Claire Muzyka

PhD advisor: Prof. Jean-Christophe M. Monbaliu

Thesis submitted in fulfillment of the requirements
for the degree of PhD of Sciences

NEW PERSPECTIVES TOWARD THE VALORIZATION OF BIO-BASED MOLECULES

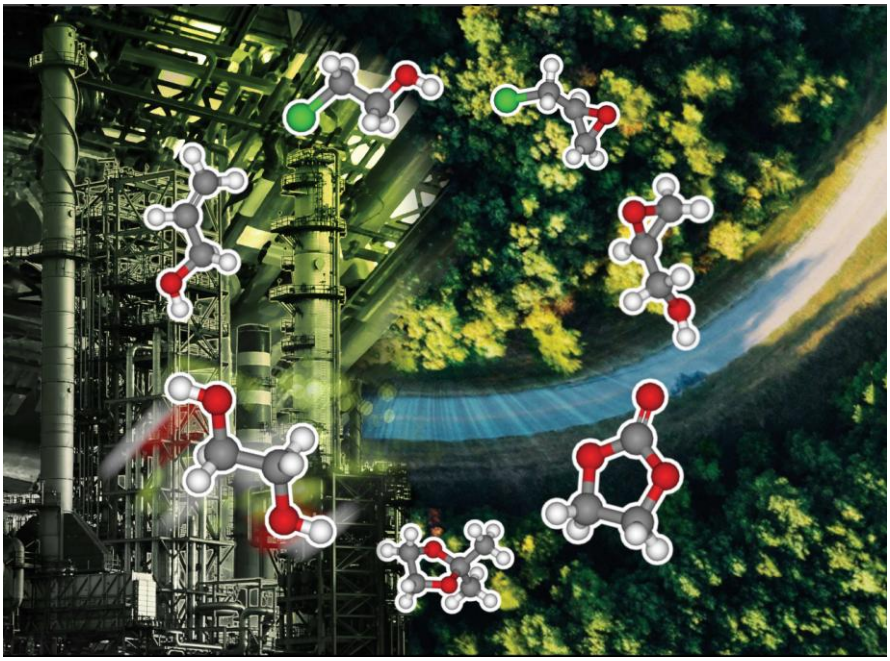

FACULTY OF SCIENCES

Department of Chemistry

Academic Year 2024-2025

ACKNOWLEDGMENT

Starting my PhD thesis in organic chemistry as a bioengineer has been one of the most demanding and rewarding challenges of my early journey. Entering a new scientific field without a formal background in chemistry required perseverance, adaptability, and resilience. This journey has been uniquely enriching, made possible thanks to the invaluable support of dedicated mentors and colleagues.

I would like to express my deepest gratitude to my PhD supervisor, Prof. Jean-Christophe Monbaliu, for offering me the opportunity to pursue this PhD in his laboratory. I am sincerely thankful for his guidance, for his trust in my ideas, and for granting me the freedom to explore them. Through his mentorship, I came to realize that the only true limit in research is our imagination.

I would also like to sincerely thank Prof. Robert Paton for the stimulating discussions on photochemistry and computational science, as well as for his support during my BAEF application. My gratitude further extends to the President of the jury, Prof. Bernard Leyh, as well as to the other jury members: Prof. François-Xavier Felpin, Prof. Christian Damblon, Dr. Christophe Detrembleur, and Dr. Bruno Grignard, for their thoughtful evaluation and valuable suggestions regarding this work.

A special thank you to Diana for her help with the writing of my articles. I am truly grateful to you for taking the time and having the patience to guide me through the challenging process of scientific writing.

I would like to thank my Master's students for their motivation, passion for research, and perseverance. Our collaborations were truly complementary and allowed us to achieve great science together. Sébastien ("Croquette"), thank you for dedicating your summer vacation to our work and the DFT teaching. I truly appreciated your commitment, and I am incredibly proud to see you now leading your own research. Tom, I wish you all the best in finding your path, one that brings you both joy and fulfillment.

Over the years at CiTOS, I had the great pleasure of meeting many people from diverse backgrounds, each bringing their own unique perspective and personality. I am especially grateful to my colleagues from the North: Guillaume, who introduced me to the world of programming; Romodo, whose artistic talent never ceased to amaze me; and Charlotte, for sharing her love of French songs. Thank you, Anita, for your constant joy, positivity, and wisdom. A warm thank you as well to Rejane, Louise, and Nicolas for the much-needed nic-nac breaks and cheerful companionship. I am also grateful to my office mates, Michele and Florian, and to the Lab 3 team, Hubert and Loïc, as well as the extended group in the M Room, with the matriarch Elyse and all the “shrimps,” past and present. Each of you has played a part in making the lab a truly unique and enriching place, shaped by people from all walks of life.

A big thanks to Bruno for the Wednesday croissant breaks, to Geoffroy for his support throughout the years, and to Christian, for everything and, of course, the coffee.

Finalement, je voudrais remercier ma famille, spécialement ma maman, mon frère et mon papa qui m'ont soutenu pendant toutes ces années, dans les meilleurs jours comme dans les plus compliqués. Grâce à vos petites attentions, votre perspective extérieure sur les situations complexes, et simplement par votre présence, j'ai pu surmonter des obstacles que je pensais infranchissables.

I also want to dedicate this work to my grandmother, Helena ('Babcha'), who was immensely proud that I contribute to helping others through research, as she always used to say.

I would like to conclude with these few words. As researchers, we are the architects of tomorrow's future. We are entitled to dream and to turn those dreams into reality, guiding society to navigate through its most challenging times. I firmly believe that research is one of the most altruistic pursuits we, as scientists, can undertake to create a brighter future for the world, ensuring equity, respect, and the well-being of all, while honoring and protecting our planet.

ABSTRACT (ENGLISH VERSION)

Bio-based chemistry is pivotal strategy in combating climate change and reducing the chemical industry's reliance on fossil resources. Concepts like Bioeconomy and Circular economy are gaining global recognition, underscoring an upcoming change of societal paradigm toward sustainability. Despite this strong momentum and the clear environmental benefits, bio-based and green chemistry face significant challenges that threaten the pace of this sustainable transition. Among them, the main issue relates to the huge difficulty to compete with established petrochemical industries, in cost, performance and scalability. Overcoming these challenges is essential to fostering secure supportive policies, drive innovation and attract investment for a sustainable chemical industry transformation.

This PhD thesis is dedicated to developing innovative strategies for advancing reactions involving bio-based polyols. These substrates are inherently complex, resulting from their high content in oxygen and the coexistence of multiple functional groups within a single molecular scaffold. This research is structured around two complementary strategies: one centered on computational chemistry and the other on advanced reactor technologies. The first strategy introduces a novel strategy integrating Python scripts to statistically decompose complex spectral datasets. This method facilitates the identification of the number of species involved in kinetic studies, serving as a foundation for the development of kinetic models that optimally balance accuracy and complexity. A separate chapter is devoted to the mechanistic investigation of the deoxydehydration reaction, which generates olefin scaffolds from polyol substrates. Although this transformation offers an attractive synthetic pathway, it currently suffers from poor selectivity control, significantly hampering its broader application. The second strategy details the intensification of glycidol carbonation with CO_2, derived from bio-sourced glycerol, by employing continuous flow technology to exploit its inherent advantages in facilitating liquid gas reaction. By combining these approaches, the thesis aims to contribute to overcoming the barriers that hinder the broader adaptation of bio-based chemistry, thereby advancing the transition toward a more sustainable chemical industry.

ABSTRACT (FRENCH VERSION)

La chimie biosourcée constitue une stratégie essentielle pour lutter contre le changement climatique et réduire la dépendance de l'industrie chimique aux ressources fossiles. Des concepts tels que la Bioéconomie et l'économie Circulaire gagnent en reconnaissance à l'échelle mondiale, soulignant l'émergence d'un changement de paradigme sociétal vers une durabilité accrue. Malgré cet élan prometteur et les avantages environnementaux évidents, la chimie verte et biosourcée se heurte à d'importants défis qui freinent le rythme de cette transition durable. Le principal obstacle réside dans la grande difficulté à rivaliser avec les industries pétrochimiques établies en termes de coût, de performance et d'échelle de production. Surmonter ces défis est essentiel pour consolider des politiques de soutien, stimuler l'innovation et attirer les investissements nécessaires à la transformation durable du secteur chimique.

Cette thèse de doctorat se consacre au développement de stratégies innovantes pour faire progresser les réactions impliquant des polyols biosourcés. Ces substrats présentent une complexité intrinsèque, liée à leur teneur élevée en oxygène et à la coexistence de multiples groupes fonctionnels au sein d'une même structure moléculaire. Les chapitres s'articulent autour de deux approches complémentaires : l'une fondée sur la chimie computationnelle, l'autre sur des technologies de réacteur avancées. La première approche propose une méthode innovante intégrant des scripts Python pour décomposer statistiquement des ensembles de données spectrales complexes. Cette méthode permet d'identifier le nombre d'espèces impliquées dans les études cinétiques, servant de base à l'élaboration de modèles cinétiques optimisant le compromis entre précision et complexité. Un chapitre distinct est consacré à l'étude mécanistique de la réaction de désoxy-déshydratation, qui permet la formation de structures oléfiniques à partir de polyols. Bien que cette transformation représente une voie de synthèse prometteuse, elle souffre actuellement d'un manque de contrôle en matière de sélectivité, ce qui limite fortement son déploiement à l'échelle industrielle. La seconde approche porte sur l'intensification de la carbonatation du glycidol avec du CO_2, issu du glycérol biosourcé, à l'aide de technologies en flux continu, tirant parti de leurs avantages intrinsèques dans les réactions liquide-gaz. En combinant ces approches, cette thèse ambitionne de contribuer à surmonter les obstacles entravant l'adoption plus large de la chimie biosourcée, et ainsi à faire progresser la transition vers une industrie chimique plus durable.

Declaration of authorship

I, Claire Muzyka, declare that this PhD thesis titled, “New Perspectives Toward the Valorization of Bio-Based Molecules” and the work presented in it are my own.

I confirm that:
This work was wholly or mainly done while in candidature for a PhD degree at the University of Liège.
Where any part of this thesis has been previously published, this has been clearly stated.
Where I have consulted the published work of others, this is always clearly attributed.
Where I have quoted from the work of others, the source is always given. With the exception of such quotations, this thesis is entirely my own work.
Where the thesis is based on work done by myself jointly with others, this has been clearly stated.
I have acknowledged all main sources of help.

TABLE OF CONTENTS

1 INTRODUCTION

1.1 THE DEVELOPING BIOECONOMY IN EUROPE

1.1.1 EUROPE, BIOECONOMY, AND CURRENT SOCIETAL CHALLENGES

The overall European Bioeconomy strategy generates a turnover around € 2.3 trillion and an added value worth € 620 million, however, the current situation is still far from what was expected by the Organization for Economic Cooperation and Development (OECD).[1] While this overall strategy is a critical pillar toward a transition for an increased sustainability, the spreading and understanding of this strategy only started a decade ago, although its first mention already dates back to 1987 (Figure 1.1). The original report published by the World Commission on Environment and Development highlighted the urgent need to transition toward sustainable development and introduced the concept of bio-based economy or Bioeconomy.[2] In Europe, the early 2000s witnessed the inception of the term Bioeconomy, also known as knowledge-based Bioeconomy, within the political sphere. It then rapidly became a major objective and was launched as global strategy advocated by the European Union. The foundations of Bioeconomy were set during several European Commission (EC) strategical agendas. To name a few examples, the White Paper (1993) stressed the key role played by biotechnologies in innovation and growth and the Lisboa Agenda (2000) aimed at boosting the EU economy through knowledge and innovations. Later in 2002, EC acknowledged life science and biotechnologies as the milestones to fulfill the main objectives of the Lisboa Agenda. Following up these strategical agendas, the sourcing and upgrading of bio-based products were identified as one of the 6 key sectors for setting new paradigms for the overall European market by the Lead Market initiative, a policy promoting EU Bioeconomy between 2007-2013.[3] Similarly, Horizon 2020 (H2020), a major EU research and innovation program (2014-2020), attempted to secure EU global competitiveness through the funding of world-class public/private collaborative research programs aimed at unlocking innovation. H2020 relied on an approximate budget of € 80 billion with supplemental private investments.[4] In the continuity of this project, Horizon Europe took over in early 2021 and will spread over 7 years with an even higher strike power compared to H2020, reaching € 95.5 billion. More than half of this budget will be dedicated to modernizing and accelerating green and digital transitions, as well as to strengthening Europe's resilience and crisis preparedness, its competitiveness and its leadership.[5] Such momentum and overall strategy fall under the umbrella of a much broader strategic EU instrument, that is, the European Strategy Forum on Research Infrastructures (ESFRI), which stimulates the creation and development of top-notch research facilities to "develop the scientific integration of Europe and to strengthen its international outreach".[6]

Based on an extended public consultation regarding Bioeconomy, EC published a report entitled "Innovating for Sustainable Growth: A Bioeconomy for Europe" in 2012. This agenda comprised 5 distinct objectives to tackle with current societal challenges: (a) ensuring food security, (b) managing natural resources sustainably, (c) reducing dependence on non-renewable resources, (d) mitigating and adapting to climate change and (e) creating jobs and maintaining European competitivity. Moreover, 3 main areas of actions were identified: (a) investments in research, innovation and skills, (b) reinforced policy interaction and

stakeholder engagement and (c) enhancement of markets and competitiveness in Bioeconomy.[7] In 2017, a review of this program stated that, although significant progresses were made through the successful mobilization of funding for research and innovation, as well as for the development of numerous national and regional bioeconomy strategies, further investments were still needed within a stable regulatory environment to encourage private investments.[8]

As a project under the umbrella of H2020, RoadToBio aimed to replace 25% of the total volume of raw organic chemicals and feedstocks with bio-based or renewable alternative feedstocks by the end of 2030. The main purposes of RoadToBio revolve around 2 milestones: a) identifying bio-based chemicals opportunities and b) developing a roadmap and general frame for both bio-based chemistry and bio-based economy.[9] The first milestone enabled to identify bio-based alternatives to 85% of existing petrochemicals, with already a successful implementation at either pilot or commercial scale.[10]

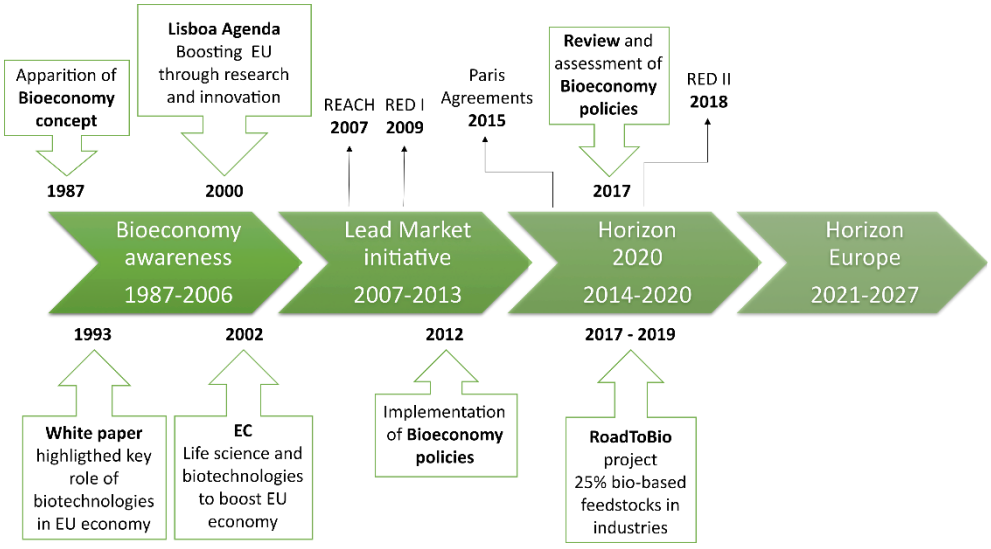

Figure 1.1 Timeline of European Bioeconomy development (1987-2021), as well as key events and projects involved in Bioeconomy within all member states.[1-3]

As very attractive indicator to assess technology maturity, the technology readiness levels (TRL) were extensively used within H2020 program to classify project status from a fundamental idea (TRL=1) to its development as fully commercialized industrial application (TRL=9). When translating this concept to H2020 first goal, it meant that all identified bio-based alternatives were associated with a TRL superior to 4, which is attributed to a demonstration prototype at laboratory scale.[11] Thus, this first purpose highlighted the fact that even if numerous bio-based technologies do exist to replace petrochemicals, they are still far from being translated at full commercial scale. Considering the second milestone, it clearly distinguished regulatory, policy and societal barriers to unlock the implementation of a durable and competitive bio-based industry.

Within the EU, numerous regulations were progressively implemented to set a stable and coherent regulatory framework toward Bioeconomy. However, owing to the legal flexibility granted by the EU to its members and the diversity of sectors involved in the bio-based economy, many specific national and even regional regulations actually hamper the development of a coherent, global and unified EU strategy. For instance, the legislative heterogeneity in EU causes the same chemical product to be considered as waste or a product and thus, can or cannot be recycled or reused within two members. Among EU legislation, different directives were highlighted as potentially problematic for the development of a bio-based economy. For instance, the Renewable Energy Directive (RED I) directly promotes the use of green energies, among others, through facilitated access to biomass feedstock. Consequently, it leads to uneven playgrounds with various bio-based industries exploiting the same resources, hence causing an extended growth of the Green Energy sector over bio-based industries. The latter achieved a 4 to 9 times higher value products compared to renewable energy and 5 to 10 times more jobs.[1] Within the frame of Circular economy, which consists in the systematic reinsertion of wastes in new pathways of valorization combined to a significant decrease in polluting emissions,[12] this directive is also very contradictory. Indeed, the use of biomass for energy is tagged as a final use whereas the upgrading of biomass to value-added products triggers a cascading use.[1] This directive was recently revised (RED II) to set new policies for reaching 32% renewable energy by the end of 2030, instead of the 20% originally scheduled in 2020.[13] Although the production of advanced biofuels is promoted, this new target could potentially escalate the pressure on biomass feedstock availability. In 2007, EU Regulation on the Registration, Evaluation, Authorization and Restriction of Chemicals (REACH) was established for promoting sustainable development, ensuring an enhanced protection of environment and public health through a better management of chemical and production hazards. Although the goals of the latter regulation fall within the walls of the green transition, it was also incriminated as a major hurdle due to the difficult, long and costly process required for the registration of new compounds, which is almost always the case for bio-based products. Another striking example concerns the exemption of import taxes or specific treatments for most of the petrochemicals, therefore leading to competitive disadvantages for bio-based products and materials. Overall, these facts clearly demonstrated that bio-based chemical and materials sectors have not yet received enough policy attention to ensure the coherency and the continuity of legal measures, as well as the required support for their growths. Besides these regulatory hurdles, the development of new bio-based industries able to compete with big petrochemical companies is still very challenging mostly due to the fact that fossil-based processes are very well optimized, come with an unbeatable cost-efficiency and are well-tailored to match the regulatory constraints.[1]

In the current regulatory landscape deeply modulated by strong measures such as the Paris agreements, the Circular Economy strategy or the Sustainable Developments Goals, EU envisions a combined approach at the interface between Bioeconomy and Circular Economy, namely, Circular Bioeconomy.[12] The Circular Bioeconomy concept advocates the exploitation of biomass-based feedstock, especially bio-based wastes to decrease green gas emissions as well as the demand for fossil carbon. The Circular Bioeconomy is however not just a superimposition of both Bioeconomy and Circular Economy; several key differences do exist. Among them, a striking example lies with green energies, which belong to the

Bioeconomy strategy but are not comprised in the Circular economy as it means the end use of a waste and prevent its further use in a reuse cycle. Additionally, some industrial sectors produce bio-based products (such as detergents and cosmetics), which is in phase with the underlying principles of Bioeconomy but cannot be recycled for health or safety considerations. Finally, numerous bio-based industrial processes were developed over the years to fulfill EU purposes, yet they were not designed to exploit their wastes, and are therefore excluded from Circular economy.[14] Nevertheless, owing to substantial EU funds involved for promoting research, innovation and competitiveness, the part of bio-based processes answering to Circular economy prerogatives will more likely increase over the years, therefore pushing European industries to converge toward a common strategy, relying on the exploitation of bio-based feedstock while maintaining high value resources as long as possible by cascading use, recycling and preserving the environment.

1.1.2 BIO-BASED CHEMISTRY

Our current standards of living rely mostly, if not exclusively, on the use of petrochemicals and fossil resources. Historically, the petrochemical revolution led to the improvement of our overall life standards. However, with an exponential increase of population worldwide, the progressive depletion of these resources accelerates, hence their shortage inevitably waves the background threat of a global collapse of the economy. In Europe, a recent study highlighted that, based on actual proven fossil resources, their future availability in 2050 will be very precarious, with reduced reserves estimated to 14% of oil, 72% of coal and 18% of gas.[15] Therefore, it becomes urgent to focus efforts on a transition toward the exploitation of sustainable and renewable resources. These past two decades witnessed the emergence of intense research efforts with the emergence of Sustainable Process Development, the introduction of the 12 principles of Green Chemistry, the highlight of several hot bio-based platform molecules by the US Department of Energy and the emergence of biorefineries toward the production of valuable platform molecules and their further upgrading. However, these processes are currently highly resource-consuming and produce extensive amounts of wastes, by contrast, quite paradoxically, to the refining of crude petroleum which is very well optimized enabling to concomitantly valorize all separated fractions and minimizing waste. In addition, the design of alternative and economically viable processes based on bio-based molecules is a great challenge to the Chemistry and Chemical Engineering communities that requires the development of innovative catalysts, process conditions and technologies, as well as substantial financial and societal support. The exploitation of biomass inherently bears the potential to produce building blocks identical to basic or more advanced petrochemicals (a.k.a. drop-in and smart drop-in bio-based chemicals, respectively– Figure 1.2), as well as to provide new opportunities (a.k.a. dedicated bio-based chemicals – Figure 1.2).[12] Regarding the latter, it becomes clear that as a consequence of their oxygen-rich unique structures, they could open new avenues toward groundbreaking applications, impossible to reach with typical petro-based hydrocarbon backbones. Although several alternative bio-based processes exist nowadays, they still suffer from poor global efficiency, as soon as the big picture is considered including the extraction of starting materiel from biomass, compared to their petro-based analog, hence preventing their widespread adoption.

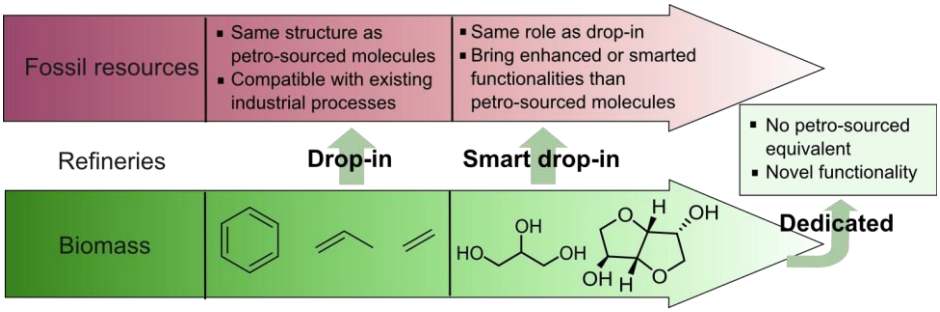

Figure 1.2 Definition of bio-based drop-in, smart drop-in and dedicated molecules.

One of the major factors to unlock relates to the high oxygen content of bio-based molecules, consequently forcing chemists and chemical engineers to adapt, rethink and redevelop established reaction conditions, processes and their overall strategies. Petro-based processes indeed rely on a different chemistry targeting hydrocarbon backbones and are historically focused on product yield, selectivity and cost-effectiveness criterions that are not anymore in phase with current societal challenges revolving around climate change, environmental footprint and pollution.

1.2 OBJECTIVES

This thesis aims to develop novel and sustainable strategies toward the upgrading of bio-based polyols, integrating computational chemistry and continuous flow technologies. The first milestone is to design an innovative approach for rationalizing new mechanisms and complex reaction networks typically associated with bio-based molecules. The second milestone focuses on leveraging the unique advantages of flow chemistry to enhance CO_2 conversion efficiency in reactions with bio-based compounds. This approach aims to support the engineering of scalable, high-throughput and waste-efficient processes for tailored polyol functionalization.

The transition toward oxygen-rich bio-based feedstocks presents a significant challenge: controlling reaction selectivity and productivity while handling molecular complexity. To address this, new tools must be designed to support chemists in navigating the inherent intricacies of bio-based compounds.

This manuscript begins with a comprehensive overview of five key reactions relevant to the transformation of vicinal diols, which helped me to frame the rest of my doctoral research: (a) deoxydehydration, (b) Williamson's or dehydrative epoxidation, (c) chlorination/dechlorination, (d) carbonation and, (e) ketalization. These reactions hold significant potential for upgrading bio-based molecules with broad industrial relevance.

Chapter 2 provides a detailed review of current synthetic methodologies and experimental conditions applied to C_2 - C_6 and cyclic polyol substrates, covering a wide array of catalytic systems developed for these purposes. This review seeks to discuss the physical and chemical challenges associated with polyols bearing multiple vicinal diols an to showcase recent technological advancements designed to overcome them. The specific goals of this review are to:

(a) establish a solid foundation to support the chemistry community in advancing bio-based processes
(b) present a library of olefins, epoxides, cyclic carbonates and ketals that can be synthesized from the five key reactions, all with significant industrial potential
(c) provide a comprehensive evaluation of the environmental metrics, including E-factor and Atom Economy, across a representative selection of processes from each reaction.

Chapter 3 focuses on the thorough understanding of preliminary steps leading to the formation of chemicals intermediates undergoing deoxydehydration. These steps involve complex dynamic covalent exchanges between polyols and orthoesters, characterized by a broad product distribution and competing reaction pathways. This chapter illustrates the intrinsic challenges of working with diols, including the intricate interplay between the reagents, products, solvents and catalysts. The main goals of Chapter 3 are to:

(a) develop a structured workflow to support in the interpretation of spectral datasets and kinetic modelling, eventually producing a robust, accurate and reliable kinetic model;

(b) apply this model to improve classical reagents and solvent screening, enabling a more systematic and quantitative approach to empirical analysis;
(c) establish an integrated kinetic and computational strategy to dissect dynamic covalent exchange network, identifying the key factors that govern reaction dynamics.

Chapter 4 investigates the deoxydehydration (DODH) of bio-based orthoesters, a reaction with considerable potential to generate renewable olefins for industrial applications. Despite its promise, the development of DODH processes has been hindered by the typically harsh conditions required (T >200 °C) and the use of reagents in excess. The main goals of Chapter 4 are:

(a) elucidate the mechanistic pathway of the DODH reaction on bio-based orthoesters and identify the key intermediates involved in olefin formation.
(b) analyze the influence of intra- and intermolecular hydrogen bonding on the reaction mechanism, and evaluate how substrate structure affects reaction selectivity and overall performance.

Chapter 5 explores the integration of bio-based polyols with abundant waste streams such as CO_2, an approach holding significant promise for advancing sustainable chemistry. Effective implementation of these transformations usually requires activated version of polyols, (e.g. epoxides), harsh conditions of temperature and pressure and carefully designed catalytic systems to overcome the inherent low reactivity of CO_2.

The first subsection of this chapter presents a comprehensive review of catalytic strategies developed under batch or flow conditions to convert common and β-hydroxylated epoxides toward glycerol carbonate, a high added value compound. The purposes of this review are to:

(a) present an in-depth discussion of the catalytic strategies for glycidol with particular emphasis on catalyst scaffolds and their mechanistic implications in the reaction;
(b) compare all reviewed processes based on the sustainability of their experimental conditions and carbonate yields, including calculated E-factors;
(c) assess the potential for industrial scale production of glycerol in continuous flow conditions.

The second subsection of Chapter 4 outlines an integrated computational and experimental approach aiming at intensifying the synthesis of glycerol carbonate via gas-liquid reactions in flow systems. The main goals of this study are to:

(a) evaluate the catalytic performances of an array of nitrogen-containing organocatalysts and rationalize the catalytic mechanism.
(b) intensify the microfluidic process and scale it up to laboratory-scale reactor, establishing a highly efficient and productive methodology for glycerol carbonate synthesis;
(c) identification of the key physicochemical parameters that limit overall reaction performance.

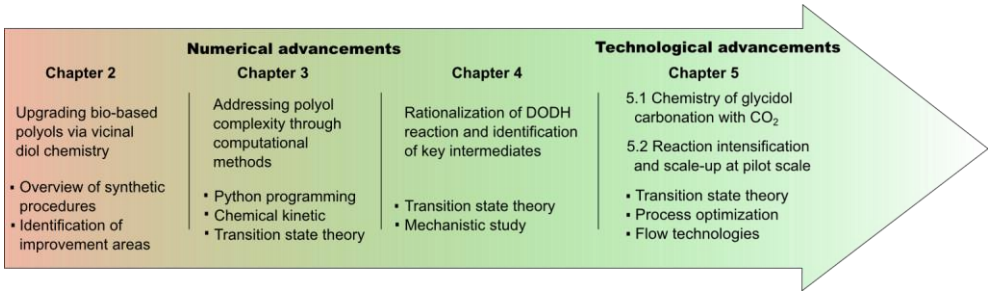

Figure 1.3 Overview of this PhD work.

1.3 REFERENCES

[1] Roadmap for the Chemical Industry towards a Bioeconomy, https://roadtobio.eu/uploads/publications/deliverables/RoadToBio_D21_RegulatoryBarriers.pdf (accessed on 10-17-21).

[2] B. R. Keeble, Med. War 1988, 4, 17–25.

[3] K. McCormick, N. Kautto, Sustainability 2013, 5, 2589–2608.

[4] What is Horizon 2020?, http://h2020ni.com/what-is-horizon-2020/ (accessed on 10-30-21).

[5] What is Horizon Europe?, https://www.horizon-eu.eu/ (accessed on 10-12-21).

[6] ESFRI: Making science happen, https://www.esfri.eu/sites/default/files/White_paper_ESFRI-final.pdf (accessed on 12-09-21).

[7] Innovation for sustainable growth: A bioeconomy for Europe, https://op.europa.eu/en/publication-detail/-/publication/1f0d8515-8dc0-4435-ba53-9570e47dbd51 (accessed on 10-5-21).

[8] Review of the 2012 European Bioeconomy Strategy, https://ec.europa.eu/information_society/newsroom/image/document/2018-6/review_of_2012_eu_bes_2E89B85F-950B-9C84-5B426D1C24851387_49692.pdf (accessed on 10-5-21).

[9] RoadToBio, https://roadtobio.eu/uploads/publications/roadmap/RoadToBio_action_plan.pdf (accessed on 10-5-21)

[10] Bio-based opportunities for the chemical industry: Where bio-based chemicals meet existing value chains in Europe, https://roadtobio.eu/uploads/publications/deliverables/RoadToBio_D11_Bio-based_opportunities_for_the_chemical_industry.pdf (accessed on 09-22-21).

[11] What are Technology Readiness Levels (TLRs) and to which Horizon 2020 call topics are they applicable? https://ec.europa.eu/info/funding-tenders/opportunities/portal/screen/support/faq/2890 (accessed on 09-09-21).

[12] Roadmap for the Chemical Industry in Europe towards a Bioeconomy: Concept of bio-based and circular economy, https://roadtobio.eu/uploads/publications/deliverables/RoadToBio_D25_Biobased_and_circular_economy.pdf (accessed on 09-16-21)

[13] Renewable Energy-Recast to 2030 (RED II), https://ec.europa.eu/jrc/en/jec/renewable-energy-recast-2030-red-ii (accessed on 10-03-21).

[14] M. Carus, L. Dammer, *Ind. Biotechnol*. **2018**, 14, 83–91.

[15] F. Martins, C. Felgueiras, M. Smitkova, N. Caetano, *Energies* **2019**, 12, 964.

2 PERSPECTIVES FOR THE UPGRADING OF BIO-BASED VICINAL DIOLS WITHIN THE DEVELOPING EUROPEAN BIOECONOMY

2.1 PREFACE

This Chapter explores the chemistry of vicinal diols and presents new alternative processes and technologies aiming at upgrading of bio-based polyols. Despite the growing momentum driven by Bioeconomy policies, bio-based processes remain far from taking over the petrochemical industry. To address this gap, five key reactions have been identified: (a) deoxydehydration, (b) Williamson's or dehydrative epoxidation, (c) chlorination/dechlorination, (d) carbonation and (e) ketalization, for their high potential in the valorization of bio-derived molecules.

This Chapter highlights the major advancements made in the five key reactions applied to C_2-C_6 and cyclic polyol substrates. The content is based on a comprehensive review published in *ChemSusChem*: C. Muzyka, J.-C. M. Monbaliu, *ChemSusChem.* **2022**, *15*, e202102391. The Chapter provides a thorough examination of synthetic methodologies, catalytic systems and technology strategies developed to overcome the physicochemical challenges associated with polyol reaction. Critical problematics such as poor selectivity control, high polarity of substrates, and solid-state nature of polyols beyond $C_4 \geq$ are thoroughly discussed. Furthermore, the chapter presents a range of value-added compounds accessible through bio-based synthetic routes, offering a comparative perspective on their petrochemical production versus current or potential bio-based alternatives. The last section discloses an environmental and waste assessment of representative procedures, emphasizing reagents and experimental conditions detrimental to the overall process efficiency while contributing to increase environmental burdens.

This work outlines the low yields observed in many synthetic procedures and the limited use of polyols containing multiple vicinal diols. These limitations significantly hinder the broader adaptation of bio-based alternatives in place of conventional petrochemical processes. This highlights the urgent need for dedicated tools to support chemists in navigating complex reaction systems. The development of such tools holds strong potential to enable accurate mapping of reaction networks, thereby enhancing the efficiency and optimization of bio-based transformations.

2.2 ABSTRACT

In the past decade, numerous European programs have been developed to stimulate and promote research and innovation relying on sustainable and renewable resources. This Review concerns the most promising process conditions and technologies targeting bio-based vicinal diols and promoting their transformation into value-added molecules of wide industrial interest, such as olefins, epoxides, cyclic carbonates, and ketals. The previous decade has witnessed a drastic increase of European incentives aimed at pushing forward the transition from an exclusively petro-based economy toward a strong and homogeneous bio-based economy. [1-15] Since 2012, numerous programs have been developed to stimulate and promote research and innovation relying on sustainable and renewable resources. Terrestrial biomass is a virtually infinite reservoir of biomacromolecules, the biorefining of which provides platform molecules of low complexity yet with tremendous industrial potential. Among such bio-based platform molecules, polyols and, more specifically, molecules featuring vicinal diols have gained tremendous interest and have stimulated an increasing research effort from the chemistry and chemical engineering communities. This Review revolves around the most promising process conditions and technologies reported since 2012 that specifically target bio-based vicinal diols and promote their transformation into value-added molecules of wide industrial interest, such as olefins, epoxides, cyclic carbonates, and ketals.

2.3 BIO-BASED POLYOLS

Terrestrial biomass represents a virtually infinite reservoir (ca. 1.7 10^{11} tons per year) of complex biomacromolecules such as vegetable oils, sugar, cellulose or starch. The specific and selective transformation of such biomass through biorefineries leads to a range of less complex, low molecular weight yet versatile molecules with a high oxygen/carbon ratio.[16] The most abundant and versatile are nicknamed bio-based platforms and were defined by the US department of Energy (US DoE) as “molecules with multiple functional groups that possess the potential to be transformed into new families of useful molecules”; the usefulness of which is to be understood from an industrial perspective. The US DoE published an initial collection of 10 bio-based platforms of wide industrial interest.[17] With the development of new technologies and transformations, the initial list was later revised in 2010 for encompassing 13 “top chemical opportunities” compounds derived from biomass. This list comprises various carboxylic acids (3-hydroxypropionic acid, aspartic acid, succinic acid, fumaric acid, malic acid, glutamic acid, levulinic acid, itaconic acid and glucaric acid), 3-hydroxybutyrolactone, 2,5-furandicarboxylic acid, and polyols (glycerol, xylitol, arabinitol and sorbitol (Figure 2.1).[18]

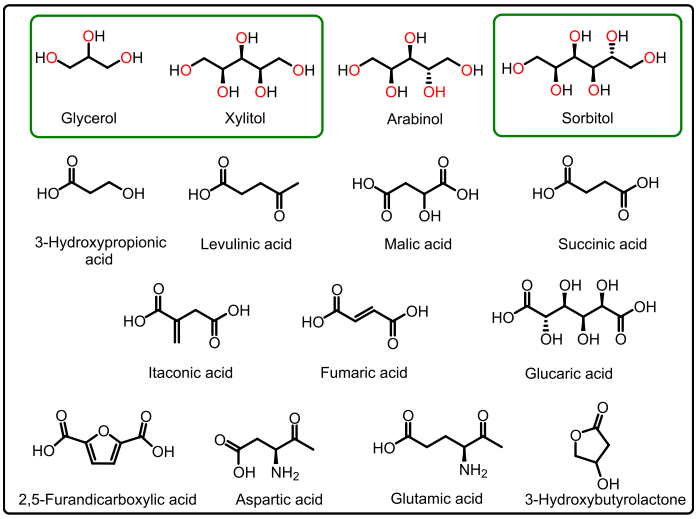

Figure 2.1 Selection of bio-based platform molecules established by the US Department of Energy (US DoE) in 2004 and emphasis on the vicinal diol backbone of bio-based polyols.[18]

Among them, bio-based polyols are among the most represented accessible class of bio-based platforms, with as common feature a specific repetition of a vicinal diol pattern (i.e., two hydroxy functions born by neighboring sp^3 carbon atoms). Aside from polyols produced from yeast fermentation or derived from the biofuel industry, this peculiar architecture is derived from plant metabolism targeting carbohydrate synthesis. More specifically, the vicinal diol pattern arises from Calvin's cycle, which is responsible for the fixation of carbon dioxide and its conversion to a 3-carbon sugar precursor called glyceraldehyde 3-phosphate (a.k.a. triose phosphate).[19] In the next metabolic step, an enzymatic cascade leads to the formation of glucose, as well as other sugars such as xylose or arabinose, which are the main reservoir of building blocks toward cellulose, starch, and hemicellulose, to name a few (Scheme 2.1).[19]

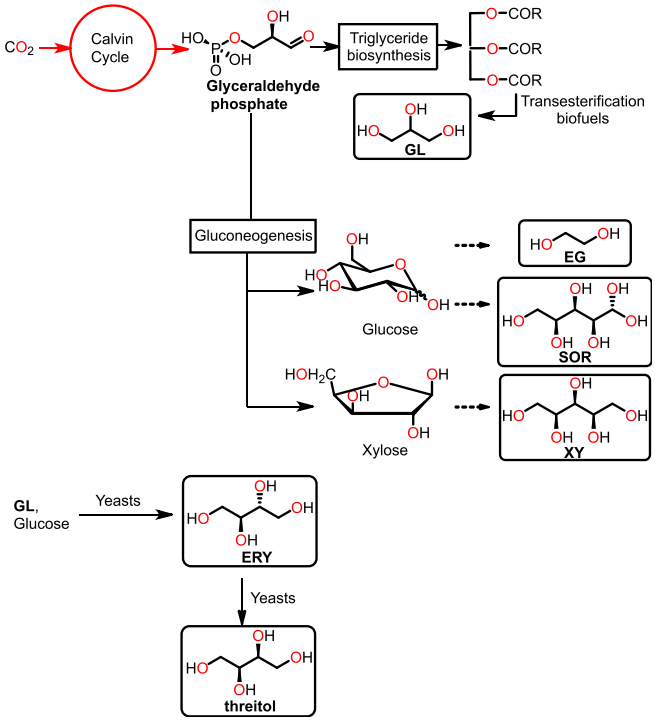

Scheme 2.1 Metabolism of CO_2 toward biosynthesis of sugars used to produce the targeted polyols ethylene glycol, glycerol, erythritol/threitol, xylitol, and sorbitol.

Based on their inherent structural features, vicinal diols bear a significant synthetic utility. Figure 2.2 depicts transformations of interest where vicinal diols are required either for the formation of either a key intermediate or an added-value product.[20--24] Indeed, the presence of two discriminable neighboring hydroxy groups opens up a large array of reactions that rely on either their inherent nucleophilicity or on the selective electrophilic activation of one of them. The outcome of such reactions is, however, quite dependent on their relative configuration. The relative configuration (*cis* or *trans*) often emerges as a determining parameter for internal vicinal diols (Figure 2.2a) where no conformational flexibility is allowed. Needless to say, the presence of multiple vicinal pairs in higher bio-based polyols exponentially increases the likelihood of competitive reactions and the formation of a wide range of products from the same starting material. This increasing complexity is illustrated in Figure 2.2b and emphasizes the paramount importance of reaction engineering and a thorough understanding of reaction mechanisms and selectivity for maintaining chemoselectivity,[22,25] which can obviously become deleterious to cost-efficiency and atom economy.

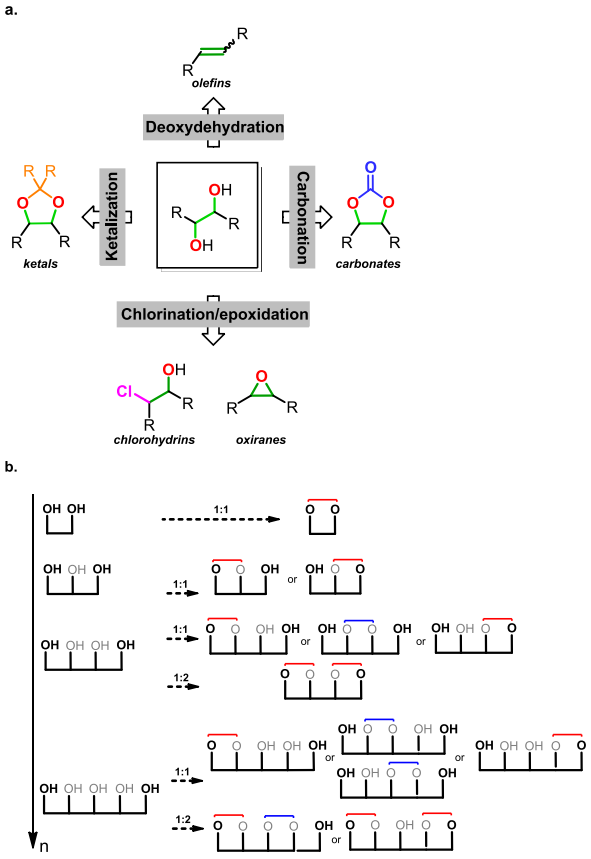

Figure 2.2 (a) Vicinal diols conversion based on their inherent reactivity (nucleophilicity or electrophilicity). (b) Correlation between multiplication of vicinal diols functions and increased complexity of reactional outcome.

Although glycerol (**GL**), xylitol (**XY**) and sorbitol (**SO**) are the only representative bio-based vicinal polyols from the updated DoE list, additional bio-based polyols of potential industrial interest are considered in this Review. Ethylene glycol (**EG**) and erythritol (**ERY**) are considered as well for providing a thorough overview of reactions and process technologies applied to C_2<C<C_6 diols (Figure 2.3), hence potentially covering a large array of drop-in, smart-drop in and dedicated bio-based industrial building blocks. While the production of **EG** is already well established at commercial scale,[26] the production of **ERY** is still at its early commercialization stage.[27] Generally, this class of chemicals displays severe differences of prices and market volumes leading to much faster progresses for widely available and cheap polyols such as **EG** or **GL** (<1200 US$ per ton) in contrast to **ERY** and **XY** (≥ 3900 US$ per ton).[21,28,29] The high costs associated with **ERY** and **XY** are also rooted in their main application in the food industry as sweeteners.[30] Indeed, the use of polyols as food additive is not recent, primary finding applications in alimentary formulations suitable for diabetes diets, these chemicals were progressively used for conventional industrial food such as candies or the manufacturing of baked goods.[31] Moreover, owing to population increase, demand for animal source food and thus animal feed is nowadays also raising. Therefore, competition for resources access seems inevitable and emerges as a major hurdle

for other industrial applications,[32] though the development of new and cost-effective technologies for their production should counterbalance a struggle for supply.

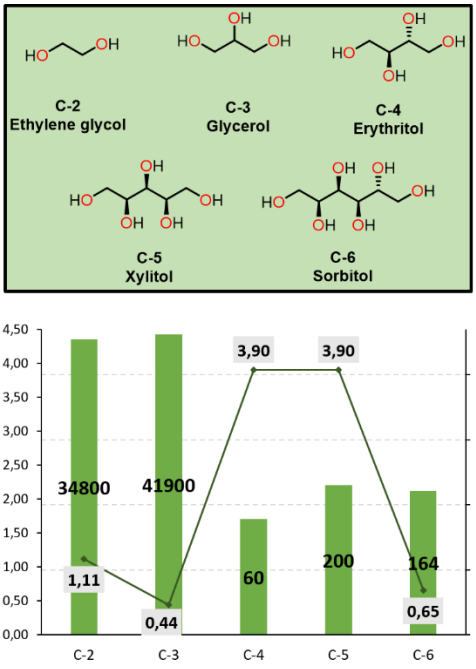

Figure 2.3 Presentation of bio-based C_2-C_6 polyols selected in this work as well as their prices per ton (light grey) and estimated global market volumes (green).

Ethylene glycol (ethane-1,2-diol, **EG**) is a very important industrial C_2 building block that expresses the simplest scenario for a vicinal diol in terms of chemistry. With a market volume of 34.8 Mt per year,[26] it is typically petro-based through partial catalytic oxidation of ethylene oxide either via direct hydration in presence of an excess of water which leads to high energy demanding purification or via a selective hydrolysis of ethylene carbonate.[33] The only industrial bio-based alternative is based on a multistep process starting from bio-ethanol. Among the main players, the bio-based **EG** process was commercialized in 2008 by India Glycol Ltd with an annual production of 175 000 t (for the production of polyethylene terephthalate) or by Greencol Taiwan Corporation (100 000 Mt y^{-1}).[26,34,35] The production of **EG** concerns 2 main huge established markets: 50% of its production is entirely dedicated to the preparation of antifreeze formulations and about 40% serves in the manufacturing of polyesters.[36]

Glycerol (propane-1,2,3-triol, **GL**) has a much larger market volume. **GL** is typically obtained from the biofuel and oleaginous sectors and is co-generated as a 10 wt% by-product from the transesterification and/or saponification of triglycerides. The worldwide production of **GL** was estimated around 8 million tons in 2020 with more than half (62%) of its production volume arising from the biodiesel industry.[10] With a foreseen growth of the biodiesel production (168 billion liters in 2022), the overall volume of **GL** is predicted to proportionally increase.[37] The main biodiesel producers are NESTE with 2.7 million t per

year (EU and Singapore), Diamond Green Diesel (USA) with 0.8 million t and Total with 0.5 million t per year (EU). US production is by far the largest, with a production capacity estimated at 11.3 billion liters.[26] Moreover, in reaction to Renewable Energy Directive II and its aim to transition toward second-generation biofuels (i.e., biofuels from waste products), new generations of plants are designed to enable their processing. For instance, Cargill invested € 150 million in Ghent (Belgium) to build a second-generation biodiesel plant with a production capacity of 150 000 tons, entirely based on the exploitation of slaughter wastes, frying fat or sewage sludge.[38] This latter comes in support to their already existing plant in Ghent (2015, ca. 367 Mt y^{-1}), which possesses a complete end to end chain of biodiesel production.[39] Given these facts, it is clear that the production of **GL** has a bright medium-term forecast, despite the threat of new generation biofuels called "hydrotreated vegetable oil (HVO)" that does not coproduce glycerol.[40] Aside from HVO, the main drawback to its worldwide and extensive use relates to its inherent production as a by-product alongside impurities such as methanol, inorganic salts, water, mono-and diglycerides as well as fatty acid residues (around 50 wt% w/v) that render the direct use of crude glycerol cumbersome.[10,41] In addition, impurity content strongly depends on the type of feedstock and the biodiesel synthesis process involved.[42] Crude **GL** is worth ca 385-500 US$ per ton,[26,43] which is quite affordable given the potential of **GL** as a starting material, yet its use in industrial processes requires extensive and costly purifications that reflect on the final cost (refined **GL** 660-1000 US$ t^{-1}).[26,37,43,44] The purification of crude **GL** typically requires several steps, among which the most straightforward ones are: (a) the neutralization of crude **GL** to remove free fatty acids, (b) distillation of methanol and partial water content. At this stage, the purity reaches an average 85% of glycerol (mass yield). The third and most cost and resource intensive purification stage, aiming to reach ≥ 95% w/w in purity, is usually performed by vacuum distillation. Careful execution is required to avoid glycerol polymerization or its dehydration under residual acidic conditions. Though, this final vacuum distillation consumes a huge amount of energy, which in the end represents around 50% of global operating costs. Alternative or additional steps including ion exchange purification or adsorption with activated carbon also often considered.[45] Despite the hurdles associated with its purification, the outstanding diversity of compounds accessible from **GL** has led to numerous applications toward high added-value chemicals.[20,25,46] As a striking example, 65% of its production is currently dedicated to its direct use in food, pharmaceuticals and personal care sectors.[10]

In contrast to **GL**, the annual production of *meso*-erythritol [(2*R*,3*S*)-butane-1,2,3,4-tetrol, ERY] only reaches 60 000 t per year through fermentative pathway of starch or glucose by yeasts and bacteria, as an osmoprotectant.[47] In 2016, the market value was around 81 million US$ and is expected to reach 150 million US$ in 2024. USA is a major supplier of **ERY**, accounting for more than 75% of the production, predominantly ensured by Cargill.[48] China accounts for a small contribution (ca. 10%) with major players including Zibo ZhongShi GeRui Biotech, Zhucheng Dongxiao Biotechnology. The main supplier in EU is Jungbunzlauer (France).[49] Large scale production of **ERY** is mostly prevented by a technology barrier; however, research toward new cheap and readily available resource pointed out in the direction of glycerol, from which advanced investigations of fermentative processes are ongoing.[27] Beside the uses of **ERY** in the food industry as flavor enhancer, humectant, stabilizer, thickener and in the pharmaceutical sector as antioxidant,[30,50] **ERY**

bears an invaluable potential as a C_4 platform toward fundamental building blocks otherwise petro-based (e.g. butadiene, vinyl ethylene oxide, vinyl ethylene carbonate, to name a few). D-threitol, a diastereoisomer of **ERY**, is also a valuable compound with a broad range of applications in the pharmaceutical industry for anti-cancer drugs.[51] This polyol is synthesized through the fermentation of **ERY** and its lower availability is directly correlated to the scarcity of yeasts able to synthesize it.[51]

Five and six carbon polyols, namely xylitol [(2*R*,3*R*,4*S*)-pentane-1,2,3,4,5-pentol, **XY**] and sorbitol [(2*S*,3*R*,4*R*,5*R*)-hexane-1,2,3,4,5,6-hexol, **SO**] are derived from naturally occurring C_5 and C_6 sugars. Classical processes to produce **XY** and **SO** consist in the hydrogenation of their respective C_5 and C_6 parent sugars, namely, xylose and glucose. These bio-based polyols display similar annual market volume with 200 000 and 164 000 t, which is quite surprising given that the cost for **SO** (650 US$ t^{-1}) is much lower compared to xylitol (3900 US$ t^{-1}).[26] The production of **SO** is mainly covered by Roquette Freres (France), as well as Cargill (USA), Ingredion Incorporated (USA) and STBC (Indonesia), accounting for 70% of the global market. Regarding **XY**, Roquette Freres and DuPont are the market leaders. Both C_5 and C_6 polyols have applications deeply rooted in the food industry as additives as well as excipient in pharmaceutical and personal care sectors. In addition, 15% manufacturing of **SO** is consumed for the production of vitamin C.[29] Again, as C_5 and C_6 bio-based platforms, **XY** and **SO** also bear a huge potential for the preparation of valuable C_5 and C_6 olefins and other industrial intermediates. The development of cost-effective and innovative processes is key for unlocking the competition with the food industry.

2.4 STAPLE REACTIONS TOWARD THE UPGRADING OF BIO-BASED VICINAL POLYOLS

The next section revolves around the 5 reactions that exploit the inherent specific reactivity of bio-based vicinal polyols and that are identified as bearing the highest potential for their upgrading toward industrially relevant building blocks. Each following subsection is dedicated to one of these 5 staple reactions and starts with a short introduction on the overall reactivity aspects, the targets that are reachable accordingly (with a comparison with current petrochemical production processes) and the associated markets. Then, the latest and most significant advances for the development of new bio-based roads, chemical processes and technologies are discussed. The discussion also emphasizes the intrinsic limitations related to the use of bio-based polyols and in particular the inherent difficulty related to the presence of multiple vicinal diol pairs in higher bio-based polyols such as *meso*-erythritol, xylitol and sorbitol with competitive reactions and complex reaction mixtures. Regarding catalytic processes, the priority is given to widely available catalysts.

2.4.1 OLEFINS FROM BIO-BASED VICINAL DIOLS: THE DEOXYDEHYDRATION (DODH) REACTION

2.4.1.1 OLEFINS AS PRIVILEGED TARGETS

Olefins are the archetype of petro-based platforms with applications deeply rooted in most of current industrial processes. The deoxydehydration (DODH) reaction enables the conversion of vicinal diols into olefins. With the wide diversity of bio-based vicinal polyols, the development of DODH protocols can therefore contribute to feeding industry with a large array of fundamental or functionalized olefin building blocks (Scheme 2.2). Among the olefins reachable through a DODH reaction, ethylene (**1**) and buta-1,3-diene (**2**) can theoretically be produced from **EG** and **ERY**, respectively. Ethylene (**1**) is the most important olefin produced around the globe with 140 Mt per year (market size of 127 billion US$ in 2017 with a cost of 1.2-1.3 US$ per kg) through steam cracking of naphtha and is considered as one of the most polluting petrochemical process regarding greenhouse gas emissions.[52] More than half its production is dedicated to the manufacturing of the most widely used plastic, namely, polyethylene, and it also contributes to the manufacturing of polystyrene and polyvinyl chloride.[53] Only 0.3% of its global capacity is provided by the fermentation of bioethanol.[54] Since the latter primarily serves as biofuel, such production scheme for ethylene (**1**) could potentially lead to a competitive struggle for the same feedstock. Hence, a complementary DODH production scheme feeding on **EG** is certainly of interest, although no development has been undertaken in that direction. Another key C_3 olefin compound is prop-2-en-1-ol (allyl alcohol, **3**), which is involved in numerous organic syntheses such as preparation of polymer crosslinking agents, resin, coatings and serves as feedstock for various value-added chemical intermediates for the manufacturing of high value added 2,3-epoxy-1-propanol (glycidol, **4**), 1-chloro-2,3-epoxypropane (epichlorohydrin, **5**), butane-1,4-diol (**6**), prop-2-enal (**7**) and prop-2-enoic acid (acrylic acid, **8**) to name a few.[55-59] Allyl alcohol **3** can be obtained through the DODH of **GL** and the primary and patent literature have witnessed an increase in related process technologies. Currently, the global production of olefin **3** mostly relies on fossil resources with an estimated market size of 0.1 Mt y^{-1} and prices ranging from 2.2-3.2 US$ per kg.[58,59] Conventional petro-based processes rely on (a) the hydrolysis of 3-chloroprop-1-ene (allyl chloride, **9**) with a base or (b) the oxidation of propene (**10**) in the presence of acetic acid (**11**) and catalyzed by palladium under O_2, followed by hydrolysis toward allyl alcohol **3**. There are alternative processes: (a) the oxidation of propene (**10**) into acrolein **7**, which next undergoes reduction toward allyl alcohol **3** in the presence of propanol (^{n}PrOH) and a catalyst such as aluminum isopropylate or (b) Lyondell's process, which relies on the isomerization of 1,2-epoxypropane (**12**) over basic Li_3PO_4.[60,61]

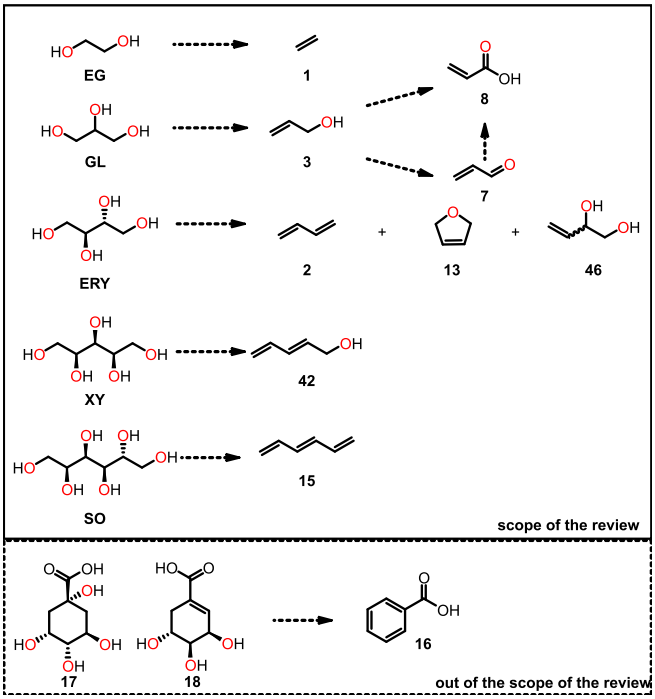

Scheme 2.2 Overview of bio-based polyols and respective olefin derivatives accessible by DODH as well as further perspectives

Allyl alcohol **3** can be converted in two major building blocks through oxidation: acrolein **7** and acrylic acid **8**. Aldehyde **7** has multiple applications that concern various fields such as the pharmaceutical sector with antibiotics and antimicrobials, the manufacturing of essential amino acid methionine as a nutritional feed additive for animals and the fragrance industry. It is also a common precursor for the preparation of acrylic acid **8**.[62] Acrylaldehyde **7** cost on the market revolves around 2.7 US$ per kg and its production volume is about 0.23 Mt y^{-1}.[62,63] Acrolein **7** is a highly toxic and hazardous chemical that is typically produced from petro-based resources. The most common production route is propene-dependent and involves a vapor-phase oxidation at 250-400 °C with oxygen in the presence of a molybdenum-bismuth-iron oxide catalyst.[60] Alternative routes do exist, including the hydration of allyl chloride **9** or the isomerization of propylene oxide **12**.[25] Acrylic acid **8** is an important building block for the polymer sector with applications including plastics, paints, coating, adhesives or superabsorbents.[60] Its global production reaches 5 Mt y^{-1} with an estimated market price of 1.63 US$ per kg.[64] The most common commercial scale process consists in the direct O_2-oxidation of propene (**10**) at high temperature in the presence of a molybdenum-based catalyst. A more sustainable road exists and relies on a sequence of glycerol dehydration and subsequent oxidation,[60] even though neither acrolein **7** nor acrylic acid **8** are currently prepared at commercial scale accordingly.[63]

1,3-Butadiene (**2**) is a C_4 petro-based platform of utmost importance and is potentially synthesizable through a double DODH of **ERY**. It stands as the most important industrial diene with applications concerning a huge diversity of synthetic rubbers, polymer resins or elastomers.[65] In 2018, its global annual production reached 18 Mt with an expected growth to 20 Mt in 2020. The costs associated with butadiene suffer from a large volatility, directly correlated to the oil market. Average prices fluctuate between 1-2 US$ per kg. 95% of its production comes from oil refining and the isolation of C_4 hydrocarbon fractions. Furthermore, an expensive and cumbersome purification is required through extractive distillation to obtain the highest grade possible, which is an essential requirement for polymerization purposes.[66] 2,5-Dihydrofuran (**13**) can also be accessed through a modified DODH of **ERY** or its dehydrated intermediate, namely, (3*R*,4*S*)-tetrahydro-3,4-furandiol (**14**). Compound **13** is a heterocyclic compound with promising future as a potential platform in the manufacturing of 1,4-epoxybutane (**15**), 2,3-dihydrofuran (**16**), 1,4-butanediol (**6**) or other fine chemicals including oxolane-3-carbaldehyde or cyclopropane derivatives.[67,68] Regarding its preparation, current industrial research focus on the ring expansion of vinyl oxiranes,[69] while alternative road relies on ring closure metathesis.[70]

1,3,5-Hexatriene (**15**), a C_6 conjugated molecule, can potentially be accessed from **SO** through a triple DODH. Since **SO** is much cheaper than **ERY**, it is expected that **15** will have a bright forecast as a dedicated bio-based building block, potentially lead to higher added-value products than butadiene **2**.[71,72]

Despite falling beyond the scope of substrates, other polyols are also of prime interest to yield cyclic compounds comprising olefin motifs. For instance, benzene can be accessible through a triple DODH of inositols, a family of natural occurring carbohydrates. Similarly, phenols are also reachable via a double DODH and consecutive dehydration.[73,74] As a reminder, phenols are predominantly involved in the polymer industry, with the manufacturing of phenolic resins and bisphenol A.[75] Benzoic acid **16** is also reachable, via renewable quinic acid (**17**) or shikimic acid (**18**), therefore, offering an alternative to the current industrial process relying on toluene oxidation. Acid **16** finds many applications such as the manufacturing of terephthalic acid, ε-caprolactam, dyes or food preservatives. In addition, its oxidative decarboxylation leads to phenol production, currently mostly generated from benzene.[75]

2.4.1.2 THE DODH PROCESS ON VICINAL DIOLS

The deoxydehydration (DODH) reaction is a classical procedure for the conversion of vicinal diols into olefins, typically operated in the presence of rhenium-based catalysts and in presence of a sacrificial reductant (Figure 2.4). Owing to the very low earth abundance of Re (estimated to 10^{-3} ppm) and the risk of rapid depletion, as well as its unknown long-term toxicity, reaction privileging alternative transition metals with a larger abundancy such as molybdenum and vanadium (1 ppm and 10^2 ppm earth crust abundance, respectively) are emerging as well.[76]

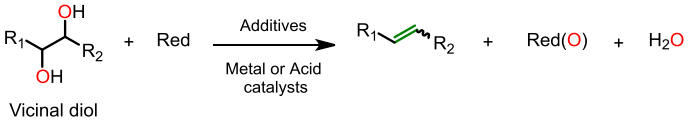

Figure 2.4 Overview of the DODH reaction for the upgrading of bio-based vicinal polyols toward olefins.[15]

Alternative, metal-free innovative DODH protocols relying on acidic catalysts receive an increasing attention from the scientific community.[24,55,70] Figure 2.5 illustrates the breakdown of DODH protocols according to the catalytic system used.[15] The direct application of DODH protocols on bio-based polyols is very challenging not only because of their inherent high hydrophilicity and their physical state (C_2, C_3: viscous liquids; $C_{\geq 4}$: solids) and the great variability of their composition/purity, but also as consequence of the usual high process temperatures to trigger the DODH process. Moreover, the inherent complexity related to bio-based polyols featuring several pairs of vicinal diols that can potentially lead to several DODH isomeric olefins or competitive products (mono vs poly-DODH extrusion) needs to be carefully addressed for controlling the regioselectivity, otherwise leading to highly unselective product distribution.[15] Developing efficient and selective processes for the upgrading of bio-based vicinal polyols that rely on scalable, low-footprint process conditions as well as environmentally benign chemicals is therefore a timely and significant goal. In the following sections, the most relevant and recent DODH protocols relying on either abundant metals or low footprint process discussions will be addressed.

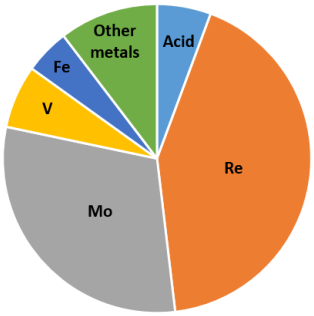

Figure 2.5 Popularity of catalytic systems (metal-based or metal-free) from the primary literature for the DODH on bio-based vicinal polyols (data from [15]).

For developing efficient DODH processes compatible with a potential industrial scale, it is mandatory to rely on readily available and inexpensive metal-based catalysts such as oxo-molybdenum and oxo-vanadium compounds.[77] In addition, efficient recyclability and low long-term toxicity are key requirements for current and future catalyst candidates. While molybdenum fulfils the health imperative,[78] vanadium exposure to high concentration level and repeated times is recognized for its toxicity toward humans.[79] Nevertheless, the use of V over Mo has several advantages: (a) V is more abundant and (b) V has less volatile market values.[76] Conventional metal-based DODH processes are also limited by the use of toxic petro-based solvents and sacrificial additives, which prevents a large-scale development. More sustainable solutions have already emerged that rely on the use of bio-based polyols both as substrates and sacrificial reductants, however, this drastically reduces the yield

toward the corresponding olefins and co-generates a significant amount of waste products.[72] In this section, we have collected some representative examples of metal-based DODH protocols on C_2<C<C_6 bio-based platforms relying on non-toxic and abundant metals, as well on metal-free alternatives. The next section also gathers some examples of metallic hydrogenolysis protocols in gaseous phase applied to **GL**. Yet not strictly related to the DODH reaction in terms of mechanism, the distribution of products is comparable and typically leads to olefins as major product, hence justifying their presence at the end of this section.

2.4.1.2.1 METAL-BASED DODH PROTOCOLS

Molybdenum. In 2014, Fristrup and co-workers developed several Mo-based DODH protocols on several vicinal bio-based diols. A preliminary screening of potential Mo candidate catalysts gave similar yields ranging from 37 to 43% for the DODH of decane-1,2-diol (used both as substrate and sacrificial reductant) toward 1-tetradecene in dodecane. Interestingly, cheap and widely available ammonium heptamolybdate [$(NH_4)_6Mo_7O_{24}$, (AHM)] gave satisfactory results with 43% yield and was therefore selected for further reactions. The authors also attempted a tentative DODH of **GL** under continuous distillation for the preparation of allyl alcohol **3** (Scheme 2.3). **GL** was used both as substrate and sacrificial reductant, under neat conditions and in the absence of any other additive. Noteworthy, the theoretical yield toward allyl alcohol **3** is limited to 50% because of the ambivalent role of the substrate. Large amounts of side products were observed with the formation of (a) acrolein **7** derived from the competitive dehydration of **GL**; (b) formaldehyde **19** from the deformylation of **GL** and (c) various acetals from the condensation of **19** with **GL**. The competitive conversion of the substrate in several acetal intermediates accounted for the modest yield of 9% toward **3**. The authors attempted a modification of the protocol to limit the competitive formation of acetal: 3% NaOH was added to the reaction medium, yet it did not improve the yield toward **3**. Instead, glycidol **4** was formed in 29% yield in the presence of NaOH, hence highlighting a potential strong competition between glycerol DODH (toward allyl alcohol **3**) and dehydration (toward glycidol **4**). Another alternative relied on a significant dilution of the reaction medium with a high boiling solvent, although this irremediably impacted the overall footprint of the process. The poor solubility of **GL** in most organic solvent was quite restrictive, and hydrophilic 1,5-pentanediol was eventually selected. The DODH under these conditions led to a significant enhancement of the selectivity and yield toward **3** with 40% yield, despite a low conversion.[80]

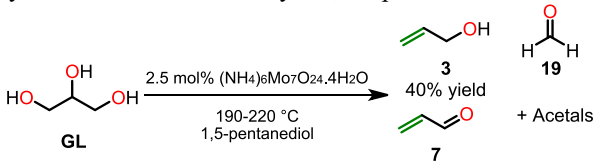

Scheme 2.3 The DODH of glycerol catalyzed by ammonium heptamolybdate (AHM) using 1,5-pentanediol without external reductant under reactive distillation, yielding allyl alcohol **3** in 40%.[80]

One year later, the same group reported an updated DODH protocol based on isopropyl alcohol (^{i}PrOH) serving as a green sacrificial reductant and as a solvent in the presence of ammonium heptamolybdate as a catalyst (Scheme 2.4). The use of ^{i}PrOH as a more oxidizable sacrificial reductant than the bio-based vicinal polyol substrate helped preventing

the competitive oxidation of **GL**, hence, enhancing the overall yield toward the corresponding DODH product. In contrast to previous studies, the addition of Bu_4NOH as a base had a positive impact on the production of the olefin product with an increase from 46% to 77% for the DODH of hexan-1,2-diol (toward 1-hexene). The optimized conditions were next applied to **GL**; the conversion was complete, but only a very modest yield toward allyl alcohol **3** (4%) was achieved, along with 19% of propene (**10**) and traces of 1,5-hexadiene. The latter was formed most likely through a reductive homocoupling of olefin **3** under the process conditions (18 h, 250 °C, 5 mol% cat. and 15 mol% of base). Next, the DODH reaction was transposed to a more complex polyol, namely, **ERY**, giving 39% of 2,5-dihydrofuran (**13**), whereas in this case, the addition of Bu_4NOH was detrimental to the formation of **13** (27% yield) arguably because of a preliminary partial substrate dehydration toward anhydroerythritol **14**. Surprisingly, DODH of **14** in presence of 15 mol% Bu_4NOH yielded 79% of **13**.[72]

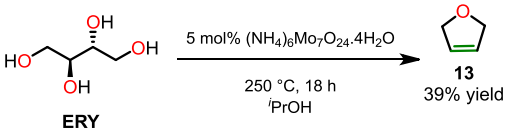

Scheme 2.4 DODH protocol based on *meso*-erythritol and AHM using a large excess of isopropyl alcohol as solvent and internal reductant.[72]

De Vos and Stalpeart studied the effect on several β-diketones ligands on Mo-based DODH (Scheme 2.5).[81] From a preliminary screening of conditions and potential catalysts, species with high electron-donating strength and large steric effect were identified as the most efficient ligands for MoO_2acac_2 as a catalyst (acac=acetylacetonate). Using 1,2-hexanediol as model DODH substrate, up to 36% yield in alkene was reached using ligand 2,2,6,6-tetramethyl-3,5-heptanedione (**20**). A similar experiment in the absence of TMHD **20** led to a lower catalyst activity, as well as the precipitation of oligomeric Mo species. The authors claimed that the formation of polymeric molybdate species was related to the absence of the bulky diketonate ligands. Implementing 4 equivalents of TMHD (2h, 200 °C), the yield jumped up to 93% yield toward 1-hexene with a TOF=4.7 h^{-1}. A large TMDH content was required to prevent the coordination of Mo with a diol scaffold, owing to the high affinity of Mo for the substrate, as well as to counterbalance the bidentate coordination of diolate compared to monodentate THMD. Under the same conditions, using widely available ammonium heptamolybdate as the Mo precursor in presence of THMD greatly improved the yield toward 1-hexene, from 12 to 80%. After optimization, the conditions were assessed on various diol substrates, among which bio-based **ERY** offered 3 and 15% yield toward buta-1,3-diene (**2**) and 2,5-dihydrofuran (**13**), respectively.

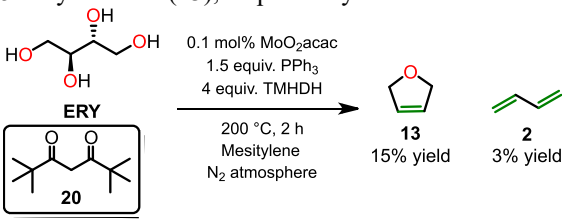

Scheme 2.5 Mo-derived catalytic system involving β-diketones ligands aiming at DODH of **ERY** with triphenylphosphine as a reductant.[81]

In 2017, Palkovits and co-workers proposed a TiO_2 supported Mo-based catalyst for the DODH of bio-based anhydroerythritol **14** with 3-octanol as the sacrificial reductant (Scheme 2.6).[82] Early work dealt with the screening of available molybdenum salts and emphasized the higher activity of $(NH_4)_6Mo_7O_{24}.4H_2O$ with 38% of 2,5-dihydrofuran (**13**). The formation of acetals from condensation between the substrate and 3-octanone, as well as the formation of octane from the dehydration of 3-octanol were also observed. Next, two different preparations for the Mo precursor were considered: (a) $(NH_4)_6Mo_7O_{24}.4H_2O$ impregnated on a TiO_2 support and (b) another precursor where an additional reduction was added to (a) to obtain $MoOx/TiO_2$ species, corresponding to the lower oxidation state of Mo. Both supported catalysts provided superior conversion and yield toward 2,5-dihydrofuran (**13**) of 48 and 55%, respectively, whereas the reduced catalyst substantially promoted the formation of 1-octene (48% yield), which was attributed to its more acidic nature. A third modality was assessed: it consisted in the simultaneous *in situ* preparation of catalyst $[(NH_4)_6Mo_7O_{24}.4H_2O+TiO_2]$ upon reaction. Such modification led to the best selectivity with 76% yield toward **13**. Recyclability of catalysts showed a gradual decrease of activity with increasing reaction cycles, whereas $MoOx/TiO_2$ displayed a higher stability. In contrast, a progressive drop in the yield of octene was observed due to deactivation of acidic sites, giving similar productivities comparable to the trials with a catalyst generated *in situ* after 5 cycles.

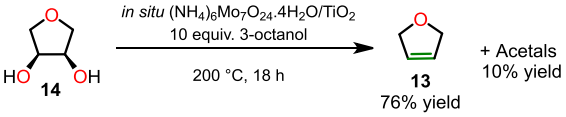

Scheme 2.6 DODH on anhydroerythritol **14** in presence of reducing agent 3-octanol and an *in situ* prepared catalyst (AHM supported on TiO_2).[82]

Okuda and co-workers reported a DODH protocol tailored for 1,4-anhydroerythritol **14** and catalyzed by molybdenum bisphenolate complexes.[83] The reaction time could be drastically reduced to 1 h under microwave irradiations, achieving 49% yield of 2,5-dihydrofuran (**13**) with the most efficient catalyst (5 mol%, Scheme 2.7), at 200 °C with 10 equivalents of 3-octanol.

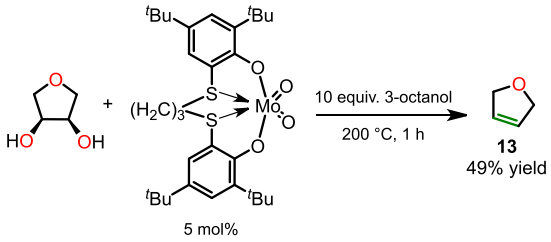

Scheme 2.7 DODH on anhydroerythritol catalyzed by a Mo-based complex featuring a (OSSO)-type bis(phenolate) ligand. [83]

Vanadium. Another widely available transition metal was explored by Fristrup in 2018, namely, Vanadium.[84] The authors developed alternative DODH protocols with vanadium-based catalysts such as NH_4VO_3, $NaVO_3$, V_2O_4, V_2O_5 and $V(acac)_3$, $VO(acac)_2$ with the emphasis on the upgrading of neat **GL** (Scheme 2.8). Among the selection of V catalysts,

ammonium metavanadate (NH_4VO_3) exhibited the highest efficiency and gave 22% yield toward allyl alcohol **3** along with 4% of acrolein **7** and only traces of propanal **31**. The process conditions involved a continuous reactive distillation setup operated at 275 °C for 5 h. Increasing the catalyst loading did not increase the yield toward **3**, whereas a lower catalytic amount was detrimental to the yield. The authors also performed a mechanistic study to identify the competitive routes leading to diverse products that relied on deuterium-labelled **GL**. The results suggested that propanal **21** and acrolein **7** were independently formed from **3**. The authors argued that aldehyde **21** would arise from a preliminary dehydration of **GL** into acetol **22**, subsequently followed with its reduction in 1,2-propanediol (**23**) and eventually leading to propan-1-ol (**24**). Acrolein **7** would arise from two consecutive dehydrations on **GL**.

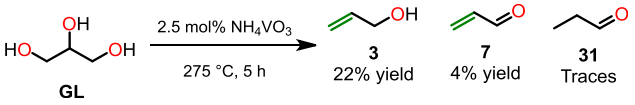

Scheme 2.8 DODH of neat glycerol with ammonium metavanadate.[84]

Niobium. Oliveira and co-workers investigated the DODH reaction with an innovative niobium catalyst and its activity in combination with silicate and silicate doped with vanadium, in the presence of a rather unusual oxidizing agent H_2O_2. Nb-Si-V showed the highest efficiency on crude **GL** followed by Nb-Si and Nb, with 95, 90 and 45% conversion, respectively (Scheme 2.9).[85] The product distribution included acetone (**25**), acetol **22** and allyl alcohol **3**. Depending on the quality of the starting **GL**, a significant impact on the selectivity of the reaction was noted. For instance, olefin **3** from refined **GL** led to approximately 14% yield, whereas it only reached a mere 4% yield with crude **GL**. Besides allyl alcohol **3**, hydroxyacetone **22** and acetone **25** were formed in 6 and 5% yield, respectively, starting from unrefined **GL**, whereas purified **GL** led only to 8 and 9% yield, respectively.

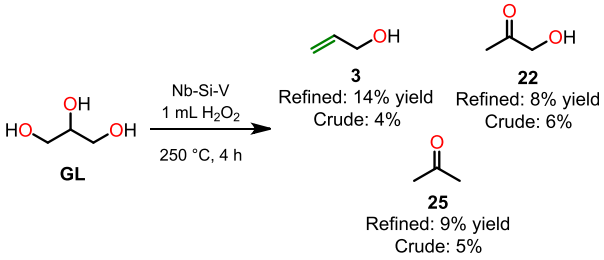

Scheme 2.9 Synthesis of allyl alcohol **3** involving either refined or crude glycerol, a niobium catalyst combined with Si and V and H_2O_2 as unusual reducer.[85]

2.4.1.2.2 METAL-FREE DODH PROTOCOLS

By contrast to metal-based DODH reactions, metal-free DODH protocols potentially offer a great opportunity for developing 100% bio-based protocols with lower environmental impacts. The most promising metal-free DODH protocols were developed with formic acid **26**, which can be manufactured from biomass or CO_2, and later with combinations of **26** and triethyl orthoformate **27**.[86]

Formic acid. Although the seminal work by Ellman and co-workers falls just out the timeframe of this Review, it pioneered an alternative metal-free DODH protocol relying on formic acid **26** on a range of vicinal diols including bio-based vicinal polyols.[70] Starting from neat **GL** and **26** as both reactant and solvent under continuous distillation, the DODH reaction proceeded very well with 80% yield after purification. The issue of substrate charring caused by air oxidation was simply alleviated under a continuous stream of nitrogen. Continuous distillation of the DODH product enabled to work at high temperature without the decomposition of allyl alcohol **3**. Mechanistic insights were collected through the application of the formic acid-assisted DODH of deuterated **GL**. The authors suggested that the reaction proceeded through the formation of 4-(hydroxymethyl)-1,3-dioxolan-2-yl)oxonium (**28**), an orthoester intermediate, which next led to a transient cyclic carbocation species that is subsequently captured with formic acid to form a 2-acyloxy-1,3-dioxolane intermediate **29**. In the last stage of the process, intermediate **29** undergoes a thermal extrusion of CO_2 (Scheme 2.10) to give allyl alcohol **3**, with a small amount of the corresponding formate **30**. They also highlighted the fact that this reaction required a vicinal diol with a *cis* relative configuration to operate. The formic acid DODH protocol was then extended to other bio-based polyols such as *meso*-**ERY** for assessing its scope. In presence of large excess of **26**, 2,5-dihydrofuran (**13**) was produced with 39% isolated yield along with water and unreacted **26** at 210-220 °C.

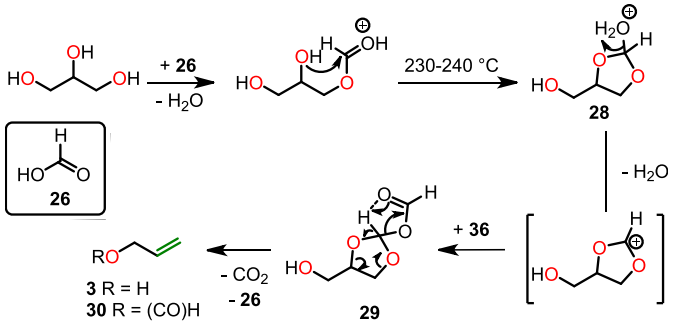

Scheme 2.10 Reaction mechanism of the formic acid-mediated DODH of **GL** toward allyl alcohol **3**.[70]

In 2015, Zhang and Li prepared acrylic acid **8** according to a two steps process that relied on a preliminary DODH reaction : (a) the preparation of intermediate allyl alcohol **3** was carried out through a formic acid-mediated DODH of **GL** and (b) a subsequent oxidation of **3** toward acrylic acid **8** (Scheme 2.11).[55] The process was operated under continuous distillation conditions with a constant supply in neat **GL** and formic acid **26**, in a 1:1.8 molar ratio. Over approximatively 2 h of distillation at 235 °C, 99% yield toward **3** was achieved, along with the collection of water and unreacted formic acid.

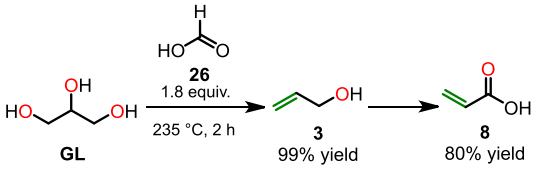

Scheme 2.11 Formic acid-assisted DODH on **GL** to allyl alcohol **3** and its subsequent oxidation to form acrylic acid **8**.[55]

A few years later, Zhang and co-workers reported the first formic acid-assisted DODH of **XY**, yielding (*E*)-2,4-pentadien-1-yl formate (**31**), which was then deoxygenated to give 1,3-pentadiene (**32**; Scheme 2.12).[87] The process was also implemented through reactive distillation using a continuous-stirred tank reactor. 1,4-Anhydroxylitol **14** was identified as the main side product due to the competition between the dehydration of **XY** and the desired DODH reaction. To limit the extent of the competitive dehydration, the addition of a solvent was envisioned to decrease the concentration of **XY**. The combined effect of dilution with tetraglyme and co-feeding the reactor with a 12:1 formic acid (**26**)/**XY** molar ratio (4.4 mL min^{-1}) gave 63% yield toward (E)-2,4-pentadien-1-yl formate (**31**) and 8% of by-product (E)-2,4-pentadien-1-ol (**33**).

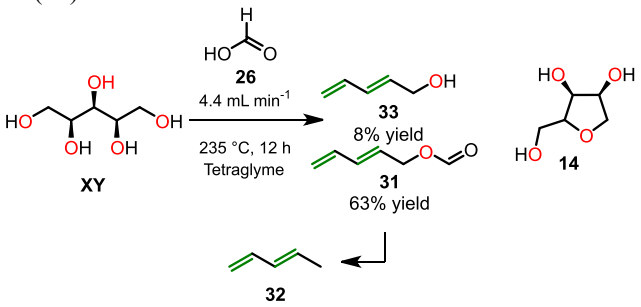

Scheme 2.12 Formic acid mediated deoxydehydration of xylitol gave 8% of (*E*)-2,4-pentadien-1-ol (**33**) and of 63% of (*E*)-2,4-pentadien-1-yl formate (**31**) used as intermediate toward the synthesis of 1,3-pentadiene (**32**).[87]

In 2017, Monbaliu and co-workers developed a continuous-flow metal-free DODH process toward allyl alcohol **3** using the synergistic combination of triethyl orthoformate **27** and formic acid **26**. Orthoformate **27** was used in stoichiometric amounts while **26** was used as a catalyst (Scheme 2.13).[24] The continuous-flow protocol, inspired by the so-called Eastwood Olefination,[88] took advantage of the installation of a dynamic covalent exchange involving **GL** and **27** to form hybrid orthoester species (as a 9:1 mixture of 2-ethoxy-1,3-dioxolan-4-yl)methanol (**34**) and 2-ethoxy-1,3-dioxan-5-ol (**35**)) with the concomitant release of ethanol, which significantly reduced the viscosity of the feed solution. The formation of such hybrid orthoesters was also critical for enabling the DODH reaction under high temperature, hence providing an original solution for the handling of highly viscous bio-based polyols without supplemental additives or solvents. The presence of an acid catalyst such as acetic acid **11** or formic acid **26** drastically improved the production of olefin **3**. Decreasing the catalyst loading below 10 mol% negatively impacted the reaction with lower yields. In-line IR monitoring conveniently offered the possibility to monitor reaction and process steadiness over time conversion. The process temperature was a very critical parameter with a profound impact on the reaction outcome: barely detectable DODH products were detected below 200 °C, whereas a cumulated yield of 86% was obtained at 250 °C with a 6 min residence time in the flow reactor. The reactor effluent was typically composed of 84: 2 ratio of allyl alcohol **3** and allyl formate (**30**). Continuous production was maintained during 12 h without noticeable alterations.

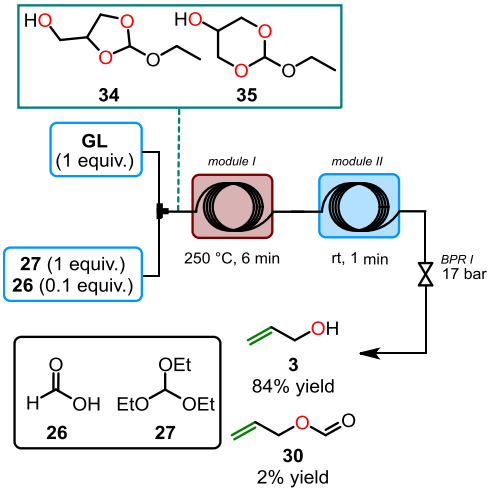

Scheme 2.13 Continuous flow setup for the triethyl orthoformate-mediated DODH of glycerol yielding 84% of allyl alcohol **3** and 2% of allyl formate **30**.[24]

In 2018, the same group further extended their DODH protocol under continuous-flow conditions for the upgrading of **ERY**.[89] The process conditions were adapted for effecting either a mono-DODH or a bis-DODH, hence producing with a high selectivity 3-butene-1,2-diol (**36**) or butadiene **2**, respectively (Scheme 2.14). 3-Butene-1,2-diol (**36**) was further upgraded to vinyl ethylene carbonate **37** through an additional carbonation reaction using dimethyl carbonate **38**. Owing to the physical state of **ERY**, solvents of high polarity were selected, namely, dimethyl sulfoxide (DMSO) and 1-ethyl-3-methylimidazolium ethyl sulfate [EMIM][ES]. Depending on several parameters including the equivalents of triethyl orthoformate **27**, the nature of the solvent and the process temperature, the distribution of products could be tuned to orient the process either to a mono-DODH (toward olefins, among which 3-butene-1,2-diol (**36**) emerged as the main product) or to a bis-DODH (toward butadiene **2**). For instance, the DODH under continuous-flow conditions on **ERY** in DMSO with 1 equivalent of **27** achieved the best yield toward 3-butene-1,2-diol (**36**) in the 250-275 °C range within only 1 min of residence time. With 2 equivalents of **27**, butadiene **2** was favored. In contrast, the process conditions using ionic liquid [EMIM][ES] led to a drastically different profile for the reactor effluent: anhydroerythritol **14** was obtained through cyclodehydration, which next gave 2,5-dihydrofuran (**13**) and but-2-enal (**39**) following up the DODH extrusion. Upon optimization of the DODH step, the authors then further upgraded 3-butene-1,2-diol (**36**) through an additional carbonation step. Neat olefin **36** was reacted with dimethyl carbonate **38** in the presence of a homogeneous organocatalyst (DBU, 2 mol%); the temperature appeared as a critical leverage, with 70% conversion at 160 °C. The addition of DMSO as a solvent, to enable the direct concatenation with the preliminary DODH step enhanced the conversion up to 95% without affecting the selectivity. Under optimized conditions and full concatenation, the authors also assessed a heterogeneous version of catalyst that offered 79% conversion and 97% selectivity toward vinyl ethylene carbonate **37** (WHSV=11.89 h^{-1}) with an excess of **38** (3 equiv.). The stability of the process was maintained over 10 h with conversion ranging from 65 to 73%, before a significant decrease to 28% after 24 h due to basic site deactivation of the catalyst.

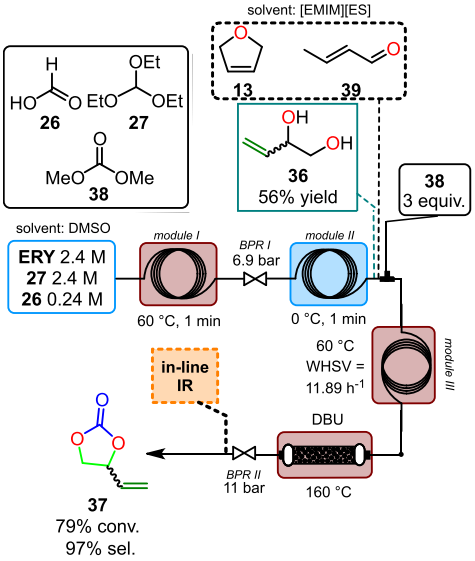

Scheme 2.14 Continuous-flow DODH of *meso*-erythritol with triethyl orthoformate catalyzed by formic acid to generate 3-butene-1,2-diol (**36**). Subsequent carbonation with dimethyl carbonate produces vinyl ethylene carbonate **37**.[89]

2.4.1.2.3 OTHER PROTOCOLS FOR THE PREPARATION OF OLEFINS FROM BIO-BASED POLYOLS

Although not related to the DODH reaction in terms of mechanism, various metallic hydrogenolysis protocols in gaseous phase have been reported on **GL** that led to similar distribution of products with typically allyl alcohol **3** as a major component of the reactor effluent.

Zirconia. Among early reports on the hydrogenolysis of **GL** toward allyl alcohol **3**, Masuda and co-workers studied the catalytic alkali metal-supported ZrO_2-FeO_x as a potent catalyst (Scheme 2.15).[90] The catalyst was used as a packing material for a packed-bed reactor for the conversion of **GL** in the gas phase. This reaction led to a variety of products in the reactor effluent: acrolein **7**, ethanal **40** as well as hydroxyacetone **22**, which then yielded carboxylic acids (such as propanoic acid **41** and acetic acid **11**) and ketones or consecutive transformation toward allyl alcohol **3** and propene **10** through a hydrogen transfer mechanism. Various alkali metals (Na, K, Rb, and Cs) supported on ZrO_2-FeO_x were investigated, all giving almost complete conversion and a higher selectivity toward **3**. The addition of potassium offered the greatest selectivity toward **3** over 6 h, before a significant decrease in performance due to catalyst deactivation by cooking. These results were explained by the large decrease of catalyst acidic site density, hence drastically reducing the preliminary dehydration of **GL**. Optimized K content in the range of 3-5 mol% achieved 27% yield toward allyl alcohol **3** [W/F=1 h; W=amount of catalyst (g), F=flow rate of feedstock (g h^{-1})] and caused a decrease of the selectivity toward other by-products. Compared to ZrO_2 -FeO_x, a significant reduction was observed both for the yields toward carboxylic acids from 21% to 7% and ketones from 9% to 5%. According to the authors, the hydrogen transfer

mechanism more likely arose from the decomposition of formic acid **26**, initially formed through the oxidation of acetol **22**, the main production arising from the dehydration of **GL**.

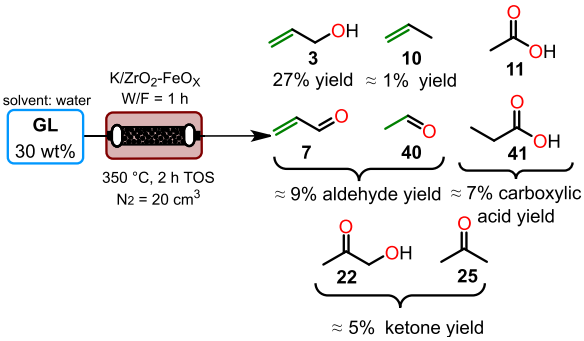

Scheme 2.15 Metallic hydrogenolysis of glycerol using a packed bed reactor with K/ZrO_2-FeO_X catalyst.[90]

The same year, Masuda and co-workers also reported a protocol for the hydrogenolysis of crude **GL** in the presence of formic acid as a H-donor catalyzed by ZrO_2-FeO_x. Taken alone, FeO_x catalysts offered a higher toward allyl alcohol **3** yield of approximately 18%, whereas the addition of ZrO_2 favored the emergence of products derived from the dehydration of **GL** (10 wt% glycerol, (W/F=5 h, 2 h). Interestingly, with 7 wt% ZrO_2, the reaction reached the highest conversion, whereas the catalyst with 27 wt% ZrO_2 gave 24% yield of propene **10**.[91]

Alumina. Stockenhuber and co-workers described protocols for the preparation of allyl alcohol **3** from **GL** based on iron catalyst supported on alumina modified with several alkali metals (Na, K, Li, Rb and Cs).[92] Assessment of the catalyst and modes of preparation indicated that catalytic material treated by washing gave the highest selectivity compared to impregnation and ion exchange, most likely due to a higher content of the active species Fe retained on the catalyst. Alkali metal addition enabled to increase the selectivity toward **3** compared to an unmodified catalyst with 4% yield (γ-alumina/Fe) and 8 to 12% (γ-alumina/Fe/alkali metal), respectively (90% conversion). Reduced catalyst deactivation was noticed compared to unmodified catalyst with 10% conversion loss instead of 20% over an extended time on stream (Scheme 2.16). The catalyst was partially regenerated but a 10% drop in conversion was observed.

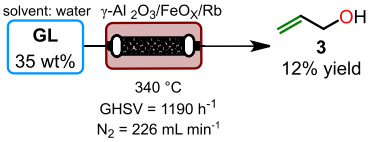

Scheme 2.16 The heterogeneous hydrogenolysis of glycerol performed at 340 °C gave 12% of allyl alcohol **3** with a γ-$Al_2O_3/FeO_X/Rb$ catalyst.[92]

In the continuity of the previous article, Stockenhuber next studied the effect of organic acids, ammonia and ammonium hydroxide as sacrificial reductants for the conversion of **GL** over γ-alumina/Fe (Scheme 2.17).[93] The presence and nature of a reducing agent was found critical to favor the formation of allyl alcohol **3** with high selectivity. Under continuous conditions, the absence of an additive led to a low yield of **3**, whereas acetol **22** emerged as

a main product. The addition of oxalic acid in a molar ratio of 0.14 to **GL** yielded **3** and aldehyde **32**, in 17.5% and 5% yield, respectively. Moreover, using a **GL**/**26** molar ratio of 0.14 neither significantly improved the reaction outcome nor decreased the selectivity toward **22**. In contrast, a higher ratio (1.9:1 26/**GL**) gave up to 19.5% yield (340 °C, 35 wt% glycerol, GHSV=1190 h^{-1}). These results were attributed to the slower decomposition of formic acid **26** compared to oxalic acid, as well as to the fact that **26** had a larger tendency to form side products. Other cheap and readily available reactants such as ammonia and ammonium hydroxide displayed similar trend that **26** and oxalic acid with 11.3 and 15.1% yield, respectively, toward allyl alcohol **3** with molar ratio of 0.14 (NH_3) and 0.75 (NH_4OH) to **GL**. To further gather insights on the reaction or mechanism, the influence of propanoic acid **41** and acetic acid **11** was also studied, yet no conclusive results were collected.

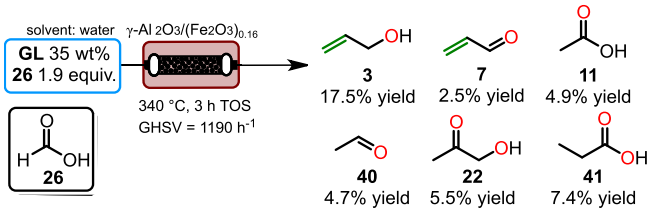

Scheme 2.17 The heterogeneous hydrogenolysis of glycerol in a vertical fixed bed reactor using γ-Al_2O_3/$(Fe_2O_3)_{0.16}$ and formic acid **26** gave 19.5% of allyl alcohol **3**.[93]

Valentini and co-workers reported the conversion of **GL** by MoAl catalyst with Cu, Ni and Co transition metals promoters.[94] In contrast to individually assessed alumina, all Mo modified catalysts exhibited good activity (ca. 75-95%) before dropping below 40% over a longer time on stream (5 h). This difference of conversion was explained by the lower number of acid sites of single γ-Al_2O_3 compared to MoAl samples, whereas their fast deactivation was caused by carbon depositions on these strong acid sites. Interestingly, Cu impregnated MoAl gave the higher conversion with 97% at 30 min of time on stream (Scheme 2.18). Given its similar acidic properties with MoAl, its superior efficiency arose from Cu and its interaction with Mo various species which enabled a higher concentration of actives sites involved in redox reactions. These results also proved that MoAl interacted differently with the several promoters. Together with NiMoAl, CuMoAl had the most elevated selectivity toward allyl alcohol **3** close to 15% and both exhibited lower selectivities toward acrolein **7** and hydroxyacetone **22**. Since several mechanisms toward olefin **3** can theoretically coexist, both **7** and **22** could be involved in the formation of **3**. Interestingly, over the first 30 min of reaction catalyzed by CuMoAl, propanol **24** was detected, the formation of which arises through the direct hydrogenation of allyl alcohol **3**.

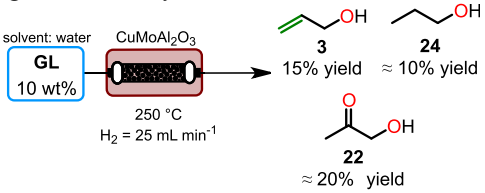

Scheme 2.18 Metallic hydrogenolysis of glycerol in a packed bed reactor with a $MoAl_2O_3$ catalyst modified with Cu at 250 °C.[94]

Zeolites. Similarly to the process reported with γ-Alumina/Fe/Rb, Stockenhuber and co-workers developed a protocol relying on an innovative zeolite (Si/Al=30) supported iron catalyst modified with rubidium deposits (ZSM-5/Fe/Rb) for the conversion of **GL** toward allyl alcohol **3**.[95] ZSM-5/Fe catalyst with the higher iron loading (13 wt%) offered complete conversion and a superior selectivity toward **3**. Modification with rubidium enabled to increase from 3% to 12% yield toward olefin **3**.

Likozar and co-workers reported another protocol for the preparation of **3** that relied on bifunctional zeolites supported FeMo and FeMoCs catalysts (Scheme 2.19).[96] A stability study over extended operation time on stream underlined a quick deactivation for the bimetallic catalysts. 2.5$Cs_{2.5}Fe_{2.5}$Mo-ZSM-5(30) and 5$Cs_{2.5}Fe_{2.5}$Mo-ZSM-5(1500) were associated with a superior activity with a conversion of 98 and 79%, respectively, after 56 h of operation. A modification with cesium was attempted to decrease the Brønsted acidity of 2.5$Cs_{2.5}Fe_{2.5}$Mo-ZSM-5(30), although it exhibited a very low selectivity toward olefin **3** due to its extended Lewis acidity inherent to low SiO_2/Al ratio of 30. Thus, this former led to very high selectivities toward acrolein **7** (ca. 45%) and acetol **22** (ca. 30%), yet the amount of allyl alcohol **3** remained low (ca. 10%). Therefore, a zeolite of higher basicity (SiO_2/Al=1500) was selected and further studied to gather information on the influence of different cesium loading. With 10 wt%, a selectivity of 52% toward **3** was obtained, although a fast drop in the conversion of **GL** occurred within 7 h. The most stable yield was achieved by 5$Cs_{2.5}Fe_{2.5}$Mo-ZSM-5(1500) and gave 45% of allyl alcohol **3**, along with around 10% of aldehyde **7** and around 20% of hydroxyacetone **22** over 26 h over operation.

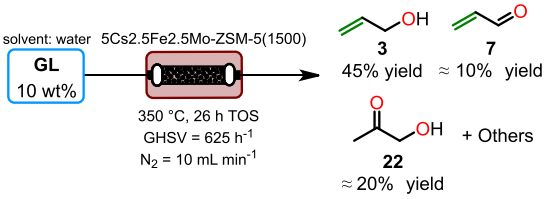

Scheme 2.19 The heterogeneous hydrogenolysis of glycerol in a fixed bed reactor catalyzed by FeMo-ZSM-5(1500) impregnated with 5 wt% of cesium.[96]

Lourenço and co-workers reported a process for the conversion of **GL** catalyzed by beta zeolite (BEA) supported V_2O_5 (Si/Al=25, 4% V) modified with cesium, in the absence of reducing additive.[97] Surprisingly, a similar trend of catalyst deactivation was observed over the first hours of operation for the 3 different samples (individual BEA, V/BEA and V/BEA/Cs). This phenomenon suggested that the dehydration rate was neither influenced by acidic site strength nor their surface density. Reaction with BEA catalyst gave a higher selectivity toward acrolein **7** (ca. 40%)>acetol **22** (ca. 30%)>acetaldehyde **40** (ca. 15%)> allyl alcohol **3** (only 2%), respectively, which matched with the well-known zeolite acidic properties, promoting the dehydration of **GL**. Modification with vanadium slightly increased the selectivity toward olefin **3** to 7%, whereas the selectivity toward aldehyde **7** increased even more (up to ca. 60% over 24 h, 320 °C, 30 mL min^{-1} N_2). To decrease the formation of **7**, an exchange of V/BEA with Cs ions was performed to reduce the acidic site density, resulting in an increase of the selectivity toward olefin **3** up to 30% while reducing the selectivity toward acrolein **7** to around 50% over 24 h of time on stream.

Silica. Jiang and co-workers developed another bimetallic catalyst based on molybdenum and iron supported on KIT-6 silica.[98] Preliminary tests were performed on single Fe, Mo and combined FeMo catalysts. Aside from the lower conversion obtained with Fe-KIT-6, similar excellent conversions (99%) of **GL** were found for the two other samples. MoFe-KIT-6 showed the highest selectivity toward ally alcohol **3** with 19% against 17% for individual metallic catalyst. Increasing the metallic loading to 0.3 led to a slightly lower conversion (94%), yet it increased the selectivity to 29% (TOS=2 h, 35 wt% aqueous solution of **GL** at 340 °C). The highest efficiency of MoFe-0.30/KIT-6 was attributed to its moderate acidic properties as well as its moderate to low reducing properties, by opposition to Fe-KIT-6.

Jiang and co-workers pursued their work on MoFe-KIT-6 catalysts by impregnation with V, Ti, and Nb (Scheme 2.20).[99] V- and Nb-modified catalysts gave higher conversion with 96% and 92%, respectively while the vanadium-based sample achieved the best selectivity toward all products with 34% for allyl alcohol **3** (Nb 18%), 17% for acrolein **7** (Nb 10%) and 14% for acetaldehyde **40** (Nb 8%; TOS=2 h). MoFe-Ti/KIT-6 gave lower conversion and selectivities, except for **40** with 20%. In comparison with results of MoFe/KIT-6, only V-based catalysts had a higher efficiency, highlighting MoFe as the active species. The authors claimed that such a higher activity was correlated to the interaction between V and MoFe oxides, the modulation of acidic properties and a well-developed and ordered mesoporous structure of catalyst. Lower conversion with MoFe-Ti/KIT-6 were linked to its poor specific surface, suggesting that it favored C-C cleavage of acetol **22** unstable intermediates (toward propanal **21** and acetone **25**) and **GL**. Whereas MoFe-Nb/KIT-6 gave a lower selectivity toward allyl alcohol **3**, most likely caused by the superior acidity of Nb_2O_5, hence promoting products derived from the dehydration of **GL**. Compared to MoFe/KIT-6, a V modified catalyst ensured both a better stability and a steady conversion at 85% during 8 h, before dropping to 70% (20% selectivity) after 24 h. Regeneration of the catalysts proved to be rather inconclusive due to a gradual decrease of activity with cycles.

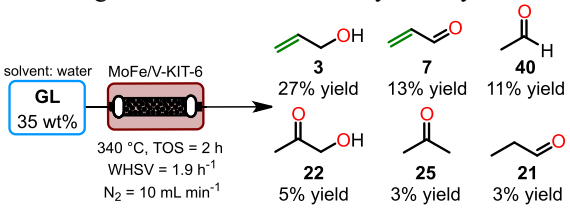

Scheme 2.20 The heterogeneous hydrogenolysis of glycerol in a packed bed reactor using MoFe/KIT-6 modified with vanadium achieved 29% of allyl alcohol **3**.[99]

ZIF (2-methylimidazole). In 2020, Hou and co-workers reported a continuous process relying on H_2 as reducing agent, catalyzed with a CoFe alloy supported on 2-methylimidazole (CoFe-ZIF; Scheme 2.21).[100] The bimetallic catalyst showed a synergistic effect between Fe (enhancing surface acidity) and Co (offering a higher ability for H_2 activation and adsorption), hence promoting the dehydration of **GL** and its consecutive hydrogenation to yield allyl alcohol **3**. Increasing the process temperature up to 250 °C favored the selectivity toward **3** at the expense of acetol **22**. By contrast, exceeding 250 °C strongly promoted the formation of side product propanol **24**. The selectivity toward olefin **3** was also positively influenced by the concentration in H_2 concentration: higher H_2/**GL** ratio leading to superior

conversion and drastically decreasing the formation of **22** from 54% to 9%. Nevertheless, the selectivities toward propanol **24** and 1,2-propanediol (**33**) also increased accordingly. A low H_2 pressure up to 20 bar was also beneficial to allyl alcohol **3**, whereas higher pressure promoted its further hydrogenation. Under optimized conditions, the process achieved 62% yield (conv. 90% sel. 69%) of **3** with TOF=48.7 h^{-1}, at 250 °C and 20 bar with H_2/**GL** ratio of 40.

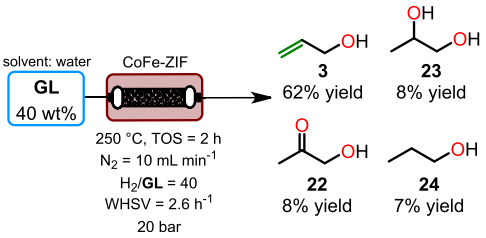

Scheme 2.21 The heterogeneous hydrogenolysis on glycerol catalysed by CoFe alloy supported on ZIF with H_2 as reducing agent reached 62% yield of olefin **3**.[100]

2.4.2 EPOXIDES FROM BIO-BASED POLYOLS: CARBOXYLATION AND CONSECUTIVE WILLIAMSON'S EPOXIDATION OR DEHYDRATIVE EPOXIDATION

2.4.2.1 OXIRANES AS HIGH ADDED VALUE BUILDING BLOCKS

Ethylene oxide **42** is the simplest cyclic ether characterized by an exceptional reactivity due to the high strain of its 3-membered ring.[101] It stands as one of the most important bulk chemicals with a global production of 31 Mt in 2018 with a predicted annual growth rate of 3-4%.[52,102] It is expected to reach a market volume of 58 billion US$ by the end of 2023.[103] Currently, 72% of the production of **42** is dedicated to the preparation of glycols, with an annual volume of 26 Mt, as well as a non-negligible part going to the preparation of ethoxylates as surfactants. Glycols have applications deeply rooted in the polymer sector with polyester fiber, poly(ethylene succinate), polyethylene terephthalate or polyurethanes manufacturing. Ethylene oxide **42** is commonly produced from the oxidation of ethylene **1** in the presence of a silver catalyst and oxygen (Scheme 2.22a).[52] There is still an intense research effort dedicated to finding new applications for further increase the scope of **42**, hence justifying the development of more sustainable processes for its preparation. An emerging more sustainable approach relies on the epoxidation of the simplest bio-based vicinal diol, namely, **EG**.

Glycidol **4** is a key monomer for the polymer industry due its high ambivalent reactivity correlated to its strained ring and its terminal hydroxy group. Among its primary applications, the production of branched polyglycidols is predominant.[104] In addition, **4** can also lead to the formation of new generation of monoalkyl glyceryl ethers with numerous applications in the fields of coatings, lubricants and high boiling solvents.[105] Oxirane **4** is also involved in the preparation of high value-added pharmaceuticals due to its inherent reactivity and was utilized as a key building block for the preparation of analgesics and human immunodeficiency virus (HIV).[59,106,107] The current market value of glycidol **4** is very high (20 US$ per kg).[59] Its main industrial road still relies on fossil resources through epoxidation

of allyl alcohol **3** with hydrogen peroxide over tungsten derived catalysts (Scheme 2.22b). This pathway displays several drawbacks: (a) it involves multiple steps, (b) the catalyst undergoes decomposition (c) and the process comes with an overall low yield. Nevertheless, recent advances were achieved with development of new supported catalysts such as Ti silicate or Ti-MCM-41.[108] Greener commercial alternative exists with the Epicerol (Solvay) or GTE (Dow) processes that feed upon **GL** for the preparation of glycidol **4**. Typically, both processes imply a preliminary chlorination step on **GL**, followed with an epoxidation and hydrolysis to **4** using diluted NaOH solution under harsh conditions (Scheme 2.22c).[59] Recently, a chloride-free industrial process was developed by Green Lizard Technologies based on the preparation of glycerol carbonate (**43**) from **GL** and dimethyl carbonate **38**, followed by its subsequent decarboxylation into glycidol **4**. The process, however, cogenerates 1 equivalent of CO_2. Lab scale translation was already successfully implemented while industrial scale up is expected by the end of 2021, with a production capacity of 10 000 t y^{-1} (Scheme 2.22d).[109,110]

These past decades, ethylene oxide **42** and glycidol **4** have been envisioned as highly reactive substrates for the exploitation of carbon dioxide, which was until there, largely impaired by its high thermodynamic stability.[111] From these oxiranes, attractive protocols toward 1,3-dioxolan-2-one (**44**) and glycerol carbonate **43** have been engineered,[112] eventually leading to the development of industrial roads by among others, Huntsman Corporation.[113,114] The next section gathers the most recent and promising protocols for the preparation of epoxides: (a) conventional direct epoxidation protocols applied to vicinal diols, including the intermolecular etherification (Williamson's epoxidation) and the dehydrative epoxidation and (b) indirect epoxidation protocols from cyclic carbonates with extrusion of CO_2.

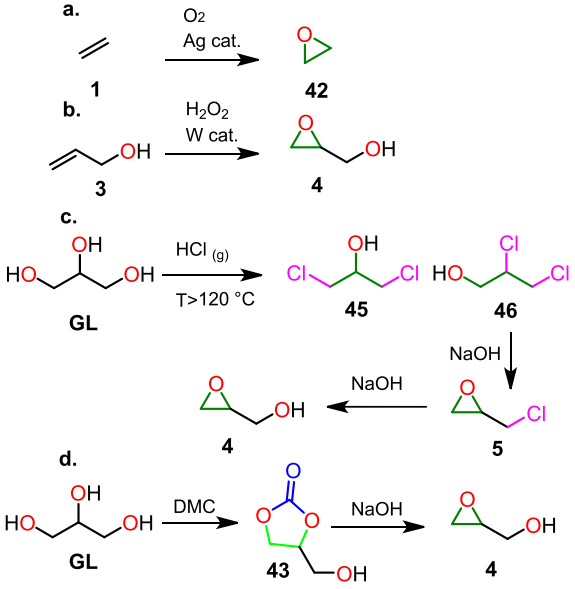

Scheme 2.22 Industrial processes for the preparation of ethylene oxide **42** and glycidol **4**. (a) Synthetic road toward ethylene oxide **42** based on ethylene (**1**) oxidation. (b) Formation of glycidol **4** from the oxidation of allyl alcohol **3**. (c) Glycerol chlorination into dichlorohydrins, Wiliamson's epoxidation and formation of glycidol **4**. (d) Alternative road to oxirane **4** by concomitant carboxylation of glycerol and decarboxylation of glycerol carbonate **43**.

2.4.2.2 DIRECT EPOXIDATION OF VICINAL DIOLS

2.4.2.2.1 INTERMOLECULAR ETHERIFICATION (WILLIAMSON'S EPOXIDATION)

A typical pathway for the conversion of **GL** toward glycidol **4** consists in the intermediate formation of monochlorinated derivatives of **GL** followed with its intramolecular Williamson's epoxidation in the presence of a base. In 2016, Proto and co-workers reported an innovative production of valuables oxiranes through the cyclization of 2-chloro-1,3-propanediol (**45**), a major by-product of the production of epichlorohydrin **5** (see below, Section 2.3).[115] This procedure simply relied on the conversion of **45** in a 1 M KOH solution in ethanol (EtOH) at room temperature for 30 min (Scheme 2.23). The reaction was first carried out on a mixture of 3-chloro-1,2-propanediol (**46**) and **45** (7.5% and 0.6% yield, respectively), previously obtained from the distillation of a reactor effluent from the chlorination of **GL**. The results were very conclusive: 99% yield was reached with 100% selectivity toward glycidol **4**. To assess the robustness and its application for downstream processing epichlorohydrin **5**, the same reaction was also implemented on a pure solution of **45**. For the latter, 90% yield and excellent selectivity were achieved with only water and KCl as by-products while ethanol could be easily recycled by distillation.

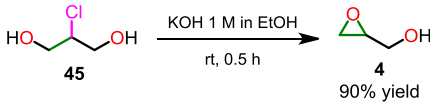

Scheme 2.23 Synthesis of glycidol **4** by the reaction between **45** and KOH in ethanol at room temperature for 30 min.[115]

More Recently, Dydo and co-workers developed an alternative road toward glycidol **4** exploiting a less conventional technology, namely, bipolar membrane electrodialysis.[116] Such technology enabled the *in situ* formation of hydroxy anions from an aqueous solution, which further reacted with **46** to generate the targeted oxirane **4** (Figure 2.6). Interestingly, the co-generated chloride anions could also be removed through anion exchange membrane (AEM). Constant voltages conditions (11 V) offered higher conversion and selectivity in contrast to constant electric current modalities. pH was also identified as critical parameter as a consequence of the high sensitivity of the product to hydrolysis, hence reforming **GL** as a side product. Upon optimization, the membrane-based system achieved afforded 100% conversion and 97% selectivity starting from a 30% aqueous solution of **46**, whereas a downstream purification step by distillation afforded 75.6% yield of glycidol **4**.

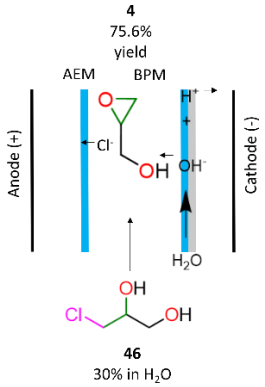

Figure 2.6 Bipolar membrane electrodialysis protocol relying on the reaction of monochlorohydrin **46** as substrate with *in situ* generated hydroxyl anions toward the synthesis of oxirane **4**.[116]

In 2019, Monbaliu and co-workers reported the first liquid-phase continuous-flow process aimed at the hydrochlorination of **GL** and its subsequent dehydrochlorination toward valuable epoxide **4**.[117] Reaction optimization was performed with acetic acid **11** as a model catalyst. Temperature and residence time showed to be critical for triggering the reaction, and the product distribution was very sensitive to both parameters. Upon optimization, 140 °C and 20 min of residence time offered both very good conversion of **GL** (88%) and cumulated yield comprising 73% monochlorohydrins (mostly **46**) and 13% dichlorohydrins (mostly **47**; Scheme 2.24). Further increase of both parameters led to the significant formation of humins and eventually led to reactor clogging. It is worth mentioning that the sealed nature of continuous-flow reactor prevented catalyst loss by evaporation, a very common issue for the process in batch.

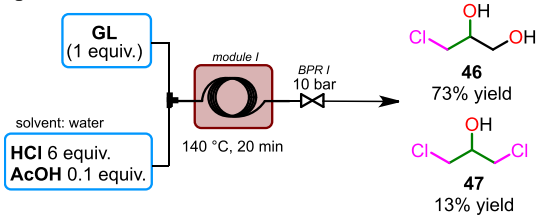

Scheme 2.24 Continuous flow process of glycerol hydrochlorination catalyzed by acetic acid **11** at 140 °C with 10 bar of counter pressure for 20 min gave 73% of **46** and 13% of **47**.[117]

2.4.2.2.2 DEHYDRATIVE EPOXIDATION

Yi and co-workers reported a gas-phase dehydration of vicinal diols from **EG**, 1,2-propanediol (**33**) and 2,3-butanediol into their corresponding epoxides (namely, ethylene oxide **42**, propylene oxide **12** and 2,3-epoxybutane) in a fixed-bed continuous-flow reactor. Using 2,3-butanediol as a model substrate, the authors performed a screening of conditions and catalysts.[118] Alkali metal oxides (Ca, Mg, Cs, Sr, K and Na) supported on SiO_2 were investigated and showed that catalysts modified with cesium displayed the higher activity with 69% selectivity toward dimethyloxirane (66% conversion), in contrast to other candidates (0-39% conversion). The authors explained this superior performance by the stronger basicity of sites generated by cesium impregnation, the lower decrease of catalyst

specific surface and the poorer extent of silicate dissolution around Cs atoms, thus, enhancing its accessibility for the dehydrative oxidation reaction compared to the other candidates. Further increasing the Cs loading was detrimental for catalyst activity, whereas the increase of its calcination temperature from 550 to 700 °C positively affected its performance. The stability of the catalyst was assessed over 30 h of operation and showed a decrease of the specific activity, defined as the formed amount of product (mol h^{-1}) on loaded amount of catalyst (mol), from 59 to 40 h^{-1} before reaching a plateau around 33 h^{-1} after 13 h of reaction. The optimized conditions were next transposed for the dehydrative epoxidation on **EG**, 36% conversion and 38% selectivity were obtained toward ethylene oxide **42** (TOF=8.3 h^{-1}) and 47% selectivity toward side product acetaldehyde **40** (SV=1.38 L min^{-1} g^{-1} total flow rate/amount of catalyst; Scheme 2.25). DFT studies for the reaction mechanism highlighted both the involvement of surface hydroxy groups from SiO_2 and basic sites in transition-state structure.

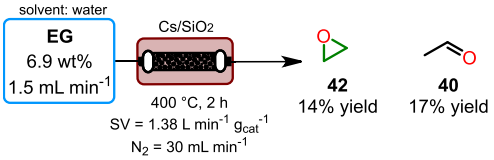

Scheme 2.25. Heterogeneous dehydrative epoxidation of ethylene glycol in a fixed bed continuous reactor using cesium deposits supported on SiO_2 at 400 °C giving 14% of ethylene oxide **42** and 17% of ethanal (**40**).[118]

Likozar and co-workers presented a continuous gas-phase flow process toward glycidol **4** catalyzed by HZSM-5 zeolite (SiO_2/Al=1500) modified with cesium (Scheme 2.26).[59] Three concentrations of alkali metal deposits were investigated to study influence of catalyst basicity on the distribution of products. Results highlighted both superior conversion and selectivity for the selected catalysts, in decreasing order of performance: 20CsZSM-5(1500)>10CsZSM-5(1500)>40CsZSM-5(1500) with 40%, 13%, 5% yield of **4**, respectively (2-3 h TOS). A longer time on stream caused substantial catalyst deactivation by cesium decomposition (reduction) and cooking. It is worth mentioning that the selectivity toward oxirane **4** continued to rise with extended TOS, more likely as a consequence of to the poisoning of non-selective active sites on the catalyst. Thermogravimetric studies provided further insights on this phenomenon, indicating that higher Cs content was correlated to a reduced porosity, hence responsible for a lower resistance to cooking with the 40 wt% Cs catalyst. Cs concentration ≥ 20% enabled to decrease the occurrence of the major side product (hydroxyacetone **22**), most likely in correlation with the increasing basic properties and the absence of measurable Lewis acidity. The authors suggested that the reaction pathway toward glycidol **4** was likely involving a direct dehydration of **GL**.

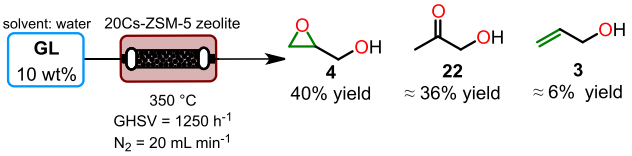

Scheme 2.26 Heterogeneous dehydrative epoxidation of glycerol into glycidol **4** catalyzed a modified ZSM-5 zeolite at 350 °C.[59]

2.4.2.3 Indirect epoxidation through the extrusion of CO_2 from cyclic carbonates

This section summarizes the decarboxylation protocols on cyclic carbonates for the preparation of the corresponding oxiranes. Most of the examples from the primary literature target glycidol **4**, the preparation of which relies on the decarboxylation of glycerol carbonate **43**. Interestingly, most research papers include the *in situ* transformation of **GL** into **43** prior the decarboxylation step.

2.4.2.3.1 Metal-catalyzed CO_2 extrusion from carbonates

Lee and co-workers developed a two-step synthesis starting first with the carbonation of **GL** and then followed with a subsequent decarboxylation of glycerol carbonate **43** toward glycidol **4** (Scheme 2.27).[119] The authors used various zinc catalysts and urea as a carbonatation reagent, in lieu of the more conventional dimethyl carbonate **38**. Under reduced pressure, the catalytic performance of $ZnCl_2$, $ZnSO_4$, $Zn(NO_3)_2$ and $Zn(OAc)_2$ were assessed for one-pot reaction conditions. The general trend disclosed good performance for the preparation of glycerol carbonate **43** with yields superior to 70%; only $Zn(OAc)_2$ achieved a significant conversion to glycidol **4** (20% yield). The Zn catalysts were found to react with **GL** to form insoluble $Zn(C_3H_6O_3)$, which are in turn inefficient for the follow-up decarboxylation to epoxide **4**, as well as ammonium salts. Interestingly, removal of this inactive species enabled to increase the yield toward **4** up to 50%, yet this was limited to the experiments with $Zn(OAc)_2$. $Zn(C_3H_6O_3)$ was preponderant upon completion of the carbonation step, therefore, deactivating the catalyst for the second decarboxylation step. When implementing this reaction with either $Zn(OAc)_2$ or NH_4OAc, the yield toward oxirane **4** did not exceed 24%, far from the preliminary results. Further investigation showed that the carbonation step also generated $Zn(NH_3)_x(OAc)_2$ species, which are more likely responsible for the decarboxylation activity. Using a NH_4AOc/ZnO mixture with a molar ratio of 4 gave the best yield toward **4** (58%; Scheme 2.27).

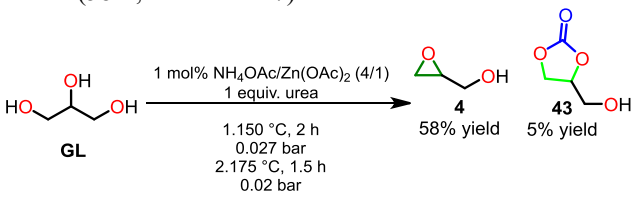

Scheme 2.27 One pot synthesis of glycidol **4** based on glycerol carbonation with urea (150 °C, 2 h) and the subsequent decarboxylation of glycerol carbonate **43** (175 °C, 1.5 h) with a catalytic system composed of 4/1 ratio of $NH_4OAc/Zn(OAc)_2$ under reduced pressure.[119]

Bañares and co-workers studied the preparation of glycidol **4** based on a ZSM-5 zeolite (SiO_2/Al=1500) and a nanoscale cobalt oxide-supported ZnO catalyst (RT-10CoZn).[120] The authors also studied the influence of various thermal devices for the activation of glycerol carbonate **43** under neat conditions. Under atmospheric pressure, both catalysts exhibited the highest performance under microwave activation with a short reaction time (30 min, 150 °C). The same conditions were carried out in an ultrasonic apparatus (60 °C over 7 h) and a conventional heating (150 °C over 23 h) gave lower conversions. With the optimized conditions in hand, RT-10CoZn gave 99% selectivity and 71% conversion toward **4**

compared to ZSM-5, owing to a decrease in its acidic properties arising from its progressive dealumination by microwave irradiations.

2.4.2.3.2 CO_2 EXTRUSION FROM CARBONATES IN IONIC LIQUIDS

In 2012, Kelkar and co-workers investigated ionic liquids (ILs) as efficient catalysts for the conversion of **GL** into oxirane **4** through a two-step process (preliminary carbonation of **GL** followed with a decarboxylation of glycerol carbonate **43** toward **4**; Scheme 2.28a).[121] Early results of one-pot synthesis indicated the extremely low poor activity of halide-derived ILs with only traces of glycerol carbonate **43** and epoxide **4**. In contrast, ILs composed of hydroxide and bicarbonate counter anions achieved conversions and selectivities toward **4** ranging from 77 to 95% and 43 to 67%, respectively. The higher efficiencies of these ILs were attributed to their stronger basicity which favored the decarboxylation of **43** into **4**. As tetramethylammonium hydroxide [TMA][OH] demonstrated the best activity, it was selected for further reaction optimization. Increasing the catalyst loading enabled to drastically enhance the selectivity up to 78% for **4** while keeping a conversion of 90% of **GL** toward glycerol carbonate **43** after 90 min of reaction time. Given that the carbonation reaction is an equilibrium, a 3:1 excess of dimethyl carbonate **38** helped to shift the equilibrium toward **43**. Overall, the best reaction conditions reached 78% selectivity in glycidol **4** and gave a **GL** conversion superior to 90% with 0.01 equivalents of [TMA][OH] at 80 °C. The recyclability of the catalyst was assessed by adding fresh reagents after the first cycle. Decrease of both conversion and selectivity around 8 and 9%, respectively, were observed, mainly imputed to changes in reaction parameters caused by the dilution of the reaction medium.

Tao and co-workers reported the preparation of four tetraethylammonium amino acid ILs (TAAILs) aimed at the decarboxylation of glycerol carbonate **43** toward **4**, which in turned was prepared *in situ* from **GL** with dimethyl carbonate **38** (Scheme 2.28b).[122] Along with TAAILs, other catalysts including tetraethylammonium acetate or sodium prolinate were tested. Tetraethylammonium pipecolinate showed a superior activity, giving 95% conversion of **GL** and 81% selectivity toward **4**. A computational study on the catalytic process indicated that IL counter anions with a higher content of negative charges on the oxygen enabled an enhanced activation of reagents; firstly, by the activating OH group from glycerol and carbonyl of DMC, and secondly this of CH from glycerol carbonate. Increasing the temperature up to 130 °C combined to an extended residence time (2 h) greatly favored both conversion and selectivity toward **4**, with an overall yield of 78% yield. After three cycles of catalyst recycling, the selectivity toward oxirane **4** progressively decreased.

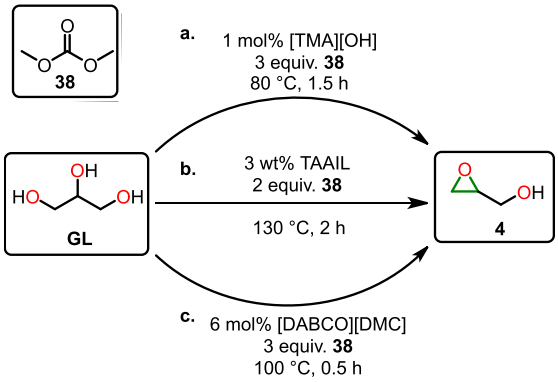

Scheme 2.28 Glycerol carbonation with dimethyl carbonate **38** and the subsequent CO_2 extrusion from glycerol carbonate using ionic liquids and various experimental conditions; (a) tetramethylammonium hydroxide [TMA][OH], (b) tetraethylammonium pipecolinate (TAAIL) and (c) 1,4-diazabicyclo[2.2.2]octane (DABCO) and its IL derivatives with dimethyl carbonate ([DABCO][DMC]).[121–123]

Several years later, Kelkar and co-workers studied basic strength impact of 1,4-diazabicyclo[2.2.2]octane (DABCO) and its IL derivatives with dimethyl carbonate **38** ([DABCO][DMC]) on the production of **4** from **GL**, again with the *in situ* formation of glycerol carbonate **43** (Scheme 2.28c).[123] Under reflux, comparative experiments highlighted higher performance of catalyst exhibiting lowest basicity, that is, [DABCO][DMC]. These results emphasized that basic properties were not sufficient to fully account for the catalyst efficiency toward epoxide **4**, despite this is widely acknowledged fact through the literature. Adjusting the DABCO-DMC IL content to 6 mol% greatly improved the selectivity toward **4**, reaching 83% selectivity while ensuring 97% conversion. Considering the reaction mechanism, the authors claimed that both cations and counter anions were involved in triggering the reaction, through a dual electrophile and nucleophile activation of the reactants. By contrast, DABCO only could interact with the hydroxy groups of the substrate, thus, displaying a lower catalytic activity.

In addition to the work of Kelkar's group, Lee and co-workers studied the influence of ILs acidity and nucleophilicity on the decarboxylation of glycerol carbonate **43** into **4** (Scheme 2.29).[124] From preliminary tests performed with various alkali metal salts, the authors stated that both the Lewis acidity of the cation and the basicity of the anion had a strong impact on the selectivity toward glycidol **4**. In addition, it was worth mentioning that NaCl showed a good activity with a surprisingly high yield (62%). To ensure a good tunability of acid-base properties, 1-butyl-3-methylimidazolium-based ILs were selected. Starting from [BMim], a library of ILs were assessed, eventually emphasizing [BMim]NO_3 and [BMim]I as the most efficient catalysts. These superior activities were correlated to a moderate hydrogen basicity (β value 0.6-0.8) of their counter anions whereas substrate conversion remained >95% for β >0.6. Using 1-butyl-3-methylimidazolium as a cation allowed to increase the selectivity toward 4 up to 73%, in comparison with the 69% provided with [BMim]NO_3. This suggested that lower Lewis acidity slightly favored the selectivity to oxirane **4**, although this was not confirmed with cations of decreasing acidity. The addition of $Zn(NO_3)_2$ seemed to play a synergic role in conjunction with ILs by lowering the basicity of NO_3^- which in turn decreased

the activation of the hydroxy groups on **43** and **4**. As major side products arose from the polymerization of epoxide **4**, the implementation of continuous feeding for glycerol carbonate **43** and distillation of **4** combined to the use of glycol dimethyl ether as a solvent (DMPEG 350) afforded an excellent 98% yield toward glycidol **4** (TOF=150 h^{-1}). The efficiency of the catalyst remained constant for the first 28 h before slightly decreasing with a TOF of 107 h^{-1} after 40 h.

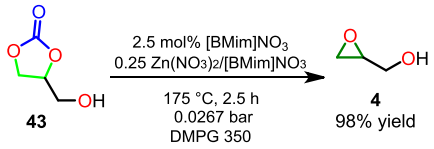

Scheme 2.29 Procedure toward glycidol **4** with a continuous feed of glycerol carbonate **43** and catalyzed by a synergistic system composed of molar ratio 1/4 of [BMim][NO_3] and $Zn(NO_3)_2$ in presence of DMPG 350 as a solvent under reduced pressure at 175 °C for 2.5 h.[124]

In 2014, Darensbourg and Yeung performed a computational study of the base- and acid-catalyzed decarboxylation of glycerol carbonate **43** (Scheme 2.30).[125] Regarding the base-catalyzed decarboxylation processes, the authors started with the conjugated basis of **43**, that is, a cyclic carbonate-alkoxide intermediate (Scheme 2.30a). Two intermediates were envisioned for the intramolecular five-membered ring opening of the cyclic carbonate, depending on which O-C bond was cleaved, giving either oxiran-2-ylmethyl carbonate (**48**) or oxetan-3-yl carbonate (**49**). Next, the free energy barriers (relative to their transition state) were calculated and led to values of 14.4 kcal mol^{-1} for the formation of the epoxide-carbonate **48** and a higher value of 19.8 kcal mol^{-1} for the formation of the oxetane-carbonate **49** intermediate (Scheme 2.30b), likely caused by steric repulsion of its eclipsed substituents. Given the fast reaction of CO_2 with an alkoxide, authors assumed that thermodynamic data were sufficient to explain the selectivity of the extrusion of CO_2.

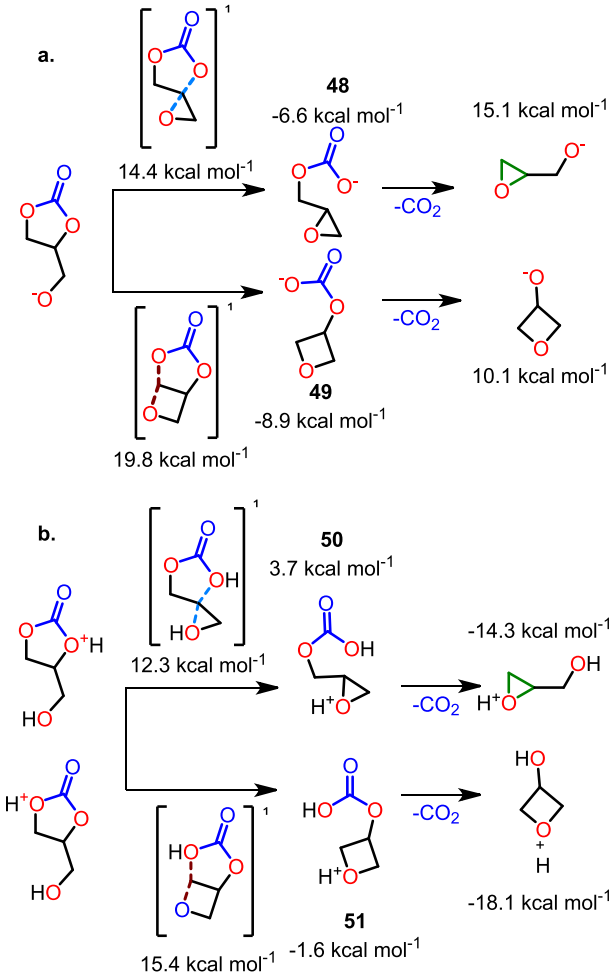

Scheme 2.30 Computed mechanism for the decarboxylation of glycerol carbonate (a) under base-catalyzed conditions and (b) under acid-catalyzed conditions.[125]

Calculations showed that this step was endergonic, even if it led to a gain of entropy, hence highlighting CO_2 extrusion as the rate determining step. Therefore, increasing the temperature could theoretically promote the extrusion of CO_2. Eventually, even if the extrusion of CO_2 from the epoxide-carbonate intermediate **48** was slightly more endergonic (21.7 vs. 19.0 kcal mol^{-1}), the authors concluded that deprotonated glycerol carbonate **43** would always form an epoxide intermediate **48**, instead of a 4-membered ring intermediate as the result of the faster kinetic for a three-membered ring closure. Epoxide intermediate **48** would then eventually lead to glycidol **4** after extrusion of CO_2. Furthermore, in the same conditions, homopolymerization of oxirane **4** was also calculated. The computational results showed that if there was sufficient heat for the decarboxylation of **43** to happen, there was also sufficient heat for the polymerization of **4**, owing to its very low activation barrier. Following a similar approach than for the base-catalyzed reaction, the authors also computed the mechanism under acidic conditions, starting from protonated glycerol carbonate **43**. Since

O-C bonds of both transition states were slightly longer, that is, emphasizing weaker interactions than for deprotonated species, free energy barriers for 2-[(carboxyoxy)methyl]oxiran-1-ium (**50**) and 3-(carboxyoxy)oxetan-1-ium (**51**; respective epoxide **50** and oxetane **51** intermediates) were also lower: 12.3 and 15.4 kcal mol^{-1}, respectively. Moreover, the extrusion of CO_2 was found to be exergonic under these conditions, indicating that the first step became rate determining step. Therefore, the acid-catalyzed decarboxylation of **GC** was also assumed to always yield glycidol **4**, in agreement with data from the primary literature.

2.4.2.3.3 MISCELLANEOUS

Haamed and co-workers reported a two-step conversion of neat **GL** catalyzed by clay mineral sepiolite (SiO_2, Al_2O_3, MgO, CaO, K_2O, Na_2O, Fe_2O_3, TiO_2) impregnated with KF.[126] Modifying sepiolite with increasing KF concentration significantly enhanced both the conversion and the selectivity toward glycidol **4** up to 30 wt%. Similar to KF impregnation, increasing catalyst loading was very beneficial for reaction outcome. By adjusting the dimethyl carbonate **48**/**GL** ratio to 2, 99% conversion and 82% selectivity were reached with 6 mol% of catalyst at 85 °C for 90 min. The authors next evaluated the recycling of the catalyst, and the results showed a progressive decrease of both conversion and selectivity down to 83% and 76%, respectively, after 4 runs. The reduction in activity was correlated to a progressive obstruction of its internal pores by reagents.

2.4.3 CHLORINATED DERIVATIVES AND OXIRANE FROM BIO-BASED POLYOLS: GLYCEROL CHLORINATION AND DECHLORINATION TOWARD EPICHLOROHYDRIN

This section specifically treats the case of epichlorohydrin **5**. Despite a closely related structure to glycidol **4**, the inherent reactivity profile of oxirane **5** with **2** highly reactive electrophilic centers justifies a separate section.

2.4.3.1 CHLORINATED DERIVATIVES AND EPICHLOROHYDRIN AS A KEY BUILDING BLOCK

Monochlorohydrins are the first intermediates compounds formed toward the production of dichlorohydrins (1,3-dichloropropan-2-ol (**47**) and 2,3-dichlorpropan-1-ol (**52**)) and epichlorohydrin **5**. Monochlorohydrin **45** is a side product as it cannot undergo a second chlorination toward dichlorohydrins **47**,**52**. As a potent way of valorization, a process was recently developed to convert **45** into glycidol **4** through simple basification of the reaction medium.[115] Dichlorohydrins are key intermediates which can be considered as both bulk and fine chemicals. Obviously, dichlorohydrins are intermediates in the synthesis of epichlorohydrin **5** and glycidol **4**. They also have niche applications in numerous sectors as starting material for the synthesis of antimicrobials compounds intended to the agricultural or health industries, involved in the production of polyesters for flame retardants for instance or surfactants.[127]

Epichlorohydrin **5**, is a high-volume commodity which stands as a pillar in the polymer industry, especially toward epoxy resins, whereas also contributing to surfactant and

pharmaceutical sector as a very potent ambivalent electrophile.[127,128] Although a large amount of **GL** is produced from triglyceride transesterification, **5** still serves as feedstock for the petro-based synthesis of high purity **GL**, essential for some drugs formulations. Its worldwide production and prices revolve around 2.2 Mt y^{-1} and approximatively 1.8-2.5 US$ per kg, respectively.[41,58,129,130] At the industrial scale, petro-based epichlorohydrin **5** (Scheme 2.31a) is prepared from a mixture of dichlorohydrins (30:70 **52**/**47**) derived from the chlorination of propene through allyl chloride **9**, which next undergoes an alkali treatment to form oxirane **5**. Epichlorohydrin **5** can also be generated starting from allyl acetate. This latter undergoes a hydrolysis to yield allyl alcohol **3** before its chlorination. The main drawbacks of these methods are multiple: (a) the petro-based nature of the starting materials, (b) inherent safety issues of these reagents, (c) the lower reactivity of dichlorohydrins **47**, **52** and (d) the poor atom economy.[127] Since 2007, alternative bio-based roads are also operational at the commercial scale with the GTE (Glycerol to Epichlorohydrin) process from DOW and the Epicerol processes from Solvay (see also Section 2.2 on glycidol **4**). Together, they feed the market with 15% of the global production for **5**, which is approximately 0.33 Mt y^{-1}.[63] The Epicerol process (Scheme 2.31b) relies on a 2-step pathway. The first step encompasses the chlorination of **GL** with gaseous hydrochloric acid (HCl) and catalyzed by caprylic acid, yielding a mixture of monochlorohydrins and dichlorohydrins. A temperature above 120 °C prevents the deleterious effect of water on the reaction equilibrium, whereas using a catalyst with long carbon chain avoids its loss by evaporation.[63] The second step implies a dechlorination of the mixture of chlorinated derivatives with an inorganic base to form the epoxide. Nowadays, this process is industrially applied up to a scale of 100 kt per year. Among the major drawbacks, the atom economy is still poor, as well as the recyclability of chemicals.[131]

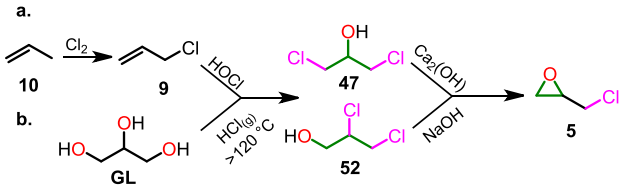

Scheme 2.31 Industrial processes for the preparation of epichlorohydrin **5**. (a) Synthesis starting from propene and (b) alternative road relying on glycerol.[60,63]

Diglycidyl ethers are polymer cross linkers with key involvement in epoxy resin synthesis. Owing to the extensive versatility of this class of polymers, it concerns a substantial market, especially in the field of painting, coating or electronics, as well as in the manufacturing of composite materials. Among the various epoxy resins, the diglycidyl ether of bisphenol A (DGEBA) represents 70% of their production worldwide. The current global market size for such resins is approximately 20 billion US$ per year with an annual average growth of 7%.[132] The preparation of DGEBA consists in the O-alkylation of bisphenol A with **5** in the presence of NaOH as a catalyst. However, although the bio-based production of **5** is now possible, bisphenol A is still prepared from petro-based acetone and phenol.[63]

Another polymeric application relies on the synthesis of glycerol ethers (GMEs), which exhibit particular biological properties such as immunostimulant or antimicrobial properties. They allow the active transport of substances through the skin and are hence widely used in

shampoos and skin creams, for example. For this goal, an industrial synthetic road toward a specific GME named Sensiva SC50 was developed at the industrial scale. This process is based on the prior etherification of epichlorohydrin **5** in the presence of fatty alcohol or phenol under basic conditions (NaOH, K_2CO_3 or tertiary amines) to give glycidol ethers precursors. The final step leading to GMEs relies on the hydrolysis of the epoxide.[61]

Epichlorohydrin **5** also possesses several commercialized niche applications with antimicrobial molecules (e.g., 1,2,4-triazinones) destined to the agrochemical or pharmaceutical sectors (sulfonamides).[127]

2.4.3.1.1 EN ROUTE TOWARD BIO-BASED EPICHLOROHYDRIN WITH CARBOXYLIC ACID CATALYST FOR THE PRELIMINARY CHLORINATION STEP

Canela-Garayoa and co-workers reviewed the preparation of chlorinated derivatives from **GL**, as well as their subsequent uses in numerous organic syntheses toward added values compounds. Most of the protocols reported in the literature for the chlorination of **GL** toward mono- and dichlorohydrins involve reacting neat **GL** with hydrochloric acid in liquid or gas phases in the presence of acetic acid **11** as a catalyst. The process conditions (temperature, pressure, HCl concentration or reaction time) have a profound impact on the selectivity toward either monochlorohydrins **45**, **46** or dichlorohydrins **47**, **52**.[127] The mechanism is depicted in Scheme 2.32.

Di Serio and co-workers studied a large diversity of carboxylic acid catalysts exploitable for the chlorination of **GL**.[20] Typical process conditions rely on aqueous HCl with dicarboxylic acids of increasing carbon chain length including malonic acid, maleic acid, fumaric acid, tartaric acid or adipic acid as catalysts. All catalysts displayed very good conversion ranging from 86% to 99% and a higher selectivities toward monochlorohydrins (63-93%). Experiments relying on aliphatic monocarboxylic acids were also described and emphasized as hexanoic and heptanoic acids as very efficient catalysts for the formation of 1,3-dichlorohydrin **47** with 87-91% selectivity and very good conversion (86-94%). Several lactones such as gamma butyrolactone or caprolactam also achieved very promising results with conversions around 87 to 96% and selectivity up to 94% toward 1,3-dichlorohydrin **47**. The authors also discussed other carboxylic acids containing additional functional groups in more or less vicinal position and their influence on the activity of the catalyst. For instance, with benzoic acid derivatives: benzoic acid **16** and 2-aminobenzoic acid were associated with a very low efficiency; 2-methylaminobenzoic acid was not catalytically active for the chlorination of **GL** while phenylacetic acid achieved very good 89% conversion and 85% selectivity toward dichlorohydrins.

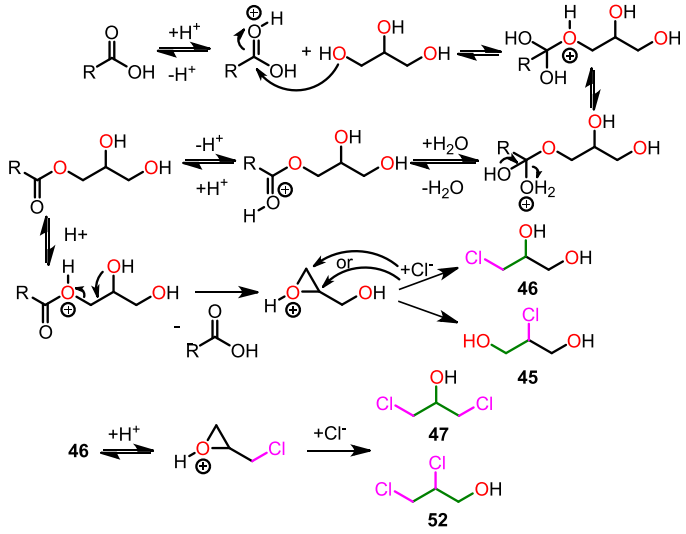

Scheme 2.32 Mechanism for the formation of monochlorohydrins and dichlorohydrins from the reaction of glycerol with hydrochloric acid (HCl).[70]

Similarly, Wang and co-workers investigated aliphatic mono- and dicarboxylic and hydroxycarboxylic acids as potential catalysts for the liquid-gas hydrochlorination of **GL** (Scheme 2.33).[133] Considering monocarboxylic acids, the transformation of **GL** into monochlorohydrins was associated with yields exceeding 70% after 2 h, whereas longer reaction times (up to 10 h) enabled the conversion of monochlorohydrins into dichlorohydrins. With a prolonged reaction, the yield toward dichlorohydrins typically ranged from 68 to 75%, with a decreasing catalytic efficiency from propionic acid>butyric acid>hexanoic acid to acetic acid. These results suggested that compounds of decreasing pK_a had better activity. The only exception was noticed from acetic acid, which displayed a slightly lower conversion compared to propionic acid, which was attributed to its lower boiling that caused evaporation and, hence, loss of the catalyst. The assessment of dicarboxylic acids showed that an increasing carbon chain length had a positive impact on the formation of 1,3-dichlorohydrin **47** (69-73% yield) with adipic acid>succinic acid>malonic acid>oxalic acid. Generally, 6-8 h of reaction was required to convert 50% of monochlorohydrins into dichlorohydrins. Oxalic acid maintained a superior selectivity toward monochlorohydrins for the whole reaction time. This result was explained by the strong steric hindrance between both neighboring carboxylic groups, hence preventing the formation of dichlorohydrins. Hydroxycarboxylic acids including lactic, malic and citric acids showed poor activity with a decreased formation of 1,3-dichlorohydrin **47**. These results clearly showed the influence of functional groups and carbon chain length on the reaction outcome. While mono- carboxylic acids of small chain length had a better efficiency compared to dicarboxylic acids of same length, the opposite trend was observed for an increasing carbon number. Thus, adipic acid was selected over propanoic acid for further optimization because of its more elevated boiling point. With an adjustment of the catalyst loading to 6.9 mol%, 1,3-dichlorohydrin **47** was obtained in 90% yield at 110 °C for 14 h.

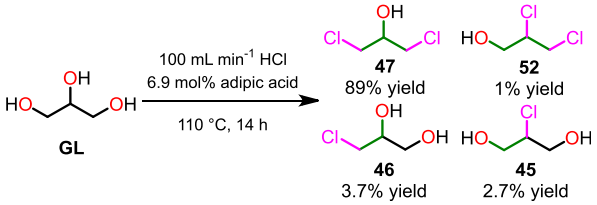

Scheme 2.33 Synthesis of monochlorohydrins and dichlorohydrins from the reaction between gaseous HCl and glycerol using adipic acid as catalyst, yielding predominantly 89% of 1,3-dichlorohydrin **47**.[133]

Other classes of carboxylic acids were investigated by Santacesaria and co-workers with several glycolic acids and amino acids in a batch reactor under gas/liquid conditions.[134] The assessment for the catalytic activity of various amino acids emphasized a very high activity for glutamic acid, with total conversion and high selectivity toward 1,3-dichlorohydrin **47** (72%). Asparagine and cysteine gave a higher selectivity toward 3-monochlorohydrin **46** (70 and 50^%, respectively). By contrast, glycolic, diglycolic thioglycolic acids gave full conversion of **GL**, yet with poor selectivity toward monochlorohydrins or dichlorohydrins, both ranging approximately between 40 and 60% (4 h, 100 °C, 8 mol% of catalyst with 4.5 bar of HCl).

Monbaliu and co-workers reported a liquid-phase continuous-flow process aimed at the hydrochlorination of **GL** as already discussed in section 2.2. (Scheme 2.34).[117] A library of homogeneous carboxylic acids was assessed to tune selectivity toward dichlorohydrins. Among them, pimelic acid displayed the best activity, including for the trials on crude **GL**. Upon optimization of the first hydrochlorination of **GL**, the authors also studied a subsequent dechlorination step with NaOH in aqueous solution, hence providing a mixture of glycidol **4** and epichlorohydrin **5**. The direct concatenation between both steps was successfully attempted, giving a very satisfying 74% cumulated yield with 30% yield of epoxide **4** and 44% yield of **5**. In line downstream purification was implemented through liquid-liquid extraction with methyl *tert*-butyl ether (MTBE) with a hydrophobic membrane separator, achieving efficient separation of both oxiranes. Glycidol **4** remained in water, whereas **5** was extracted in MTBE and used for the preparation of active pharmaceutical ingredients from the β-aminoalcohol class. The scalability of dehydrochlorination step was evaluated in a commercial mesofluidic reactor (Corning Advanced-Flow G1 SiC reactor, 60 mL internal volume) using a model solution simulating a typical output for the hydrochlorination of **GL**. The results indicated a complete conversion of dichlorohydrins and monochlorohydrins, with a short residence time of 90 s.

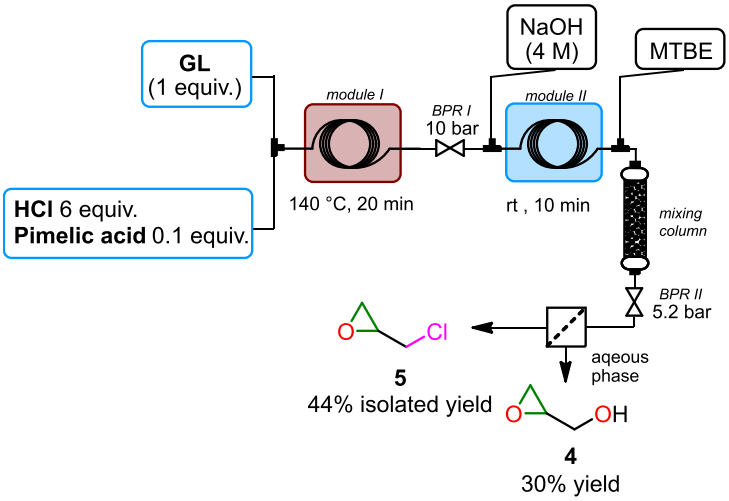

Scheme 2.34 Continuous flow setup of concatenated reactions of glycerol hydrochlorination and subsequent Williamson's epoxidation, followed by liquid-liquid extraction with MTBE to obtain 44% isolated yield of **5** and 30% yield of **4**.

In 2014, Brandi and co-workers proposed a novel approach for the chlorination of **GL** based on trimethylchlorosilane (TMSCl) in the presence of acetic acid as a catalyst (Scheme 2.35).[135] Various experiments were implemented to determine the influence of reactional parameters on the distribution of products. While setting the temperature at 100 °C, trials relying on a large excess of TMSCl (≥ 2.5 equivalents) led to complete conversion and very good selectivity toward 1,3-dichlorohydrin **47**, after 6 h of reaction, exceeding 85% in yield. 96% yield was achieved after 12 h with 2.9 equivalents of TMSCl. Decreasing the temperature to 60 °C and lowering the excess of TMSCl to 1.8-2.5 equivalents had a deleterious impact on the conversion, though the formation of 3-monochlorohydrin **46** was favored (68-78% yield). Under these conditions, full conversion of **GL** could only be reached for a prolonged reaction time of 18 h. Based on these results, a fine tuning of the selectivity was tested on a 52:48 **GL**/monochlorohydrin aqueous mixture (10% w/w solution) obtained from the transesterification of sunflower oil with TMSCl. The authors used a similar excess of 2.7 mol of TMSCl per mole of hydroxy groups for all trials. While high selectivity and yield toward 1,3-dichlorohydrin **47** (96% yield) was reached at 100 °C (12 h reaction time), a lower process temperature (60 °C) gave mostly 3-monochlorohydrin **46** after 9 h of reaction (68:30 **46**/**47** molar ratio). The authors detected hexamethyldisiloxane as a side product formed by 2 equivalents of TMSCl and claimed that it could be recovered through distillation prior its recycling with HCl and ZCl_2 to form fresh TMSCl.

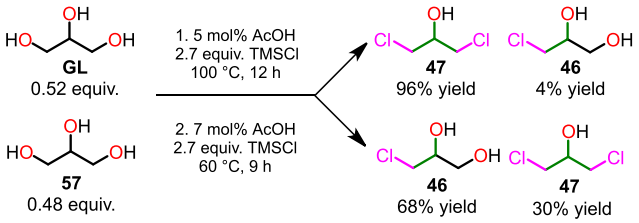

Scheme 2.35 New synthetic pathways leading to the synthesis of mono- and dichlorohydrins through the reaction between glycerol with TMSCl. Modulation of experimental conditions enabled a tunable reaction output toward either 1,3-dichlorohydrin **47** (5 mol% cat., 100 °C, 12 h) or 3-monochlorohydrin **46** (7 mol% cat., 60 °C, 9 h).[135]

Santacesaria and co-workers studied the behavior of homologous chlorinated series of catalysts including acetic, monochloroacetic, dichloroacetic and trichloroacetic acids for the chlorination of **GL** under gas-liquid conditions (Scheme 2.36).[136] Comparative experiments showed that chlorinated derivatives promoted the selectivity toward **46** (27-70% yield), in opposition to acetic acid, which comes with a very high selectivity toward **47** (typ. 90%). In addition, an increasing chloride content on the catalysts led to a decrease of the conversion; only acetic acid ensured full conversion. However, the similarity between the boiling point of acetic acid and the process temperature led the authors to select monochloroacetic acid as a catalyst. The authors argued that this selection would alleviate catalyst loss through evaporation. The authors also studied the impact of the pressure on the chlorination of **GL**. Rising the pressure led to an increase of the conversion, although the selectivity toward 3-monochlorohydrin **46** dropped in favor of the formation of 1,3-dichlorohydrin **47** (ca. 35% yield).

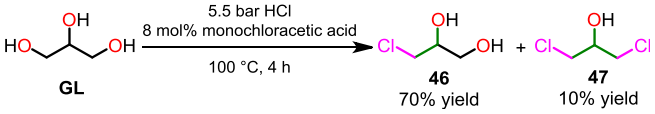

Scheme 2.36 Reaction between glycerol and HCl catalyzed by monochloroacetic acid at 100 °C for 4 h.[136]

2.4.3.1.2 CHLORINATION OF GLYCEROL WITH ACYL CHLORIDES

In 2016, Serio and co-workers reported acyl chlorides as both catalysts and reagents for the chlorination of **GL**, relying on the *in situ* formation of gaseous HCl.[137] The authors compared carboxylic acids such as acetic, propionic, adipic, succinic and malonic acids with their respective acyl chlorides in catalytic amounts (8 mol%) in the presence of gaseous HCl. The results highlighted that acyl chlorides led to a faster formation of 1,3-dichlorohydrin **47**, though the selectivity over an extended reaction time remained relatively similar compared to the parent carboxylic acid catalysts. By contrast, acyl chlorides gave a higher yield toward dichlorohydrins for short reaction times. For instance, a significant difference was obtained with adipoyl dichloride, which achieved roughly 90% selectivity whereas adipic acid only offered about 65%. This phenomenon was rationalized by the authors based on mechanistic specific features: in the carboxylic acid-mediated hydrochlorination, the formation of 2,3-dihydroxypropyl acetate (**53**), the intermediate ester that forms from the addition of the polyol substrate on the catalyst, is an equilibrium, whereas with acyl chloride, the reaction is quantitative, owing to the enthalpic activation of the acyl chloride. Moreover, the equilibrium that concerns carboxylic acids generates water, whereas the formation of an ester from an

acyl chloride does not. In addition, in comparable conditions, the ester from the acyl chloride is more concentrated than for the carboxylic acid counterpart and the generation of HCl for the former catalyzes the subsequent step toward the oxonium, hence greatly favoring the second step (Figure 2.7). The authors also observed that addition of acyl chloride in one time was deleterious to the reaction due to sharp increase of HCl pressure which negatively impacted both the selectivity toward dichlorohydrins and the reaction rate. Therefore, the authors considered a continuous injection of acyl chloride of 2 mL min^{-1} (and *in situ* release of HCl) that gave a very good yield of 92% of 1,3-dichlorohydrin **47** in less than 2 h. The authors also reported that the NaCl content in raw **GL** slightly enhanced the selectivity toward **47**.

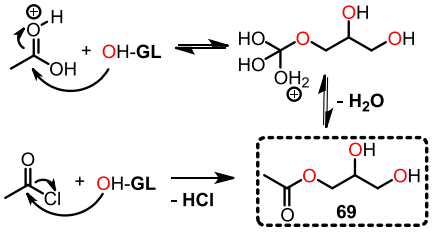

Figure 2.7 Comparison of the mechanisms of hydrochlorination with carboxylic acids and acyl chlorides (illustrated on glycerol).[137]

2.4.3.1.3 CHLORINATION OF GLYCEROL WITH HYDROTALCITES

Ramirez and co-workers developed a continuous gas-phase fixed bed process based on the dehydrochlorination of dichlorohydrins catalyzed by Lewis basic Mg-Al mixed oxides derived from hydrotalcites.[131] An assessment of the reaction parameters highlighted that the process temperature had a critical impact on the catalyst activity. For temperatures ranging from 130 to 150 °C, a high selectivity (80-100%) toward epichlorohydrin **5** was achieved, whereas a further increase of the temperature (150-300 °C) had a deleterious effect with almost no selectivity nearly toward oxirane **5**. This was explained by the thermal isomerization of **5** toward 1-chloropropan-2-one. At 150 °C and WHSV=1.2 h^{-1}, the conversion decreased to 15% within the first hour while the selectivity toward **5** reached 80% after 3 h.

2.4.3.1.4 CHLORINATION OF GLYCEROL IN THE ABSENCE OF A CATALYST

Salmi and co-workers reported the hydrochlorination of neat glycerol under gas-liquid conditions.[138] Experiments in the absence of a catalyst were performed and, surprisingly, displayed substantial conversion of **GL** in monochlorohydrins. Varying the temperature from 70 °C to 120 °C enabled to increase the conversion of **GL** from roughly 25% to 75% after 200 min, emphasizing that the great temperature dependence of the hydrochlorination of **GL** without catalyst.

2.4.3.1.5 ENZYMATIC FORMATION OF EPICHLOROHYDRIN

Hu and co-workers reported biotransformation of 1,3-dichlorohydrin **47** in epichlorohydrin **5** using halohydrin dehalogenases expressed by recombinant Escherichia coli BL21 (DE3). To prevent enzyme inhibition caused by elevated concentration of **5**, the authors implemented a resin-based *in situ* product removal to continuously eliminate **5** by adsorption. Using a 10%

HZD-9 resin (w/v), the production of oxirane **5** achieved 88% yield after 20 min at 45 °C.[139] Zheng and co-workers described the enantioselective conversion of 1,3-dichlorohydrin **47** in (*S*)-5 with a mutant (P175S/W249P) expressing the haloalcohol dehalogenase gene. The latter displayed a high enantiomeric excess (*ee*) of 95%, which was enhanced by use of an epoxide hydrolase to reach a yield of 91% of *(S)*-5 with ≥99^% *ee*.[140] Zheng also developed a process relying on halohydrin dehalogenases that are rather insensitive to high **5** concentration. The addition of NO_2 as a nucleophile in the reaction medium enabled to synthesize (*R*)-5 with 41% yield and ≥ 99% *ee*.[141] The same team also reported an alternative to halohydrin dehalogenases for the enantioselective production of (*R*)-5. The authors relied on a recombinant A. radiobacter epoxide hydrolase expressed through Escherichia coli. Based on the hydrolysis of **5** racemate, a maximal yield of 48% was achieved with *ee*> to 99% due to substrate and product inhibition.[142]

2.4.4 FIVE-MEMBERED CYCLIC CARBONATES FROM BIO-BASED POLYOLS: DIRECT OR INDIRECT CARBONATION OF VICINAL DIOL

2.4.4.1 BIO-BASED CYCLIC CARBONATES AS NEW DROP-IN MOLECULES AND ALTERNATIVE MONOMERS

Ethylene carbonate **44** is a key cyclic carbonate with low toxicity and high biodegradability. Owing to its high boiling point and low viscosity, it stands as a sustainable alternative to common aprotic polar solvents such as DMF, DMSO and NMP. However, owing to its high melting temperature, it is under solid state at room temperature and further requires the use of another compound, usually dimethyl carbonate **38**, to enable its use as solvent under standard conditions.[143] This carbonate is also extensively used in lithium ion batteries as co-solvent for electrolytes,[144] as well as a carbonating reagent for transesterification reactions with diols and cross-linking agent in the polymer sector.[64,145] Carbonate **44** (Figure 2.8) is already available at commercial scale and is produced from the cycloaddition of ethylene oxide **42** with CO_2, with an annual production of 0.2 Mt at an average price of 1.5 US$.[145] The main drawbacks of this process are related to the inherent toxicity of oxirane **42**, its volatile costs and its petro-based nature.[143]

Glycerol carbonate **54** (Figure 2.8) is one of the most appealing derivatives of **GL** because of its renewable carbon content ranging from 76 to 100% according to its production scheme, its low toxicity, non-flammability and biodegradability. As an alternative to conventional polar solvents, glycerol carbonate **43** has also appealing physicochemical proprieties comprising a high boiling point and vapor tension, as well as its hydrophilic nature.[146] Moreover, carbonate **43** has other notable applications such as bio-lubricant due to its adhesion to metallic surfaces and formulating agent as well as monomer for polymer sector.[25,147] Carbonate **43** also exhibits a very interesting multipurpose reactivity with an ambivalent electrophile/nucleophile character. Finally, **43** has also found utility in Li-based batteries as an electrolyte liquid carrier.[146] Overall, the large array of applications concerned by glycerol carbonate led to huge interest from industrials with worldwide key players comprising Huntsman International, UBE industries, InKemia Green Chemicals, TCI Chemicals to name a few.[148,149] Recent estimations approximated its production to 3 Mt y^{-1} in 2020 and with a cost of 25000-34000 US$,[42,58] which is quiet contradictory.

Historically, the first preparations of carbonate **43** were carried out through the reaction of **GL** with phosgene or with its derivatives such as alkyl chloroformates or carbonylimidazoles. However, given intrinsic toxicity and corrosive nature of phosgene, and the high cost and high-water sensitivity of its derivatives, greener and safer roads were developed, including processes with urea, dimethyl carbonate **38** or CO_2.[21,119,150--152] Nowadays, the major hurdle for a widespread use of glycerol carbonate worldwide is its relatively high cost.[153] Current research efforts are now being focused on the design of new synthetic strategies involving the exploitation of waste derived-catalysts and affordable carbonation reagents, which could significantly reduce the current market price for carbonate **43**.[154] Efforts are also being devoted to the development of process conditions and reagents that can accommodate crude **GL** rather than refined.

Over the past decades, bio-based five membered carbonates gained a significant interest in the polymer sector, especially as promising renewable sources of monomers aimed at the production of poly(β-hydroxyurethane)s (PUHs).[155] PUHs are extensively used in elastomers, rigid and soft foams, coatings or additives[156,157] As polymerizable building blocks, cyclic carbonates have the potential to offer a more sustainable manufacturing of macromolecules as well as valorizing bio-based feedstock and carbon dioxide. Especially, the use of five membered cyclic carbonates offers an alternative route to PUH production based on hazardous toxic phosgene and isocyanates (for PUHs).[158] Just to have a glimpse at the inherent potential of cyclic carbonates as monomers, the markets associated with PUHs is estimated to 62 billion US$ with global productions of 18 Mt y^{-1}.[156,159]

Among cyclic carbonates reachable through biomass, (4*S*,4'*R*)-[4,4'-bis(1,3-dioxolane)]-2,2'-dione (erythritol dicarbonate, **54**; Figure 2.8) is obtained from a petro-based route relying on the CO_2 carboxylation of 2,2'-bioxirane, obtained through the epoxidation of butadiene **2**.[160] Erythritol dicarbonate **54** can also be obtained from the double carbonation of **ERY** in high yield using various carbonating agents.[161] Recently, sustainable procedures relying on dimethyl or diphenyl carbonates **38**, **55** were developed. Due the bicyclic nature of erythritol decarbonate **54**, it stands as a promising monomer for the polymer industry, especially, some studies already showed applications in the field of non-isocyanate polyurethanes.[160,161] Other examples of polycyclic carbonates, (3*R*,4*R*,6*R*)-4-[(*S*)-2-oxo-1,3-dioxolan-4-yl]tetrahydrofuro[3,4-d][1,3]dioxol-2-one [56, sorbitol bis(cyclo-carbonate), Figure 2.8]) is an emerging compound, constituted of a tetrahydrofuran derivative bearing two cyclic carbonates produced by the reaction of **SO** with dimethyl carbonate **38**. Tricyclic compound **56** is considered a potent platform to compete with polycyclic species such as (3*R*,3*R*,6*S*,6*R*)-hexahydrofuro[3,2-b]furan-3,6-diol (**57**, isosorbide), which had a market size of 190 million US$ in 2018 and stands to increase to 350 million US$ in 2023, with many applications deeply rooted in the polymer industry and commercial applications in electronic, packaging or biomedical sectors.[162,163] (4*R*,4'*S*,4"*S*,5'*S*)-[4,4':5',4"-ter(1,3-dioxolane)]-2,2',2"-trione (**58**, sorbitol tricarbonate, Figure 2.8), which can be accessible through a threefold carbonation of **SO** using diphenyl carbonate **55**, was also recently reported as a potential candidate in non-isocyanate polyurethanes (NIPU) manufacturing.[164]

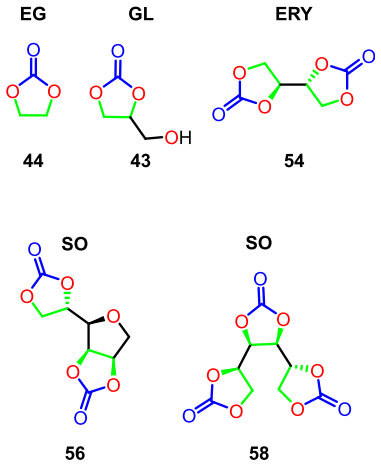

Figure 2.8 Common bio-based carbonates. The parent bio-based vicinal polyol is indicated above the corresponding structures.

2.4.4.2 THE CARBONATION OF VICINAL DIOLS

The carbonation reaction is a common strategy toward 5-membered cyclic carbonates that starts from a vicinal diol and a carbonating reagent. Under the term carbonation, there are actually two main variants: (a) direct and (b) indirect processes. Direct processes use CO_2 or CO in the presence of various catalysts. Indirect processes can be further subdivided into 3 subclasses: (i) indirect processes involving a coupling agent to fix CO_2 prior to its transesterification with a polyol; (ii) indirect processes involving linear or cyclic carbonates and urea as carbonation reagents; (iii) procedures involving the preactivation of vicinal diols into their corresponding epoxides and their subsequent reaction with CO_2. In other words, the latter category of indirect processes corresponds to a cycloaddition of CO_2 and epoxides, which is the current privileged industrial road toward carbonates. Overall, all these synthetic roads are selective toward the 5-membered ring species rather than the 6 membered isomer.[165]

The term “carboxylation” is also widely encountered in the primary literature for describing the carbonation of polyols, although it theoretically refers to the functionalization of a substrate with a carboxylic acid group. Within the frame of polyol carbonation, it is used to describe the incorporation of a CO fragment onto the structure of carbohydrate derivatives. Similarly, their direct carbonation with CO_2 can be expressed as the “carbonylation of a vicinal diol”, which corresponds to the incorporation of CO to yield the cyclic carbonate.

Carbon dioxide stands theoretically as the perfect C_1 feedstock since it is considered as a widely available and low-cost building block. Moreover, developing industrial processes that consume CO_2 is very appealing to mitigate the overall greenhouse gas emissions. Such processes have the potential to globally supply a wide range of industrial applications for the production of large array of linear and cyclic carbonates starting from bio-based vicinal polyols. With such context, several Green Chemistry principles can be fulfilled and chemical processes with high atom economy can be devised.[143] Currently, the global production of

CO_2 is estimated at 37 000 Mt per year whereas its exploitation in various fields of applications only approximately reaches 200 to 300 Mt y^{-1} at best.[166] Moreover, the production of cyclic carbonates at industrial scale only represents approximately 100 kt y^{-1}, mostly through the cycloaddition of CO_2 on epoxides (in 2013).[167] This fact foresees a huge potential for further developing carbonation routes from bio-based vicinal polyols.

However, reactions involving carbon dioxide as reactant are severely hampered by equilibrium limitations and the inherent stability of CO_2, hence, only achieving low yields. Consequently, several works investigated the implementation of harsh conditions of pressure and temperature, which resulted in high energy demanding processes. In addition, the activation of CO_2 was also studied via several elaborated catalytic systems yet there is still plenty of room for optimizing the substrate conversion. One of the most efficient systems was developed by Tomishige and co-workers, based on lanthanide cerium oxide in presence of an excess of additive pyridine-2-carbonitrile (**59**) at 130 °C and 50 bar CO_2 for 1-2 h. This procedure enabled to convert a library of 1,2- and 1,3-diols with yields ranging between 62 and 99%.[168] Despite the good performances of catalytic candidate, CeO_2 is toxic and displays a low crustal abundancy, which causes its high cost.[76] Overall, the design of new affordable and low toxicity catalysts able to offer high yields and enhanced stability over extended time on stream is still a very challenging subject for the scientist community.

2.4.4.2.1 DIRECT CARBOXYLATION OF VICINAL DIOLS

One of the prototype reactions involves **GL** as a bio-based vicinal polyols, which enables the direct production of glycerol carbonate **43** with a very high atom economy, superior to 87%.[151,169] Unfortunately, this reaction is largely hampered by a unfavorable equilibrium constant ($K=6.4\ 10^{-5}$ at 25 °C, 1 atm) as well as the formation of water as a by-product.[170] The latter can hydrolyze the cyclic carbonate product back to **GL**. As a result, a wide diversity of catalysts was assessed to lower the energetic barrier for the direct reaction with CO_2, in conjunction with a library of dehydrating agents in stoichiometric amount to shift the equilibrium. Nevertheless, the use of additives is not desirable due to the inherent generation of wastes and its negative impact on the atom economy; it also comes with a significant cost for complex purification steps.[171,172] Despite that the direct carboxylation of **GL** with CO_2 is a very timely research area that bears significant potential for the preparation of the corresponding carbonate **43**, and cyclic carbonates in general, this reaction has received less attention over the two past decades than the cycloaddition between epoxides and CO_2.[151] One of the main reasons is that the reaction with epoxides, in the current state of the art, achieves superior results at milder conditions for a plethora of internal and terminal epoxides than the direct carboxylation of vicinal polyols.

Metal-based catalysts. In 2017, Ozorio and Mota studied several metal oxides including ZnO, SnO_2 and Fe_2O_3 supported on polyvinyl alcohol aimed at the direct carboxylation of **GL** under supercritical CO_2 conditions without the addition of any dehydrating agent (Table 2.1, entry 1).[173] Preliminary tests were performed using Fe_2O_3 showed that a very high CO_2 pressure was required to obtain a poor yield in glycerol carbonate **43** (4%) within 3 h. Extending the reaction time to 12 h enabled to reach the thermodynamic equilibrium, affording 7% yield of carbonate **43**. Among various metal oxides, ZnO exhibited the highest catalytic activity with 8.1% yield of glycerol carbonate **43** at 180 °C, under 150 bar of CO_2,

whereas a mere 3% was obtained without catalyst. The gradual formation of a layer of $ZnCO_3$ led to a progressive deactivation of the catalyst. Nevertheless, it could be fully regenerated through by calcination, ensuring similar results over 4 reaction cycles.

Table 2.1 Overview of the various protocols dedicated to the direct carbonation of glycerol using CO_2.

Entry	Catalyst	Conditions	**43** (%)	Ref.
1	ZnO	150 bar CO_2, 180 °C, 12 h	8.1	[173]
2	CuO	1.2 equiv. **59** 150 °C, 5 h, 40 bar CO_2, DMF	39	[169]
3	$ZnWO_4$-ZnO	150 °C, 6h, 50 bar CO_2, DMF	6.3	[172]
4	Co-ZIF-67	210 °C, 12 h, 3 bar CO_2, acetonitrile	29	[174]
5	-	3 equiv. **59**, 180 °C, 12 h, 150 bar CO_2	18.7	[151]
6	$Zn(OTf)_2$ /phe[a]n[a]	5 equiv. CaC_2, 180 °C, 24 h, NMP, 50 bar CO_2	92	[170]

[a] 1,10-phenanthroline

Eljah, Kurdhani, and Wang reported the conversion of **GL** with CO_2 based on a set of metal oxide nanoparticles (NiO, CuO and Co_3O_4) in the presence of both a dehydrating agent 2-cyanopyridine **59** and DMF as a solvent (Table 2.1, entry 2). Preliminary results identified higher performances of CuO>Co_3O_4>NiO with yields of glycerol carbonate **43** of 39%, 8% and 6%, respectively. Notably, the catalyst activity could be tuned through the modification of the NP size using calcination. Raising the process temperature from 300 to 400 °C led to a great improvement in the selectivity (from 39% to 80%), whereas the conversion only slightly increased to 49% (45% at 300 °C). Relying on the structural characterization of the CuO catalyst, the authors correlated its superior activity to a high specific surface and a higher redox ability combined to a large density of basic active sites. The catalyst could be recycled up to 4 times without any significant loss of activity. However, further use required its regeneration by calcination.[169]

He and Liu focused on a series of powder catalysts-based composed of a blend of $ZnWO_4$ and ZnO, in the absence of a dehydrating agent.[172] Using DMF as a solvent, the catalyst performances were assessed as a function of its W content (Table 2.1, entry 3). Increasing the W deposition from 1 to 10 wt% had a positive effect on the production of glycerol carbonate **43**, achieving up to 6.3% (vs. 2% under the initial conditions). These results were correlated to a superior specific surface of the catalyst, hence, enabling an enhanced exposure of active sites and a larger occurrence of moderate Lewis acidic sites, by contrast to pure ZnO, which displayed an elevated content of strong basic sites. The temperature was an important parameter as well with optimal conditions at 150 °C; higher process temperatures led to the formation of by-products likely arising from competitive reactions with the solvent or the polycondensation of **GL** itself.

Huang and co-workers reported another process catalyzed by a zeolite imidazole framework-67 containing cobalt metal centers with acetonitrile acting both as dehydrating agent and solvent (Table 2.1, entry 4). Rising the temperature from 120 °C to 210 °C had a positive impact on the selectivity that increased from 32% to 49%, whereas the conversion remained relatively similar (in the 25-30% range). By contrast, extending the reaction time from 6 h to 12 h significantly increased the selectivity up to 92%, giving 29% yield toward carbonate **43** with only 3 bar of CO_2. By-products arose mainly from the reaction of water with acetonitrile, giving acetamide and acetic acid **11**. Catalyst removal from the crude reaction mixture was largely hampered by its fine particle size and by the viscosity of **GL**, hence leading to a very poor recyclability.[174]

Metal-free conditions. Zhao and co-workers reported a catalyst-free carboxylation of **GL** using various cyanopyridine species both as a dehydrating agent and as a reaction promoter, in the absence of any additional catalyst or additives.[151] The authors started by determining the influence of various isomers of cyanopyridine on the reaction outcome. While pyridine-3-carbonitrile (**60**) and pyridine-4-carbonitrile (**61**) offered yields in glycerol carbonate **43** of 5.3 and 3.8%, respectively, the 2-cyano isomer **59** gave 11.4% yield in carbonate **43**. This experimental observation was supported with a DFT study (B3LYP/aug-cc-pVDZ), which helped to identify and rationalize the mechanism and selectivity though the interaction of the various cyanopyridine isomers and CO_2.

Whereas 3- and 4-cyanopyridines **60** and **61** showed two connecting structures characterized by high absorption energies (CO_2-N in pyridine: 67-75 kcal mol^{-1}; CO_2-N of cyano group: ca. 92 kcal mol^{-1}), 2-cyanopyridine **59** displayed a third form, consisting in a dual concomitant interaction with CO_2 through the nitrogen atom of the pyridine ring and the nitrogen atom of the cyano group, thus generating a stable 5-membered ring intermediate of lower energy (57.71 kcal mol^{-1}; Figure 2.9a&b). As a consequence, this species interacted much more easily with CO_2, hence enhancing its activation and further reaction with **GL**. The dehydrating agent was converted to 2-pyridinecarboxamide (**62**) through reaction with water.

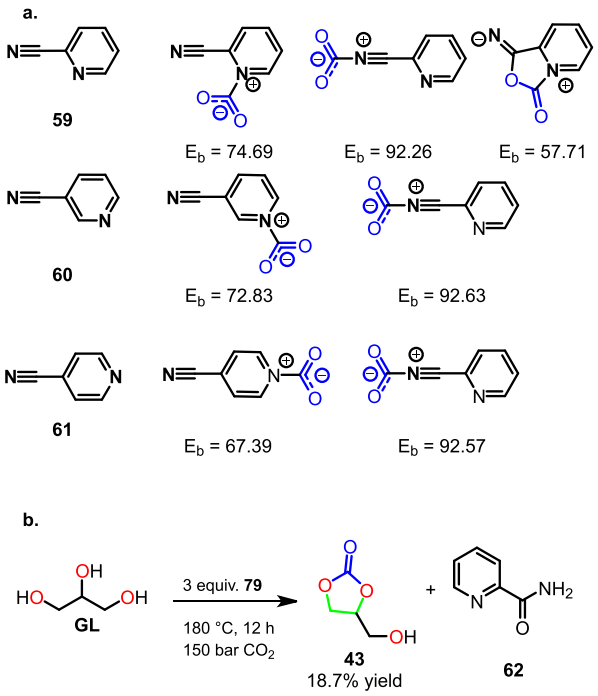

Figure 2.9 (a) Computed structures and binding energies (in kcal mol^{-1}) for the interactions of CO_2 with the three species of cyanopyridines.[151] (b) Carbonation of glycerol with 2-cyanopyridine.[151]

Upon process optimization, increasing the CO_2 pressure from 20 to 200 bar enhanced the conversion from 29.3% to 46%. The optimal excess of 2-cyanopyridine **59** was of 3 equivalents (in respect to **GL**), affording 18.7% yield of glycerol carbonate 43 after 12 h at 180 °C under 150 bar of CO_2 (Table 2.1, entry 5). Besides cyanopyridine species, Choi and co-workers reported another alternative, namely, calcium carbide (CaC_2) as a cheap and widely available dehydrating agent.[170] In presence of 1-methyl-2-pyrrolidinone (NMP) as a solvent, the authors screened various zinc-based catalysts with phenanthroline as a ligand, including $ZnSO_4$, $ZnCl_2$, $ZnBr_2$, ZnI_2, $Zn(OAc)_2$ and $Zn(OTf)_2$. All catalysts, but $Zn(OTf)_2$ gave poor to moderate yields of glycerol carbonate **43**, ranging from 25 to 67%. $Zn(OTf)_2$ outclassed the other Zn-based catalysts with an excellent yield of 92%, which was attributed to its stronger Lewis acidity. Other ligand scaffolds were studied, and the results of the study indicated that electron-donating substituents positively influenced the yield toward carbonate **43**, whereas electron-withdrawing groups had a deleterious effect. Furthermore, disubstituted ligands also diminished the activity of the catalyst, owing to stronger hindrance. A concomitant increase of both the temperature and the reaction time favored the formation of glycerol carbonate **43**. Moreover, an excess of calcium carbide (5:1 in respect to **GL**) also favored the production of **43**. Upon optimization, the protocol was also successfully applied to a library of diverse vicinal diols with yields in the 83-98% range over 24 h of reaction time (Table 2.1, entry 6).

2.4.4.2.2 INDIRECT CARBONATION OF VICINAL DIOLS

The indirect carbonation of a vicinal diol involves a third reactant, namely, a coupling agent, to overcome the thermodynamic barrier of carbon dioxide. The process consists in the *in situ* carboxylation of the coupling agent, generating a reactive carbonylation agent, and its consecutive transesterification with the vicinal diol to yield the corresponding cyclic carbonate. Among the various reported coupling agents, propylene oxide **12** and 4,4-dimethyl-5-methylene-1,3-dioxolan-2-one (**63**) are currently the most widely studied. Compound **63** is often seen as the prototype of the α-alkylidene cyclic carbonate family of compounds. One of the major hurdles of this strategy is ascribed to the large formation of wastes and low atom economy arising from the use of a coupling agent,[151] as well as its typical petro-based nature and complex purifications.[175,176] Though, green road toward the manufacturing of **12** already exists at laboratory scale, via the epoxidation of 1,2-propanediol (**33**) directly synthesized from **GL**.[177] Regarding precursors of α-alkylidene cyclic carbonates such as **63**, some propargylic alcohol derivatives can be obtained from acetylene and formaldehyde. Moreover, these propargylic precursors are quite tunable, therefore offering a broad range of cyclic carbonates structures, with a huge potential in applications related to polymer or organic chemistries.[175]

Metal-free carbonations with a coupling agent. Jang and co-workers reported a metal-free carbonation based on dibromomethane acting both as solvent and coupling agent, in the presence of DBU as a base and 1-butyl-3-methylimidazolium hexafluorophosphate to enhance the solubility of CO_2.[178] DBU displayed a dual action for the activation of CO_2 through (a) the formation of DBU-CO_2 adducts and (b) the activation of a hydroxy group of the vicinal polyol to form a more nucleophilic alkoxide moiety (Scheme 2.37).
This eventually leads to a bromo alkylated intermediate that undergoes an intramolecular substitution to form the desired cyclic carbonate. Notably, control experiments with (*S*)-1-phenylethane-1,2-diol (**64**) only produced the corresponding (*S*)-4-phenyl-1,3-dioxolan-2-one (**65**), indicating that the chirality of on the substrate was conserved. Interestingly, ethylene carbonate **44** was obtained in up to 74% yield starting from **EG** at 70 °C (8 h under 10 bar of CO_2). Though, this process led to the formation of undesirable halogenated wastes and inherently has a low atom economy.

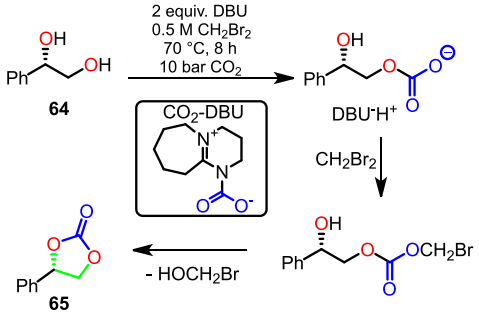

Scheme 2.37 Reaction mechanism of diol carbonation with CO_2/DBU and dibromomethane as coupling agent on a model substrate.[178]

A few years later, Oyamada and co-workers proposed a process relying on coupling agent 1-bromobutane under mild reaction conditions and dichloromethane as solvent.[179] The transformation of **EG** in its corresponding cyclic carbonate **44** was achieved in 95% yield at 25 °C after 24 h of reaction time. Similarly, Mizuno and co-workers reported glycerol indirect carbonation with butyl bromide catalyzed this time by Barton's base (*tert*-butyl tetramethylguanidine), using NMP as solvent.[180]

Han and co-workers developed an alternative one-pot carbonation process based on propylene oxide **12** as coupling agent (Scheme 2.38).[150] In the presence of CO_2, **12** was converted into propylene carbonate (**66**) prior a subsequent transesterification with **GL** to produce **43** and by-product propylene glycol **33**. Screening of several alkali halides catalysts including NaCl, NaBr, NaI, KCl, KBr and KI demonstrated that higher efficiency was determined by the nucleophilicity of the counter anion and its leaving group ability. Among them, KI displayed a superior activity at a very low catalyst loading (0.75 mol%) in respect to **12**. Surprisingly, tuning **12**/**GL** molar ratio to 4:1 offered a conversion of **GL** exceeding 90%, even though KI is well known for displaying a low catalytic activity toward the cycloaddition of CO_2 onto epoxides. Hence, the authors assumed the occurrence of a co-catalytic mechanism enabling epoxide **12** activation by hydrogen bonding via OH groups of the vicinal polyol substrate that progressively formed propylene glycol **33** (Scheme 2.38). It was worth mentioning that as for the transesterification of **GL** it is an equilibrium-controlled reaction; thus, increasing the amount of carbonation reagent propylene carbonate (**66**) had also a positive effect on the formation of the desired glycerol carbonate **43**.

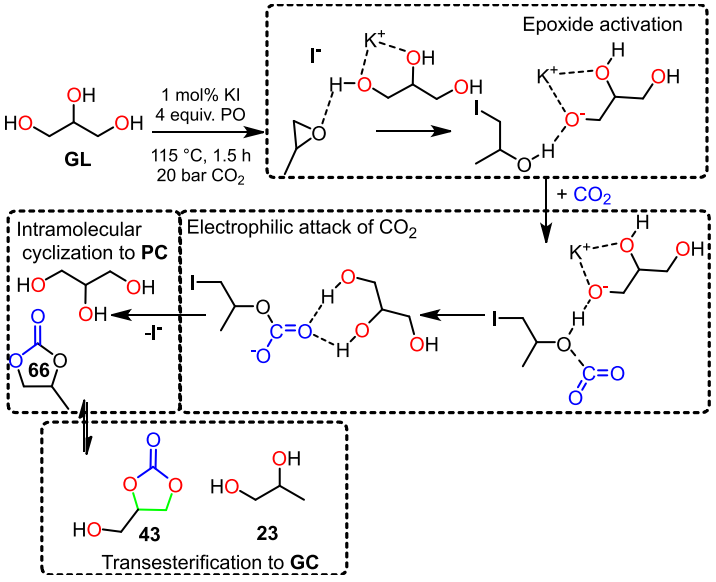

Scheme 2.38 One-pot catalytic carbonation process based on propylene oxide **12** as coupling agent.[150]

Using similar reactional conditions, Pescarmona and co-workers reported cheap and readily accessible catalytic system based on ion exchange-type amberlite polymeric beads (ammonium forms) bearing iodide or hydroxy counter anions.[181] Preliminary study of **GL**

transesterification identified Amb-OH-910-OH as the most active resin, ascribed to higher basicity of OH^- compared to I^-, hence facilitating substrate deprotonation. Amb-OH-910-I was found to be the most efficient for the cycloaddition of CO_2 on epoxides. Next, a one-pot synthesis was performed using a combination of both catalysts in various proportions. Remarkably, Amb-OH-910-I used as single catalyst achieved the best yield toward glycerol carbonate **43** and propylene glycol **33** (27 and 37%, respectively). A higher content of **33** was attributed to residual water contained in glycerol which led to the hydrolysis of propylene oxide **12**. When introducing Amb-OH-910-OH to the catalytic system, it was found to be detrimental to the reaction outcome, with increasing loading correlated to decreasing yields of glycerol carbonate **43**. These results supported that besides Amb-OH-910-OH activity toward transesterification, it was also involved in the catalysis of **12** hydrolysis, resulting in lower production of propylene carbonate **66**. Furthermore, the poor efficiency of Amb-OH-910-I for the cycloaddition of CO_2 with epoxides was counterbalanced by the activation of epoxides through hydrogen bonding with the OH groups of the substrate. Under optimized conditions, 69% yield of 43 and 67% yield of 66 were obtained (115 °C for 2 h under 20 bar of CO_2). Finally, the stability of the catalyst was validated for 4 successive runs with only a slight deactivation caused by iodide exchange with other anions.

Xia and co-workers described another process for the indirect carbonation of neat **GL** catalyzed by heterogeneous 1-vinyl-3-butylimidazolium bromide network using reticulating agent divinyl benzene (DVB).[182] The preparation of the catalyst was determinant for the reaction outcome: samples produced by the functionalization of an imidazolium monomer with nBuBr prior their polymerization [P-DVB-(vIm-BuBr)] gave superior performances, reaching up to 81% yield in glycerol carbonate **43** over 69% obtained for a sample prepared trough copolymerization of imidazolium monomers and DVB, prior its functionalization [P-(DVB-vIm)-BuBr]. These results were correlated with the lower content in IL on P-(DVB-vIm)-BuBr. The optimum conditions with such heterogeneous IL catalyst (4 wt%) involved heating at 100 °C for 4 h under 20 bar of CO_2 with a 4 :1 **12**/**GL** ratio. The catalyst reusability was ensured over 5 cycles without noticeable drop of activity.

Liu and al. described indirect carbonation of a library of diols using propargylic alcohol (**67**) and organocatalyst DBU in DMF.[22] Propargylic alcohol **67** acted as a coupling agent and reacted with CO_2 to produce an α-alkylidene cyclic carbonate intermediate **84**, which was then consumed to generate the corresponding cyclic carbonates and 3-hydroxy-3-methylbutan-2-one (**68**) as a by-product. The authors notably observed a higher yield in by-product **68** compared to the desired cyclic carbonate, which was imputed to the competitive hydrolysis of **63**. Nevertheless, increasing temperature to 120 °C narrowed the difference between both product contents, in other words, it promoted the carbonation reaction toward cyclic carbonate, thus improving the yield toward glycerol carbonate **43** (120 °C for 10 h under 30 bar of CO_2). A likely mechanism relied on (a) the activation of CO_2 and propargylic alcohol **67** with DBU, followed by (b) formation of cyclic intermediate **63**. It is worth mentioning that the presence of an exocyclic olefin led to a higher cyclic carbonate ring strain, resulting in an enhancement of their reactivity with diols. Intermediate alcoholysis consisted in the nucleophilic attack of a diol alkoxide, yielding an enol species which tautomerizes into a ketone, and thus, to catalyst recycling (Scheme 2.39).[175] The fast rearrangement of the enol intermediate into a more stable tautomer ketone is seen as the

driving force of the reaction.[183] In the last step (Scheme 2.39), the desired carbonate and the α-hydroxyketone by-product **68** are generated through intramolecular cyclization of ketone intermediate.[22]

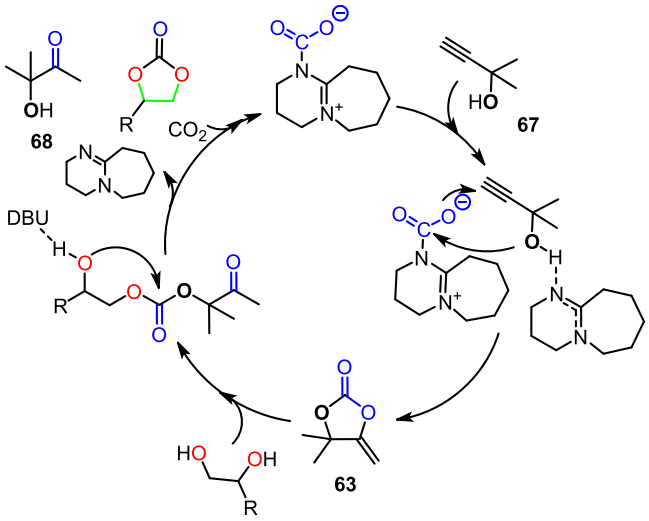

Scheme 2.39 Catalytic cycle for the carbonation of polyols with CO_2/DBU and propargylic alcohol **67**.[22,175,183]

Lu and co-workers developed a versatile cascade synthesis with propargylic alcohol **67** as coupling agent, catalyzed by a dual system Lewis/Brønsted bases under mild conditions (25 °C and 1 atm of CO_2).[21] The conditions also include the presence of 1-methyl-1,5,7-triazabicyclo[4.4.0]dec-5-ene (TBD) as a catalyst and acetonitrile as a solvent. Both steps were performed within 24 h of reaction time. Once optimized, such one-pot synthesis was extended to various bio-based polyols including **GL**, **ERY**, **XY** and **SO**. Given their multiple reactive sites, the chemoselectivity is very cumbersome to control. The authors attempted to tune the selectivity through various **67**/substrate molar ratios. For instance, the carbonation of **ERY** with one equivalent of **67** led to anhydroerythritol carbonate **69**, whereas the reaction in the presence of 2 equivalents mainly produced erythritol dicarbonate **54**. Overall, the results obtained for the conversion of polyols toward the corresponding cyclic carbonates in DMF gave variable results, mostly according to the nature of the substrate, with yields ranging from 33 to 92%. Noteworthy, such process conditions enabled the retention of the stereochemistry of the substrate (Figure 2.10).

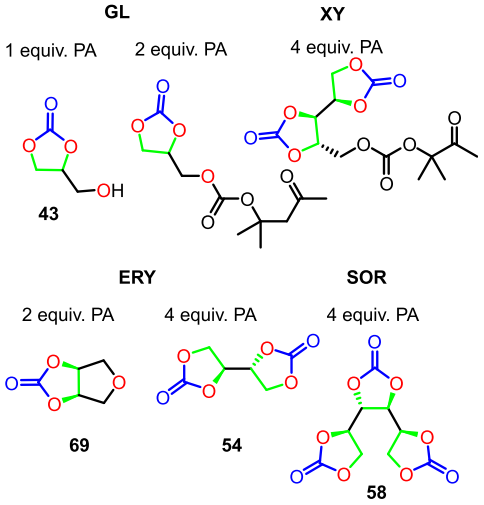

Figure 2.10 Scope of Lu's protocol on various bio-based polyols (**GL**, **ERY**, **XY** and **SO**). The parent bio-based vicinal polyol is indicated above the structures of the corresponding carbonates.[21]

Carbonates and carbamide as carbonation agents. With an increasing number of reports on the development of innovative carbonation technologies, a broad range of carbonating agents were developed overtime.[152] The safety and environmental concerns associated with the use of phosgene led to the development of other, less problematic carbonation reagents.[184] By contrast, urea is a very appealing carbonating agent widely available at low cost and much safer to use than phosgene, despite the release of corrosive gaseous ammonia as by-product. Urea also requires elevated temperature under vacuum pressure or continuous gas flow to shift the equilibrium upon the carbonation of diols,[185] and besides urea as a solid typically imposes the use of a solvent,[25] hence negatively impacting on the overall environmental footprint. Another alternative relies on diphenyl carbonate **55**, which enables to work with smaller excess in respect to substrate compared to dimethyl carbonate **38**, although it generates phenol as a side product and still requires the use of a solvent.[185] As more reactive species, yet considered as safe, dimethyl carbonate **38**, diethyl carbonate, ethylene carbonate **44** and propylene carbonate **66** carbonates are valuable and well-studied alternatives. In particular, **38** is widely studied because of its low toxicity as well as it can be prepared from urea.[186] The transesterification of diols with **38** under relatively smooth conditions in the presence of a suited catalysts.[154] Despite the efficiency of **38** as a carbonation reagent and its ease of handling as a liquid, it is a poor solvent for bio-based vicinal polyols, hence resulting in mass transfer issues. Such hurdles add up to other technical challenges inherent to bio-based vicinal diols such as a spare solubility, viscosity (**GL**) or the need for adding polar solvents for solid polyols.

Over the past decade, **GL** emerged as a privileged substrate for the transesterification toward glycerol carbonate **43** using carbonation reagents is extensively covered in recent reviews concerning both batch,[19,114,153,154,187,188] and continuous conditions.[25,46,189] Consequently, the carbonation of **GL** with dimethyl carbonate **38** is not presented in the scope of this Review. The next paragraphs deal with carbonation of less common bio-based vicinal polyol

substrates, namely, **EG**, **ERY**, **XY** and **SO**. It is worth mentioning that among the numerous reported procedures, several synthetic procedures eventually led to a commercial scale application.[114]

Using dimethyl carbonate **38** both as a solvent and a carbonation agent, Mayakova and co-workers reported metal complex-based processes achieving the selective conversion **EG** (95% yield) when using air sensitive $Co(CO)_8$. In contrast, $W(CO)_6$ gave quantitative conversion with a 1,2-dimethoxyethane/ethylene carbonate **44** product distribution of 1.8:1 (1 h, 180 °C, 4 equiv. DMC, Table 2.2, entry 1), thus indicating partial methylation of glycols.[190]

Ebitani and co-workers described a process toward cyclic carbonates based on a basic hydrotalcite-hydromagnesite (HT/HM) catalyst in DMF. The ratio between both composites had a noticeable impact on the reaction rate with an optimal HM/HT 0.5:1 composition, whereas further increase in hydromagnesite content was detrimental, ascribed to the too large decrease of HT active sites density. Notably, HM composite did not exhibit any catalytic activity but the authors highlighted its ability to inhibit HT aggregation, as well as its efficient capacity of substrate adsorption, which had a key involvement on HT performances. Indeed, it was observed that the activity of HT strongly depended on substrate concentration in reactional medium; the coexistence of HM on the catalytic surface enabled to modulate diols concentration to fit within optimal working conditions of HT sites. Under optimized conditions, the authors reported a yield of 89% in ethylene carbonate **44** within 70 min of reaction time, at 100 °C in presence of 5 equivalents of dimethyl carbonate **38** (Table 2.2, entry 2).[191]

Xiao, Gao and Hong reported the transesterification of neat **EG** with dimethyl carbonate **38** as carbonation agent catalyzed by heterogeneous Ca-Mg-Al hydrotalcite modified with KF depositions (KF/HT). Using an excess of **38** (**GL**/**38** 1:3 ratio), the conversion of **EG** into the corresponding carbonate **44** reached 98% yield (100% select.) at 80 °C within 30 min of residence time (Table 2.2, entry 3). The optimal catalyst loading was of 5 mol% and its stability could be maintained for up to 10 reaction runs.[192]

Bruijnincx and co-workers reported a system based on N-heterocyclic carbenes with an imidazole derived organocatalyst (NHC) toward production of cyclic carbonates. With an optimized catalyst, ethylene carbonate **44** reached 58% yield at 74 °C after 6 h of reaction with 1 mol% catalyst (Table 2.2, entry 4).[158]

Hou and co-workers developed an innovative catalytic system relying on CO_2/DBU/alcohol aimed at the transesterification of alcohols with dimethyl carbonate **38** (Table 2.2, entry 5). Using ethanol as model substrate, the introduction of CO_2 up to 10 bar was beneficial to the yield, which was attributed to the formation of an ionic liquid species ([DBUH][$O(CO)OCH_2CH_3$]). However, increasing the pressure had a negative effect, putatively imputed to the diminution of DBU content due to its increasing immobilization to form [DBUH][$O(CO)OCH_2CH_3$], hence leading to a decrease in available active species. Remarkably, when the reaction was carried out between 70-80 °C, it gave lower yields in presence of carbon dioxide, whereas an opposite trend was noticed at a process temperature

≥ 90 °C. This clearly emphasized a temperature dependency for such catalytic system CO_2/DBU/alcohol. This was later confirmed by experiments studying the DBU/[$DBUH^+$] molar ratio as a function of temperature, resulting in an increasing ratio at higher temperature, supposedly caused by the thermal degradation of ionic liquid species. This explanation was also supported by the occurrence of ionic product under solid state at low temperature in a non-polar solvent (toluene). At a higher temperature (90 °C), complete miscibility was noticed. Besides this fact, the solid state of catalyst greatly facilitated its recovery and recycling. Finally, the authors proposed a combined mechanism consisting in the conventional road with nucleophilic activation of carbonation agent by DBU, forming the N-alkoxycarbonyl DBU derivative [$DBU(CO)OCH_3$], which could subsequently be activated by strong hydrogen bonding with [$DBUH^+$] conjugated acid, eventually leading to the desired cyclic carbonate. This study clearly showed that the basicity of the catalyst was not sufficient to predict both the conversion and selectivity for such transesterification reaction. This process was next extended to **EG** (46% yield) and a library of carbamates and aliphatic carbonates could be also synthesized (yields ranging from 46 to 85%). Owing to incomplete recovery of the catalyst after reaction, the conversion progressively decreased, yielding 80% after 5 runs, whereas the selectivity remained steady. Nevertheless, given the need for a stoichiometric amount of DBU, the global efficiency of the process is questionable.[193]

In 2018, Kim, Lee, and Baral proposed a transesterification procedure for vicinal diols based on TBD as an organocatalyst and diphenyl carbonate **55** as the carbonation reagent in 2-methyltetrahydrofuran (2-Me-THF). Although DMC stands as a much greener alternative, its lower reactivity compared to diphenyl carbonate **55** required the implementation of more drastic reaction conditions. Though, the use of diphenyl carbonate **55** was conditioned by the presence of a solvent to ensure miscibility with vicinal diols. 91% yield of ethylene carbonate **44** was obtained at very low temperature of 30 °C (2 h reaction time), with a nearly stoichiometric amount of **55** (1.1:1 **GL**/**55** ratio) and 2 mol% TBD. A variety of sterically tri- and tetra-substituted carbonates was also reachable at yields ranging at 56-98% yields (Table 2.2, entry 6).[184]

Table 2.2 Summary of reactions dedicated to the indirect carbonation of ethylene glycol toward **44** with carbonating agents.

Entry	Catalyst	Conditions	**44** (%)	Ref.
1	$Co(CO)_8$	4 equiv. **38**, 180 °C, 1 h	95	[190]
2	HT/HM	5 equiv. **38**, 100 °C, 70 min, DMF	89	[191]
3	KF/HT	3 equiv. **38**, 80 °C, 0.5 h	98	[192]
4	NHC	6 equiv. **38**, 74 °C, 6 h	58	[158]
5	DBU	3 equiv. **38**, 100 °C, 14 h, toluene, 10 bar CO_2	46	[193]
6	TBD	1.1 equiv. **55**, 30 °C, 2 h, Me-THF	91	[184]
7[a,b]	Barton's base	3 equiv. **38**, 135 °C, 2 min, 7 bar	65	[185]
8[a,b]	TBAB	3 equiv. **38**, 180 °C, 3 min, 11 bar	75	[152]
9[a,b]	-	15 equiv. **38**, 240 °C, 15 min, 50 bar	82	[194]

A series of articles featured the use of new process technologies for the preparation of cyclic organic carbonates. For instance, in 2018, Monbaliu and co-workers studied the performances of a library of organic bases for the development of a continuous-flow preparation of a library of cyclic carbonates derived from vicinal diols (Scheme 2.40). The screening of catalysts was performed with **GL** as a valuable model substrate and involved candidates with pK_{BH+} in the range of 23.6-32.9. Barton's base (2-tert-butyl-1,1,3,3-tetramethylguanidine) and various sterically hindered phosphazenes emerged from the screening as the most potent catalysts (conv. 94-97%, select. 83-87%; Table 2.2, entry 7). Interestingly, phosphazenes were associated with superior conversions but lower selectivities toward glycerol carbonate **38**, due the competitive decarboxylation of glycerol carbonate **38** toward glycidol **4**. The much higher costs associated with phosphazenes eventually led to the selection of Barton's base as the best compromise. Next, their heterogeneous version was also assessed over extended time on stream, highlighting a similar drop of catalyst activity within the first hours of reaction and reaching a plateau around 80% yield after 80 h of operation. The heterogeneous version of the catalysts was seen as a way to simplify downstream processing, although the decrease of the conversion led the authors to select the homogeneous strategy. The latter was successfully transposed to several substrates featuring apical and/or internal diols, with yields ranging between 57 and 84%. This process was further translated at pilot scale under mesofluidic conditions (reactor with a total internal volume of 40 mL) with Barton's base, offering a productivity of glycerol carbonate about 8 kg per day (98% conv., 80% sel.) within 2 min of residence time, at 135 °C, 1 mol% DBU and 3 equivalents of dimethyl carbonate **38** (7 bar).[185]

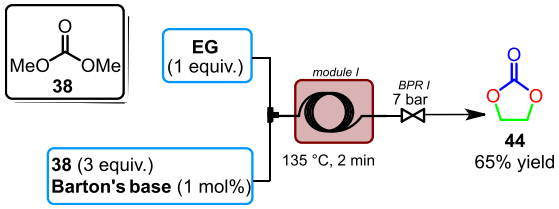

Scheme 2.40 Continuous flow procedure aiming at the carbonation of ethylene glycol with dimethyl carbonate catalyzed by Barton's base.[185]

One year later, Monbaliu and co-workers reported a similar continuous-flow process relying on a much cheaper and widely available quaternary ammonium salt catalyst. The optimized conditions with 3.5 mol% of tetrabutylammonium gave 88% yield toward **EC** within 3 min of residence time at 180 °C and 3 equivalents of dimethyl carbonate **38** (11 bar; Table 2.2, entry 8).[152]

In parallel, Selva and co-workers reported a catalyst-free thermal transesterification of vicinal diols with dimethyl carbonate **38** in continuous-flow reactor. Under superheated conditions, **EG** was converted to reach 82% yield at 240 °C (50 bar) with a residence time of 15 min, in presence of a large excess of **38** (15 equiv.; Table 2.2, entry 9).

In 2017, Mülhaupt and co-workers proposed a synthetic procedure toward erythritol dicarbonate **54** with diphenyl carbonate **55** and zinc acetate in dimethyl sulfoxide. Under a

reduced pressure of 30 mbar at 120 °C (19 h reaction time), the by-product phenol was continuously distilled off to yield 80-90% erythritol dicarbonate **54** after recrystallization.[160] The same group also developed a related process toward sorbitol tricarbonate **58** catalyzed by K_2CO_3. Recrystallization of the crude material in acetone afforded a 70% yield of STC. The authors also proposed another sequential process consisting in the dimerization of acrolein **7** to form hexa-1,5-diene-3,4-diol, followed by a transesterification with diethyl carbonate. Afterwards, the olefins were subjected to epoxidation using meta-chloroperoxybenzoic acid (mCPBA) and their further carboxylation with CO_2, to eventually yield sorbitol tricarbonate **58** (Scheme 2.41).[164]

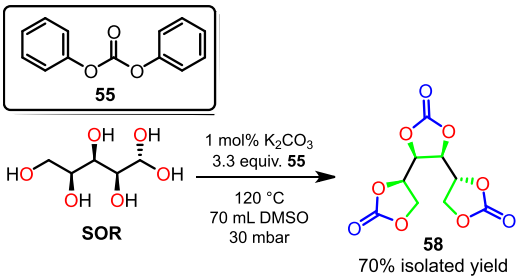

Scheme 2.41 Carbonation of sorbitol with 3.3 equiv. of diphenyl carbonate at 120 °C under reduced pressure to yield 70% of **58**.[164]

In contrast to Mülhaupt *et al.*, Meier and Dannecker developed a greener and more sustainable transesterification of **ERY** with dimethyl carbonate **38** both as a solvent and a reagent in the presence of TBD as an organocatalyst. Although **ERY** was sparingly soluble in **38**, heating the reaction mixture to 60 °C gradually enabled its dissolution. The reaction was carried out under reduced pressure to continuously remove methanol and shift the equilibrium toward the formation of erythritol dicarbonate **54** that was obtained in 90% yield after 40 min of reaction time. Through simple product filtration, the reaction medium could be recycled by adding both fresh **38** and **ERY** and the catalytic activity was maintained for 8 consecutive runs. Interestingly, the reaction time was shortened to 25 min, most likely due to the presence of seeds of erythritol dicarbonate **54** which promoted its crystallization.[161]

In 2012, Rockiki and co-workers studied the formation of tetrahydrofuran derivatives containing five-membered cyclic carbonates using dimethyl carbonate **38**, complex polyols and basic K_2CO_3 as a catalyst under reduced pressure. 1,4-Dioxane was used as solvent to partially overcome the usual mass transfer issue. When this reaction was implemented on **ERY**, it was found that the distribution of products could be tuned according to molar ratio of **ERY**/**38**. With a stoichiometric amount, the reaction mainly led to 1,4-anhydroerythritol **14**, whereas with an excess **38**, the carbonated version of **14** was obtained. Remarkably, the same reaction was performed at 70 °C in place of 90 °C and gave an unexpectedly low content of erythritol dicarbonate **54** (5% yield), suggesting that a lower temperature tends to decrease the extent of polyol etherification to the benefit of its double carbonation. With **SO**, the outcome of the reaction depended on which pair of vicinal diols the installation of the first cyclic carbonate would proceed. At position 6, a competitive additional decarboxylation of the intermediate resulted in an etherified species bearing a vicinal diol in *cis* position as well as another on aliphatic chain, thus yielding a tricyclic derivative of tetrahydrofuran

containing two cyclic carbonates (43% yield) **56**. In contrast, the carbonation of the primary OH group at position 1 led to the formation of a tetrahydrofuran intermediate species featuring a *trans* vicinal diol which could not be carbonated due to highly strained ring, eventually leading to isosorbide **57** (Scheme 2.42).[195]

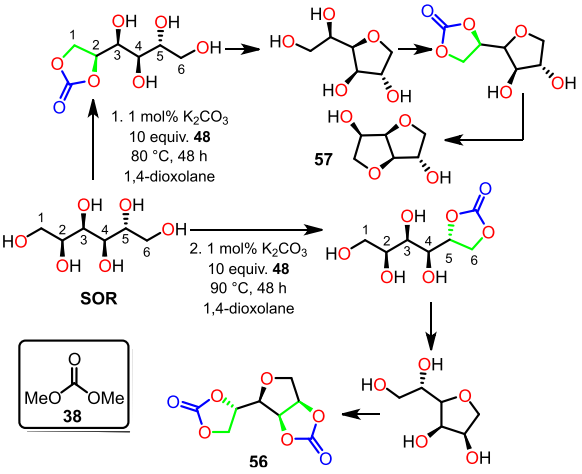

Scheme 2.42 Carbonation of sorbitol with dimethyl carbonate showing the competitive pathways.[195]

Zachara and co-workers reported the production of sorbitol bis(cyclo-carbonate) **56**. Since their previous work underlined the poor solubility of **SO** in 1,4-dioxane, the authors switched to more polar solvents. Surprisingly, methanol was selected, even if it is co-generated as side product of the carbonation with dimethyl carbonate **38**. The authors argued that the presence of methanol promoted the conversion of undesirable linear carbonates into their corresponding cyclic carbonate. The conversion of **SO** relied on a 2-step process starting with the complete solubilization of the polyol under reflux (3 h, 60 °C) and followed with the removal of methanol by distillation over 24 h, giving a precipitate. Depending on the vicinal diol pair involved in the carbonation process, the corresponding tetrahydrofuran intermediate would bear a pair of hydroxy groups positioned in *cis* or *trans* hence leading to two distinct products: the target compound **56** (40% yield) and the side product. Since dimethyl carbonate **38**/methanol formed an azeotrope (thus decreasing the overall process atom economy), a combination of diethyl carbonate and ethanol was also assessed but only achieved very low conversion (4% yield, Scheme 2.43).[196]

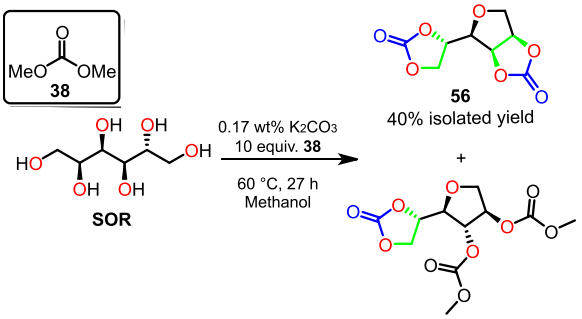

Scheme 2.43 Reaction of sorbitol with dimethyl carbonate toward sorbitol bis(cyclo-carbonate) **56**.[196]

Furtwengler and Avérous investigated a library of organic, organometallic and inorganic catalysts aimed at the carbonation of D-**SO** with dimethyl carbonate **38** as both reagent and solvent. The results identified TBD as the most efficient catalyst, which gave 45% yield of sorbitol bis(cyclo-carbonate) **56** over 48 h reaction time at 75 °C. A lower temperature negatively impacted the process due to a lower catalyst solubility in the reaction medium. To prevent **38** losses through evaporation, a continuous supply of **38** (15 mL h^{-1}) was implemented to the distillation setup to maintain a constant and optimal **38**/**SO** molar ratio of 3.35, achieving 50% yield of bicarbonate **56** in 16 h.[162]

2.4.5 CYCLIC KETALS FROM BIO-BASED POLYOLS: KETALIZATION OF VICINAL DIOL

2.4.5.1 KETALS AS VERSATILE COMPOUNDS AND BIODEGRADABLE MONOMERS

The ketalization of carbonyl compounds with diols is a common transformation (Figure 2.11), which is typically implemented to ensure chemoselective transformation upon protection of aldehydes or ketones within the frame of complex organic synthesis,[197] though it also concerns the production of fuel additives and the manufacturing of building blocks toward high added-value. Ketals have also a promising future in the polymer industry as biodegradable smart polymers.[198] The formation of ketals typically involves toxic solvents and is catalyzed by homogeneous acids such as HCl, H_2SO_4, CF_3CO_2H or *p*-toluenesulfonic acid, which require specific equipment and are harmful and difficult to recycle.[199,200] Furthermore, they often require complex and expensive purification steps.[201] Given these numerous drawbacks, heterogeneous catalysts were often seen as potential alternatives for improving the global efficiency, through easier catalyst recovery and the absence of neutralization step. Nevertheless, up to now, the use of heterogeneous catalysts did not reach comparable performances compared to sulfuric acid, underlying the challenging features of this reaction.[202,203]

Considering **EG**, its condensation with ketones leads to a 1,3-dioxolane backbone such as **EG** acetone ketal **70** (Figure 2.11) which finds various applications in the preparation of pharmaceuticals, polymers or even fragrance formulations. It has a versatile backbone, the substitution of which offers a versatile pool of chiral derivatives associated with large array of biological activities.[204] 2,2-Dimethyl-1,3-dioxolane-4-methanol (aka solketal, **71**) is a well-known upgraded polyol synthesized from the reaction between **GL** and acetone **35** (Figure 2.11). Its preparation comes with an appealing atom economy and has a current market value estimated to 22 billion US$ per year.[23,205] Solketal **71** is primarily used as a fuel additive. The incorporation of **71** in fuel enables to minimize the formation of small particles upon combustion in engines; it also enhances the viscosity and the cold flow properties of the resulting fuel blend. However, it increases the fuel density, which in turn has a negative impact on the engine operation.[23,37] Solketal **71** is considered as non-toxic for mammals, and is therefore also used as a suspending agent or as precursor in pharmaceutical preparations.[206]

Glycerol levulinate ketal (**72**) is a novel bio-based compound arising from the ketalization of **GL** with methyl levulinate (**73**; Figure 2.11). Owing to its unique molecular structure, it is expected to develop several applications in the field of biodegradable surfactants, polymers, additives or as green solvent due to its broad solubility, as well as in plasticizers and coatings.[207,208] Given the promising wide spectrum of applications of this compound, the development of commercial scale production facilities is undergoing, such as with Segetis Inc.[209] Globally, this growing interest is not only limited to glycerol levulinate ketal **72** but is extended to all levulinic acid derived ketals, such as glycerol levulinic acid ketal (**74**).[207] (4*R*,4'*S*)-2,2,2',2'-tetramethyl-4,4'-bis(1,3-dioxolane) (aka erythritol bisacetone ketal, **75**), which is synthesized through a double condensation of acetone on **ERY**, offers an attractive symmetrical 1,3-dioxolane structure system with lots of potential for the design of innovative biodegradable polymers (Figure 2.11).[198] Similarly, (1*S*,2*S*)-1,2-bis(2,2-dimethyl-1,3-dioxolan-4-yl)ethane-1,2-diol (aka sorbitol bisketal, **76**) is also reachable through a double ketalization of the two apical pairs of vicinal diols on **SO**. Recently, Xu and co-workers reported the preparation of sorbitol bisketal **75** in the frame of a strategy to specifically control internal OH groups etherification toward isosorbide **57**, which is typically manufactured from a poorly selective double dehydration of **SO** (Figure 2.11).[210]

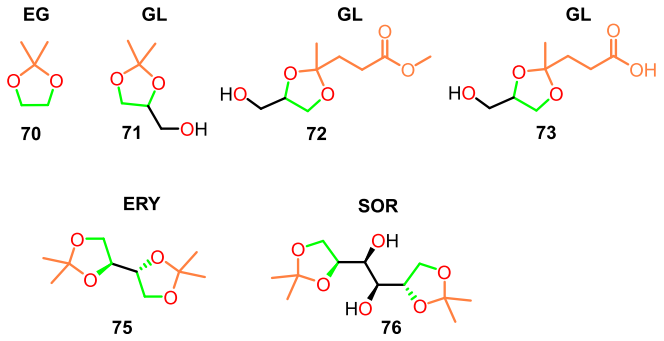

Figure 2.11 Overview of most common -based ketals. The parent bio-based vicinal polyol is indicated above the structures.

2.4.5.2 KETALIZATION OF BIO-BASED VICINAL DIOLS WITH ACETONE

A typical ketalization reaction is catalyzed either by Brønsted or Lewis acids. A classical reaction outcome starting with **GL** is composed of two ketals: a 5-membered ring ketal **71** and a 6-membered ring ketal **77**, the former being predominant. The favored formation of the 5-membered ketal is typically explained by steric hindrance in the 6-membered ketals caused by one of the methyl group at the axial position (Scheme 2.44).[23]

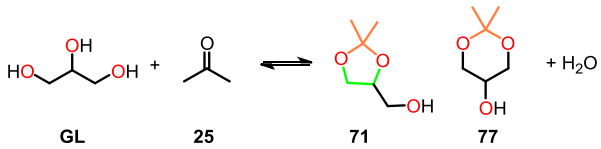

Scheme 2.44 5-membered and 6-membered ketals generated from the reaction between glycerol and acetone **25**.[23]

The formation of a ketal is an equilibrium that cogenerates water, which means that without actions to remove water, the formation of a ketal will be limited by the equilibrium thermodynamic constant.[205] Consequently, dehydration additives are often required, as well as the use of one of the reagents in excess. At the lab scale, a Dean-Stark apparatus is often relied on in conjunction with solvents such as cyclohexane, benzene or toluene. Similar to glycerol carbonate **38**, solketal **71** has received a significant attention over the last decades due to its promising future as fuel additive. Its preparation and use have already been covered by recent and thorough reviews in the presence of homogeneous and heterogeneous catalysts in both batch and continuous flow conditions.[23,25,37,206,211] Therefore, the preparation of **71** from **GL** will not be detailed here. The next paragraphs will be devoted to the ketalization bio-based vicinal diols and are organized according to the nature of the catalyst.

Homogeneous acidic catalysts. As an illustration of homogeneous acidic catalysis for the ketalization of **EG**, Xie and co-workers reported a ketalization process with HCl as a catalyst in the presence of trimethyl orthoformate **78** as a dehydration additive (Table 2.3, entry 1). With orthoformate **78**, reaction completion was observed within 12 h, whereas in the absence of **78**, a very low conversion (7%) was observed even after 24 h. In presence of 1.2 equivalents of **78**, the reaction with **EG** as substrate, and for some examples as solvent, gave 91% with pentane-3-one (ketal **79**) and 94% with cyclopentanone (ketal **80**) after 24 h at room temperature (Scheme 2.45). Other examples are ketals **81** and **82**.[197]

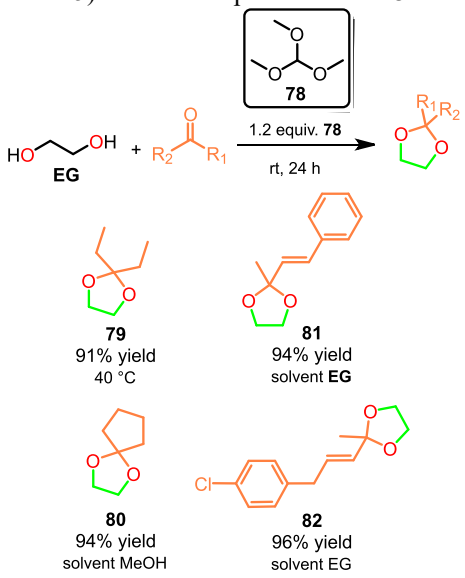

Scheme 2.45 Scope of Xie's work on ketalization of various diols substrates.[197]

Xu and co-workers reported a protocol toward glycerol levulinate ketal **72** based on methyl levulinate and sulfuric acid. Upon optimization, 1 equivalent of methyl levulinate **73** was reacted with 4.4 equivalents of **GL** and 0.27 mmol of catalyst, yielding 72 in 97.2% at 123 °C (under 90 kPa) in 30 min reaction time with a Dean-Stark apparatus (Table 2.3, entry 2 and Scheme 2.46). When the optimized conditions were transposed to crude **73**, the yield decreased to 85%.[209]

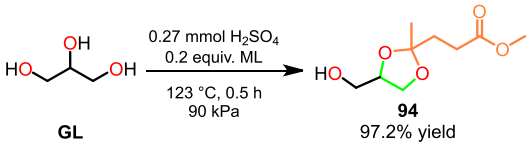

Scheme 2.46 Preparation of glycerol levulinate ketal **72**.[209]

Heterogeneous metal-based catalysts. Yang and co-workers described a cobalt-based catalyst with dimethylglyoxime (DH_2) as a ligand for the ketalization of vicinal diols under neat conditions. Several cobalt-based salts were assessed with $CoCl_2$, $Co(NO_3)_2$, $CoSO_4$ and $Co(OAc)_2$ as catalysts for the ketalization of 1,2-propanediol (**23**) in the presence of cyclohexanone (Table 2.3, entry 3). $CoCl_2$ gave the highest conversion (95%, ≥ 99% selectivity) followed by $Co(NO_3)_2$ and $CoSO_4$ with 90 and 49%, respectively. These results were explained by the axial unoccupied sites of the intermediate cobaloxime species (Scheme 2.47a). In the case of $CoCl_2$, the formation of the active catalytic species led to the generation of 2 equivalents of HCl, which could easily be removed from the reaction medium at 70 °C under 0.05 bar, hence, creating 2 catalytic sites (Scheme 2.47b). Similarly, the reaction with $Co(NO_3)_2$ produced HNO_3, that was removed from the reaction mixture through its degradation in NO_2. The authors stated that, in contrast with the previous cobalt salts, the use of $CoSO_4$ would generate H_2SO_4, which is more difficult to remove from the reaction medium hence resulting in a lower activity. $Co(OAc)_2$ did not give any conversion. Based on this process, various carbonyl compounds were assessed to obtain ketal and acetal derivatives of vicinal diols such as **EG**, giving yields ranging from 79 to 99%.[212]

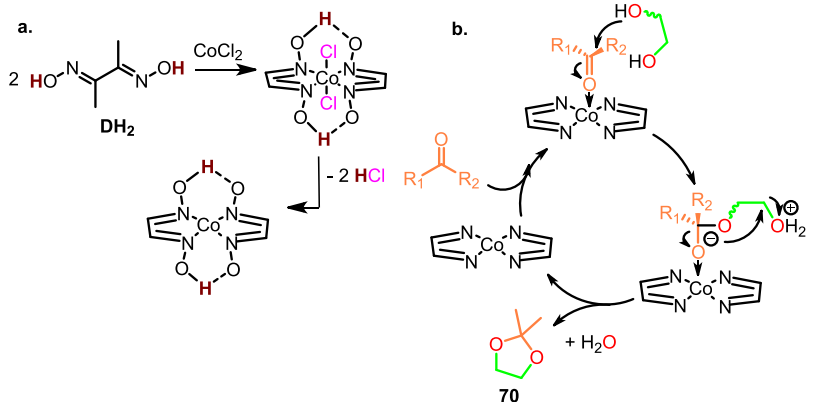

Scheme 2.47 (a) Formation of catalytic species using cobalt based salt and diglyoxime as well as (b) mechanism of ketal formation from **EG**.[212]

Su and co-workers studied CuI metal-organic frameworks with phosphine ligands in presence of diverse counterions such as Br^-, Cl^- and $PF6^-$. Among the various candidates, samples with $PF6^-$ (CuL-PF6) exhibited the higher activity, indicating that catalytic performances depend on the nature of the anion (Table 2.3, entry 4). Owing to the low coordination of $PF6^-$, the metal center was largely available for the substrate. The authors also assessed the impact of the bulkiness of the ketone substrates on reaction outcome, showing that compounds with increasing steric hindrance led to decreasing yields of the respective ketal (2-

butanone>cyclohexanone>1-phenylethan-1-one>diphenylmethanone). This phenomenon was also attributed to lower accessibility of metal center and thus, demonstrating the size dependency of the reaction. Furthermore, the weak Lewis acidity of CuI was expected to have a stronger impact on the reactivity of electron rich substrates such as 2-butanone and cyclohexanone than on electron deficient compounds. Nevertheless, the catalytic stability was only ensured for three cycles.[213]

Under similar reactional conditions, Oliver and co-workers developed an alternative process relying on MOF constituted of barium centers organized in layers and covalently linked by ethanedisulfonate bridges ($Ba_2F_2[OSC_2H_4SO_3]$) that remained less active (37% yield) than CuL-PF6 for the reaction of **EG** with 2-butanone (Table 2.3, entry 5).[214]

Shao, Ou, and Zhong described a process using a phosphorous incorporated solid SO_4^{2-}/TiO_2 catalyst while ensuring similar performances for the ketalization of **EG** with cyclohexanone (99% yield) over 6 successive batch experiments (Table 2.3, entry 6).[203]

In 2016, Nascimento and co-workers studied several heterogeneous catalysts including niobium phosphate, sulfonic resin and zeolite aimed at the ketalization of ethylene glycol with ethyl 4-oxopentanoate. Among catalytic samples, NbP was the only candidate able to selectively form the ketal derivative (conv. 54%, sel. 100%) without side reactions arising from diol transesterification (Table 2.3, entry 7). These results were attributed to the lower acidity of the catalyst upon the other samples.[215]

Heterogeneous metal-free catalysts. A series of reports concerned the development and use of silica-based heterogeneous catalysts. Čejka and co-workers investigated the catalytic performances of weak acidic germanosilicate zeolites with the large pores IWW (Si/Ge=4.2) and extra-large-pores UTL (Si/Ge=7.2) over commercial aluminosilicates zeolites β (BEA) and mordenites (MOR), both depicting strong Brønsted and Lewis acidic properties. Under solvent-free conditions, comparative experiments using **GL** demonstrated the superior catalytic efficiency of IWW in comparison to UTL, whereas the latter was characterized by a higher content of Ge and a larger crystal size and volume of micropores. Thus, textural features seemed to suggest that UTL were associated with higher mass transfer limitation than IWW. Moreover, UTL only displayed Lewis acidic centers whereas IWW also possessed water induced Brønsted acid sites, which appeared to be more active for diol ketalization. Increasing the activation temperature up to 300 °C had a positive impact on IWW activity, which was correlated to an increased Lewis acidity and a decrease of Brønsted acidity. When used for the ketalization of **GL** toward solketal **71**, IWW exhibited similar performance (55% yield of solketal) over commercial catalyst BEA while outperforming MOR (14%). Since the formation of ketal **71** is an equilibrium, increasing the excess of acetone **35** to 25 equivalents had a positive impact on the production of **71** (>99%) at room temperature within 3 h. Catalyst stability was ensured for 3 reactions cycles with no leaching of Ge. This process was then successfully extended to the ketalization of **EG** with 35 (>99%) or with methyl ethyl ketone (95%; Table 2.3, entry 8). By contrast, more complex polyols such as butane-1,4-diol (**6**) gave much lower yields (18-68%).[216]

Duan and co-workers proposed $H_4SiW_6Mo_6O_{40}/SiO_2$ as catalytic system for ketalization of **EG** with cyclohexanone, offering 80% yield of 1,4-dioxaspiro[4.5]decane in 50 min of reaction time whereas maintaining similar activity over 4 reaction runs (Table 2.3, entry 9).[201]

In 2014, Song reported a heterogeneous catalyst $H_4[SiW_{12}O_{40}]$ supported on SiO_2 to prevent an important leaching of H-SiW_{12} in the reaction medium. Under solvent-free conditions, the ketalization of **EG** proceeded well with 83% yield in 6 h (Table 2.3, entry 10); comparable results were ensured over 10 cycles.[217]

Tang and co-workers studied catalyst efficiency of zeolite nanofiber assemblies (NB-MOR), its H-form analog produced from NH^{4+} ion exchange (HNB-MOR) and mesoporous aluminosilicate (Al-MCH-41). From preliminary tests involving the ketalization of alcohols, mordenite composites depicted superior activities over Al-MCH-41, caused by aluminosilicate weaker acidic properties. The authors also compared a series of alcohols of different bulkiness and showed that the conversion of smaller alcohols was similar for both MOR samples, whereas reactions involving bulkier alcohols led to low catalytic activity for NB-MOR, owing to mass-transfer limitation. Assessment of a library of ketones highlighted the higher performance of HNB-MOR, for example the ketalization of **EG** with cyclohexanone that gave 91% (50 °C, 12 h 0.2:0.6 cyclohexanone/**EG**; Table 2.3, entry 11). The catalyst remained active for 10 cycles with similar performance.[218]

Table 2.3 Overview of reactions performed on ethylene glycol, glycerol or *meso*-erythritol ketalization with diverse ketones.

Entry	Ketone agent (equivalents)	Conditions	Ketal (%)	Ref.
1[a]	Cyclopentone (0.8)	rt, 1.2 equiv. **78**, MeOH, HCl	94	[197]
2[a,b,c]	Methyl levulinate (0.2)	123 °C, 90 kPa, 0.5 h, H_2SO_4	97.2	[209]
3[d,e]	Cyclohexanone (0.7)	70 °C, 1 h, 0.05 bar, $CoCl_2/DH_2$	99	[212]
4[b,d]	Cyclohexanone (1)	110 °C, toluene, 12 h, CUL-PF_6	93	[213]
5[b,d]	2-Butanone (1)	110 °C, toluene, 12 h, $Ba_2F_2[OSC_2H_4SO_3]$	37	[214]
6[b,d]	Cyclohexanone (0.8)	80 °C, cyclohexane, 2 h, SO_4^{2-}/TiO_2-P cat.	99	[203]
7[b,d]	Ethyl levulinate (0.5)	110 °C, toluene, 4 h, NbP	54	[215]
8[d,e]	Acetone (0.5)	80 °C, 3 h, UTL	99	[216]
9[b,d]	Cyclohexanone (0.7)	80 °C, cyclohexane, 50 min, $H_4SiW_6Mo_6O_{40}/SiO_2$	80	[201]
10[d,e]	Cyclohexanone (0.7)	60 °C, 6 h, $H_4[SiW_{12}O_{40}]/SiO_2$	83	[217]
11[d]	Cyclohexanone (0.33)	50 °C, acetonitrile, 12 h, HNB-MOR	91	[218]
12[b,d,e]	Cyclohexanone (0.83)	90°C, 1 h, cyclohexane, SC-34-SO_3H	98	[202]
13[d,e]	Cyclohexanone (1)	50 °C, 2 h, BAL-MOR	70	[219]
14[d]	2-Butanone (6)	25 °C, 2.5 h, ethanol, H-Sulfo-POSS	≈80%	[220]
15[d,e,f]	0.15 levulinic acid	190 °C, 1.5 h, D-Hβ	34	[221]
16[d,e]	Cyclohexanone (0.55)	85 °C, 3 h, SWIL/B-SBA-16	83	[222]
17[b,d]	Cyclohexanone (0.66)	120–125 °C, 1.25 h, cyclohexane, SBA-15/Al-IL	85	[223]
18[d,e]	Acetophenone	80 °C, 12 h, Clay H^+	66	[225]
19[d,e]	Acetone (0.5)	40 °C, 24 h, PILCs-Al-Zr	19	[199]
20[b,d]	Cyclohexanone (0.76)	120 °C, 2 h, cyclohexane, M-ZrPO	98	[226]
21[d,e]	2-Butanone (0.5)	90 °C, 14 h, $[Sb_2O_2(OH)]^+$	55	[227]
22[d,g]	Isopropenyl acetate (1)	30 °C, THF, Amberlyst-15	23	[228]
23[c, d,g]	Isopropenyl acetate (3)	30 °C, 16 h, Acetic acid, 5 equiv., Amberlyst-15	91	[229]
24[b,d]	Levulinic acid (0.1)	80 °C, 20 min, benzene, Amberlyst-15	88	[207]
25[b,d,h]	Acetone (3)	80 °C, 24 h, Amberlyst-15, benzene	53	[198]

Peng, Kun, Lin designed a strong acidic catalyst based on a mesoporous silica SBA-15 composite coated with polycyclic carbon layer using furfuryl alcohol and following functionalization with sulfonic acid (SC-34-SO_3H). The use of furfuryl alcohol rather than sucrose as a carbon source provided a uniform coating onto silica that prevented pore blockage and an improved substitution of SO_3H, therefore leading to superior acidic properties of SC-34-SO_3H (Table 2.3, entry 12).[202]

Yang's team reported a Brønsted acidic ionic liquid (SO_3H) catalyst supported on mordenite (BAL@MOR). In stoichiometric amount, **EG** reacted with cyclohexanone to yield the respective cyclic ketal around 70% after 2 h of reaction time at 50 °C (Table 2.3, entry 13).[219]

Vogt, Esteban, and Söderholm synthesized polystyrene-based sulfonate-octaphenyl POSS (polyhedral oligomeric silsesquioxanes) compounds (H-Sulfo-POSS) to catalyze the ketalization of **GL** reaction with 2-butanone at 25 °C (Table 2.3, entry 14). Three candidates of different sulfonation degrees were prepared and compared to commercial references such as para-toluenesulfonic acid (PTSA) and its heterogeneous analog Amberlyst-36. Ethanol was used as solvent to solubilize all partners. Higher catalytic performance was correlated with an increasing degree of sulfonation with TOS of 2601 h^{-1}, 1844 h^{-1} and 1587 h^{-1}, respectively, whereas PTSA reached 2256 h^{-1} and 213 h^{-1} Amberlyst-36. The assessment of the recyclability of the catalyst showed that the efficiency of H-Sulfo-POSS-3 progressively decreased over 10 runs to yield a mere 3% for the ketalization of **GL** with 2-butanone. The authors argued that the high solubility of the catalyst in the reaction medium was the primary case leading to poor recyclability.[220]

Parikh, Chakraborty and Umrigar reported a ketalization/esterification process on various vicinal diols with levulinic acid (**83**) under continuous-flow and microwave irradiated conditions catalyzed by a desilicated zeolite. The desilication technique enabled the selective extraction of silicon to increase Si/Al ratio, hence increasing the intrinsic acidic properties of the material, as well as improving molecular transport toward actives sites. Implementing a tubular reactor at 190 °C, reaction with levulinic acid **83** in presence of 8 equivalents of **EG** afforded 42% yield of 2-hydroxyethyl-4-oxopentanoate (**84**), 26% yield of ketone 3-(2-methyl-1,3-dioxolan-2-yl)propanoic acid (**85**) and 31% yield of keto-ester 2-hydroxyethyl-(2-methyl-1,3-dioxolan-2-yl)propanoate (**86**; Scheme 2.48 and Table 2.3, entry 15). For the same substrate under microwave irradiation, quantitative conversion was reached, yet the selectivity toward the three identified products was lower compared to the continuous-flow experiments: 24% for ester **112**, 34% for ketal **85**, 14% for ester ketal **86**, as well other products.[221]

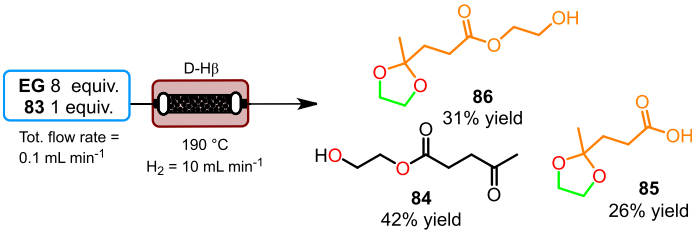

Scheme 2.48 Reaction output arising from the reaction of ethylene glycol with levulinic acid **83** under continuous flow conditions.[221]

Jiang and co-workers designed a heterogeneous catalyst based on boron modified SBA-16 nano-cages (large pore mesoporous silica) functionalized with tungstosilicic ionic liquid (SWIL/B-SBA-16) to both increase the number of acidic sites and enhance the acidity of the support. Boron content was determinant for the reaction outcome with an optimum Si/B=15; higher concentration of boron was detrimental due to occurrence of mass limitation caused by partial destruction of nano-cages. In the absence of both solvent and dehydrating agent, 1.8 equivalents of **EG** reacted with 1 equivalent of cyclohexanone to give the corresponding ketal derivative in 83% yield at 85 °C for 3 h (Table 2.3, entry 16). Interestingly, the use of a dehydrating agent did not improve the yield and required the addition of toluene. The catalyst could be reutilized for 8 cycles, with a moderate drop of activity, eventually yielding the corresponding ketal in 69.5%.[222]

Alternatively, Jiang and co-workers developed an immobilized chlorine-aluminate catalyst supported on SBA-15 aimed at **EG** ketalization with cyclohexanone (Table 2.3, entry 17).[223]

Xu and co-workers developed a novel process toward highly selective synthesis of isosorbide **57** via the ketalization of the apical vicinal diols of **SO** catalyzed by a H-beta zeolite, yielding sorbitol bisketal derivatives (Scheme 2.49). This strategy enabled an accurate control of the selective intramolecular etherification of internal OH groups to yield the targeted tetrahydrofuran derivatives. Using methyl isobutyl ketone as both reagent and solvent, **SO** gave 93% yield of isosorbide **57** underlying the efficiency of polyol ketalization in these conditions (170 °C, 2 h). This protocol was also extended to **ERY** and **XY**, giving 90% and 71%, respectively, of the corresponding tetrahydrofuran derivatives (Table 2.3, entry 18).[224]

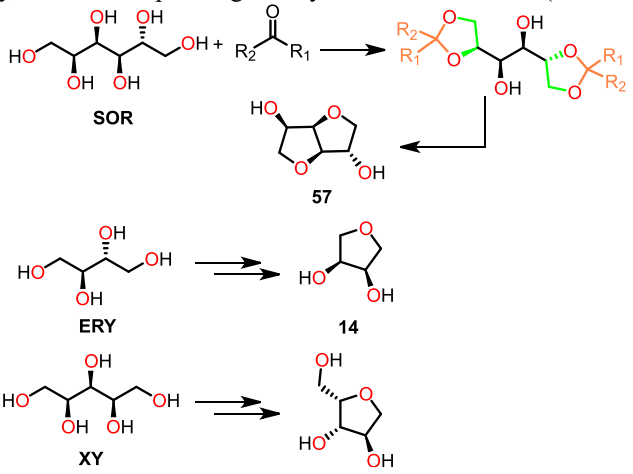

Scheme 2.49 Ketalization of the two apical pairs of sorbitol's vicinal pairs with a ketone agent.[224]

Miscellaneous. Besbes and co-workers developed an acid-activated clay (clay-H0.5) for the ketalization of **EG** (1 equiv.) and acetophenone **87** toward dioxolane **88**.[225] Compared to an inactivated catalyst that gave 29% yield of **EG** ketalization product **88**, the acid-activated clay gave 66% yield under the same reaction conditions (Scheme 2.50 and Table 2.3, entry 19), which was correlated to superior acidic sites density. Though, the catalytic activity gradually decreased over 6 successive runs, to afford a 61% yield of ketal **88**.

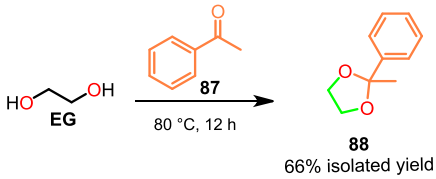

Scheme 2.50 Ketalization of **EG** with acetophenone toward 2,2-diphenyl-1,3-dioxolane (**119**).[199]

Another example was reported by Srasra and Ghnimi: the authors prepared sodium pillared interlayered clays (PILCs) modified by zirconium and alumina via cation exchange reaction, achieving ≈ 19% yield of 2,2-dimethyl-1,3-dioxolane (**70**) through the ketalization of **EG** and acetone **25** (0.5 equiv.) in 24 h reaction time at 40 °C.[199]

Chou and co-workers developed a ketalization process using a mesoporous zirconium oxophosphate (M-ZrPO) catalyst. Among the various ratio of P/Zr assessed, M-ZrPO-0.75-500 depicted the higher mesostructured uniformity as well as larger specific surface and pore volume, overall offering an enhanced accessibility of reactive sites. The determination of catalytic acidic properties by NH_3-TPD showed the occurrence of both Brønsted and Lewis acid sites, with the latter displaying stronger acidity. Under optimized conditions, the ketalization of **EG** was performed on a series of ketones, yielding the corresponding ketal product in 81 to 98% (Table 2.3, entry 20). The catalyst was reused up to 5 times without significant activity drop.[226]

Fei and Yin designed a process based on an inorganic two-dimensional network of antimony oxide hydroxide under solvent-free conditions. After 14 h of reaction time at 90 °C, up to 55% yield was obtained for the ketalization of **EG** with methyl ethyl ketone (Table 2.3, entry 21).[227]

Selva and co-workers reported a tandem reaction based on the conversion of vicinal diols with isopropenyl esters catalyzed by a heterogeneous acid Amberlyst-15 in a fixed-bed reactor (Scheme 2.51). Using prop-1-en-2-yl acetate (**89**) as reagent and THF as solvent, the transesterification with **EG** led to the generation of 2-hydroxyethyl acetate (**90**; conv. 94%, sel. 67%) and prop-1-ene-2-ol (**91**) in stoichiometric amount. Through enol-keto tautomerization, **91** was converted in the corresponding acetone **25**, which subsequently reacted with **EG** to yield 70 (sel. 31%), the ketal derivative of **EG** (Table 2.3, entry 22). In contrast, under optimized conditions, a reaction cascade with 1,2-propanediol (**23**) yielded an approximate 50:50 selectivity distribution toward monoester 2-hydroxypropyl acetate (**92**)/ketal 2,2,4-trimethyl-1,3-dioxolane (**93**) products. **EG** lower results were attributed to its faster transesterification, that is, decreased substrate availability for ketalization.[228]

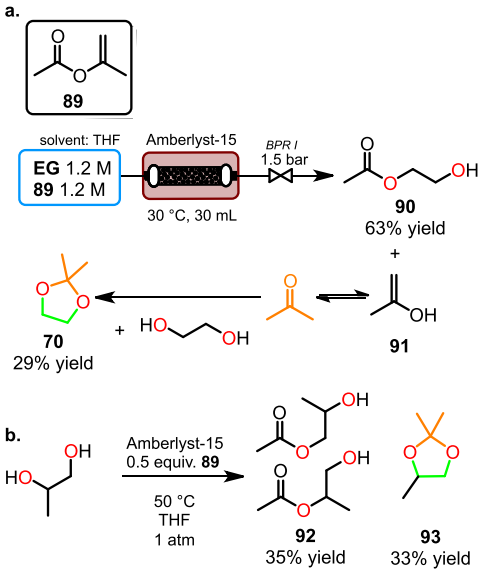

Scheme 2.51 (a) Continuous flow procedure for the reaction between ethylene glycol and isopropenyl acetate.[228] (b) Procedure for the reaction between propylene glycol and isopropenyl acetate.[228]

The same team also developed a ketalization/acetylation tandem one-pot sequence using **GL**, isopropenyl acetate **89**, acetone **25** and acidic Amberlyst-15 in presence of acetic acid **11** as solvent. Acetone **25**, which was produced *in situ* either from the tautomerization of **91** or the solvolysis of **89** with AcOH, reacted with **GL** to form a binary mixture of 5-membered ring and its 6-membered ring ketal analogs with a 97:3 ratio. The authors evaluated the impact of various reaction parameters on the reaction outcome and highlighted that the molar ratio and reaction time were paramount to control the selectivity. Indeed, increasing isopropenyl acetate **89**/**GL** ratio to 1:10 and extending reaction time to 32 h led to 51% yield of solketal acetate (**94**) and 49% yield of triacetin (**95**). Adjusting the **89**/**GL** ratio to 4 and adding a large excess of co-ketalizing agent acetone (20 equiv.) led to the complete disappearance of solketal **71**/2,2-dimethyl-1,3-dioxan-5-ol (**77**) for the benefit of solketal acetate **94**/2,2-dimethyl-1,3-dioxan-5-yl acetate (96; 85%) and the concomitant formation of triacetin **95** (Scheme 2.52 and Table 2.3, entry 23). Further experiments highlighted that modulation of the AcOH content to 1.5 equivalents in conjunction with an external intake of acetone **25** (tune to 5 equiv.) led to the formation of solketal acetate **94** as the major product (91%) and only traces of **71**/**77** (3%), as well as 2% 1,2-diacetin **97**/1,3-diacetin (**98**) and 7% triacetin **95**.[229]

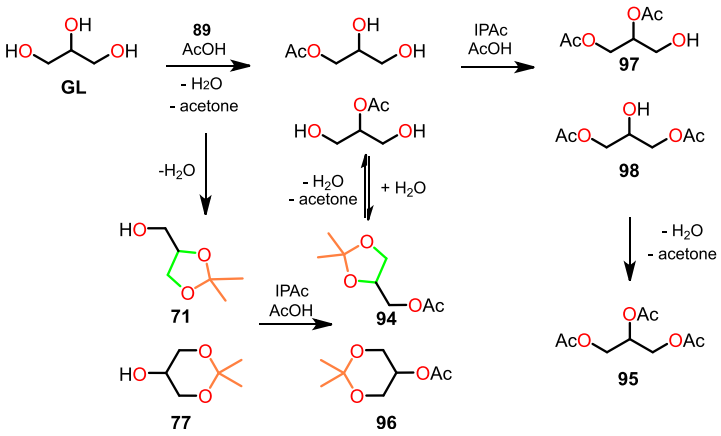

Scheme 2.52 Pathways toward the different reactional products formed through the reaction of glycerol and isopropenyl acetate **121**.[229]

Animashaun and Amarasekara described a one-pot ketalization/esterification toward the manufacturing of ketals derivatives of **EG** and levulinic acid **83** in presence of either Amberlyst-15 or homogeneous *p*-toluenesulfonic acid. The authors relied on benzene as solvent for assessing both catalysts. Indeed, *p*-TsOH activity generated predominantly the corresponding ester in 75% yield, whereas heterogeneous Amberlyst-15 led to 88% yield of the corresponding ketone **85** after 20 min; for prolonged reaction time (180 min), the ketone started to be converted into the corresponding ketone ester **86** (ca. 55% 86, ca. 45% **85**; see Scheme 2.48 and Table 2.3, entry 24).[207]

Timofeeva and co-workers studied the influence of homogeneous and heterogeneous Brønsted acids catalysts for the ketalization of **ERY** with various ketones (Scheme 2.53). Considering homogeneous catalysts such as *p*-toluenesulfonic acid (conditions a in Scheme 2.53) and 1-(3-propylsulfonic)-3-methyl-imidazolium chloride (conditions b in Scheme 2.53), total selectivity (conv. 92-95%) was achieved toward bis-ketal **75** with acetone **25** (Table 2.3, entry 25). By contrast, heterogeneous catalysts such as Amberlyst-15 (conditions c in Scheme 2.53) and $SiO\text{-}SO_3H$ (conditions d in Scheme 2.53) promoted partial or complete dehydration of **ERY** toward anhydroerythritol **14** and its subsequent ketalization toward ether ketal **99** in the presence of acetone **25**. Then, similar experiments were also performed with cyclic ketones. Their results showed complete selectivity toward bis-ketals species for all catalysts; cyclopentanone on the contrary gave complete selectivity toward the corresponding ketal ether with the heterogeneous catalysts. Overall, the results indicated that the steric hindrance of the ketone backbone was a critical parameter driving the selectivity. The authors also performed computations (HF/3-21G) to further characterize the driving forces controlling the selectivity; computations showed that the bis-ketal species was always the most thermodynamically stable compound, whereas ketals formed with acyclic ketones of increasing bulkiness were increasingly less stable thermodynamically.[198]

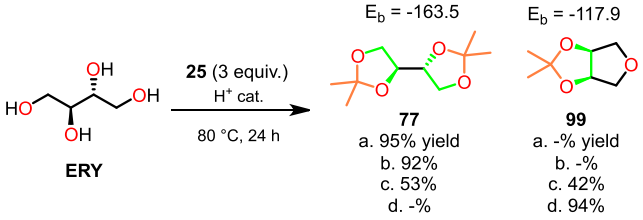

Scheme 2.53 Conversion of erythritol into bis-ketal **75** derived and ether ketal **99** with indication of the computed energies (in kcal mol^{-1}).[198]

2.4.6 GENERAL CONSIDERATIONS ON THE GREEN METRICS OF BIO-BASED PROCESSES

Despite the large variety of successful achievements for the development of process conditions aimed at the upgrading of bio-based vicinal polyols and the many incentives advocating a transition from petro-based to bio-based resources, the exploitation of bio-based platform molecules still stands as a major challenge for chemists and chemical engineers. Biomass refining toward bio-based platform molecules is currently far from offering similar performances compared to petro-based platforms and are typically generating a significantly higher volume of waste products. With respect to the central topic of this Review, the polyol backbone also imposes the development of new synthetic approaches to access the various drop-in, smart drop-in and dedicated bio-based platforms discussed in this manuscript. As detailed in the previous sections, the upgrading of bio-based vicinal polyols relies on the use of specific additives, appropriate solvents, suitable catalytic systems, unprecedented operating conditions or innovative technologies. Though, their implementation for the upgrading of bio-based platforms weighs a lot when it comes to assessing their global efficiency. The global process efficiency can be assessed through a diversity of metrics (so-called "green metrics") to quantify the overall environmental footprint.[230-233] Among the various green metrics available, the environmental factor (E-factor) developed by Sheldon in the 90s is still widely used as pertinent parameter to assess waste generation. It is defined as the ratio of the total mass of waste on the mass of synthesized product while lower value is interpreted as a process with a global low environmental footprint.[15] The E-factor value is inherently related to the nature and the context of process: (a) oil refining is usually associated with a very low E-factor (<1); (b) production roads leading to bulk chemical are usually characterized with E-factors ranging from 1 to 5; (c) processes toward fine chemicals procedures have E-factors in the 5-50 range and (d) the production of pharmaceuticals should not exceed an E-factor of 100.[234,235] These numbers are correlated with the complexity and the number of steps. As the upgraded molecules discussed in this work have predominant applications at the interface between bulk chemicals and fine chemicals, processes with E-factors ranging from 1 to 50 would be acceptable. Besides the E-factor, the Atom Economy, introduced by Trost in 1995,[236] is another very handy metric that enables to quantify both the effectiveness and the sustainability of a given process (or the compliance with most of 12 principles of Green Chemistry).[237] It is defined as the percentage of atoms from the reagents that are maintained in the final product. A reaction with 100% atom economy indicates the complete incorporation of reagents in the targeted product, thus, with no waste atoms. These metrics should be carefully handled since they exclude important process parameters such as

the temperature, pressure and specific chemical hazards. They remain, however, good and reliable indicators of the overall efficiency and suitability of a process within the context of lowering the overall environmental impact.

We have selected a few representative examples from the above sections and have subjected them to both E-factor and AE calculations. Table 2.4 summarizes the overall efficiency and environmental footprints for a selection of representative processes. A first overview of Table 2.4 shows that three selected processes are associated with an AE below 30%; 18 processes are associated with an AE between 30 and 65% and 9 processes have an AE superior to 65%. Based on the AE, it can already be stated that two third of alternative processes assessed in this work only incorporate 30-65% of atoms invested via the reagents and additives, hence impacting negatively the overall environmental footprint. To have deeper insights into waste generation, the E-factor is next considered for the same selection of process. It was calculated to consider solvent and catalyst mass, as well as all products (including by- and side-product), in contrast to AE. Table 2.4 shows favorable E-factor values comprised between 0.45 and 50 when excluding the example of DODH that relies on a very large excess of isopropyl alcohol (solvent and reductant), processes using high volumes of solvents intended for Dean-Stark apparatus and the carbonation protocols with CO_2. Although the amount of waste generated is important to consider, another fundamental aspect relies on the evaluation of the hazards and environmental impact of the waste products.[238]

Knowing that solvents represent the largest fraction of waste associated with a given process, it often becomes a determining factor in the calculation of the E-factor as it can represent up to half of the material used in a chemical process.[238] For instance, the use of methanol in the synthesis of sorbitol bis(cyclo-carbonate) **56** causes a significant increase of E factor value from 12.48 to 15.14 (Table 2.4, entry 24). It is clear that the selection of a solvent must be strictly guided to select the most suitable alternatives. Solvent selection guides are available, and among them, the CHEM21 selection guide is among the most elaborated and used of solvents as recommended and thus widely promoted as first solvent candidate to implement.[238] Coming back to the DODH example (Table 2.4, entry 4) that requires a large excess of isopropyl alcohol (as solvent and reductant), the less favorable E-factor (77.61) is somehow mitigated with the low toxicity of isopropanol, which is a recommended CHEM21 solvent.

The use of CO_2 even in large excess, is also highly encouraged to as a potential strategy to decrease atmospheric levels. Unfortunately, the processes developed so far are usually highly energy consuming and require additives; overall leading to unfavorable green metrics (Table 2.4, entries 17-20) and a poor global efficiency. Noteworthy, calculation of E-factor (Table 2.4) without considering CO_2 input enables to reach more acceptable processes.

Given the results of the two common metrics, it is clear that most of the examples presented in Table 2.4 fulfill neither the atom economy nor the waste prevention principles of Green Chemistry. It is therefore important to insist on the fact that sustainable processes have to be distinguished from bio-based processes, defined as chemical procedures exploiting bio-based molecules. The use of bio-based resources is a necessary condition, but it is not a sufficient condition to claim sustainability. The road toward sustainable bio-based processes is ahead

of us but still requires significant contributions from both the chemistry and chemical engineering communities.

2.4.7 CONCLUSION

As a direct consequence of the growth of the bio-based economy, numerous new alternative processes and technologies aimed at the upgrading of bio-based polyols are thriving under the drive of strong EU incentives toward a transition from classical petro-based processes. Despite many significant advances both from chemical and from process technology standpoints, bio-based processes are not ready yet to take over the petrochemical industry. Numerous challenges remain ahead. One of the main hurdles relates to their technology-readiness levels, which are typically around TRL 4-5 and thus still far from implementation at industrial scale and further commercialization. These processes rely on novel chemistries and conditions that are often drastically different from those developed for petro-based platforms, and usually display lower yields and selectivities than their petro-based analogs. With the increasing complexity of some higher bio-based polyols, managing chemoselectivity becomes overwhelming and requires the development of selective catalysts or process conditions to improve reaction selectivity, stoichiometry and the global reaction outcome. Much effort has been devoted to the identification of high-performing and benign catalytic systems with extended stability. However, a non-negligible proportion of catalysts still rely on low and extremely scarce volume elements such as the DODH reaction and the preponderant use of rhenium-derived catalysts, sacrificial reagents, and additives, as well as solvents with significant environmental impact. It is also critical to develop process conditions, additives, and catalysts that are amenable to low-purity, unrefined bio-based platforms to increase the cost-effectiveness of such processes. Most of these processes feeding on bio-based platforms are inherently associated with unfavorable sustainability metrics, which hence clearly pinpoint the areas of research where improvements and the next research efforts must be focused, such as solvents, additives, and process technologies with a lower environmental footprint. These are the mandatory steps to merge bio-based and sustainable processes toward an effective and radical shift in the current petro-based industrial paradigm.

From this overview, it can be stated that bio-based processes have the potential to supply industry with numerous building blocks (drop-in, smart drop-in, and dedicated platforms) including olefins, oxiranes, cyclic carbonates, and ketals. There is, however, still plenty of room for improvement in terms of selectivity, performance, and environmental footprint. Similarly, the organic chemistry dedicated to the exploitation of complex polyols including erythritol, xylitol, and sorbitol toward high added-value compounds is currently in its infancy. However, these polyols depict privileged structures for the manufacture of new chemical motifs, such as conjugated systems and cyclic carbonates, and therefore potentially stand as starting materials for new technological innovations. This Review was structured as a reference guide of five staple reactions that exploit vicinal diols and concrete examples of attainable molecules starting from bio-based polyols. It also aims to provide support for further advances and stimulate the creativity of chemists and chemical engineers involved in the development of bio-based processes.

Table 2.4 Calculation of environmental factor and atom economy for selected reactions of the five staple reactions discussed in this work.

Entry	Bio-based polyol	Category	Reagents & solvent (equivalents)	Temperature; Reaction time	Reaction conditions	Typical product(s) & yields [a]	E factor [b,d]	Atom economy [c]	Ref.
Olefins from bio-based vicinal diols – the deoxy-dehydration (DODH) reaction									
1	GL	Homogeneous metal	AHM= $(NH_4)_6Mo_7O_{24}.4H_2O$ (0.025) 1,5-pentanediol (0.33)	190 °C, up to completion	Reactive distillation	**3** 40% yield	18.64 (4.29)[f]	63.08	[80]
2			NH_4VO_3 (0.01)	275 °C, 5 h	Reactive distillation	**3** 22% yield **7** 4% yield	5.21	63.08	[84]
3		Homogeneous metal free	Triethyl orthoformate (1) Formic acid (0.1)	250 °C, 6 min	Continuous flow	**3** 22% yield **30** 8% yield	0.45[e]	24.17	[24]

Entry	Bio-based polyol	Category	Reagents & solvent (equivalents)	Temperature; Reaction time	Reaction conditions	Typical product(s) & yields [a]	E factor [b,d]	Atom economy [c]	Ref.
Olefins from bio-based vicinal diols – the deoxy-dehydration (DODH) reaction									
4	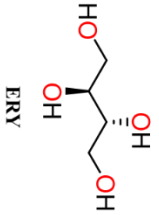 **ERY**	Homogeneous metal	AHM= $(NH4)_6Mo_7O_{24}.4H_2O$ (0.05) Isopropyl alcohol (32.75)	250 °C, 18 h	Under N_2[d]	 **13** 39% yield	77.61	57.39	[72]
5		Homogeneous metal free	Formic acid (2)	210-220 °C, 30 h	N_2[d], 3 cycles of distillation-cooling	 **13** 39% isolated yield	6.84	41.68	[70]
6	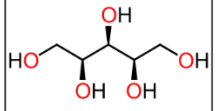 **XY**	Homogeneous metal free	Formic acid (12) Tetraglyme (0.29)	235 °C, 12 h	Batch continuous distillation	 **33** 8% yield 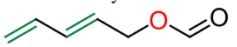 **31** 63% yield	8.92 (8.11)[j]	42.45	[87]

Entry	Bio-based polyol	Category	Reagents & solvent (equivalents)	Temperature; Reaction time	Reaction conditions	Typical product(s) & yields [a]	E factor [b,d]	Atom economy [c]	Ref.
Epoxides from bio-based polyols: carboxylation and consecutive Williamson's epoxidation or dehydrative epoxidation									
7	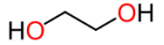 **EG**	Heterogeneous metal	Water (370) Cs/SiO_4 (0.1 g)	400 °C	Continuous flow	 **42** 14% yield  **40** 14% yield	1.95	70.97	[118]
8	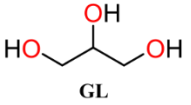 **GL**	Homogeneous metal	Urea (1) ZnO (0.002)/NH_4(OAc) (0.008)	1. 150 °C, 2 h, 0.027 bar 2. 175 °C, 1.5 h, 0.02 bar	Batch continuous distillation	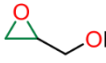 **4** 83% yield 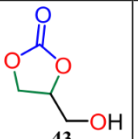 **43** 16% yield	2.13	48.69	[119]
9	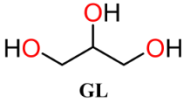 **GL**	Homogeneous metal free	Dimethyl carbonate (3) [DABCO][DMC] (0.06)	100 °C, 0.5 h	Batch	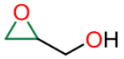 **4** 58% yield 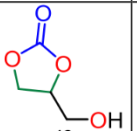 **43** 5% yield	3.66	40.67	[123]
10			HCl 35% (6) NaOH 4M (9) Acetic acid (0.1)	1.140 °C, 20 min 2. rt, 10 min	Continuous flow	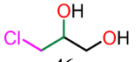 **46** 65% yield 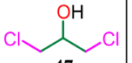 **47** 14% yield	6.83[k]	65.59	[117]

Entry	Bio-based polyol	Category	Reagents & solvent (equivalents)	Temperature; Reaction time	Reaction conditions	Typical product(s) & yields [a]	E factor [b,d]	Atom economy [c]	Ref.
Epoxides from bio-based polyols: carboxylation and consecutive Williamson's epoxidation or dehydrative epoxidation									
11		Homogeneous metal free	HCl (6.48) Adipic acid (0.069)	110 °C, 14 h	Reactor (distillation) was purged with N_2[d] before reaction	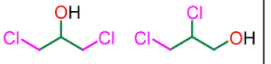 **47** 89% yield **52** 1% yield 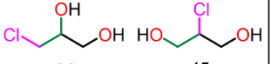 **46** 3.7% yield **45** 2.7% yield	1.92	78.18	[133]
12			HCl 35% (6) NaOH 4M (9) Pimelic acid (0.1) MTBE (23.37)	140 °C, 20 min	Continuous flow	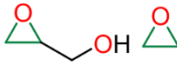 **4** 83% yield 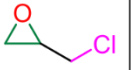 **5** 44% isolated yield	43,49[k,o]	54.90	[117]

Entry	Bio-based polyol	Category	Reagents & solvent (equivalents)	Temperature; Reaction time	Reaction conditions	Typical product(s) & yields [a]	E factor [b,d]	Atom economy [c]	Ref.
Epoxides from bio-based polyols: carboxylation and consecutive Williamson's epoxidation or dehydrative epoxidation									
13		Homogeneous metal free	Acyl chloride (1.38)	100 °C, less than 2 h	Batch	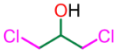 **47** 92% yield 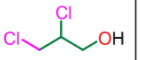 **52** 4% yield 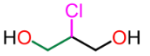 **45** 4% yield	0.56	51.79	[135]
14	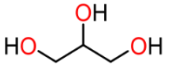 **GL** 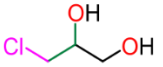 **3-MCH**		TMSCl (2.7) Acid acetic (0.05)	100 °C, 12 h	Batch	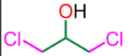 **47** 96% yield 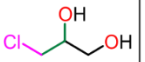 **46** 4% yield	2.59	61.54	[135]

Entry	Bio-based polyol	Category	Reagents & solvent (equivalents)	Temperature; Reaction time	Reaction conditions	Typical product(s) & yields [a]	E factor [b,d]	Atom economy [c]	Ref.
Five membered cyclic carbonates from bio-based polyols – direct or indirect carbonation of vicinal diol									
15	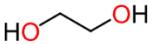 **EG**	Heterogeneous metal	KF/Ca-Mg-Al HT (0.05) DMC (3)	80 °C, 0.5 h	Distillation	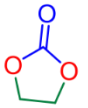 **44** 98% yield	2.85	57.88	[192]
16		Homogeneous metal free	Barton's base (0.01) DMC (3)	135 °C, 2 min	Continuous flow	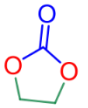 **44** 78% yield	3.86	57.88	[185]
17	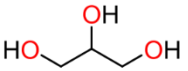 **GL**	Homogeneous metal	CO_2 (26.54) CaC_2 (5) $Zn(OTf)_2$ (0,05) 1,10-phenanthroline (0.15) NMP (62.34)	180 °C, 24 h	Batch	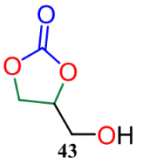 **43** 92% yield	21565 (60.10)[g] (21507)[j]	86.77	[118]

Entry	Bio-based polyol	Category	Reagents & solvent (equivalents)	Temperature; Reaction time	Reaction conditions	Typical product(s) & yields [a]	E factor [b,d]	Atom economy [c]	Ref.
Five membered cyclic carbonates from bio-based polyols – direct or indirect carbonation of vicinal diol									
18		Homogeneous metal free	CO_2 (15.94) 2-cyanoporidine (3)	180 °C, 12 h	Batch	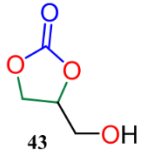 **43** 18.7% yield	2561 (17.33)[g]	86.77	[181]
19		Heterogeneous metal free	CO_2 (26.54) Propylene oxide (4) Amb-OH-910[l] Mesitylene (0.3)	115 °C, 2 h	Batch	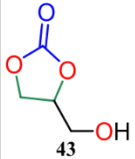 **43** 18.7% yield 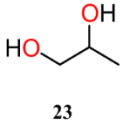 **23** 67% yield	84.12f (1.76)[g,f] (83,85)[j,f]	60.82	[181]
20		Homogeneous metal free	CO_2 (0.01) Propargylic alcohol (1.5) DBU (40) DMF (25.83)	120 °C, 10 h	Batch	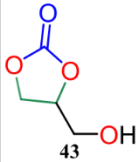 **43** 69% yield 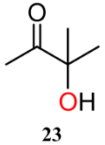 **23** 67% yield	11772.26 (11.11)[g] (7527.16)[j]	61.46	[22]

Entry	Bio-based polyol	Category	Reagents & solvent (equivalents)	Temperature; Reaction time	Reaction conditions	Typical product(s) & yields [a]	E factor [b,d]	Atom economy [c]	Ref.
Five membered cyclic carbonates from bio-based polyols – direct or indirect carbonation of vicinal diol									
21	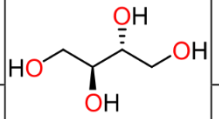 **ERY**	Homogeneous metal free	DPC (2.10) $Zn(OAc)_2.2H_2O$ (0.01) DMSO (2.77)	120 °C, 19 h	Vacuum distillation (30 mbar)	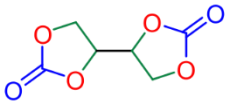 **54** 85% isolated yield	4.24 (2.78)[j]	31.62	[84]
22		Homogeneous metal free	DMC (29.70) TBD (0.05)	60 °C, 40 min	Vacuum distillation (314 mbar)	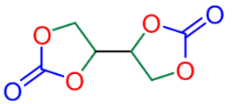 **54** 90% isolated yield	16.89	57.60	[161]

Entry	Bio-based polyol	Category	Reagents & solvent (equivalents)	Temperature; Reaction time	Reaction conditions	Typical product(s) & yields [a]	E factor [b,d]	Atom economy [c]	Ref.
Five membered cyclic carbonates from bio-based polyols – direct or indirect carbonation of vicinal diol									
23	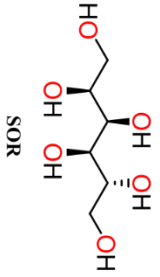 SOR	Homogeneous metal free	DPC (3.3) DMSO (3.3) K_2CO_3 (0.01)	120 °C	Vacuum distillation (30 mbar)	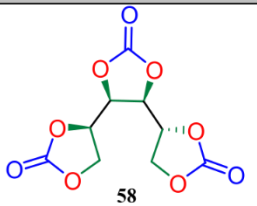 **58** 70% isolated yield	5.30 (3.89)[j]	31.54	[164]
24			MeOH (7.18) DMC (10) K_2CO_3 (0.22)	66 °C, 27 h	Reflux for 3 h followed by MeOH distillation	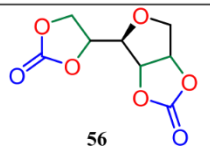 **56** 40% isolated yield	15.14 (12.48)[j]	47.48	[196]
25			DMC (3.5) TBD (0.05)	75 °C, 16 h	Distillation	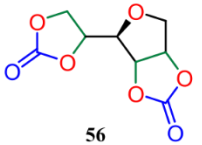 **56** 50% isolated yield	45.43	47.48	[162]

Entry	Bio-based polyol	Category	Reagents & solvent (equivalents)	Temperature; Reaction time	Reaction conditions	Typical product(s) & yields [a]	E factor [b,d]	Atom economy [c]	Ref.
Cyclic ketals from bio-based polyols: the ketalization of vicinal diols									
26	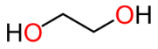 **EG**	Heterogeneous metal	Cyclohexanone (1) Toluene (1.2) Cu-PF6 (0.002)	90 °C, 12 h	Dean-Stark	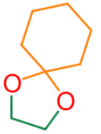 93% yield	1.07 (0.24)[j]	88.75	[213]
27			Acetone (5) UTL[m]	80 °C, 3 h	Dean-Stark	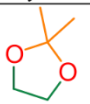 **70** 99% yield	2.50	85.00	[216]
28			Isopropenyl acetate (1) THF (10.23) Amberlyst-15 (0.8 g)	30 °C, 0.19 h	Continuous flow	 **70** 29% yield 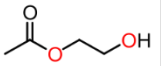 **90** 63% yield 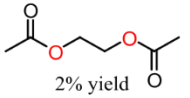 2% yield	8.18 (0.)[j]	62.97	[228]

Entry	Bio-based polyol	Category	Reagents & solvent (equivalents)	Temperature; Reaction time	Reaction conditions	Typical product(s) & yields [a]	E factor [b,d]	Atom economy [c]	Ref.
Cyclic ketals from bio-based polyols: the ketalization of vicinal diols									
29	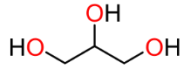 **GL**	Homogeneous metal free	Methyl levulinate (0.23) H_2SO_4 (0.002)	123 °C, 0.5 h	Vacuum distillation (90 kPa)	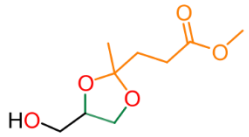 **72** 97% yield	1.70[p]	91.90	[209]
30	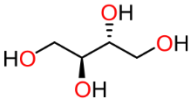 **ERY**	Homogeneous metal free	Cyclohexanol (0.76) Amberlyst-15[n,i] (0.05) benzene (112.12)	80 °C, 24 h	Vacuum distillation (90 kPa)	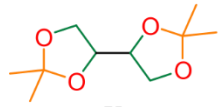 **75** 54% yield	81.96[f] (1.75)[i,f]	84.68	[198]

[a] All represented reaction products are considered as valuable. [b] calculated with the formula E-factor = (mass of total inputs) – (mass of valuable products)/mass of valuable products. [c] atom economy = [(M.W. of targeted product)/(∑M.W. of reagents); d inert gases are not included in the E factor calculation. [d] inert gases are not included in the E factor calculation. [e] ethanol is not considered as a waste since it can be distilled off before allyl alcohol; [f] the catalyst quantity is divided by the number of cycles; [g] CO_2 is not included in E-factor calculation. [h] Gas volume is hypothetically fixed to reactor volume. [i] indirectly determined from the catalyst H+ concentration and catalyst molar mass of 314 g/mol; [j] solvent is not considered in E-factor calculation; [k] water is not considered in E-factor calculation; [l] 0.095 g of catalyst for 5 mmol of ethylene glycol; [m] 0.005 g of catalyst for 0.001 mol of glycerol; [n] 0.01 g of catalyst for 2 mmol of glycerol; [o] purification step comprised into E factor calculation.

2.5 REFERENCES

[1] Roadmap for the Chemical Industry towards a Bioeconomy, https://roadtobio.eu/uploads/publications/deliverables/RoadToBio_D21_RegulatoryBarriers.pdf (accessed on 10-17-21).

[2] B. R. Keeble, *Med. War* **1988**, *4*, 17–25.

[3] K. McCormick, N. Kautto, *Sustainability* **2013**, *5*, 2589–2608.

[4] What is Horizon 2020?, http://h2020ni.com/what-is-horizon-2020/ (accessed on 10-30-21).

[5] What is Horizon Europe?, https://www.horizon-eu.eu/ (accessed on 10-12-21).

[6] ESFRI: Making science happen, https://www.esfri.eu/sites/default/files/White_paper_ESFRI-final.pdf (accessed on 12-09-21).

[7] Innovation for sustainable growth: A bioeconomy for Europe, https://op.europa.eu/en/publication-detail/-/publication/1f0d8515-8dc0-4435-ba53-9570e47dbd51 (accessed on 10-5-21).

[8] Review of the 2012 European Bioeconomy Strategy, https://ec.europa.eu/information_society/newsroom/image/

document/2018-6/review_of_2012_eu_bes_2E89B85F-950B-9C84-5B426D1C24851387_49692.pdf (accessed on 10-5-21).

[9] RoadToBio, https://roadtobio.eu/uploads/publications/roadmap/

RoadToBio_action_plan.pdf (accessed on 10-5-21)

[10] Bio-based opportunities for the chemical industry: Where bio-based chemicals meet existing value chains in Europe, https://roadtobio.eu/uploads/publications/deliverables/

RoadToBio_D11_Bio-based_opportunities_for_the_chemical_industry.pdf (accessed on 09-22-21).

[11] What are Technology Readiness Levels (TLRs) and to which Horizon 2020 call topics are they applicable? https://ec.europa.eu/info/funding-tenders/opportunities/portal/screen/support/faq/2890 (accessed on 09-09-21).

[12] Roadmap for the Chemical Industry in Europe towards a Bioeconomy: Concept of bio-based and circular economy, https://roadtobio.eu/uploads/publications/deliverables/

RoadToBio_D25_Biobased_and_circular_economy.pdf (accessed on 09-16-21)

[13] Renewable Energy-Recast to 2030 (RED II), https://ec.europa.eu/jrc/en/jec/renewable-energy-recast-2030-red-ii (accessed on 10-03-21).

[14] M. Carus, L. Dammer, *Ind. Biotechnol*. **2018**, 14, 83–91.

[15] F. Martins, C. Felgueiras, M. Smitkova, N. Caetano, *Energies* **2019**, 12, 964.

[16] N. N. Tshibalonza, J. C. M. Monbaliu, *Green Chem.* **2020**, 22, 4801–4848.

[17] Top Value Added Chemicals from Biomass Volume I-Results of Screening for Potential Candidates from Sugars and Synthesis Gas Produced by the Staff at Pacific Northwest National Laboratory (PNNL) National Renewable Energy Laboratory (NREL) Office of Biomass, http://www.osti.gov/bridge (accessed on 10-5-21).

[18] J. J. Bozell, G. R. Petersen, *Green Chem.* **2010**, 12, 539–554.

[19] D. Voet, J. G. Voet, *Biochemistry*, 2nd edn., J. Wiley & Sons (New York, US), **1996**, pp. 649-655.

[20] J. ten Dam, U. Hanefeld, ChemSusChem 2011, 4, 1017–1034.

[21] E. Santacesaria, R. Vitiello, R. Tesser, V. Russo, R. Turco, M. Di Serio, *Ind. Eng. Chem. Res.* **2013**, 53, 8939–8962.

[22] H. Zhou, H. Zhang, S. Mu, W.-Z. Zhang, W.-M. Ren, X.-B. Lu, *Green Chem.* **2019**, 21, 6335–6341.

[23] L. H. Han, J. Y. Li, Q. W. Song, K. Zhang, Q. X. Zhang, X. F. Sun, P. Liu, *Chinese Chem. Lett.* **2020**, 31, 341–344.

[24] I. Corrêa, R. P. V. Faria, A. E. Rodrigues, *Sustain. Chem.* **2021**, 2, 286–324.

[25] N. N. Tshibalonza, J.-C. M. Monbaliu, *Green Chem.* **2017**, 19, 3006–3013.

[26] R. Gérardy, D. P. Debecker, J. Estager, P. Luis, J. C. M. Monbaliu, *Chem. Rev.* **2020**, 120, 7219–7347.

[27] Y. Nakagawa, T. Kasumi, J. Ogihara, M. Tamura, T. Arai, K. Tomishige, *ACS Omega* **2020**, 5, 2520–2530.

[28] A. Rywińska, M. Marcinkiewicz, E. Cibis, W. Rymowicz, *Prep. Biochem. Biotechnol.* **2015**, 45, 515–529.

[29] O. Rosales-Calderon, V. Arantes, Biotechnol. *Biofuels* **2019**, 12, 240.

[30] M. Rakicka-Pustułka, A. M. Mirończuk, E. Celińska, W. Białas, W. Rymowicz, *J. Clean. Prod.* **2020**, 257, 120533.

[31] Reducing Added Sugars with Polyols, https://www.ift.org/news-and-publications/food-technology-magazine/issues/2016/november/features/reducing-added-sugars-with-polyols (accessed on 09-20-21).

[32] A. Muscat, E. M. de Olde, I. J. M. de Boer, R. Ripoll-Bosch, *Glob. Food Sec.* **2020**, 25, 100330.

[33] A. N. Marchesan, M. P. Oncken, R. Maciel Filho, M. R. Wolf Maciel, *Green Chem.* **2019**, 21, 5168–5194.

[34] Ethylene glycols, https://www.indiaglycols.com/divisions/ethylene_glycols.htm (accessed on 09-24-21).

[35] Bio-Based Chemicals: A 2020 Update, https://www.ieabioenergy.com/wp-content/uploads/2020/02/Bio-based-chemicals-a-2020-update-final-200213.pdf (accessed on 09-17-21).

[36] S. Rebsdat, D. Mayer, Ullmann's Encyclopedia of Industrial Chemistry, 6th edn., Wiley-VCH Verlag GmbH & Co. KGaA(Weinheim, DE), **2012**, pp. 531–546.

[37] I. Zahid, M. Ayoub, B. B. Abdullah, M. H. Nazir, M. Ameen, Zulqarnain, M. H. Mohd Yusoff, A. Inayat, M. Danish, *Ind. Eng. Chem. Res.* **2020**, 59, 20961–20978.

[38] Cargill production of biodiesel using sewage water, https://www.lecho.be/entreprises/energie/cargill-produira-a-gand-du-diesel-a-partir-d-eaux-usees/10259573.html (accessed on 10-11-21).

[39] Bioro Biodiesel Refinery, https://www.cargill.com/agriculture/bioro-biodiesel-refinery (accessed o10-11-21).

[40] H. Aatola, M. Larmi, T. Sarjovaara, *SAE Int. J. Engines* **2009**, 1, 1251–1262.

[41] J. Kaur, A. K. Sarma, M. K. Jha, P. Gera, *Biotechnol. Reports* **2020**, 27, e00487.

[42] S. Nomanbhay, M. Y. Ong, K. W. Chew, P.-L. Show, M. K. Lam, W.-H. Chen, *Energies* **2020**, 13, 1483.

[43] H. Russmayer, M. Egermeier, D. Kalemasi, M. Sauer, *Biotechnol. Adv.* **2019**, 37, 107395.

[44] L. Kumar, R. Kaur, R. Tyagi, P. Drogui, *Bioresour. Technol.* **2021**, 323, 124565.

[45] A. Rodrigues, J. C. Bordado, R. G. dos Santos, *Energies* **2017**, 10, 1817.

[46] R. S. Varma, C. Len, Curr. Opin. *Green Sustain. Chem.* **2019**, 15, 83–90.

[47] A. R. Abbasi, J. Liu, Z. Wang, A. Zhao, H. Ying, L. Qu, M. A. Alam, W. Xiong, J. Xu, Y. Lv, Front. *Bioeng. Biotechnol.* **2021**, 9, 648382.

[48] H. Schiweck, A. Bär, R. Vogel, E. Schwarz, M. Kunz, C. Dusautois, A. Clement, C. Lefranc, B. Lüssem, M. Moser, S. Peters, Ullmann's Encyclopedia of Industrial Chemistry, 6th edn., Wiley-VCH Verlag GmbH & Co. KGaA (Weinheim, DE), **2012**, pp. 1–37.

[49] Erythritol Market Report 2021, https://www.wboc.com/story/44457236/erythritol-market-report-2021-production-capacity-demand-and-supply-sales-margin-cost-analysis-2024 (accessed on 10-29-21).

[50] S. N. Gunasekara, J. Stalin, M. Marçal, R. Delubac, A. Karabanova, J. N. Wei Chiu, V. Martin, *Energy Procedia* **2017**, 135, 249–262.

[51] P. Chi, S. Wang, X. Ge, M. Bilal, P. Fickers, H. Cheng, *Biochem. Eng. J.* **2019**, 149, 107259.

[52] W. H. Faveere, S. Van Praet, B. Vermeeren, K. N. R. Dumoleijn, K. Moonen, E. Taarning, B. F. Sels, *Angew. Chemie Int. Ed.* **2021**, 60, 12204–12223.

[53] J. B. Greenblatt, D. J. Miller, J. W. Ager, F. A. Houle, I. D. Sharp, *Joule* **2018**, 2, 381–420.

[54] A. Mohsenzadeh, A. Zamani, M. J. Taherzadeh, *ChemBioEng Rev.* **2017**, 4, 75–91.

[55] X. Li, Y. Zhang, *ACS Catal.* **2016**, 6, 143–150.

[56] C. V. Pramod, R. Fauziah, K. Seshan, J. P. Lange, *Catal. Sci. Technol.* **2018**, 8, 289–296.

[57] T. T. N. Nguyen, M. Huchede, E. Blanco, F. Morfin, J. L. Rousset, L. Massin, M. Aouine, V. Bellière-Baca, J. M. M. Millet, *Appl. Catal. A Gen.* **2018**, 549, 170–178.

[58] G. M. Lari, G. Pastore, M. Haus, Y. Ding, S. Papadokonstantakis, C. Mondelli, J. Pérez-Ramírez, Energy *Environ. Sci.* **2018**, 11, 1012–1029.

[59] A. Kostyniuk, D. Bajec, P. Djinović, B. Likozar, *Chem. Eng. J.* **2020**, 394, 124945.

[60] K. Weissermel, H.-J. Arpe, P. Kalck, B. Zahner, Chimie Organique Industrielle, 3th edn., DeBoeck Université (Louvain-la-Neuve, BE), **2000**, pp. 1–453.

[61] M. Sutter, E. Da Silva, N. Duguet, Y. Raoul, E. Métay, M. Lemaire, *Chem. Rev.* **2015**, 115, 8609–8651.

[62] I. Pala-Rosas, J. L. Contreras, J. Salmones, B. Zeifert, R. López-Medina, J. Navarrete-Bolaños, S. Hernández-Ramírez, J. Pérez-Cabrera, A. A. F.-M. de Oca, *Catalysts* **2021**, 11, 360.

[63] M. Pagliaro, Glycerol, 1st edn., Elsevier (Sawston, UK), **2017**, pp. 23–57.

[64] R. A. Dagle, A. D. Winkelman, K. K. Ramasamy, V. L. Dagle, R. S. Weber, *Ind. Eng. Chem. Res.* **2020**, 59, 4843–4853.

[65] E. V. Makshina, M. Dusselier, W. Janssens, J. Degrève, P. A. Jacobs, B. F. Sels, *Chem. Soc. Rev.* **2014**, 43, 7917–7953.

[66] A. C. Dimian, N. I. Bezedea, C. S. Bildea, *Ind. Eng. Chem. Res.* **2021**, 60, 8475–8492.

[67] S. R. Schmidt, Catalysis of Organic Reactions: Twenty-first Conference, 1st edn., CRC Press (Boca Raton, US), **2006**, pp. 80–90.

[68] T. J. L. Mustard, D. J. MacK, J. T. Njardarson, P. H. Y. Cheong, *J. Am. Chem. Soc.* **2013**, 135, 1471–1475.

[69] L. A. Batory, C. E. McInnis, J. T. Njardarson, *J. Am. Chem. Soc.* **2006**, 128, 16054–16055.

[70] E. Arceo, P. Marsden, R. G. Bergman, J. A. Ellman, *Chem. Commun.* **2009**, 3357–3359.

[71] J. R. Dethlefsen, P. Fristrup, *ChemSusChem* **2015**, 8, 767–775.

[72] J. R. Dethlefsen, D. Lupp, A. Teshome, L. B. Nielsen, P. Fristrup, *ACS Catal.* **2015**, 5, 3638–3647.

[73] M. Shiramizu, F. D. Toste, *Angew. Chemie Int. Ed.* **2012**, 51, 1–6.

[74] M. Shiramizu, F. D. Toste, *Angew. Chemie - Int. Ed.* **2013**, 52, 12905–12909.

[75] E. Arceo, J. Ellman, R. Bergman, *ChemSusChem* **2010**, 3, 811–813.

[76] P. C. K. Vesborg, T. F. Jaramillo, *RSC Adv.* **2012**, 2, 7933–7947.

[77] G. Chapman, K. M. Nicholas, *Chem. Commun.* **2013**, 49, 8199–8201.

[78] J. A. Novotny, C. A. Peterson, *Adv. Nutr.* **2018**, 9, 272–273.

[79] A. Wilk, B. Wiszniewska, Postep. *High Med Dosw* **2017**, 71, 850–859.

[80] J. R. Dethlefsen, D. Lupp, B. C. Oh, P. Fristrup, *ChemSusChem* **2014**, 7, 425–428.

[81] M. Stalpaert, D. De Vos, *ACS Sustain. Chem. Eng.* **2018**, 6, 12197–12204.

[82] L. Sandbrink, K. Beckerle, I. Meiners, R. Liffmann, K. Rahimi, J. Okuda, R. Palkovits, *ChemSusChem* **2017,** 10, 1375–1379.

[83] K. Beckerle, A. Sauer, T. P. Spaniol, J. Okuda, *Polyhedron* **2016**, 116, 105–110.

[84] A. R. Petersen, L. B. Nielsen, J. R. Dethlefsen, P. Fristrup, *ChemCatChem* **2018**, 10, 769–778.

[85] H. S. Oliveira, P. P. Souza, L. C. A. Oliveira, *Catal. Today* **2017**, 289, 258–263.

[86] Y. Zhang, F. Sun, H.-Y. Zhang, G. Ying, J. Zhao, *Ind. Eng. Chem. Res.* **2018**, 57, 4553–4561.

[87] R. Sun, M. Zheng, X. Li, J. Pang, A. Wang, X. Wang, T. Zhang, *Green Chem.* **2017**, 19, 638–642.

[88] G. Crank, F. Eastwod, Aust. J. *Chem.* **1964**, 17, 1385–1391.

[89] N. N. Tshibalonza, R. Gérardy, Z. Alsafra, G. Eppe, J.-C. M. Monbaliu, *Green Chem.* **2018**, 20, 5147–5157.

[90] A. Konaka, T. Tago, T. Yoshikawa, A. Nakamura, T. Masuda, *Appl. Catal. B Environ.* **2014**, 146, 267–273.

[91] A. Konaka, T. Tago, T. Yoshikawa, H. Shitara, Y. Nakasaka, T. Masuda, *Ind. Eng. Chem. Res.* **2013**, 52, 15509–15515.

[92] G. Sánchez, J. Friggieri, C. Keast, M. Drewery, B. Z. Dlugogorski, E. Kennedy, M. Stockenhuber, *Appl. Catal. B Environ.* **2014**, 152–153, 117–128.

[93] G. Sánchez, J. Friggieri, A. A. Adesina, B. Z. Dlugogorski, E. M. Kennedy, M. Stockenhuber, *Catal. Sci. Technol.* **2014**, 4, 3090–3098.

[94] R. C. R. Santos, D. M. V. Braga, A. N. Pinheiro, E. R. Leite, V. N. Freire, E. Longhinotti, A. Valentini, *Catal. Sci. Technol.* **2016**, 6, 4986–5002.

[95] G. Sánchez, B. Z. Dlugogorski, E. M. Kennedy, M. Stockenhuber, *Appl. Catal. A Gen.* **2016**, 509, 130–142.

[96] A. Kostyniuk, D. Bajec, P. Djinović, B. Likozar, *Chem. Eng. J.* **2020**, 397, 125430.

[97] R. Almeida, M. F. Ribeiro, A. Fernandes, J. P. Lourenço, *Catal. Commun.* **2019**, 127, 20–24.

[98] H. Lan, X. Xiao, S. Yuan, B. Zhang, G. Zhou, Y. Jiang, *Catal. Letters* **2017**, 147, 2187–2199.

[99] H. Lan, Q. Yao, Y. Zhou, B. Zhang, Y. Jiang, *Mol. Catal.* **2020**, 498, 111279.

[100] H. Zhao, Y. Jiang, H. Liu, Y. Long, Z. Wang, Z. Hou, *Appl. Catal. B Environ.* **2020**, 277, 119187.

[101] M. H. Barecka, M. Skiborowski, A. Górak, *Chem. Eng. Res. Des.* **2017**, 123, 295–316.

[102] D. Zhang, P. Hang, G. Liu, J. Clean. *Prod.* **2020**, 275, 122773.

[103] L. G. Pinaeva, A. S. Noskov, *Pet. Chem.* **2020**, 60, 1191–1206.

[104] M. Bochenek, N. Oleszko-Torbus, W. Wałach, D. Lipowska-Kur, A. Dworak, A. Utrata-Wesołek, *Polym. Rev.* **2020**, 60, 717–767.

[105] M. Ricciardi, F. Passarini, I. Vassura, A. Proto, C. Capacchione, R. Cucciniello, D. Cespi, *ChemSusChem* **2017**, 10, 2291–2300.

[106] A. Wróblewska, A. Fajdek, J. *Hazard. Mater.* **2010**, 179, 258–265.

[107] E. Petit, L. Bosch, A. M. Costa, I. Rodríguez-Izquierdo, D. Sepúlveda-Crespo, A. M. Muñoz-Fernández, J. Vilarrasa, *ChemMedChem* **2021**, 16, 2217–2222.

[108] A. Wróblewska, A. Fajdek, J. Wajzberg, E. Milchert, *J. Hazard. Mater.* **2009**, 170, 405–410.

[109] Green glycidol pilot plant in the UK, https://www.thechemicalengineer.com/news/green-glycidol-pilot-plant-in-the-uk (accessed on 10-28-21).

[110] Green Lizard Technologies: Green Glycidol, https://greenlizardtechnologies.com/what-we-do/green-glycidol-glycerol/ (accessed on 10-26-21).

[111] Y. A. Alassmy, Z. A. Pour, P. P. Pescarmona, *ACS Sustain. Chem. Eng.* **2020**, 8, 7993–8003.

[112] J. Sun, J. Ren, S. Zhang, W. Cheng, *Tetrahedron Lett.* **2009**, 50, 423–426.

[113] J. C. J. Bart, N. Palmeri, S. Cavallaro, Biodiesel Science and Technology: From Soil to Oil, Elsevier (Sawston, UK), **2010**, pp. 571–624.

[114] M. O. Sonnati, S. Amigoni, E. P. Taffin De Givenchy, T. Darmanin, O. Choulet, F. Guittard, *Green Chem.* **2013**, 15, 283–306.

[115] D. Cespi, R. Cucciniello, M. Ricciardi, C. Capacchione, I. Vassura, F. Passarini, A. Proto, *Green Chem.* **2016**, 18, 4559–4570.

[116] A. Milewski, D. Czechowicz, A. Jakóbik-Kolon, P. Dydo, ACS Sustain. *Chem. Eng.* **2019**, 7, 18640–18646.

[117] R. Morodo, R. Gérardy, G. Petit, J. C. M. Monbaliu, *Green Chem.* **2019**, 21, 4422–4433.

[118] T. Y. Kim, J. Baek, C. K. Song, Y. S. Yun, D. S. Park, W. Kim, J. W. Han, J. Yi, *J. Catal.* **2015**, 323, 85–99.

[119] Y. K. Endah, M. S. Kim, J. Choi, J. Jae, S. D. Lee, H. Lee, *Catal. Today* **2017**, 293–294, 136–141.

[120] C. L. Bolívar-Diaz, V. Calvino-Casilda, F. Rubio-Marcos, J. F. Fernández, M. A. Bañares, *Appl. Catal. B Environ.* **2013**, 129, 575–579.

[121] S. M. Gade, M. K. Munshi, B. M. Chherawalla, V. H. Rane, A. A. Kelkar, *Catal. Commun.* **2012**, 27, 184–188.

[122] Y. Zhou, F. Ouyang, Z. Bin Song, Z. Yang, D. J. Tao, *Catal. Commun.* **2015**, 66, 25–29.

[123] M. K. Munshi, S. M. Gade, V. H. Rane, A. A. Kelkar, *RSC Adv.* **2014**, 4, 32127–32133.

[124] J. S. Choi, F. S. H. Simanjuntaka, J. Y. Oh, K. I. Lee, S. D. Lee, M. Cheong, H. S. Kim, H. Lee, *J. Catal.* **2013**, 297, 248–255.

[125] D. J. Darensbourg, A. D. Yeung, *Green Chem.* **2013**, 16, 247–252.

[126] Y. T. Algoufi, U. G. Akpan, M. Asif, B. H. Hameed, *Appl. Catal. A Gen.* **2014**, 487, 181–188.

[127] A. Canela-Xandri, M. Balcells, G. Villorbina, P. Christou, R. Canela-Garayoa, *Molecules* **2020**, 25, 2511.

[128] B. M. Bell, J. R. Briggs, R. M. Campbell, S. M. Chambers, P. D. Gaarenstroom, J. G. Hippler, B. D. Hook, K. Kearns, J. M. Kenney, W. J. Kruper, D. James Schreck, C. N. Theriault, C. P. Wolfe, *Clean - Soil, Air, Water* **2008**, 36, 657–661.

[129] M. Ricciardi, D. Cespi, M. Celentano, A. Genga, C. Malitesta, A. Proto, C. Capacchione, R. Cucciniello, *Sustain. Chem. Pharm.* **2017**, 6, 10–13.

[130] Epichlorohydrin prices in Europe, https://publications.jrc.ec.europa.eu/repository/handle/

(accessed on 10-21-21).

[131] G. M. Lari, G. Pastore, C. Mondelli, J. Pérez-Ramírez, *Green Chem.* **2018**, 20, 148–159.

[132] G. Gibson, Brydson's Plastics. Materials, 8th edn., Elsevier Inc. (Sawston, UK), **2017**, pp. 773–797.

[133] X. Hou, Y. Fu, X. Zhu, H. Yin, A. Wang, *Asia-Pacific J. Chem. Eng.* **2015**, 10, 626–632.

[134] R. Vitiello, V. Russo, R. Turco, R. Tesser, M. Di Serio, E. Santacesaria, Chinese *J. Catal.* **2014**, 35, 663–669.

[135] D. Giomi, M. Malavolti, O. Piccolo, A. Salvini, A. Brandi, *RSC Adv.* **2014**, 4, 46319–46326.

[136] R. Tesser, M. Di Serio, R. Vitiello, V. Russo, E. Ranieri, E. Speranza, E. Santacesaria, *Ind. Eng. Chem. Res.* **2012**, 51, 8768–8776.

[137] R. Vitiello, R. Tesser, E. Santacesaria, M. Di Serio, *Ind. Eng. Chem. Res.* **2016**, 55, 1484–1490.

[138] C. A. de Araujo Filho, K. Eränen, J. P. Mikkola, T. Salmi, *Chem. Eng. Sci.* **2014**, 120, 88–104.

[139] S. P. Zou, E. H. Du, Z. C. Hu, Y. G. Zheng, *Biotechnol. Lett.* **2013**, 35, 937–942.

[140] F. Xue, Z. Q. Liu, Y. J. Wang, H. Q. Zhu, N. W. Wan, Y. G. Zheng, *Catal. Commun.* **2015**, 72, 147–149.

[141] H. X. Jin, Z. C. Hu, Z. Q. Liu, Y. G. Zheng, Biotechnol. *Appl. Biochem.* **2012**, 59, 170–177.

[142] H. X. Jin, Z. Q. Liu, Z. C. Hu, Y. G. Zheng, *Eng. Life Sci.* **2013**, 13, 385–392.

[143] P. P. Pescarmona, Curr. Opin. *Green Sustain. Chem.* **2021**, 29, 100457.

[144] M. Metzger, B. Strehle, S. Solchenbach, H. A. Gasteiger, *J. Electrochem. Soc.* **2016**, 163, A1219–A1225.

[145] K. Shukla, V. C. Srivastava, *Catal. Rev. Sci*. Eng. **2017**, 59, 1–43.

[146] G. Fiorani, A. Perosa, M. Selva, *Green Chem.* **2018**, 20, 288–322.

[147] J. Granados-Reyes, P. Salagre, Y. Cesteros, *Appl. Catal. A Gen.* **2017**, 536, 9–17.

[148] Glycerol Carbonate Market, https://www.transparencymarketresearch.com/glycerol-carbonate-market.html (accessed on 10-14-21).

[149] Glycerol Carbonate Market and applications, https://www.transparencymarketresearch.com/glycerol-carbonate-market.html (accessed on 10-04-21).

[150] J. Ma, J. Song, H. Liu, J. Liu, Z. Zhang, T. Jiang, H. Fan, B. Han, *Green Chem.* **2012**, 14, 1743–1748.

[151] X. Su, W. Lin, H. Cheng, C. Zhang, Y. Wang, X. Yu, Z. Wu, F. Zhao, *Green Chem.* **2017**, 19, 1775–1781.

[152] R. Gérardy, J. Estager, P. Luis, D. P. Debecker, J. C. M. Monbaliu, *Catal. Sci. Technol.* **2019**, 9, 6841–6851.

[153] W. K. Teng, G. C. Ngoh, R. Yusoff, M. K. Aroua, *Energy Convers. Manag.* **2014**, 88, 484–497.

[154] S. Sahani, S. N. Upadhyay, Y. C. Sharma, *Ind. Eng. Chem. Res.* **2020**, 60, 67–88.

[155] S. Dabral, U. Licht, P. Rudolf, G. Bollmann, A. S. K. Hashmi, T. Schaub, *Green Chem.* **2020**, 22, 1553–1558.

[156] C. Carré, Y. Ecochard, S. Caillol, L. Averous, *ChemSusChem* **2019**, 12, 3410–3430.

[157] F. Siragusa, E. Van Den Broeck, C. Ocando, A. J. Müller, G. De Smet, B. U. W. Maes, J. De Winter, V. Van Speybroeck, B. Grignard, C. Detrembleur, *ACS Sustain. Chem. Eng.* **2021**, 9, 1714–1728.

[158] J. A. Stewart, R. Drexel, B. Arstad, E. Reubsaet, B. M. Weckhuysen, P. C. A. Bruijnincx, *Green Chem.* **2016**, 18, 1605–1618.

[159] S. W. Shao, C. H. Chen, J. R. Chan, T. Y. Juang, M. M. Abu-Omar, C. H. Lin, *Green Chem.* **2020**, 22, 4683–4696.

[160] S. Schmidt, F. J. Gatti, M. Luitz, B. S. Ritter, B. Bruchmann, R. Mülhaupt, *Macromolecules* **2017**, 50, 2296–2303.

[161] P.-K. Dannecker, M. A. R. Meier, *Sci. Rep.* **2019**, 9, 9858.

[162] P. Furtwengler, L. Avérous, *Sci. Rep.* **2018**, 8, 1–14.

[163] D. J. Saxon, A. M. Luke, H. Sajjad, W. B. Tolman, T. M. Reineke, *Prog. Polym. Sci.* **2020**, 101, 101196.

[164] S. Schmidt, B. S. Ritter, D. Kratzert, B. Bruchmann, R. Mülhaupt, *Macromolecules* **2016**, 49, 7268–7276.

[165] H. C. Brown, J. H. Brewster, H. Shechter, *J. Am. Chem. Soc.* **1954**, 76, 467–474.

[166] F. Nocito, A. Dibenedetto, Curr. Opin. *Green Sustain. Chem.* **2020**, 21, 34–43.

[167] A. J. Kamphuis, F. Picchioni, P. P. Pescarmona, *Green Chem.* **2019**, 21, 406–448.

[168] M. Honda, M. Tamura, K. Nakao, K. Suzuki, Y. Nakagawa, K. Tomishige, *ACS Catal.* **2014**, 4, 1893–1896.

[169] A.-K. JMH, H. Wang, E. Elhaj, *J. Mater. Sci. Eng.* **2019**, 8, 1000523.

[170] Q. Zhang, H. Y. Yuan, X. T. Lin, N. Fukaya, T. Fujitani, K. Sato, J. C. Choi, *Green Chem.* **2020**, 22, 4231–4239.

[171] J. A. Castro-Osma, C. Alonso-Moreno, A. Lara-Sánchez, J. Martínez, M. North, A. Otero, *Catal. Sci. Technol.* **2014**, 4, 1674–1684.

[172] J. Liu, D. He, *J. CO_2 Util.* **2018**, 26, 370–379.

[173] L. P. Ozorio, C. J. A. Mota, *ChemPhysChem* **2017**, 18, 3260–3265.

[174] C. Hu, M. Yoshida, H. C. Chen, S. Tsunekawa, Y. F. Lin, J. H. Huang, *Chem. Eng. Sci.* **2021**, 235, 116451.

[175] C. Ngassam Tounzoua, B. Grignard, A. Brege, C. Jerome, T. Tassaing, R. Mereau, C. Detrembleur, *ACS Sustain. Chem. Eng.* **2020**, 8, 9698–9710.

[176] V. Aomchad, À. Cristòfol, F. D. Monica, B. Limburg, V. D'Elia, A. W. Kleij, *Green Chem.* **2021**, 23, 1077–1113.

[177] Z. Yu, L. Xu, Y. Wei, Y. Wang, Y. He, Q. Xia, X. Zhang, Z. Liu, *Chem. Commun.* **2009**, 3934–3936.

[178] Y. N. Lim, C. Lee, H.-Y. Jang, European *J. Org. Chem.* **2014**, 2014, 1823–1826.

[179] T. Kitamura, Y. Inoue, T. Maeda, J. Oyamada, *Synth. Commun.* **2016**, 46, 39–45.

[180] M. Mihara, K. Moroga, T. Iwasawa, T. Nakai, T. Ito, T. Ohno, T. Mizuno, *Synlett* **2018**, 29, 1759–1764.

[181] Y. A. Alassmy, P. J. Paalman, P. P. Pescarmona, *ChemCatChem* **2021**, 13, 475–486.

[182] X. Song, Y. Wu, D. Pan, J. Zhang, S. Xu, L. Gao, R. Wei, G. Xiao, *J. CO_2 Util.* **2018**, 28, 326–334.

[183] B. Grignard, C. Ngassamtounzoua, S. Gennen, B. Gilbert, R. Méreau, C. Jerome, T. Tassaing, C. Detrembleur, *ChemCatChem* **2018**, 10, 2584–2592.

[184] E. R. Baral, J. H. Lee, J. G. Kim, *J. Org. Chem*. **2018**, 83, 11768–11776.

[185] Z. Wang, R. Gérardy, G. Gauron, C. Damblon, J. C. M. Monbaliu, *React. Chem. Eng.* **2019**, 4, 17–26.

[186] S. Asghari, M. Ghiaci, *Ind. Eng. Chem. Res.* **2020**, 59, 6405–6415.

[187] J. R. Ochoa-Gómez, O. Gómez-Jiménez-Aberasturi, C. Ramírez-López, M. Belsué, *Org. Process Res. Dev.* **2012**, 16, 389–399.

[188] S. Christy, A. Noschese, M. Lomelí-Rodriguez, N. Greeves, J. A. Lopez-Sanchez, *Curr. Opin. Green Sustain. Chem.* **2018**, 14, 99–107.

[189] C. Len, F. Delbecq, C. Cara Corpas, E. Ruiz Ramos, *Synthesis* **2018**, 50, 723–741.

[190] R. I. Khusnutdinov, N. A. Shchadneva, Y. Y. Mayakova, *Russ. J. Org. Chem.* **2014**, 50, 948–952.

[191] A. Kumar, K. Iwatani, S. Nishimura, A. Takagaki, K. Ebitani, *Catal. Today* **2012**, 185, 241–246.

[192] M. Hong, L. Gao, G. Xiao, *J. Chem. Res.* **2014**, 38, 679–681.

[193] Q. Gu, J. Fang, Z. Xu, W. Ni, K. Kong, Z. Hou, *New J. Chem.* **2018**, 42, 13054–13064.

[194] S. Guidi, R. Calmanti, M. Noè, A. Perosa, M. Selva, *ACS Sustain. Chem. Eng.* **2016**, 4, 6144–6151.

[195] K. M. Tomczyk, P. A. Guńka, P. G. Parzuchowski, J. Zachara, G. Rokicki, *Green Chem.* **2012**, 14, 1749–1758.

[196] M. M. Mazurek-Budzyńska, G. Rokicki, M. Drzewicz, P. A. Guńka, J. Zachara, *Eur. Polym. J.* **2016**, 84, 799–811.

[197] J.-L. Dong, L.-S.-H. Yu, J.-W. Xie, *ACS Omega* **2018**, 3, 4974–4985.

[198] A. S. Amarasekara, S. R. Ali, H. Fernando, V. Sena, T. V. Timofeeva, SN *Appl. Sci.* **2019**, 1, 1–8.

[199] S. Mnasri-Ghnimi, N. Frini-Srasra, Appl. Clay *Sci.* **2014**, 88–89, 214–220.

[200] T. Rohand, J. Savary, I. E. Markó, *Monatshefte fur Chemie* **2018**, 149, 1429–1436.

[201] S. J. Yang, L. Yu, Y. K. Huang, G. Bin Duan, *Adv. Mater. Res.* **2012**, 430–432, 289–292.

[202] L. Fang, K. Zhang, L. Chen, P. Wu, Chinese *J. Catal.* **2013**, 34, 932–941.

[203] S. Zhong, Q. Ou, L. Shao, J. Chil. *Chem. Soc.* **2015**, 60, 3005–3008.

[204] O. Mhadhbi, N. Besbes, Moroccan *J. Heterocycl. Chem.* **2020**, 19, 89–98.

[205] D. Rigo, R. Calmanti, A. Perosa, M. Selva, *Green Chem.* **2020**, 22, 5487–5496.

[206] M.R. Khodadadi, J. Thiel, R. S. Varma, C. Len, *J. Flow Chem.* **2021**, 11, 725–735.

[207] A. S. Amarasekara, M. A. Animashaun, *Catal. Letters* **2016**, 146, 1819–1824.

[208] S. Dutta, N. S. Bhat, *ChemCatChem* **2021**, 13, 3202–3222.

[209] P. Li, Z. Xiao, C. Chang, S. Zhao, G. Xu, *Ind. Eng. Chem. Res.* **2019**, 59, 17520–17528.

[210] J. Ma, S. Shi, X. Jia, F. Xia, H. Ma, J. Gao, J. Xu, *J. Energy Chem.* **2019**, 36, 74–86.

[211] A. R. Trifoi, P. Ş. Agachi, T. Pap, Renew. *Sustain. Energy Rev.* **2016**, 62, 804–814.

[212] Y. Zong, L. Yang, S. Tang, L. Li, W. Wang, B. Yuan, G. Yang, *Catalysts* **2018**, 8, 48.

[213] X. Tan, L. Li, J. Zhang, X. Han, L. Jiang, F. Li, C. Y. Su, *Chem. Mater.* **2012**, 24, 480–485.

[214] Y. Abdollahian, J. L. Hauser, D. L. Rogow, A. G. Oliver, S. R. J. Oliver, *Dalt. Trans.* **2012**, 41, 12630–12634.

[215] F. A. Freitas, D. Licursi, E. R. Lachter, A. M. R. Galletti, C. Antonetti, T. C. Brito, R. S. V. Nascimento, *Catal. Commun.* **2016**, 73, 84–87.

[216] I. Podolean, J. Zhang, M. Shamzhy, V. I. Pârvulescu, J. Čejka, *Catal. Sci. Technol.* **2020**, 10, 8254–8264.

[217] S. Zhao, Y. Jia, Y. F. Song, *Catal. Sci. Technol.* **2014**, 4, 2618–2625.

[218] T. Liu, W. Fu, X. Zheng, J. Jiang, M. Hu, T. Tang, *RSC Adv.* **2014**, 4, 18217–18221.

[219] Z. M. Li, Y. Zhou, D. J. Tao, W. Huang, X. S. Chen, Z. Yang, *RSC Adv.* **2014**, 4, 12160–12167.

[220] V. Söderholm, J. Esteban, D. Vogt, *Catal. Sci. Technol.* **2021**, 11, 4529–4538.

[221] V. Umrigar, M. Chakraborty, P. Parikh, *Int. J. Chem. Kinet.* **2019**, 51, 299–308.

[222] Y. Xie, Q. Zhao, G. Gao, T. Jiang, *Dalt. Trans.* **2019**, 48, 17106–17116.

[223] L. Dai, Q. Zhao, H. Zhao, Y. Li, T. Jiang, Korean *J. Chem. Eng.* **2017**, 34, 1358–1365.

[224] P. Che, F. Lu, X. Si, H. Ma, X. Nie, J. Xu, *Green Chem.* **2018**, 20, 634–640.

[225] W. Hagui, R. Essid, S. Amri, N. Fares, M. Khabbouchi, O. Tabbene, F. Liman, E. Srasra, N. Besbes, Turkish *J. Chem.* **2019**, 43, 435–451.

[226] Z. Miao, L. Xu, H. Song, H. Zhao, L. Chou, *Catal. Sci. Technol.* **2013**, 3, 1942–1954.

[227] J. Yin, H. Fei, *Dalt. Trans.* **2018**, 47, 4054–4058.

[228] D. Rigo, G. Fiorani, A. Perosa, M. Selva, *ACS Sustain. Chem. Eng.* **2019**, 7, 18810–18818.

[229] D. Rigo, R. Calmanti, A. Perosa, M. Selva, *Green Chem.* **2020**, 22, 5487–5496.

[230] D. J. C. Constable, A. D. Curzons, V. L. Cunningham, *Green Chem.* **2002**, 4, 521–527.

[231] C. Jiménez-González, D. J. C. Constable, C. S. Ponder, *Chem. Soc. Rev.* **2012**, 41, 1485–1498.

[232] S. Maurya, D. Yadav, K. Pratap, A. Kumar, *Green Chem.* **2017**, 19, 629–633.

[233] J. Andraos, Reactions green metrics: problems, exercices and solutions, 1st edn, CRC Press (Boca Raton, US) Group, **2018**, pp. 1–604.

[234] R. A. Sheldon *Ser. IIc Chem.* **2000**, 3, 541–551.

Author contributions

CM prepared and wrote the manuscript.

JCMM advised for the overall structure and corrected the manuscript.

3 COMPUTER-AIDED KINETIC NETWORK MODELING OF COMPLEX ORTHOESTER-POLYOL DYNAMIC COVALENT EXCHANGES

3.1 PREFACE

Chapter 3 dives into the tedious and cumbersome task of elucidating mechanisms and kinetics for unknown reactions, echoing to the high complexity of compounds with multiple functional groups such as polyols. To address this problematic, we aim to develop a new computational strategy to ease the analysis of complex spectral data and provide a framework to develop a robust and accurate kinetic model of reaction. We selected dynamic covalent exchanges toward orthoesters with diols as our model reaction due to the limited mechanistic and kinetic insights available in literature. This reaction is particularly relevant, as it produces intermediates that can undergo deoxydehydration to form valuable olefins. Such orthoester derived scaffolds also have applications in drug delivery and recycling materials.

Our numerical strategy involves decomposing multi-dimensional spectral datasets into interpretable components (e.g., number of species in the kinetic study) using tensor-based methods (Figure 3.1). Tensors (X) are defined as mathematical objects that can store data in any number of dimensions (dimension > 2), making it a powerful tool for the representation of complex relationships and multi-dimensional data. In our case, 3D tensors are composed of time, chemical shifts and signal intensities of our kinetic monitoring. To solve such datasets, implementation Tucker decomposition (TD) allows to reduce the high-dimensional spectral data into a parsimonious set of components representing the underlying species of our kinetic study for the three dimensions. TD models the data tensor X as follows:

$$X \approx G \times A^{(1)} \times A^{(2)} \times A^{(3)}$$

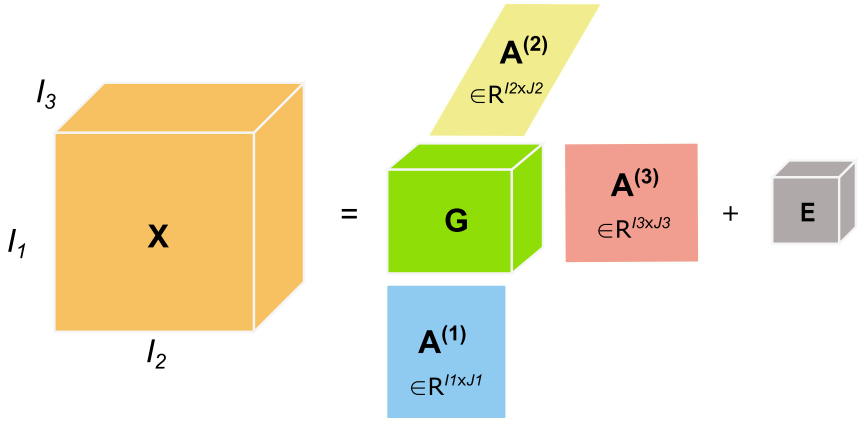

Figure 3.1 Representation of Tucker decomposition of a 3D tensor into the tensor core (G) and the three factors ($A^{(1)}$, $A^{(2)}$ and $A^{(3)}$) and, the residual error (E).

Here, G corresponds to the core tensor, capturing the interactions between factor matrices $A^{(1)}$, $A^{(2)}$ and $A^{(3)}$, each corresponding to a factor (time, chemical shifts or signal intensities) and E denotes the residual error between the original and reconstructed dataset. Through the operation of n-mode product, the core tensor is multiplied by each factor matrix to approximate the original dataset.

A key principle in dataset factorization is parsimony, defined as the ability to represent multi-dimensional data with the minimal number of significant components without overfitting. In other words, parsimony is essential to constrain the model to only capture significant contributions, avoiding the integration of noise or artefacts. Overall, TD provides a framework to extract latent factors while maintaining physical interpretability. Latent factors are unobservable variables statistically determined. In our case, their physical interpretation theoretically corresponds to entities such as the spectrum of individual pure species identified with TD and the profiles of species concentration over time.

The second script aims to numerically solve differential equation modelling a chemical reaction (Figure 3.2). This is performed by the implementation of non-linear least squares optimization. This method allows to find the mathematical model that best explains the experimental dataset. In our case, this strategy relies on the minimization of the sum of the squared differences (residuals) between the experimental observations (e.g. species concentrations) and the values predicted by the model. The overall aim of this method is to minimize the residuals as much as possible, to achieve the most accurate theoretical modelling.

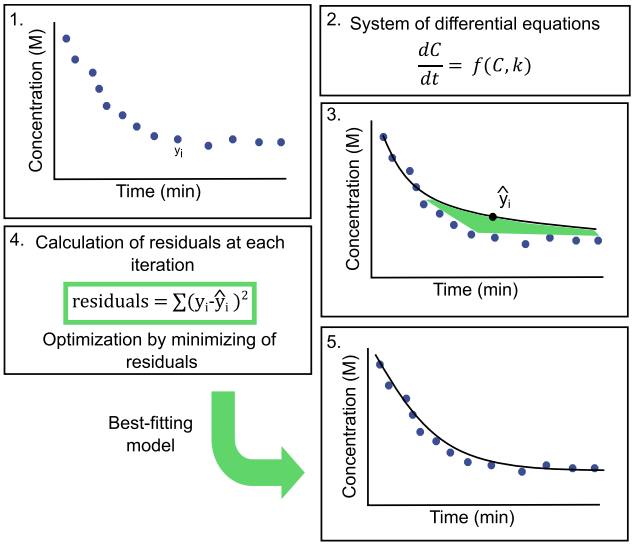

Figure 3.2 Stepwise kinetic model refinement: from initial fit to optimized parameter estimation.

By combining these two complementary mathematical approaches, we aim to develop a user-friendly and open-accessed workflow to facilitate the mechanistic and kinetic understanding of dynamic covalent exchanges between orthoesters and diols.

3.2 ABSTRACT

Kinetic modeling is a powerful tool for unraveling complex reaction mechanisms, yet integrated workflows combining spectral data interpretation and kinetic system modeling remain scarce. This work addresses this gap by developing a Python workflow that enables comprehensive analysis of intricate reaction networks, specifically targeting dynamic covalent exchanges toward orthoesters with diols (DCE). Through rigorous kinetic modeling and experimental validation, we uncovered DCE's complex system of interconnected species, governed by multiple competitive pathways. All pathways featured the same reaction sequence, involving the formation of a carbocation or carbene intermediate by orthoester activation, followed by nucleophilic substitution or cyclization with a free alcohol group. Our multidisciplinary approach quantified how solvent properties and reagent nature (by-product: MeOH, EtOH, iPrOH) influence reaction kinetics. While solvents and alcohol by-products with strong hydrogen bonding capacity enhanced transition state stabilization, they also promoted the formation of energetically favorable complexes with the catalyst. These resulted in limited catalyst availability and consequently reduced overall reaction rates. Catalyst screening identified dicarboxylic acids as particularly effective, especially oxalic acid, which achieved substrate conversion under 30 seconds, contrasting with formic acid requiring 45 minutes. DFT analysis revealed that enhanced catalytic performance stemmed from intramolecular hydrogen bonding between active and non-active acid sites, which lowered activation barriers beyond simple acidity considerations.

3.3 INTRODUCTION

Organic chemistry is a constantly evolving field, where understanding chemical reactions remains a major challenge. Traditionally, addressing this imperative has required extensive experimental work, including reaction monitoring, screening of experimental conditions, catalysts or solvents. These processes generate vast amounts of raw data that require expertise in systematic processing and modeling. However, the rise of computational science has revolutionized this approach, offering powerful and user-friendly tools for analyzing complex datasets. Open-access numerical algorithms now allow chemists to extract meaningful insights from large reaction datasets, reducing reliance on purely empirical methods.

One particularly promising application is kinetic modeling, which aims to deconstruct intricate reaction systems into fundamental interconnections between reagents and products. By mapping complex reaction networks, researchers strive to simplify system complexity into elementary reactions, potentially uncovering new mechanisms and enabling efficient reaction optimization.[1–3]

Python is widely regarded as an essential tool in computational science, thanks to its open-source nature, ease of use, adaptability, and rich collection of scientific libraries. Leveraging these advantages, most open-access chemical kinetics packages are now programmed into Python, enabling the simulation of kinetic chemical systems across various fields, including metabolic networks, enzyme biotransformation, or physical, inorganic, and analytical chemistry.[4–6] While simulation packages are widely available, far fewer are specifically engineered for fitting experimental data in chemical kinetics.[7–10] Among these, ODEnlls and

chemical kinetics packages stand out, enabling the adjustment of kinetic models to experimental data using non-linear least squares to calculate rate constants and concentrations of the reaction. However, ODEnlls primary focuses on the chemical kinetic simulations and only facilitates comparison with experimental data. Moreover, neither of these packages include a systematical statistical analysis of the fitted model or efficient visualization of the calculated output.[11,12]

Such enhancements are crucial for accurately modeling complex reaction networks and refining their kinetics models. One field that particularly demands such improvements is system chemistry, where dynamic covalent chemistry (DCC) stands out as a promising area. DCC is characterized by the formation of reversible covalent bonds, often leading to complex molecular architectures.[13,14] DCC has driven significant innovations in various areas, including drug delivery and bioconjugation,[15–17] the synthesis of recyclable polymers or adaptative materials,[18–20] as well as the construction of discrete complex assemblies,[21–24] and organic frameworks.[25–27] Among the diverse exchange reactions within the DCC toolbox,[28,29] we are particularly interested in the reactions between simple orthoesters and alcohols.[30] These transformations not only expand the possibilities for dynamic systems and supramolecular chemistry,[31] but also offer alternative pathways for converting biobased compounds into value-added olefins.[32–35]

Little is known about the equilibrium networks underlying DCC systems. Previous study on the acidic-mediated exchange of alcohols with O,O,O-orthoester between trimethyl orthoacetate and ethanol (EtOH) consistently reached the thermodynamic minimum (Scheme 3.1). This resulted in the same statistical product distribution regardless of the catalyst or the solvent used.[31] A computational study also revealed that ammonium orthoesters cryptates undergo a concerted mechanism involving protonation and C-O bond cleavage.[22] However, a comprehensive computational and kinetic modeling approach for these systems has yet to be developed.

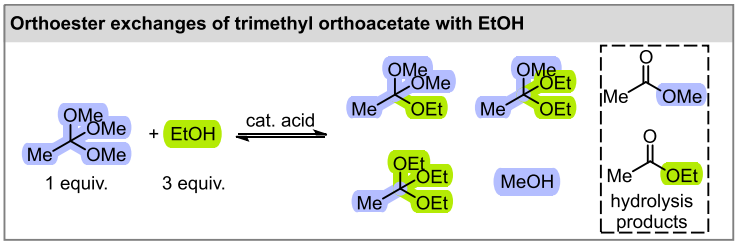

Scheme 3.1 Illustration of acid-catalyzed orthoester exchanges between ethanol and trimethyl orthoacetate and resulting product distribution.[31]

Herein, we present a comprehensive experimental and computational study of dynamic covalent exchanges (DCE) involving polyols and orthoesters. This challenging system was elucidated through the combined use of computer programming, DFT computations, and experimental data. A custom Python script was developed to estimate the number of compounds present in complex NMR spectra. It can handle mixtures containing up to 12 different species and facilitates the detailed characterization of the individual products. An existing kinetic modeling Python script was adapted to organic chemistry systems, and

supplemented with statistical tools to enable efficient evaluation of model accuracy.[11,12] The kinetic model thus derived provided a complete mapping of the DCE network, clearly identifying the underlying reaction mechanisms. This model was further used to assess the kinetic differences arising from variations in experimental conditions, solvent choice, and orthoester reagents. In parallel, a DFT study was performed to identify key factors influencing the reactivity and the stability of orthoesters under the different experimental conditions screened.

3.4 Results and discussion

3.4.1 Computer-assisted estimation of species in the DCE network

In-line benchtop NMR (43 MHz) monitoring of solutions containing a 1:1 ratio of ethylene glycol (**1**) and triethyl orthoformate (**2b**) in presence of 10 mol% of formic acid (FA) in acetonitrile was used to define suitable conditions (temperature, reagent concentration, and reaction time) that would allow the formation of multiple DCE products in detectable amounts (Section S5 in the Supporting Information). The reaction was then performed under the selected conditions and monitored over 3 h using offline high-field NMR (700 MHz) (Section S3.2 in the Supporting Information). The variety of species present in the NMR spectra represented a challenge for precise interpretation. We therefore turned to computer programming and data fitting to estimate the number of distinct species present. Our goal was to develop a broadly applicable approach capable of determining the number of components in NMR spectra of DCE crude mixtures acquired during kinetic experiments, but without requiring prior signal assignment or preliminary data preprocessing.

We explored a wide array of factorization methods to identify the most suitable algorithm capable of considering the chemical shifts and intensity within a large spectral dataset, as well as changes over time (Section S6.1 in the Supporting Information). Ultimately, we opted for a tensor decomposition due to its ability to perform non-negative factorization, and to handle higher-dimensional data and complex patterns. A Python script based on the Tucker decomposition algorithm was developed (Figure 3.1), allowing direct upload of unprocessed NMR spectra files. The program then evaluates the quality of the fit as a function of the number of species assumed to be present in the mixture (Section S6 in the Supporting Information).

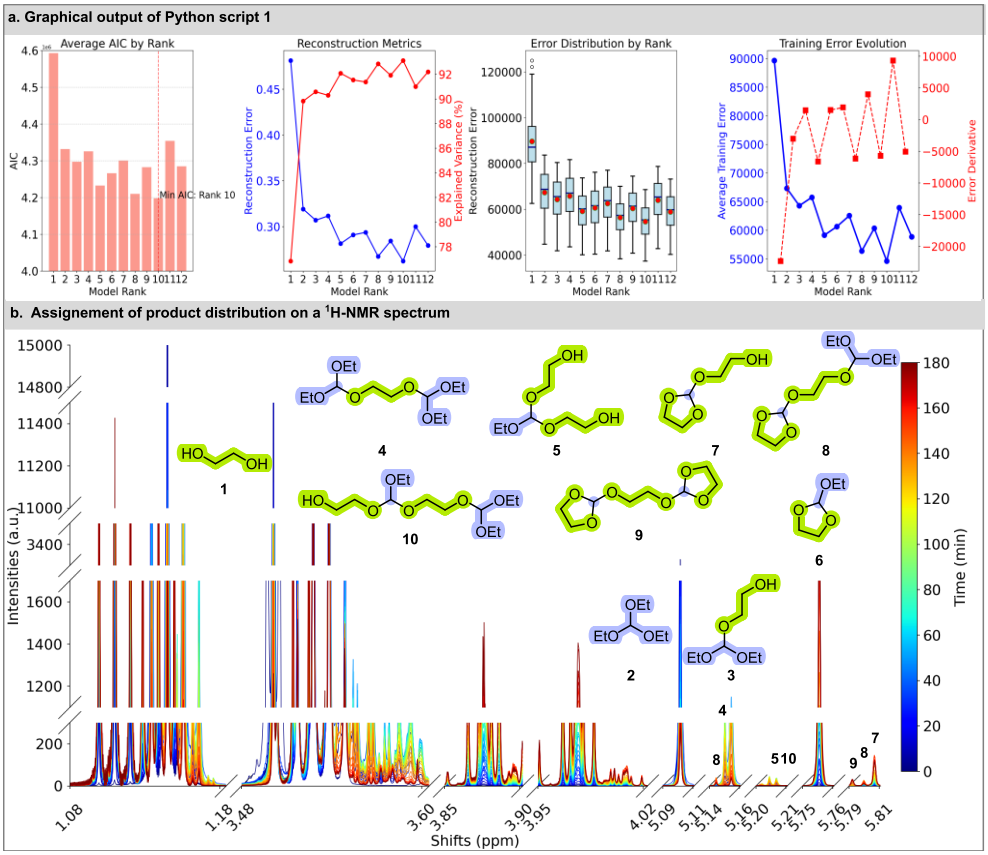

Figure 3.3 (a) Evaluation of the computer assisted data fitting to determine the number of compounds in solution. Comparative analysis of dimensionality reduction performance for ranks 1-12 including the AIC, the reconstruction error and the explained variance ratio, the reconstruction error box plots, the first derivative of the reconstruction error and the training error evolution. (b) ^{1}H-NMR kinetic profile of the reaction between **1** and **2b** (1:1 ratio) with 10 mol% of formic acid (FA) as catalyst in acetonitrile.

To evaluate the accuracy of the data reconstruction per number of species considered, we employed a statistical tool known as the Akaike Information Criterion (AIC).[36] AIC is used to evaluate the optimal trade-off between model fit and complexity. Increasing the number of presumed compounds improves the fit to the spectra but also introduces the risk of overfitting by adding unnecessary components or capturing measurement noise. An optimal model corresponds to the minimum AIC value. Figure 3.3a shows the calculated AIC when assuming between 1 to 12 ranks (*i.e.*, different compounds populating molecular diversity) in the mixture, with the AIC minimum obtained at 10 compounds. The accuracy of the model was confirmed by a rapid improvement of reconstruction error and explained variance, indicating improved accuracy, as well as a boxplot showing a narrowing error distribution. The derivative of the error showed abrupt fluctuations between ranks 8 and 10, pointing to a transition zone between the model best performance and overfitting (Section S6 in the

Supporting Information). Together, these analyses suggest 10 compounds as the best estimate of the number of species present throughout the kinetic monitoring of this reaction.

3.4.2 CRUDE CHARACTERIZATION

After gaining insights on the extent of molecular diversity formed through the DCE network under standardized experimental conditions, we set out to assign the signals in the spectra based on literature and knowledge of NMR interpretation. Cyclic hybrid orthoester species such as **6**, **7**, **9** have been previously reported and could be readily identified by the characteristic singlet of the orthoformate methine proton (in the 5.75 to 5.90 ppm range).[37–39] In contract, cyclic compound **8** and acyclic orthoesters (e.g. **3**, **4**, **5**) were either never reported or poorly characterized in the prior literature background. However, a characteristic singlet in the 5.00 to 5.30 ppm area could be identified, and was attributed to the orthoformate methine proton of each acyclic orthoesters or cyclic species **8** (Figure 3.3b). These signals were unambiguously assigned through 2D-HMBC analysis, which allowed to correlate these orthoformate methine protons to their vicinal methylenoxy neighbors. For example, the methine proton of parent orthoester **2b** showed a single correlation with a vicinal methylenoxy group from the ethoxy limb, whereas the methine proton of cyclic hybrid orthoester **3** gave an additional correlation from its ethylene glycol moiety (Section S4 in the Supporting Information). Structures of acylic **3**, **4**, and **5** were later confirmed by preparative isolation of the compounds. Structural identity was confirmed through NMR and GC-MS (Section S12 in the Supporting Information).

3.4.3 COMPUTER-ASSISTED KINETIC MODELING

Having identified the diversity of DCE products by high-field ^{1}H-NMR, quantification with an internal standard was performed, and a speciation curve (*i.e.*, concentration of compounds over time) was built. A second Python script, based on the chemical kinetic package developed by Boudoire *et al.*, was then used to solve the differential equations that describe the concentration over time of each species in the DCE system.[12] The script developed for our work enables the calculation of the kinetic constant for each compound and offers quantitative and graphical tools to evaluate the quality of the model.

The overall strategy relied on solving equilibrium expressions involving an increasing number of species detected by NMR. For each iteration, a kinetic model was constructed to fit the speciation curves and estimate the forward and reverse rate constants for the proposed exchange pathways. Reactions with negligible kinetic contributions were excluded from the model. This model then served as the basis for subsequent iterations, allowing the progressive incorporation of additional species and/or alternative reversible interconversions. The process was repeated until all species were incorporated, and a highly accurate fitting of the data was obtained. Further details on the methodology for model development and iterative refinement are provided in Section S7 of the Supporting Information. **Model I** (Figure 3.4a) considered only the bidirectional steps connecting the starting materials (ethylene glycol **1** and parent triethyl orthoformate **2b**) to the primary hybrid orthoester **3**, along with its subsequent interconversion into secondary acyclic hybrid orthoester **5** and cyclic hybrid orthoester **6** (Section S7.4 of the Supporting Information). The calculated equilibrium

constants indicated that the formation of **3** is reversible but thermodynamically favored (K = 3), while its conversion to **6** proceeds essentially irreversibly (K = 164.7).

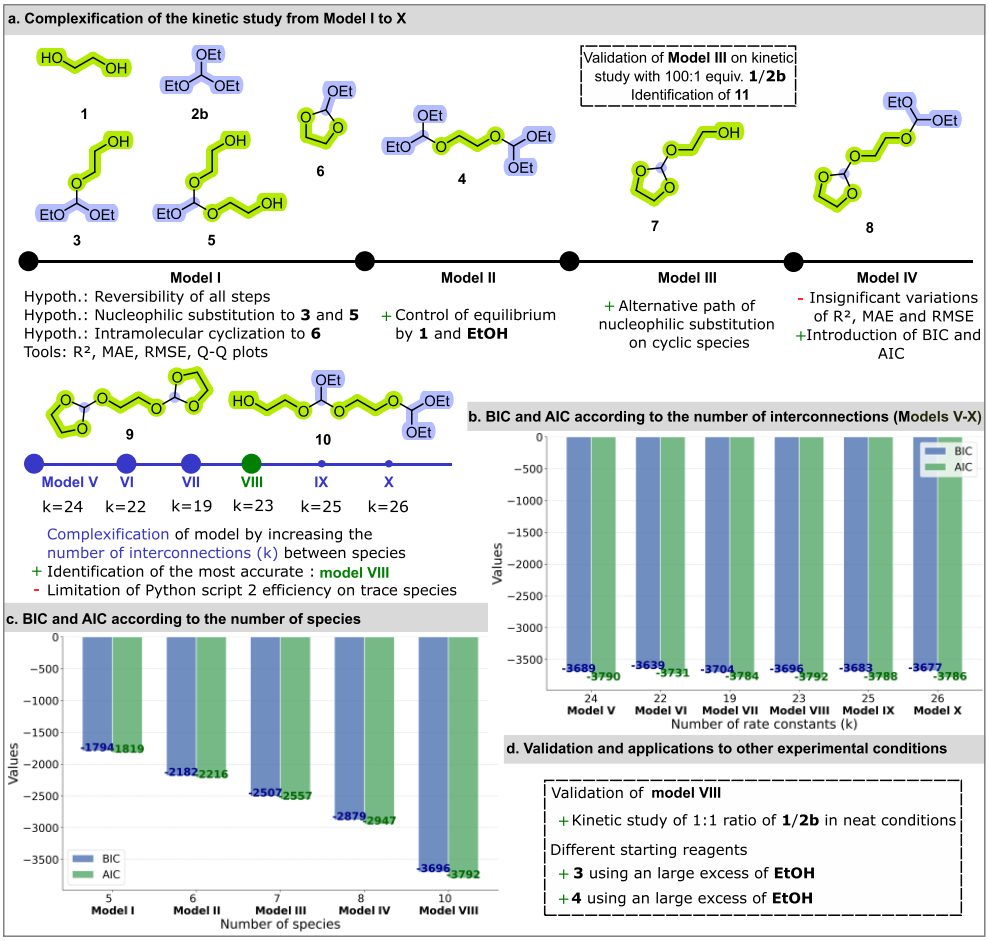

Figure 3.4 (a) Strategy toward the complexification of the model according to the number of species and the number of interconnections. (b) Calculated BIC and AIC for models **V** to **X**. (c) Calculated BIC and AIC for final models **I**, **II**, **III**, **IV** and **VIII** and, (d) Validation (kinetic study under neat conditions) and applications to other experimental conditions (kinetic studies starting from **3** or **4** in presence of an excess of **EtOH**).

This provided the basis for **Model II** (Figure 3.4a), which integrated the formation of dimeric species **4**. Two alternate paths were considered for its formation: (IIa) the reaction of parent orthoformate **2b** with primary hybrid orthoester **3**, releasing ethanol; and/or (IIb) the self-condensation of **3**, releasing ethylene glycol (**1**). The model fitting obtained by including each individual equilibrium pair, as well as their combination (IIa+IIb) were evaluated using four statistical metrics: the coefficient of determination (R^2), root mean squared error (RMSE), mean absolute error (MAE), and quantile-quantile (Q-Q) plots (see Section S7.5 of the Supporting Information). All tested paths returned high R^2 values ($R^2 > 0.95$) for most species but **5**. Only pathway (IIb) gave a high R^2 for **5** (R^2 = 0.98), whereas alternative models

resulted in significantly lower values ($R^2 < 0.73$). Analysis of residuals via MAE and RMSE further confirmed that pathway (b) substantially reduced the fitting error for compound **5**.

Model III (Figure 3.4a) expanded the reaction network to include the formation of species **7** via two alternative dynamic covalent paths: (IIIa) the intramolecular cyclization of **5** and/or (IIIb) reversible exchange between compound **6** and ethylene glycol (**1**). Kinetic analysis revealed that the cyclization (path IIIa) proceeds irreversibly, whereas path IIIb is reversible (K = 0.5), and under the strong influence of the relative concentrations of **6** and **1**. The contribution of path IIIb was experimentally validated by increasing the excess of **1** (100:1 **1**/**2b** ratio), which shifted the equilibrium in favor of species **7** (Section S7.7 in the Supporting Information).

Model IV (Figure 3.4a) further elaborated the exchange network by incorporating the formation of species **8** through three competing dynamic routes: (IVa1) the reaction of **7** with primary hybrid orthoester **3** or (IVa2) the reaction of **7** with parent orthoformate **2b**, and (IVb) the reversible interconversion involving **6** and **3**. All possible combinations of these paths (seven in total) were considered to account for the bidirectional connectivity within the network. Comparative analysis based on R^2, RMSE, and MAE showed minimal statistical variation across the tested models (Section S7.8 in the Supporting Information). To address model selection in light of such an increased complexity, both the Akaike Information Criterion (AIC) and Bayesian Information Criterion (BIC) were used (Section S6.2 in the Supporting Information).[40] Although a combination of paths IIIa1 and IIIa2 yielded the lowest penalized fit scores, the differences remained marginal and statistically inconclusive. The limited discriminative power was attributed to the low steady-state concentration of species **8**, which reduced the sensitivity of model validation (Section S7.8. in the Supporting Information).

The last products identified by NMR were species **9** and **10**, both detected at low concentrations (> 6 mM). Due to their low abundance and the increasing complexity of the dynamic network, reliable assessment of the associated exchange pathways became more challenging. To mitigate such challenge, the possible paths leading to species **8**, **9** and **10** were evaluated separately through a new series of **Models** (**V** to **X**). Each of these models encompassed the full set of species (**1** to **10**), but they differed in the number and the topology of dynamic covalent interconnections (k).

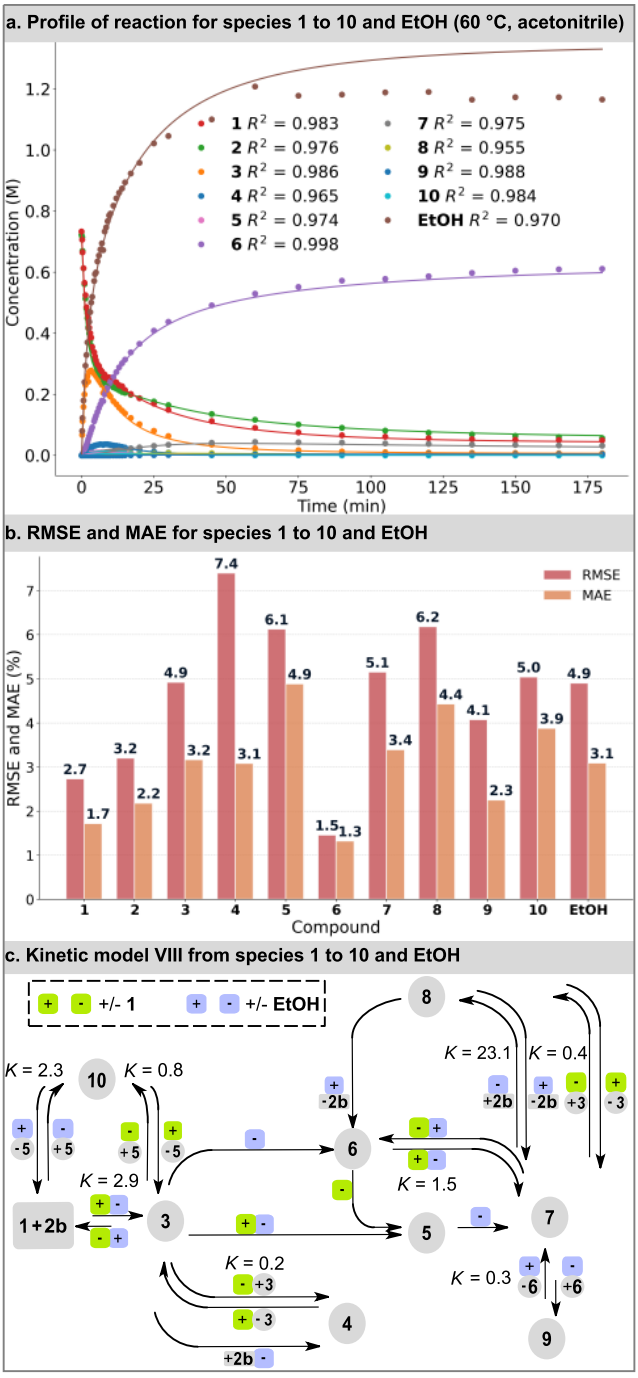

Figure 3.5 (a) Speciation curve for compounds **1** to **10** and **EtOH** and their corresponding coefficient of determination (R^2) for **Model VIII**. (b). Calculated root means square error (RMSE) and mean average error (MAE) for **Model VIII** (c) Finalized kinetic **Model VIII** developed through computer-assisted modeling.

Model comparison based on AIC and BIC revealed only modest differences among candidates, with **Models V** and **VIII** offering the best statistical fits. Examination of the RSME and MAE discarded **Model VI** and **VII** due significant residual errors, particularly in the fitting of species **8** (Section S2.7.8 in the Supporting Information) due to the large error for compound **8**. **Model VIII** was ultimately preferred to **Model V** for its reduced complexity while maintaining comparable accuracy (Figure 3.4b). From a mechanistic standpoint, the choice of **Model VIII** over **Model V** implies that the exchange between **6** and **3** leading to **8** contributes negligibly under our conditions, and can be considered non-reversible within the network. The refinement of the kinetic model resulting in **Model VIII** was demonstrated to improve accuracy, as indicated by the decreasing values of BIC and AIC with the inclusion of additional species, as shown in Figure 3.4c.

3.4.4 VALIDATION AND APPLICATION OF THE MODELS TO OTHER CONDITIONS

Model VIII provided an excellent fit to the experimental data, with individual species obtaining coefficients of determination (R^2) between 0.95 and 0.99, and most residuals falling within the 5% of confidence interval (Q-Q plot, Section S7.9.2 in the Supporting Information). To further test its applicability and robustness, **Model VIII** was applied to three additional kinetic data sets: (i) using compound primary hybrid orthoester **3** as the initial substrate, (ii) using dimeric species **4** as starting material, and (iii) carrying out the reaction under neat conditions.

The use of alternative starting materials (*i.e.*, **3** and **4**) required their preparative isolation, since no commercial sources or protocols were available. The synthesis of **3** was guided by prior kinetic insights: a short reaction time (2 min) and a reduced temperature minimized overreaction and enabled isolation in *ca*. 70% yield via vacuum distillation (with ~30% of **1** remaining). Compound **4** was selectively prepared with a larger excess of parent orthoformate **2b**, and purified using the same method as **3**.

Each of the isolated compounds was subjected to kinetic analysis in the presence of ethanol. The resulting speciation profiles were input into **Model VIII**, which reproduced the experimental data with high accuracy ($R^2 > 0.90$) without requiring further parameter adjustment. This confirms the predictive reliability of **Model VIII**, and its capacity to generalize across varying initial experimental conditions.

Performing the reaction under neat conditions enabled the detection of minor species in higher concentrations. Aside from compounds **8**, **9**, and **10**, which were previously observed in trace amounts, several unidentified species emerged in the NMR spectra. Distinct singlets in the 5.00 to 5.30 ppm area suggested the formation of new acyclic orthoester derivatives. When **Model VIII** was applied to this dataset, it continued to provide an excellent overall fit ($R^2 > 0.92$) for most species. However, the fit for compound **8** remained limited ($R^2 > 0.50$), likely reflecting the increased complexity of the reaction mixture. Models including other possible exchange paths between compounds **1** to **10** failed to provide gains in accuracy (Section S7.11 in the Supporting Information). While including the newly observed species

could further enhance the predictive performance, their structural elucidation and integration were considered beyond the scope of this study.

3.4.5 Analysis of kinetic Model VIII

The final kinetic model (**Model VIII**) emphasizes species **3** and **7** as central intermediates within the DCE network, due to their high degree of interconnectivity with other network members. Both compounds bear available hydroxyl moieties that enable multiple exchange reactions, thus making them central & multidirectional hubs through which reactivity flows. Overall, the progression of the equilibrium relies on the transient buildup of **3** and **7** before the system stabilizes toward later downstream products.

The initial reaction between **1** and parent orthoester **2b** favors the formation of primary hybrid orthoester **3** (K = 2.9), which is then rapidly converted to cyclic product **6** through an intramolecular process. Early in the reaction (~ 3 min), dimer **4** is formed reversibly from **3**, but once **3** is consumed through its irreversible conversion to **5** and **6**, **4** undergoes back-exchange to regenerate **3** and is ultimately depleted. The transformation of **3** to **5** is also irreversible, resulting the sustained presence of **5** until it is converted. The conversion of **5** to **7**, after approximately 50 min, follows again an irreversible step.

Whereas species **4** and **5** are only transiently present, compound **6** accumulates and becomes the dominant species in the DCE network. Kinetic modeling shows the major consumption path for **6** is its conversion to **7**. However, this step requires at least one equivalent of **1**, which is largely depleted after the first hour of reaction, thereby limiting the extend of conversion. When ethylene glycol (**1**) is supplied in large excess (e.g., 100 equivalents) the equilibrium shifts significantly toward the formation of **7**, confirming that this transformation depends on substrate availability. Furthermore, the transformation of **6** to **7** is reversible, both directly and through an intermediate path involving species **8**, further contributing to the persistence of **6** in the system. Compounds **9** and **10** are present in low concentration due to their reliance on **5** and **7**, which are themselves short-lived and subject to reversible formation.

Computer-assisted solving of the reaction kinetics provides valuable insight into equilibrium position and the relative importance of competing reactions. However, direct comparison of rate (k) or equilibrium (K) constants are sometimes limited by differing reaction orders. Furthermore, predictions for minor species remain uncertain, and the kinetic model does not capture the forces driving the equilibrium at the molecular level. To address these limitations and gain a more comprehensive understanding, a computational study using Density Functional Theory (DFT) was performed.[41]

3.4.6 COMPUTATIONAL INVESTIGATION OF DCE MECHANISM

The mechanism of the DCE system was studied using DFT. It can be categorized into two main stages: (a) activation of an orthoester to generate a reactive intermediate, either a carbocation (a1) or a carbene (a2), and (b) a subsequent nucleophilic attack by a hydroxyl group, occurring either intermolecularly or intramolecularly (Figure 6; see Sections S10–S11 in the Supporting Information).
Step (a1) proceeded through a concerted activation of acyclic orthoesters (e.g., compounds **2b**, **3**, **5**) by formic acid (FA), to yield carbocationic intermediate **int.1** (Figure 3.6a1). The resulting transition state (TS) involves simultaneous protonation of one ethoxy group by the acidic proton of FA and cleavage of the corresponding C–O bond. This C–O bond scission is stabilized via hydrogen bonding between the orthoester proton and the carbonyl oxygen of FA (**TS.1-int.1**). When the orthoester bears a free hydroxyl group, such as in compounds **3** and **5**, Natural Population Analysis (NPA) indicated that the hydroxyl proton (partial charge +0.50 e^-) is more acidic than the orthoformate methine proton (+0.26 e^-). Consequently, the geometry of the TS shifts: FA preferentially forms a hydrogen bond with the hydroxyl group, altering the TS geometry (e.g., **TS.2-3**) and stabilizing the resulting carbocationic intermediates **int.2** (ΔG^{rea} = 12.5 kcal mol^{-1}) compared to **int.1** (ΔG° = 13.2 kcal mol^{-1}). This confirms the influence of the availability of free hydroxyl moieties on reactivity and intermediate stabilization.

The activation of cyclic orthoester derivatives (e.g., compounds **6**, **7**, **8**, **9**) proceeded through the formation of a carbene intermediate (step a2; Figure 3.6a2). For compound **6**, an asynchronous mechanism was identified, involving an initial carbocation generation followed by deprotonation of the orthoformate methine proton to yield carbene intermediate **int.6** (Section S11.3 in the Supporting Information). In contrast, the same transformation computed for species **7** showed a stabilized carbocation intermediate (**int.7**), that subsequently formed carbene intermediate **int.11**. This mechanistic divergence, from concerted to stepwise mechanism was attributed to the greater stabilization of the carbocation in **7**, arising from an intramolecular hydrogen bonding interaction with its hydroxyl group. Energetically, **int.7** was more stable (ΔG^{rea} = 16.8 kcal mol^{-1}) than carbene **int.6** (23.6 kcal mol^{-1}). **TS.1-int.7** shows a stereoelectronic interaction (second order stabilization energy of 7.3 kcal mol^{-1}) between the hydroxyl group and the departing ethoxide, which contributed to a lower activation barrier of 4.5 kcal mol^{-1} compared to **TS.1-int.6**.

Following the activation step, the reactive intermediates formed in step (a), whether carbocationic (a1) or carbonic (a2), undergo a nucleophilic attack by an oxygen atom in step (b), either inter- or intramolecularly. This nucleophilic attack was consistently found to have a low activation barrier ($\Delta G^{\neq} < 3$ kcal mol^{-1}) and a strong thermodynamic driving force (ΔG^{rea} < -11 kcal mol^{-1}). These results indicate that step (b) is both fast and highly favorable under the reaction conditions.

Computational analysis supported the reversible formation of primary hybrid orthoester **3** from **1** and parent orthoformate **2b**, as previously suggested by kinetic modeling. The activation barrier for the reverse reaction, corresponding to the release of **1** from **3**, and the formation of **int.1**, was found to differ by less than 1 kcal mol^{-1} from the forward reaction

(loss of EtOH, **TS.1-int.2**). This fact supports a near-equilibrium process. The subsequent reaction of **3** with **1** to form **5** was confirmed as kinetically favored. The reverse reaction (release of **1** from **5**) had an activation barrier ($\Delta G^{\neq}$) of 14.9 kcal mol^{-1}, which is slightly higher than the 13.4 kcal mol^{-1} computed for the forward step, confirming a kinetically favorable progression. Once formed, **5** undergoes rapid intramolecular cyclization to **7** ($\Delta G^{\neq}$ = 13.5 kcal mol^{-1}).

All three primary forward reactions of **3** leading to compounds **4**, **5** and **6** are fast, with $\Delta G^{\neq}$ < 2.3 kcal mol^{-1}. Thermodynamically, compound **5** was slightly more stable than **4** (of –1.3 kcal mol^{-1}) and **6** (of –2.3 kcal mol^{-1}). However, experimental data consistently showed that compound **6** predominates. This discrepancy was ascribed to the fast depletion of **1** and **2b** at the onset of the reaction, which limits the formation of **4** and **5**, while also reducing the extent of the conversion of **6** into **7**. Once formed, the orthoformate methine proton in **6** becomes less acidic, thus decreasing its affinity for FA. Furthermore, the activation of **6** requires the formation of carbene **int.6** which has the highest activation barrier among all intermediates studied ($\Delta G^{\neq}$ of 23.8 kcal mol^{-1}, **TS.1-int.6**), further hindering its progression.

Interestingly, despite the high activation barrier, kinetic analysis indicated that the net transformation of **6** towards **7** remains favored. This apparent contradiction can be rationalized by two factors: first, FA principally interacts with the more acidic hydroxyl group in **7**, rather than with the orthoformate methine proton on **6**, thus limiting the backward step; second, the concentration of **7** remains low compared to **6**, due to its ongoing conversion to downstream products **8** and **9**. This shifts the equilibrium toward continued formation of **7**. As a result, compound **6** accumulates as the predominant species within the DCE network, while **7**, **8**, and **9** are present in lower amounts.

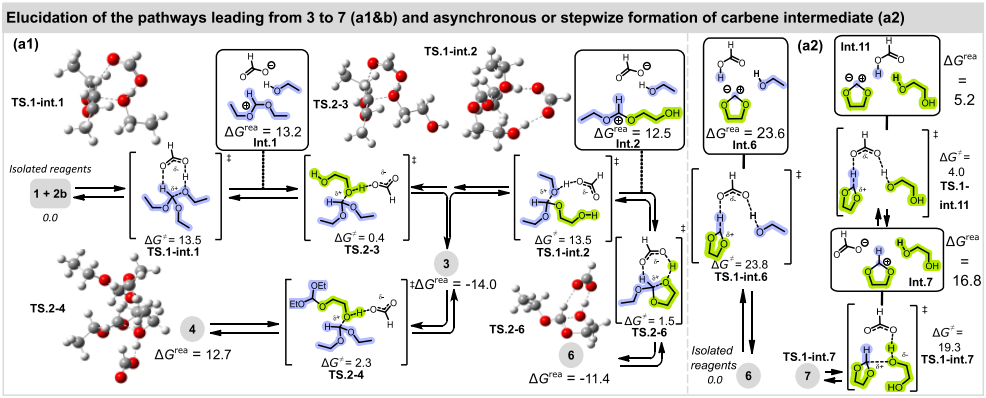

Figure 3.6 (a1) Computational investigation of the pathways including transition states structures and resulting products from **3** to **7**. (a2) Stepwise or asynchronous mechanisms leading to the formation of **int.6** or **int.7** and **int.11** calculated at the B3LYP-GD3BJ/6-31+G* level of theory (SMD = MeCN).[41] Activation barriers ($\Delta G^{\neq}$) and Gibbs energy (ΔG^{rea}) are given in kcal mol^{-1}.

3.4.7 TUNING DCE NETWORKS BY CHANGING THE CATALYST, SOLVENT EFFECTS AND PARENT ORTHOESTER

To complement the kinetic and mechanistic mapping of the DCE system, the influence of Brønsted acid catalysts, solvent effects and the nature of the parent orthoesters on reactivity was systematically investigated through a combination of experimental screening and DFT computations (Figures 3.7, 3.8). These parameters were found to exert distinct yet intertwined effects on both the rate and selectivity of the dynamic covalent exchange, enabling precise modulation of the reaction network. They further confirmed that the rate-determining steps (RDS) involves orthoester activation via protonation and C–O bond cleavage, consistent with the formation of a stabilized carbocation intermediate.

The catalytic performance of a panel of mono- and dicarboxylic acids was evaluated by monitoring the conversion of compound **2b** and the formation of the most abundant products (**3** and **6**) over a 45-minute period. Experimental data was collected using various organic acids (Figure 3.7a) including acetic acid (AA), pimelic acid (PA), benzoic acid (BA), succinic acid (SA), oxalic acid (OA), trichloro- and trifluoro- acetic acid (TCA and TFA).

The activation ($\Delta G^{\neq}$) and reaction (ΔG^{rea}) parameters for the forward step connecting primary hybrid orthoester **3** to cationic **int.2** decreased linearly with decreasing pK_a of the acid (Figure 3.7b) as a result of the greater proton exchange ability between the acid and substrate. However, the screening of catalysts revealed that acid strength alone was insufficient to predict reactivity trends. Carboxylic acids of comparable strength, such as AA (pK_a = 4.76) and PA (pK_a = 4.71), led to similar activation parameters ($\Delta G^{\neq}$ (AA) = 17.7 kcal mol^{-1}, $\Delta G^{\neq}$ (PA) = 17.4 kcal mol^{-1}, respectively). A modest conversion of parent orthoester **2b** (~41%), mostly to form primary hybrid orthoester **3** (~30%) and **6** as minor component (~5%), was experimentally observed (Figure 3.7c). Slightly increasing the acidic strength with BA (pK_a = 4.20) substantially improved the conversion (69%), with the formation of **6** in 21%. Interestingly, dicarboxylic acids featuring a short carbon backbone (C ≤ 4) such as SA (pK_a = 4.16) and OA (pK_a = 1.20), exhibited superior catalytic activity. OA, in particular, led to complete conversion of parent orthoester **2b** in less than 30 s and yielded over 85% of **6**. These effects were rationalized by DFT calculations, which showed that intramolecular hydrogen bonding (HBD) between the two carboxyl groups in dicarboxylic acids significantly stabilized the transition state. When the second carboxylic acid moiety became involved in an HBD interaction with the catalytically active one, $\Delta G^{\neq}$ decreased from 16.5 kcal mol^{-1} to 11.6 kcal mol^{-1} (see **TS.OA.H** in Figure 3.5b). This stabilization highlights the critical role of noncovalent interactions in promoting DCE.

In contrast, stronger acids such as TCA or TFA (p*K*a = 0.77 and 0.33, respectively) led to extensive degradation of orthoesters, forming hydrolysis products, such as ethyl formate (**13**) and 3-hydroxypropyl formate (**14**), in 65% overall yield (section S11.4 in the Supporting Information). These observations underscore the need for catalytic activation that is both potent and selective, avoiding overactivation that diverts the reaction into non-productive or destructive pathways.

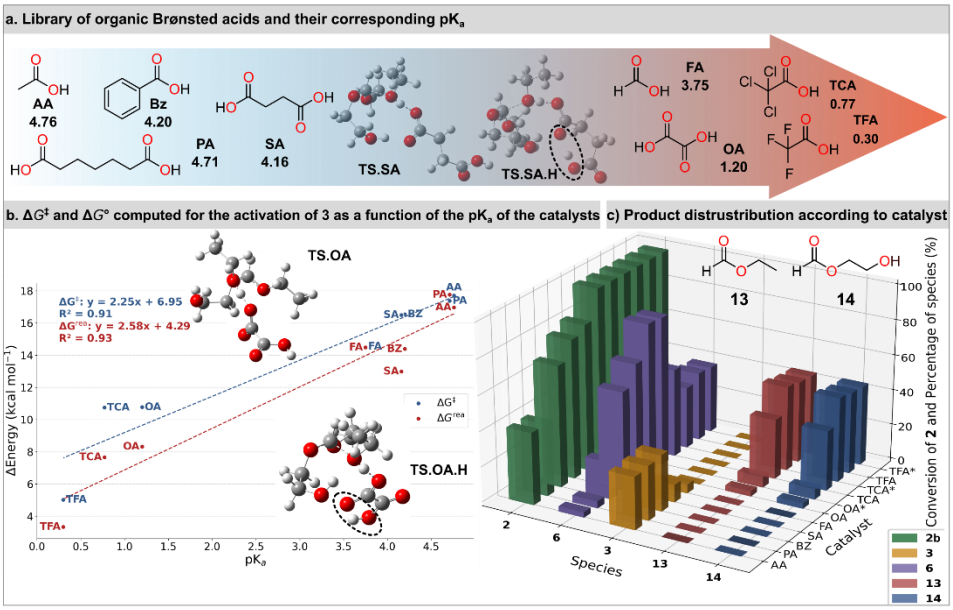

Figure 3.7 (a) Library of various homogeneous Brønsted acids with their pK$_a$,[42] (b) Correlation of the activation barriers and reaction Gibbs free energies with the pK$_a$ of a range of acid catalysts. Free Gibbs energies (ΔG^{rea}, in red) and activation barriers ($\Delta G^{\neq}$, in blue) plotted as a function of pK$_a$ of the catalysts for the activation of **3** into **int.2**. (c) Experimental conversion of **2b** and resulting product distribution obtained for each catalyst with a loading at 5 or 10 mol% (marked with *).

We were also interested in understanding better how differences in solvent properties impact the reaction system. One strong incentive was the natural propensity of the reaction to self-modify solvent composition. Indeed, as the DCE network expands, ethanol is increasingly released, with the final solvent composition reaching a 13:1 ratio between acetonitrile and ethanol. Several metrics were selected to quantify the impact of the solvent: Hansen parameters for dispersion (δ_d), polarity (δ_p) and hydrogen bonding ability (δH), Guttman's donor (DN) and acceptor numbers (AN) (Figure 3.8a). Aside from acetonitrile, two additional solvents were screened: dimethyl sulfoxide (DMSO) and dimethylformamide (DMF). Both experimental and computational data sets using FA as a catalyst (Section S11.4 in the Supporting Information) were used to clarify the effect of solvents. Experimental kinetics (over 45 min) were analyzed using **Model VIII** to obtain the corresponding rate constants. The results indicated that solvent modulation clearly introduced an additional layer of complexity by modulating both TS stabilization and catalyst availability. This phenomenon was also accounted for in the DFT computations, where both implicit and explicit solvation (trimers) were considered (Section S11.5 in the Supporting Information).

Among the aprotic solvents tested, DMSO (DN = 29.8), DMF (DN = 26.6), and MeCN (DN = 14.1) differed substantially in their influence. DFT calculations showed that DMSO provided the most effective stabilization of the carbocationic transition state ($\Delta G^{\neq}$ = 9.3 kcal mol^{-1}), followed by MeCN ($\Delta G^{\neq}$ = 11.6 kcal mol^{-1}) and DMF ($\Delta G^{\neq}$ = 12.8 kcal mol^{-1}). However, this benefit came at a cost: DMSO also formed highly stable solvation complexes with formic acid (ΔE_{diss} = -2.3 kcal mol^{-1}), which effectively reduced the free concentration

of catalyst in solution. In contrast, MeCN, with a positive dissociation energy (ΔE_{diss} = +6.0 kcal mol^{-1}), preserved the catalyst availability, while still offering sufficient transition state stabilization in contrast to DMF (ΔE_{diss} = 4.2 kcal mol^{-1}). These computational results matched experimental observations (Figure 3.8a): reactions carried out in MeCN, which is associated with both lower DN and δ_H, were consistently associated with higher rates and yields than those in DMSO or DMF. It is also expected that the reaction is further accelerated by the consequent release of EtOH. These effects translate through the highest yields of compound **6** under otherwise identical conditions. Other solvent parameters such as London dispersion forces (δ_d) or polarity (δ_p) appear to have little influence on reaction kinetics based on the data in Figure 3.8a. Optimal solvent choice must therefore balance polarity, hydrogen bonding ability, and catalyst coordination to favor productive exchange over sequestration or deactivation, hence modulating the entire DCE network.

In addition to catalyst and solvent effects, the structure of the parent orthoester itself was shown to play a pivotal role in shaping the reaction kinetics (Figure 3.8b). Specifically, the identity of the alcohol released during exchange, *i.e.*, methanol (MeOH, from **2a**), ethanol (EtOH, from **2b**), or isopropanol (*i*PrOH, from **2c**) had a dual impact on the system. On one hand, DFT demonstrated that smaller, more polar alcohols provided better TS stabilization: $\Delta G^{\neq}$ of 6.8 kcal mol^{-1}, 7.2 kcal mol^{-1} and 8.6 kcal mol^{-1} were computed for MeOH, EtOH and *i*PrOH (explicit solvation with a trimer). On the other hand, these same alcohols had distinct inhibition behavior through catalyst complexation. MeOH, with its high hydrogen-bond donor ability (δ_H = 10.9 cal mol$^{-1/2}$, DN = 19.0), formed the most stable FA–alcohol complex (ΔE_{diss} = -6.7 kcal mol^{-1}), significantly reducing the effective catalytic activity and reducing the rate. In contrast, *i*PrOH (δ_H = 8.0 cal mol$^{-1/2}$, DN = 21.1) exhibited weaker interactions with FA (ΔE_{diss} = +2.4 kcal mol^{-1}), allowing for faster turnover despite a lower TS stabilization. Experimental results corroborated these insights: triisopropyl orthoformate **2c** yielded the highest rate constants among the three orthoester derivatives tested, followed by triethyl (**2b**) and trimethyl orthoformates (**2a**).

Figures 3.7 and 3.8 illustrate that optimal performance in DCE networks does not stem from maximizing any single parameter, such as acidity, solvent polarity, or leaving group ability, but rather from achieving a finely tuned balance among them. Catalysts featuring cooperative hydrogen-bonding motifs (e.g., OA), solvents with low catalyst-binding affinity (e.g., MeCN), and parent orthoesters that release weakly coordinating alcohols (e.g., **2c**) consistently led to the most favorable reactivity profiles. These components collectively influence not only the rates of individual elementary steps, but also the topology and directionality of the overall reaction network. Taken together, these results establish a coherent framework for modulating DCE reactivity through rational design of medium composition. The combined effects of catalyst structure, solvent environment, and substrate identity define the accessible kinetic landscape and enable the emergence of fast, selective, and robust exchange processes. These general principles potentially extend beyond the present model system and could offer generalizable guidelines for controlling dynamic behavior in complex molecular assemblies, supramolecular systems, and adaptive materials.

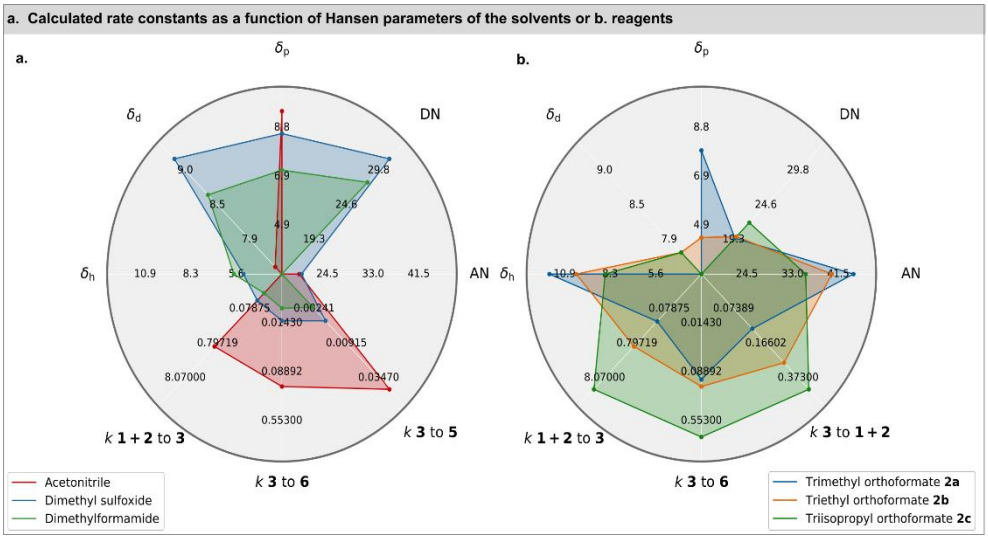

Figure 3.8 (a) Chart representing the calculated rate constants for the reaction of **1** with **2b** (1:1 ratio) using various solvents including acetonitrile (MeCN), dimethyl sulfoxide (DMSO) and dimethylformamide (DMF) as a function of their Hansen parameters and Guttman numbers (logarithmic scale). (b) Calculated rate constants for the reaction of **1** with **2** (1:1 ratio) using trimethyl orthoformate (**2a**), triethyl orthoformate **2b** and triisopropyl orthoformate **2c** in acetonitrile.

3.4.8 CONCLUSION

Kinetic analysis forms the cornerstone of reaction optimization, enabling precise catalyst selection, scalable processes, and waste reduction through mechanistic understanding. To empower chemists in this critical task, we developed two complementary Python tools aiming to assist in the interpretation of complex spectral datasets. The first script automates signal processing of data before tensorial decomposition to yield statistical metrics to estimate the number of compounds in spectral kinetic datasets. Predictions made with our script proved to be accurate, as ten compounds were identified through combination of NMR and GC-MS. Once the product distribution was identified, an intuitive kinetic modeling script was developed based on an existing code, which adjusts experimental data with a theoretical model. This script enables the development of mechanistically grounded models from the DCE between orthoesters and alcohols while rapidly testing hypotheses. The overall model elaborated in this work displayed R^2 values above 0.95 for all the ten species characterized and demonstrated its successful transposition to other experimental conditions ($R^2 > 0.90$).

Kinetic analysis, supported with DFT computations, confirmed the kinetic model developed using script 2. Both acyclic and cyclic orthoesters were observed to produce carbocations. In the case of cyclic orthoesters, an additional step involving deprotonation led to the formation of carbene species. These intermediates could then react further with nucleophiles. The only exception was compound **6**, which followed an asynchronous reaction mechanism, directly leading to the carbene. A combined experimental and computational screening of catalysts revealed an enhanced stabilization of dicarboxylic acids compared to monocarboxylic acids.

This effect was evidenced by comparable activation energy barriers for OA, TCl_3 and TF_3, despite the lower acidity of the dicarboxylic acid, and similar conversion rates of **2b** within the same timeframe. The nature of the solvent and alcohol by products were also found to be critical for the reaction kinetic. Aprotic solvent with high DN and δ_H efficiently stabilized the carbocation transition states but also promoted catalyst trapping through favorable formation of solvent-catalyst complexes. In contrast, systems solvated with alcohols exhibited even greater stabilization of carbocations although energetically favorable formation of MeOH-FA reduced catalyst availability. Overall, the highest reaction rates were achieved with aprotic solvents featuring low Lewis basicity and hydrogen bonding ability, along alcohol by-products that formed energetically unfavorable complexes with the catalyst.

By integrating computational and experimental tools, this study goes beyond empirical optimization, offering a generalizable strategy to dissect complex reaction networks while balancing mechanistic accuracy with experimental feasibility. Moreover, it establishes a solid foundation for the development of predictive models capable of guiding the design of specific medium compositions through tailored experimental conditions.

3.5 REFERENCES

[1] Deem, M. C.; Cai, I.; Derasp, J. S.; Prieto, P. L.; Sato, Y.; Liu, J.; Kukor, A. J.; Hein, J. E. Best Practices for the Collection of Robust Time Course Reaction Profiles for Kinetic Studies. ACS Catal. **2023**, 13 (2), 1418–1430.

[2] D-T Nielsen, C.; BurésBur, J. Visual Kinetic Analysis. Chem. Sci. **2019**, 10, 348–353.

[3] Orito, Y. Practical Methodology in Kinetic Modeling for Complex Reactions: Weighted Error Manipulation to Allow Effective Model Evaluation in a Borderline S_N Reaction. *ACS Omega* **2025**, *10*, 9,9266-9274.

[4] Dahlgren, B. ChemPy: A Package Useful for Chemistry Written in Python Software. *J. Open Source Softw* **2018**, *3* (24), 565.

[5] Ashraf, C.; Pfaendtner, J. Assessing the Performance of Various Stochastic Optimization Methods on Chemical Kinetic Modeling of Combustion. *Ind. Eng. Chem. Res.* **2020**, *59* (43), 19212–19225.

[6] Gillespie, D. T. Stochastic Simulation of Chemical Kinetics. *Annu. Rev. Phys. Chem.* **2007**, *58*, 35–55.

[7] Saadat, N. P.; van Aalst, M.; Ebenhöh, O. Network Reconstruction and Modelling Made Reproducible with Moped. *Metabolites* **2022**, *12* (4), 275.

[8] Finnigan, W.; Cutlan, R.; Snajdrova, R.; Adams, J. P.; Littlechild, J. A.; Harmer, N. J. Engineering a Seven Enzyme Biotransformation Using Mathematical Modelling and Characterized Enzyme Parts. *ChemCatChem* **2019**, *11* (15), 3474–3489.

[9] Badenhorst, M.; Barry, C. J.; Swanepoel, C. J.; van Staden, C. T.; Wissing, J.; Rohwer, J. M. Workflow for Data Analysis in Experimental and Computational Systems Biology: Using Python as 'Glue. *Processes* **2019***, 7* (7), 460.

[10] Müller, C.; Pascher, T.; Eriksson, A.; Chabera, P.; Uhlig, J. KiMoPack: A Python Package for Kinetic Modeling of the Chemical Mechanism. *J. Phys. Chem. A* **2022**, *126* (25), 4087–4099.

[11] Newville, M.; Stensitzki, T.; Allen, D. B.; Rawlik, M.; Ingargiola, A.; Nelson, A. Lmfit: Non-Linear Least-Square Minimization and Curve-Fitting for Python. *Astrophys. Source Code Lib.* **2016**, ascl:1606.014.

[12] Liu, Y.; Le Formal, F.; Boudoire, F.; Guijarro, N. Hematite Photoanodes for Solar Water Splitting: A Detailed Spectroelectrochemical Analysis on the PH-Dependent Performance. *ACS Appl. Energy Mater.* **2019**, *2* (9), 6825–6833.

[13] You, L. Dual Reactivity Based Dynamic Covalent Chemistry: Mechanisms and Applications. *Chem. Commun.* **2023**, *59* (87), 12943–12958.

[14] Brachvogel, R. C.; von Delius, M. The Dynamic Covalent Chemistry of Esters, Acetals and Orthoesters. *Eur. J. Org. Chem.* **2016**, 2016 (22), 3662–3670.

[15] Xin, X.; Zhang, Z.; Zhang, X.; Chen, J.; Lin, X.; Sun, P.; Liu, X. Bioresponsive Nanomedicines Based on Dynamic Covalent Bonds. *Nanoscale* 2021, *13* (27), 11712–11733.

[16] Frei, P.; Hevey, R.; Ernst, B. Dynamic Combinatorial Chemistry: A New Methodology Comes of Age. *Chem. – Eur. J.* **2019**, *25* (1), 60–73.

[17] Ulrich, S. Growing Prospects of Dynamic Covalent Chemistry in Delivery Applications. *Acc. Chem. Res.* **2019**, *52* (2), 510–519.

[18] Qin, B.; Liu, S.; Huang, Z.; Zeng, L.; Xu, J. F.; Zhang, X. Closed-Loop Chemical Recycling of Cross-Linked Polymeric Materials Based on Reversible Amidation Chemistry. *Nat. Commun.* **2022**, *13* (1), 1–9.

[19] Zheng, N.; Xu, Y.; Zhao, Q.; Xie, T. Dynamic Covalent Polymer Networks: A Molecular Platform for Designing Functions beyond Chemical Recycling and Self-Healing. *Chem. Rev.* **2021**, *121* (3), 1716–1745.

[20] Winne, J. M.; Leibler, L.; Du Prez, F. E. Dynamic Covalent Chemistry in Polymer Networks: A Mechanistic Perspective. *Polym. Chem.* **2019**, *10* (45), 6091–6108.

[21] Hollstein, S.; von Delius, M. The Dynamic Chemistry of Orthoesters and Trialkoxysilanes: Making Supramolecular Hosts Adaptive, Fluxional, and Degradable. *Acc. Chem. Res.* **2023**, *18*, 25.

[22] Wang, X.; Shyshov, O.; Hanževački, M.; Jäger, C. M.; Von Delius, M. Ammonium Complexes of Orthoester Cryptands Are Inherently Dynamic and Adaptive. *J. Am. Chem. Soc.* **2019**, *141* (22), 8868–8876.

[23] Shyshov, O.; Brachvogel, R. C.; Bachmann, T.; Srikantharajah, R.; Segets, D.; Hampel, F.; Puchta, R.; von Delius, M. Adaptive Behavior of Dynamic Orthoester Cryptands. *Angew. Chem. Int. Ed.* **2017**, *56* (3), 776–781.

[24] Brachvogel, R. C.; Hampel, F.; Von Delius, M. Self-Assembly of Dynamic Orthoester Cryptates. *Nat. Commun.* **2015**, *6* (1), 7129.

[25] Hu, J.; Gupta, S. K.; Ozdemir, J.; Beyzavi, M. H. Applications of Dynamic Covalent Chemistry Concept toward Tailored Covalent Organic Framework Nanomaterials: A Review. *ACS Appl. Nano Mater.* **2020**, *3* (7), 6239–6269.

[26] Haase, F.; Lotsch, B. V. Solving the COF Trilemma: Towards Crystalline, Stable and Functional Covalent Organic Frameworks. *Chem. Soc. Rev.* **2020**, *49* (23), 8469–8500.

[27] Jiang, J.; Zhao, Y.; Yaghi, O. M. Covalent Chemistry beyond Molecules. *J. Am. Chem. Soc.* **2016**, *138* (10), 3255–3265.

[28] Hollstein, S.; Erdmann, P.; Ulmer, A.; Löw, H.; Greb, L.; Delius, M. von. Trialkoxysilane Exchange: Scope, Mechanism, Cryptates and PH-Response. *Angew. Chem. Int. Ed.* **2023**, *135* (26), e202304083.

[29] Brachvogel, R. C.; von Delius, M. The Dynamic Covalent Chemistry of Esters, Acetals and Orthoesters. *Eur. J. Org. Chem.* **2016**, *2016* (22), 3662–3670.

[30] Crank, G.; Eastwod, F. W. Derivatives of Orthoacids. I. Bicyclic Orthoesters. *Aust. J. Chem.* **1964**, *17* (12), 1385–1391.

[31] Brachvogel, R. C.; Von Delius, M. Orthoester Exchange: A Tripodal Tool for Dynamic Covalent and Systems Chemistry. *Chem. Sci.* **2015**, *6* (2), 1399–1403.

[32] Muzyka, C.; Monbaliu, J. C. M. Perspectives for the Upgrading of Bio-Based Vicinal Diols within the Developing European Bioeconomy. *ChemSusChem* **2022**, *15* (5), e202102391.

[33] Arceo, E.; Marsden, P.; Bergman, R. G.; Ellman, J. A. An Efficient Didehydroxylation Method for the Biomass-Derived Polyols Glycerol and Erythritol. Mechanistic Studies of a Formic Acid-Mediated Deoxygenation. *Chem. Commun.***2009**, *23*, 3357–3359.

[34] Li, R.; Greenchem, /; Tshibalonza, N. N.; Monbaliu, J.-C. M.; Chemistry, G. The Deoxydehydration (DODH) Reaction: A Versatile Technology for Accessing Olefins from Bio-Based Polyols. *Green Chem.* **2020**, *22* (15), 4801–4848.

[35] Tshibalonza, N. N.; Monbaliu, J. C. M. Revisiting the Deoxydehydration of Glycerol towards Allyl Alcohol under Continuous-Flow Conditions. *Green Chem.* **2017**, *19* (13), 3006–3013.

(36) Burnham, K. P.; Anderson, D. R. Multimodel Inference: Understanding AIC and BIC in Model Selection. *Sociol. Methods Res.* **2004**, *33* (2), 261–304.

[37] Shiner, C. S.; Tsunoda, T.; Goodman, B. A.; Ingham, S.; Lee, S. hung; Vorndam, P. E. (Dialkoxymethyl)Lithiums: Generation, Stability, and Synthetic Transformations. *J. Am. Chem. Soc.* **1989**, *111* (4), 1381–1392.

[38] Thomas, C. A.; Carmody, W. H. *Decolorization of Resins. U.S. Patent 2060404,* **1936**.

[39] Pittman, C. U.; Mcmanus, S. P.; Larsen, J. W. 1,3-Dioxolan-2-Ylium and Related Heterocyclic Cations. *Chem. Rev* .**1972**, *72* (4), 357–438.

[40] Kass, R. E.; Raftery, A. E. Bayes Factors. *J. Am. Stat. Assoc.* **1995**, *90* (430), 773–795.

[41] Gaussian 16, Revision C.01, M. J. Frisch, G. W. Trucks, H. B. Schlegel, G. E. Scuseria, M. A. Robb, J. R. Cheeseman, G. Scalmani, V. Barone, G. A., Petersson, H. Nakatsuji, X. Li, M. Caricato, A. V. Marenich, J. Bloino, B. G. Janesko, R. Gomperts, B. Mennucci, H. P. Hratchian, J. V. Ortiz, A. F. Izmaylov, J. L. Sonnenberg, D. Williams-Young, F. Ding, F. Lipparini, F. Egidi, J. Goings, B. Peng, A. Petrone, T. Henderson, D. Ranasinghe, V. G. Zakrzewski, J. Gao, N. Rega, G. Zheng, W. Liang, M. Hada, M. Ehara, K. Toyota, R. Fukuda, J. Hasegawa, M. Ishida, T. Nakajima, Y. Honda, O. Kitao, H. Nakai, T. Vreven, K. Throssell, J. A. J. Montgomery, J. E. Peralta, F. Ogliaro, M. J. Bearpark, J. J. Heyd, E. N. Brothers, K. N. Kudin, V. N. Staroverov, T. A. Keith, R. Kobayashi, J. Normand, K. Raghavachari, A. P.

Rendell, J. C. Burant, S. S. Iyengar, J. Tomasi, M. Cossi, J. M. Millam, M. Klene, C. Adamo, R. Cammi, J. W. Ochterski, R. L. Martin, K. Morokuma, O. Farkas, J. B. Foresman, D. J. Fox, Gaussian Inc., Wallingford CT, **2016**.

(42] Williams, R. pKa Data https//organicchemistrydata.org/hansreich/ resources/pka/pka_data/pka-compilation-williams.pdf, (2025-05-01).

Author Contributions

Claire Muzyka: Conceptualization, Experimental Work, Writing - Original Draft

Tom Perreira Rodrigues: Experimental Work

Diana Silva: Writing – review & editing

Jean-Christophe M. Monbaliu: Project Administration, Supervision, Funding acquisition, Writing – review & editing.

4 THE DEOXYDEHYDRATION REACTION OF BIO-BASED ORTHOESTERS

4.1 PREFACE

Olefins are essential industrial building blocks for the petrochemical industry, with applications spanning nearly every industrial sector. While our society still relies heavily on fossil resource, the drive toward a green transition is pushing the industry to develop processes based on renewable feedstocks. One such approach is the deoxydehydration (DODH) reaction, which converts vicinal diols into olefins. Specifically, in the context of sourcing abundant bio-based building blocks, polyols, including vicinal polyols, are quite abundant. The DODH reaction thus bears a significant potential to produce olefins starting from biobased vicinal diols. This transformation is typically achieved via two main methodologies: one employing transition metal catalysts derived from rhenium or molybdenum with sacrificial reducing reagents,[1] and the other utilizing acidic catalysts.[2] Metal-free methods are particularly attractive due to the renewable nature of the reagents and the reduced safety risks. Several studies have demonstrated the successful conversion of bio-based molecules comprising glycerol, *meso*-erythritol, xylitol into their respective olefins.[3–8] Although formic acid–based processes, in which formic acid serves as both reagent and catalyst, deliver high olefin yields, its thermal instability requires a large excess of the acid. To address this limitation, two-step strategies were designed, involving the dynamic covalent exchanges between orthoesters and diols to form dioxolane intermediates, which then undergo a thermal treatment inducing CO_2 extrusion and olefins formation. However, the detailed mechanism underlying olefin formation remains poorly understood, and the presence of multiple vicinal diols in bio-based molecules further complicates the reaction.

4.2 INTRODUCTION

The deoxydehydration reaction of dioxolane derivatives has been reported to proceed via the formation of cyclic dioxocarbenes (**1**) derived from orthoesters (**2**) (Figure 4.1a).[9] These divalent carbene species undergo thermal two-bond β-cleavages in a highly exothermic process, yielding CO_2 and the corresponding olefin (**3**).[10] The extrusion of CO_2 is generally proposed to occur through a symmetrical and concerted cleavage of both C–O σ bonds in the ring, a pathway considered energetically favorable.[11] However, an alternative mechanism involving the cleavage of a single C–O bond has been explored, leading first to a diradical species (**4**) before molecular fragmentation (Figure 4.1a). Computational analysis of the associated transition state (TS) reveals a lower activation barrier of 8.8 kcal·mol^{-1} compared to the concerted fragmentation pathway. This difference is attributed primarily to a reduction in the O–C–O bond angle, by approximately 2.2°, resulting in a more bent geometry than that observed in the concerted CO_2 extrusion.[12] Another hypothesis postulates the formation of an acidic 4,5-dihydro-1,3-dioxol-1-ium cation (**5** - Figure 4.1b), commonly observed for N-heterocyclic carbenes, prior to the formation of dioxolidin-2-ylidene (**6**). The authors consider this pathway more favorable than the direct carbene formation.[13] Notably, thermal fragmentation of acyclic dialkoxycarbene (**7**) and its corresponding carbene (**8**) has also been reported, producing a pair of radicals: a methoxycarbonyl radical (**9**) and an allylic radical (**10** – Figure 4.1c).[14]

Interestingly, other methodologies for producing deoxydehydrated products have been described, without proceeding by dioxocarbene intermediates. One such method involves a pinacol rearrangement mediated by trimethyl orthoformate (**11**), leading to the formation of the corresponding ketone. In this case, the authors propose a mechanism based on the initial formation of a dioxolane species from the *cis*-vicinal diol in the presence of Lewis acid $SnCl_4$. Subsequent C-O cleavage is further mediated by $SnCl_4$ to form intermediate **12**, inducing the rearrangement leading to the ketone formation (Figure 4.1d).[15] Alternatively, Ellman *et al.* suggest that the reaction proceeds via the generation of 2-acyloxy-1,3-dioxolane (**13**) from a carbocation intermediate, and subsequent hydrogen abstraction and CO_2 elimination (Figure 4.1e).[4]

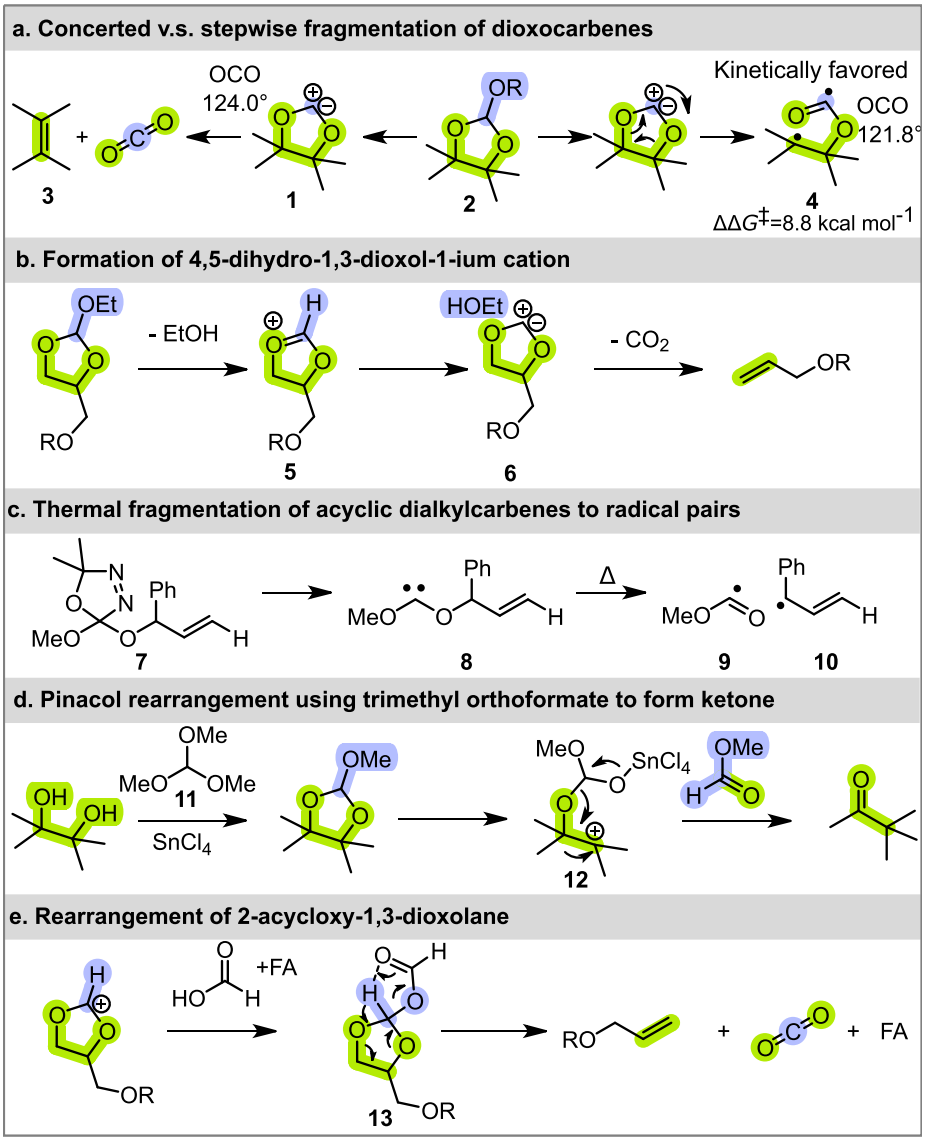

Figure 4.1 (a) Stepwise *versus* concerted fragmentation of orthoesters, yielding dioxocarbene (**1**) or single C-O bond fragmentation product (**4**).[12] (b) Formation of an acidic 4,5-dihydro-1,3-dioxol-1-ium cation (**5**) prior to the formation of dioxolidin-2-ylidene (**6**).[13] (c) Thermal fragmentation of acyclic dialkylcarbene (**8**) in a methoxycarbonyl radical (**9**) and an allylic radical (**10**).[14] (d) Alternative methodology based on pinacol rearrangement with trimethyl orthoformate as additive, with formation of 2-yl-methyl carbonate (**12**).[15] (e) Rearrangement of 2-acyloxy-1,3-dioxolane to induce CO_2 extrusion and olefin formation.[4]

Herein, we present a comprehensive DFT investigation of reaction mechanisms involved in the conversion of cyclic orthoesters derived from bio-based C_2 to C_4 diols into olefin derivatives (Figure 4.2). This study systematically examines all potential reaction products,

including orthoesters formed from apical, internal, and double vicinal diol scaffolds (dashed boxes in Figure 4.2). Our findings elucidate the mechanism of dioxocarbene formation and its subsequent transformation into olefins. A detailed analysis of the influence of substrate structural factors on dioxocarbene formation is also conducted. Furthermore, solvation effects and intermolecular interactions with key reactive species are thoroughly explored. Overall, this study offers valuable insights into the interplay of molecular geometry, electronic effects, and solvent interactions, aiming to provide a rational framework for understanding such transformations.

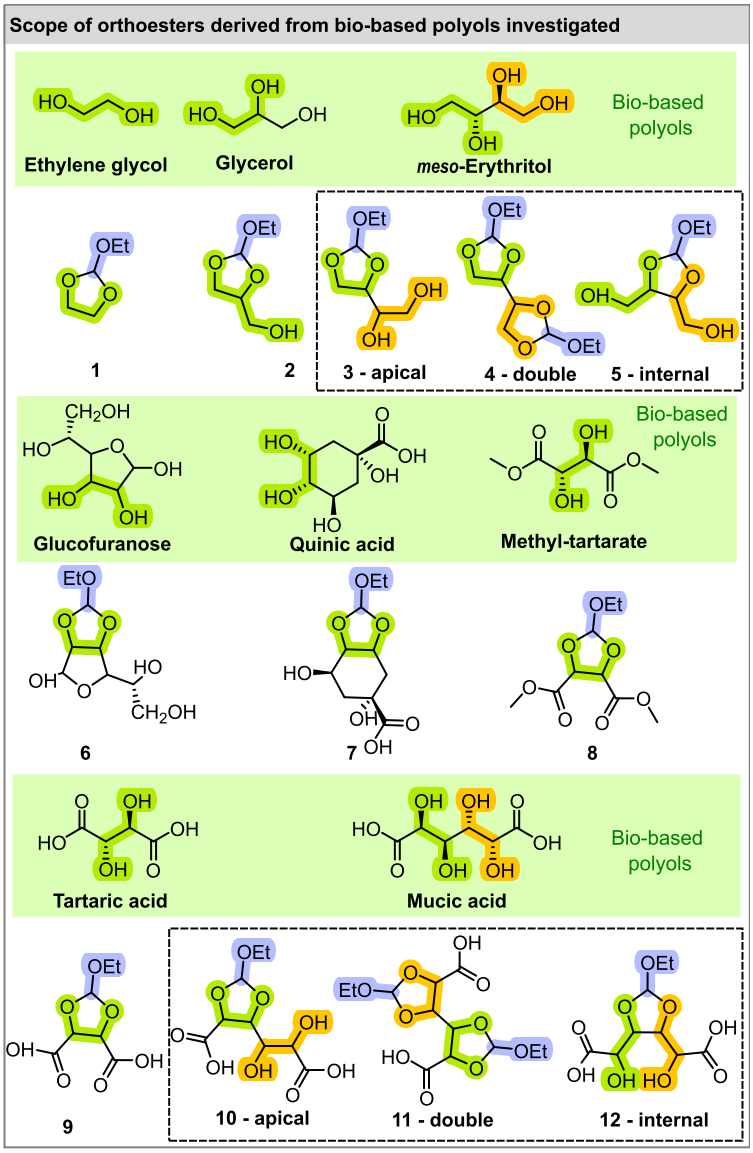

Figure 4.2 Scope of substrates potentially accessible through bio-sourced polyols undergoing dynamic covalent exchanges to form cyclic orthoesters.

4.3 RESULTS AND DISCUSSION

4.3.1 ASYNCHRONOUS FORMATION OF DIOXOCARBENE INTERMEDIATES

DFT computations were performed using the Gaussian 16 (Revision C.01) software package.[16] All stationary points were optimized and localized at the B3LYP-GD3BJ/6-31+G*(d) level of theory. The SMD method was used to model solvent effects using the built-in parameters for acetonitrile (MeCN, ε = 38.8) at 273 K. Stationary points were characterized by frequency calculations (local minima with only real frequencies and transition states with one imaginary frequency) and a systematic attempt to locate the lowest-energy conformers. Transition states were further validated by intrinsic reaction coordinate (IRC) calculations.

Starting with the simplest structure of cyclic orthoesters, e.g., **1**, in presence of a Bronsted acid (formic acid - FA), the formation of 2-acyloxy-1,3-dioxolane carbene (**int. 1**) was identified to happen through an asynchronous mechanism (Figure 4.3a). Initially, protonation and subsequent removal of the ethoxy group occurred, followed by the deprotonation of the acidic proton of the ring by the conjugated base of FA, led to transition state (TS) **TS.1 int.1** and intermediate **int. 1**.

To explore the influence of polyol derived scaffolds on carbene reactivity, a diverse array of orthoester derived from bio-sourced polyols was systematically investigated through computational methods. For molecules bearing two adjacent vicinal diols such as *meso*-erythrtiol and mucic acid, various structural combinations including apical, internal and bi-cyclic orthoesters were examined to provide comprehensive insights onto their electronic properties.

DFT calculations revealed remarkable consistency in the electronic character of carbenes derived from unfunctionalized orthoesters containing only vicinal diols, comprising compounds **1** to **7**. These carbene intermediates (**int. 1** to **7**) showed activation barriers ($\Delta G^{\neq}$) ranging from 22.0 to 24.1 kcal mol^{-1},with natural charges on the carbene atom comprised between +0.4420 and +0.4453 e$^-$ (Figure 4.3a). The consistent natural charge values across the substrate scope indicate that these intermediates share a fundamental similar electronic structure, characterized by significant polarization of the carbene center. This polarization appeared to be primarily governed by stereoelectronic interactions between the adjacent oxygens and the carbene center, complemented by the electro-withdrawing inductive effect of the dioxolane oxygen atoms. Natural bond orbital (NBO) analysis of **int. 2** highlighted two significant donor-acceptor interactions where electron density from the carbene's lone pair delocalizes into the σ^* antibonding orbitals of the adjacant C-O bonds. Each interaction provided a second-order pertubative stabilization energy (E^2) of 9.80 kcal.

The subtle variations in activation barriers among the various polyol-derived carbenes could be attributed to secondary inductive effects arising from the backbone of alkyl substitutents. These effects slightly modulated the stability of the transition states leading to carbene formation, while preserving the essential electronic nature of the reaction center.

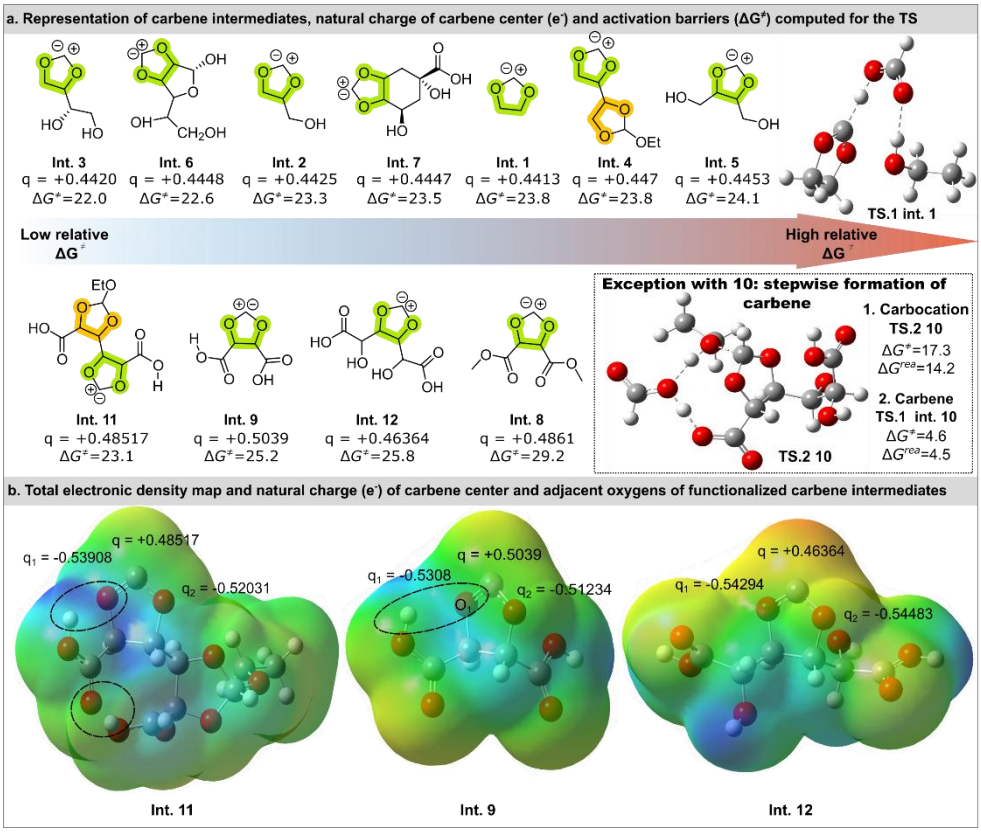

Figure 4.3 (a) Computational analysis of dioxocarbene intermediates derived from bio-based substrates (B3LYP-GD3BJ/6-31+G*(d) level of theory, SMD = MeCN at 273 K), including activation barriers ($\Delta G^{\neq}$, in kcal mol^{-1}) of their respective transition state (TS) and natural charges at the carbene center. (b) Electronic density distribution and natural charges for intermediates **9**, **11**, and **12**, highlighting the carbene center and adjacent oxygen atoms, as well as intramolecular hydrogen bonding (HBD) occurring in the species (dashed circles). Activation barriers ($\Delta G^{\neq}$) and reaction Gibbs free energies (ΔG^{rea}) are reported in kcal mol^{-1}.

Our investigation was extended to the transition state analysis of carbene formation from polyols bearing carboxylic and ester functionalities in close proximity of vicinal diols, including **8** to **12**. Comparison of their $\Delta G^{\neq}$ with benchmark species **1** clearly established a reactivity hierarchy with **TS.1 int. 1** at 23.8 kcal mol^{-1}, **TS.1 int. 9** at 25.2 kcal mol^{-1} and **TS.1 int. 8** at 29.2 kcal mol^{-1}. This ascending sequence of $\Delta G^{\neq}$ clearly demonstrated the negative influence on electron withdrawing groups (EWG) on carbene formation (Figure 4.3a). Notably, the TS leading to carbene intermediate **9** came with a significantly lower $\Delta G^{\neq}$ compared to its methyl ester counterpart. This likely indicates that electronic effects are not the sole contributors to carbene reactivity. It was expected that **TS.1 int. 9** had a higher $\Delta G^{\neq}$, owing to the stronger electron withdrawing effect of carboxylic acids. Natural population analysis (NPA) performed on tartaric acid derived carbene **int. 9** revealed a slightly uneven electronic distribution between both adjacent oxygens (q_1 = -0.5308 and q_2 = -0.5123 - Figure 4.3b). Structural analysis of **int. 9** indicated that the endocyclic oxygen atom (O_1) was

engaged in a intramolecular hydrogen bond with the carboxylic acid group. This resulted in a partial delocalization of carbene electron density, thereby attenuating the electron withdrawing influence of the carboxylic acid moiety. Structural analysis of **TS.1 int. 11** revealed the presence of intramolecular hydrogen bonding, similar to that observed with **TS.1 int. 9**. Moreover, a second hydrogen bonding interaction was identified between the carboxylic groups, further stabilizing the overall transition state. This hydrogen bond network potentially reduces $\Delta G^{\neq}$ (23.1 kcal mol^{-1}). By contrast, hydrogen bond donor interactions are absent in **TS.1 int. 8**, which compromises the additional stabilizing effects provided by the dioxolane's oxygens. This electronic perturbation decreases the stabilization of the transition state and the intermediate, thus translating into activation and reaction parameters above 29 kcal mol^{-1}. **TS.1 int. 12** represents an intermediate case before **TS.1 int. 8**, which can be attributed to a much lower electron-withdrawing influence resulting from the increased spatial separation between the carboxylic groups and the carbene center.

4.3.2 STEPWISE FORMATION OF DIOXOCARBENES VIA CARBOCATION INTERMEDIATES

Interestingly, analysis of carbene intermediate generation from **10** identified an unexpected mechanistic divergence from previously established pathways.[9] Rather than proceeding via a concerted carbene formation, DFT computations highlighted a stepwise mechanism involving the formation of carbocation followed by subsequent deprotonation to yield the carbene species. This mechanistic pathway featured more accessible intermediates, with the formation of the corresponding carbocation associated with a $\Delta G^{\neq}$ of 17.3 kcal mol^{-1} and a subsequent low $\Delta G^{\neq}$ (4.6 kcal mol^{-1}) for the generation of the carbene species. The formation of carbocation **int.2 10** proceeded via a concerted mechanism involvong the dissociation of the most acid proton (e.g. mucic acid's carboxylic group), the protonation of the catalyst and the subsequent removal of an ethoxy group (Figure 4.3a – **TS.2 10** – dashed box).

To investigate the role of hydrogen bonding in stabilizing carbocationic intermediates, orthoesters **2** and **9** were used as model subtrates. **9** followed a mechanism similar to **10**, forming the carbocation intermediate **int.2 9** ($\Delta G^{\neq}$ = 18.5 kcal mol^{-1}) upon catalyst protonation by its carboxylic acid group (Figure 4.4a – blue circles). The formation of **int.2 9** was also found to be directly autocatalyzed by its own carboxylic group, with the corresponding transition state **TS.2 9-a** displaying a comparable activation barrier to this of **TS.2 9** (Figure 4.4a – blue circles).

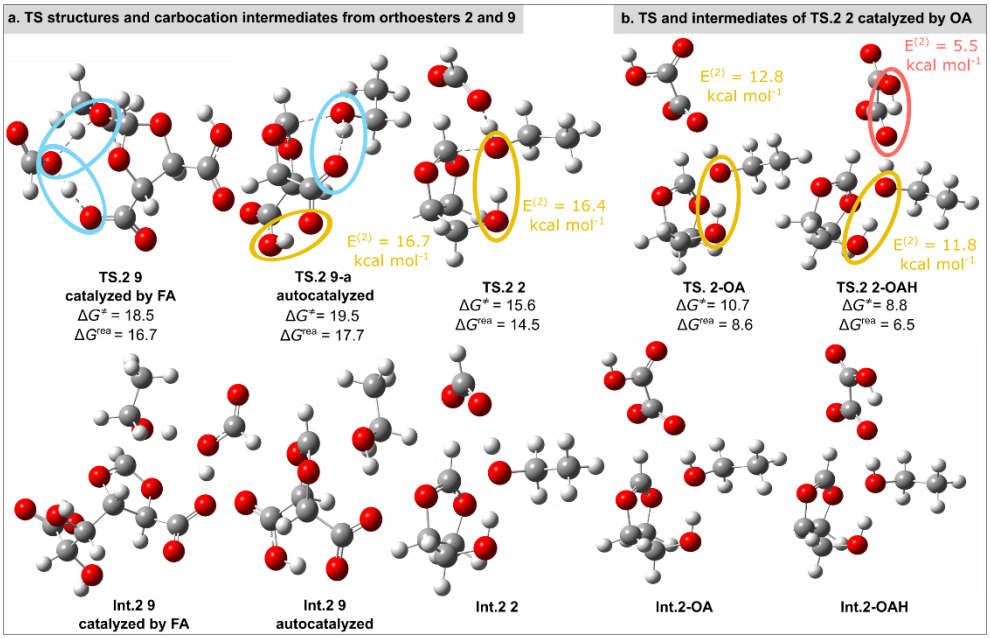

Figure 4.4 (a) Intramolecular hydrogen bond stabilization of transition states **TS.2 9.** and **TS.2 9-a** (yellow circles) in the FA-catalyzed formation of intermediates **int.2 9**, **int 2 9-a** (proton exchanges highlighted in blue circles) and **int 2 2**; (b) OA-catalyzed formation of **int 2 2** shown with/without intramolecular hydrogen bond stabilization between OA's carboxylic groups (highlighted in a red circle) Activation barriers ($\Delta G^{\neq}$) and reaction Gibbs free energies (ΔG^{rea}) are presented in kcal mol^{-1}.

Furthermore, intramolecular hydrogen bonding between an adjacent free alcohol or a carbocylic group and the leaving ethoxy moiety were found to facilitate the generation of the carbocationic intermediate (Figure 4.4a – yellow circles). This phenomenom was also observed with the formation of **int.2 3** dervied from *meso*-erythritol (details in the Supporting Information Section S3.1.2), further supporting the importance of hydrogen bonding intereactions in these complex reaction networks.

The potential protonation of the endocyclic oxygen atoms was also computationnally explored, but the results were inconclusive. Instead, the formation of the carbocation was found to proceed through a classical mechanism involving the protonation of the ethoxy limb followed with the elimination of ethanol. Subsequent nucleophilic addition by a free alcohol groups yielded a bicyclic orthoester derivative (details in the Supporting Information Section S3.1.3).[17]

Oxalic acid (OA), a stronger Bronsted acid (pK_a = 1.2) compared to formic acid (FA, pK_a = 3.75),[18] was next assessed. We aimed to determine its potential effect on the formation of carbocation **int.2 2**. While intramolecular stabilization remained necessary to facilitate the formation of **TS.2 2**, the stronger acidity of OA reduced the activation barrier of about 5 kcal mol^{-1} compared to **TS.2 2** involving FA (**TS.2 2-OA**: $\Delta G^{\neq}$ = 10.7 kcal mol^{-1}, **TS.2 2** : $\Delta G^{\neq}$ = 15.6 kcal mol^{-1}, Figure 4.4b). Further analysis integrating hydrogen bonding stabilization

between both catalyst's carboxylic acid groups resulted in a further decrease in $\Delta G^{\neq}$ (8.8 kcal mol^{-1}, **TS.2 2-OAH)**.

The formation of cyclic orthoesters trhough dynamic covalent exchanges generates significant amounts of alcohol by-products,[19] enriching the reaction medium with active hydrogen bond species. This prompted further analyze of their influence on the reaction mechanism. Methanol (MeOH), ethanol (EtOH), and isopropanol (*i*PrOH) by-products derived from the three most prevalent orthoester reagents (namely, trimethyl, triethyl and triisopropyl orthoformates) were considered. To asses the impact of intermolecular hydrogen bonding on carbocation stabilization, a small cluster featuring three molecules of MeOH was incorporated in TS calculation (**TS.2 2**).

In the reagent system (Figure 4.5), the two oxygen atoms of **2** formed hydrogen bonds with two methanol molecules (MeOH^{1}and MeOH^2), while a third methanol (MeOH^3) bonded to the catalyst's carbonyl group (FA). These hydrogen bond interactions were also observed in the **TS.2-2** (Figure 4.5). In contrast, $MeOH_2$ from the product system reoriented to stabilize the conjugate base via hydrogen bonding. Simultaneously, MeOH^1 positioned symmetrically between both oxygen atoms of **int.2-2**, stabilizing its negative charges and the nearby carbocation.

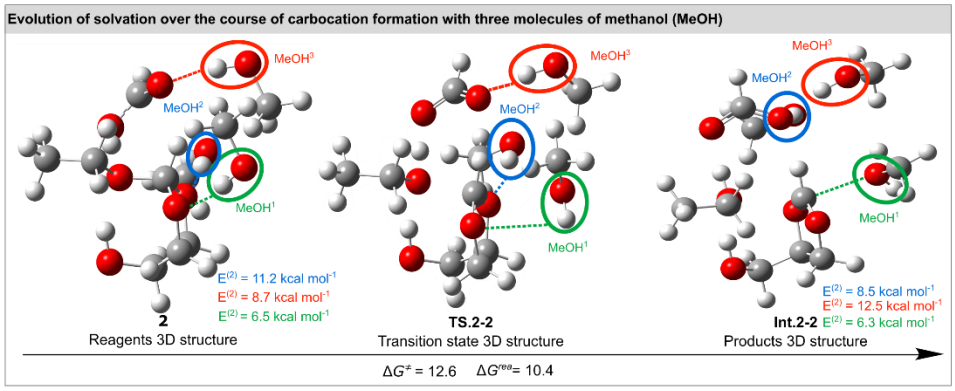

Figure 4.5 Solvation clusters for the reagent (**2** and FA), transition state (**TS.2-2**) and carbocation systems (**int.2-2**), highlighting the reorganization of the cluster of methanol (MeOH$^{1/2/3}$) with the formation of the carbocation **int.2 2** and second order stabilization energy (kcal mol^{-1}). The dashed lines represent the hydrogen bonds or donor - acceptors interactions between the alcohol molecules and the structures.

Overal, the formation of the carbocationic intermediate **int.2-2** triggered the rearrangement of the molecules cluster, further enhancing the stability of the carbocation system. This resulted in lowered activation barrier and the Gibbs free energy of 12.6 and 10.4 kcal mol^{-1} for methanol and of 14.8 and 9.9 kcal mol^{-1} for ethanol, respectively (compared to 15.6 and 14.5 kcal mol^{-1} for **TS.2 2** with only implicit solvation). The stronger hydrogen bonding capability of methanol, due to its higher acidity,[20] provided enhanced stabilization of **TS.2-2** relative to the other alcohol.

Two competitive mechanisms were identified for the generation of a dioxocarbene from carbocation **int.2 2**. The first pathway (Path 1 – Figure 4.6a) involves the deprotonation of **int.2 2** by the conjugated base of FA (which is generated from the activation of the cyclic orthoester **2** in **int.2 2**). Path 2 proceeds via a stepwise mechanism leading to the formation of **13**, which subsequently induces the extrusion of CO_2 (Figure 4.6b).

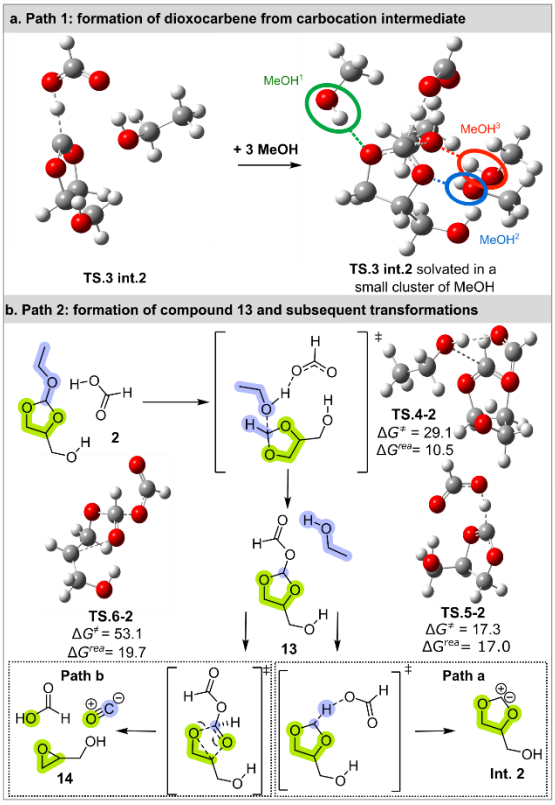

Figure 4.6 (a) Path 1: formation of dioxocarbene from carbocation intermediate **int.2 2** and. (b) Path 2: formation of compound **13**, with competing downstream pathways (a and b) leading to either the dioxocarbene intermediate or epoxide **14**. Key transition state structures (**TS.4-2**, **TS.5-2**, **TS.6-2**) are shown along their computed activation ($\Delta G^{\neq}$) and reaction Gibbs free energies (ΔG^{rea}).

Path 1 is enabled by alcohol-mediated stabilization of the carbocation-carbene reaction sequence (Figure 4.6a). Computational analysis of **TS.3 int. 2** with MeOH, EtOH and *i*POH revealed specific solvation patterns, different from those arising from carbocation species: two molecules of alcohol participate in hydrogen bonding with the endocyclic oxygens ($MeOH^{1/2}$), whereas a third molecule ($MeOH^{3}$) stabilizes the conjugated base of the catalyst. The transition state **TS.3 int. 2**, obtained from **int.2 2**, came with activation and reaction parameters of 6.1 kcal mol^{-1} and 8.3 kcal mol^{-1}, respectively, toward the carbene species (in MeOH). Likewise, a cluster of ethanol led to the same activation barrier, but a lower stabilization of the reaction intermediate by 1.8 kcal mol^{-1}.

Path 2 was elucidated based on the seminal work of Ellman *et al* (Figure 4.6b).[4] The formation of **13** was computed and indicated a highly endothermic process, along with a high activation barrier (**TS.4 2**; 29.1 kcal mol^{-1}) (Figure 4.6a). Subsequent mechanistic investigations on **13** led us to identify two alternative one-step pathways: path (a) the formation of carbene intermediate **int.2** via a concerted elimination of the formate moiety and proton abstraction (**TS.5 2** and **int. 2**) and, path (b) ring compression through the concomitant elimination of formic anhydride (**TS.6 2** ;decomposition into formic acid and carbon monoxide) and an intramolecular cyclization to yield glycidol (**14**). Comparing both energy profiles led us to conclude that the carbene route (path a) is favored over path b. Indeed, path a proceeds with a significantly lower activation barrier (17.3 kcal mol^{-1}) compared to 53 kcal mol^{-1} for path b. Although previous literature reports documented the conversion of diols to epoxides via orthoester intermediates,[21] this transformation is unlikely under our conditions. Similarly, the formation of compound **13** is highly disfavored compared to the stepwise mechanism leading to carbocation generation described previously.

4.3.3 DEOXYDEHYDRATION OF CARBENE INTERMEDIATES

The final step of the DODH process consists in the extrusion of CO_2, concomitant with the detruction of the dioxocarbene species and the installation of a carbon-carbon insaturation. This step proceeds via an heterolytic cleavage of the endocyclic C-O bonds, as reported in 2017.[13] Computations indicated that transition states structures (**TS.1 int.9**, **TS.1 int.8** and **TS.1 int.11**) associated with less stabilized carbene intermediates were assoaciated with lower activation barriers ($\Delta G^{\neq}$ = 5.4 - 7.9 kcal mol^{-1}; products **22**, **23** and **26**; Figure 7a) for the CO_2 extrusion process. This lowered energetic pathway seems to arise from an enhanced electronic polarization of the carbene center (quantified by natural population analysis, exceeding +0.48 e^-). In contrast, systems with a lower electronic polarization on the carbene center, potentially due to weaker electron-withdrawing substituents, led to higher activation barriers for the formation of olefin **15** to **21** and **23** to **26** ($\Delta G^{\neq}$ = 11.3 kcal mol^{-1} -13.0 kcal mol^{-1}; Figure 7b).

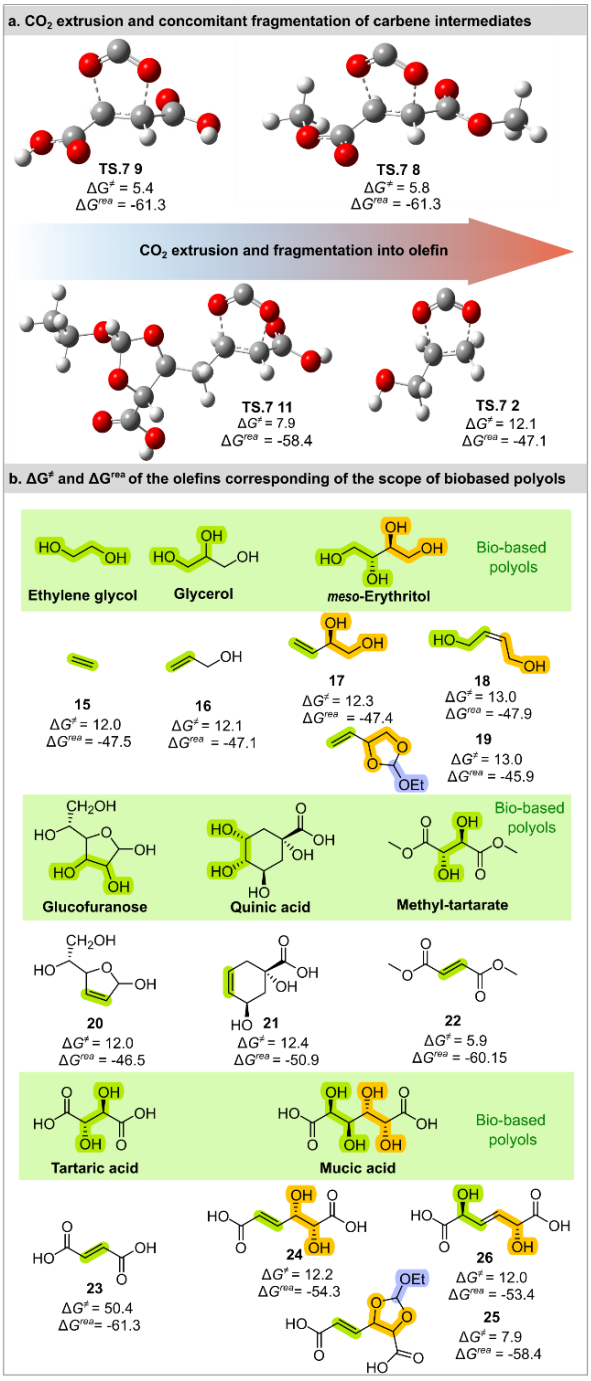

Figure 4.7 Illustration of CO_2 extrusion and molecular fragmentation of dioxocarbenes **int. 2**, **8**, **9** and **11**; (b) Activation barriers ($\Delta G^{\neq}$) and Gibbs free energy of reaction (ΔG^{rca}) of the scope bio-based orthoesters (**1** to **12**) converted in olefins (**15** to **26**).

4.3.4 CONCLUSION

This work aimed to gain deeper insights into the deoxydehydration reaction of bio-based orthoesters. The formation of dioxocarbene intermediates is rationalized through an asynchronous mechanism involving initial protonation and elimination of the orthoester ethoxy group, followed by deprotonation of the acidic proton. Carbene formation is stabilized by steroelectronic interactions between the carbene lone pair and the adjacent C-O σ* antibonding orbitals. Conversely, carbene stabilization was found rather independent of the substrate strucutre, except those substituted with electron witdrawing groups, with significant increase of activation barriers.

Intramolecular hydrogen bonding was shown to play a crucial role in the reaction mechanism, allowing the stabilization of carbocation intermediates. This stepwise mechanism occurs via the stabilization of the carbocation through a free adjacent alcohol or carboxylic acid group that is not constraint by cyclic geometry. The combined effect of intra- and intermolecular hydrogen bonding were investigated using small cluster of alcohols, with compound **2** as model subtrate. Activation barriers were observed to decrease with increasing solvent acidity. Notably, solvation with 3 molecules of methanol reduced the activation barrier from 15.6 to 12.6 kcal mol^{-1} for the TS whithout explicit solvation.

Two mechanisms were identified for dioxocarbene formation: one involving deprotonation of solvated carbocation intermediates, and the other proceeding via formation of acyloxy-1,3-dioxolane, followed by fragmentation and CO_2 extrusion. The former pathway was found to be kinetically promoted, with a activation barrier of 6.1 kcal mol^{-1} compared to 29.1 kcal mol^{-1} required for the generation of **13**. Asynchronous cleavage of both C-O bonds yielded a variety of potential olefins, with activation barrier ranging between 12 and 13 kcal mol^{-1}. The only exception was observed for dioxocarbenes substituted with EWG, which exhibited reduced activation barriers below 6 kcal mol^{-1}.

Overall, while this work provides valuable theoritical insights in the reaction of deoxydehydration, experimental work is strongly needed to confirm these hypotheses Additionnaly, molecular dynamics simulations would offer unique insights into the evolution of hydrogen bond formation throughout the reaction and its impact on reaction selectivity. Nonetheless, this study emphasizes the promising applications of DODH for olefin production as key buidling block of the industrial sector.

4.4 REFERENCES

[1] Tshibalonza, N. N.; Monbaliu, J. C. M. The Deoxydehydration (DODH) Reaction: A Versatile Technology for Accessing Olefins from Bio-Based Polyols. Green Chem. **2020**, 22 (15), 4801–4848.

[2] Muzyka, C.; Monbaliu, J. C. M. Perspectives for the Upgrading of Bio-Based Vicinal Diols within the Developing European Bioeconomy. ChemSusChem **2022**, 15 (5), e202102391.

[3] Sun, R.; Zheng, M.; Li, X.; Pang, J.; Wang, A.; Wang, X.; Zhang, T. Production of Renewable 1,3-Pentadiene from Xylitol via Formic Acid-Mediated Deoxydehydration and Palladium-Catalyzed Deoxygenation Reactions. Green Chem. **2017**, *19*, 638.

[4] Arceo, E.; Marsden, P.; Bergman, R. G.; Ellman, J. A. An Efficient Didehydroxylation Method for the Biomass-Derived Polyols Glycerol and Erythritol. Mechanistic Studies of a Formic Acid-Mediated Deoxygenationw. Chem. Commun, **2009**, 3357-3359.

[5] Rodriguez Herrero, Y.; Ullah, A. Rapid, Metal-Free, Catalytic Conversion of Glycerol to Allyl Monomers and Polymers. ACS Sustainable Chem. Eng. **2021**, *9* (28), 9474-9485.

[6] Arceo, E.; Ellman, J. A.; Bergman, R. G. A Direct, Biomass-Based Synthesis of Benzoic Acid: Formic Acid-Mediated Deoxygenation of the Glucose-Derived Materials Quinic Acid and Shikimic Acid a. *ChemSusChem* **2010**, *3* (7), 811–813.

[7] Tshibalonza, N. N.; Gérardy, R.; Alsafra, Z.; Eppe, G.; Monbaliu, J. C. M. A Versatile Biobased Continuous Flow Strategy for the Production of 3-Butene-1,2-Diol and Vinyl Ethylene Carbonate from Erythritol. *Green Chem.* **2018**, *20* (22), 5147–5157.

[8] Tshibalonza, N. N.; Monbaliu, J. C. M. Revisiting the Deoxydehydration of Glycerol towards Allyl Alcohol under Continuous-Flow Conditions. *Green Chem.* **2017**, *19* (13), 3006–3013.

[9] Sauers, R. R. Extrusion Reactions of Carbon Dioxide from Orthoesters and Derivatives: An Ab Initio Study of Some Cyclic Carbenes. *Tetrahedron Lett* .**1994**, *35* (39), 7213–7216.

[10] Xu, G.; Chang, T.-M.; Zhou, J.; McKee, M. L.; Shevlin, P. B. An Unsual Cleavage of an Energetic Carbene. *J. Am. Chem. Soc* **1973**, *121*, 7150–7151.

[11] Sauers, R. R. An Ab Initio Study of Some Heterocyclic 6π-Carbenes. *Tetrahedron Lett.* **1996**, *37* (2), 149–152.

[12] Feller, D.; Davidson, E. R.; Borden, W. T. Theoretical Study of Concerted vs. Stepwise Fragmentation of 2-Carbena-1,3-Dioxolane. *J. Am. Chem. Soc.* **1981**, *103* (10), 2558–2560.

[13] Tshibalonza, N. N.; Monbaliu, J. C. M. Revisiting the Deoxydehydration of Glycerol towards Allyl Alcohol under Continuous-Flow Conditions. *Green Chem.* **2017**, *19* (13), 3006–3013.

[14] Venneri, P. C.; Warkentin, J. Homolysis of Carbenes. Free Radicals from Dialkoxycarbenes [1]. *J. Am. Chem. Soc.* **1998**, *120* (43), 11182–11183.

[15] Kita, Y.; Yoshida, Y.; Mihara, S.; Fang, D. F.; Higuchi, K.; Furukawa, A.; Fujioka, H. Efficient Pinacol Rearrangement Mediated by Trimethyl Orthoformate. *Tetrahedron Lett.* **1997**, *38* (48), 8315–8318.

[16] Gaussian 16, Revision C.01, M. J. Frisch, G. W. Trucks, H. B. Schlegel, G. E. Scuseria, M. A. Robb, J. R. Cheeseman, G. Scalmani, V. Barone, G. A., Petersson, H. Nakatsuji, X. Li, M. Caricato, A. V. Marenich, J. Bloino, B. G. Janesko, R. Gomperts, B. Mennucci, H. P. Hratchian, J. V. Ortiz, A. F. Izmaylov, J. L. Sonnenberg, D. Williams-Young, F. Ding, F. Lipparini, F. Egidi, J. Goings, B. Peng, A. Petrone, T. Henderson, D. Ranasinghe, V. G. Zakrzewski, J. Gao, N. Rega, G. Zheng, W. Liang, M. Hada, M. Ehara, K. Toyota, R. Fukuda, J. Hasegawa, M. Ishida, T. Nakajima, Y. Honda, O. Kitao, H. Nakai, T. Vreven, K. Throssell, J. A. J. Montgomery, J. E. Peralta, F. Ogliaro, M. J. Bearpark, J. J. Heyd, E. N. Brothers, K. N. Kudin, V. N. Staroverov, T. A. Keith, R. Kobayashi, J. Normand, K. Raghavachari, A. P. Rendell, J. C. Burant, S. S. Iyengar, J. Tomasi, M. Cossi, J. M. Millam, M. Klene, C. Adamo, R. Cammi, J. W. Ochterski, R. L. Martin, K. Morokuma, O. Farkas, J. B. Foresman, D. J. Fox, Gaussian Inc., Wallingford CT, **2016**.

[17] Crank, G.; Eastwood, F. W. Derivatives of Orthoacids. I. Bicyclic Orthoesters. *Aust. J. Chem.* **1964**, *17* (12), 1385.

[18] Williams, R. pKa Data https//organicchemistrydata.org/hansreich/ resources/pka/pka_data/pka-compilation-williams.pdf, (2025-05-01)

[19] Brachvogel, R. C.; Von Delius, M. Orthoester Exchange: A Tripodal Tool for Dynamic Covalent and Systems Chemistry. *Chem. Sci.* **2015**, *6* (2), 1399–1403.

[20] Vrhovšek, A.; Gereben, O.; Jamnik, A.; Pusztai, L. Hydrogen Bonding and Molecular Aggregates in Liquid Methanol, Ethanol, and 1-Propanol. *J. Phys. Chem. B* **2011**, *115* (46), 13473–13488.

[21] Block, E. Olefin Synthesis by Deoxygenation of Vicinal Diols. *Org. React.* **1984**, *30*, 457–566.

5 THE CATALYTIC COUPLING OF CO_2 AND GLYCIDOL TOWARD GLYCEROL CARBONATE

5.1 PREFACE

This chapter specifically addresses the carbonation of epoxides, e.g. activated analogs of bio-based polyols, using gaseous carbon dioxide. The first subsection explores catalytic approaches developed to overcome the high thermodynamic stability of CO_2. The second subsection showcases the intensification of the carbonation of glycidol with CO_2, including it scale-up to pilot-scale mesofluidic reactor.

Subsection 1 outlines the two principal synthetic approaches for the preparation of glycerol carbonate. The first synthetic route utilizes common epoxides and proceeds through a nucleophile-catalyzed mechanism, while the second path employs β-hydroxylated-epoxides, which undergo transformation via the proton shuttle mechanism. This work is based on an exhaustive review published in *ACS Catalysis*: C. Muzyka, D. Silva-Brenes, B. Grignard, C. Detrembleur, J.-C. M. Monbaliu, *ASC Catalysis*, **2024**, 14, 12454-12493. These two pathways differ in their catalytic activation; one targeting the epoxide ring, while the other involves the activation of β-hydroxylated moiety. Over the past 10 years, a wide variety of catalysts have been designed to optimize epoxide-CO_2 cycloadditions, aiming for mild experimental conditions, minimal waste and excellent productivity. These include metal-based, organic, and ionic-liquid derived systems, often functionalized with hydrogen bond donor, Lewis acidic sites or chemisorptive groups. Additional strategies have leveraged porous materials, porous ionic liquids or dual component catalysts. Despite these advancements, structure-activity relationships between catalyst design on mechanism pathways remain elusive, preventing rational optimization of processes. This review examines the overall catalytic structure, clarify the role of their functional groups within the respective mechanism, and provides a sustainability assessment of their performances in term of overall efficiency and glycerol carbonate productivity.

This work highlights that despite the extensive development of catalysts for epoxide carbonation, very little attention is given to reactor technologies. Among them, continuous flow reactors inherently feature appealing advantages to efficiently handle gas-liquid reactions.

Building on the knowledge gained in the catalyst discussion, subsection 2 presents the design of novel, intensified flow process for the carbonation of glycidol, a β-hydroxylated-epoxide, catalyzed by a Bronsted base. This experimental work was published in *Angewandte Chemie International Edition*: C. Muzyka, S. Renson, B. Grignard, C. Detrembleur, J.-C. M. Monbaliu, *Angew. Chem. Int. Ed.*, **2024,** 63, e202319060. Liquid-gas reactions are notoriously limited by biphasic mass transfer in batch reactors, often resulting in low yields and poor selectivity. Continuous flow reactors address these issues through their huge surface to volume ratio, reducing diffusion distances from several centimeters in batch to only a few micrometers.

Apart from channel geometry, the volumetric mass transfer coefficient (k_La), which quantifies the efficiency of gas transfer to a liquid, is significantly impacted by fluid dynamics and the contact area between liquid and gas (Figure 5.1). In microfluidic reactors (channels diameters <100 µm), laminar flow prevails due to a low Renolds number (typically Re < 1000 in such systems). While molecular diffusion plays a significant role, mass transfer in Taylor flow (gas-liquid segmented flow) benefits from two synergetic mechanisms: an enhanced interface area and improved homogeneity of liquid slugs due to pseudo-convective mixing.

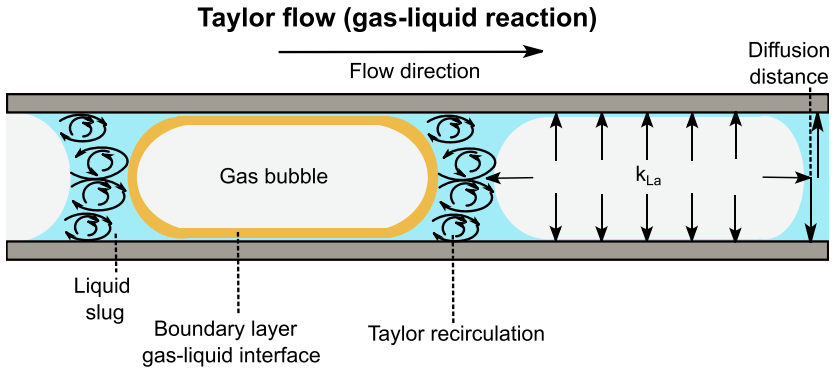

Figure 5.1 Taylor flow and mass transfer in gas-liquid reaction.

Scaling up to mesofluidic reactors (channel diameters <850 µm) enables flow rates exceeding microfluidic limits, reaching transitional-to-turbulent flow regimes (Re ≈ 2000-5000). This elevates energy dissipation rates driving two-phase flow advantages: promote bubble fragmentation and dispersion (smaller, more uniform bubbles), reduce concentration boundary layers near gas-liquid interfaces and enable continuous homogenization of liquid slugs via chaotic mixing paths and constant renewal of liquid layers.

Continuous flow reactors also support high operating pressures, which significantly increases gas solubility and promote the formation of small gas droplets with large interfacial area for mass transfer. High pressure operation also allows reactions to be performed at superheated conditions (e.g. above solvent boiling point), thereby accelerating reaction kinetics. Moreover, the high surface-to-volume ratio efficiently ensures heat transfer, yielding an accurate and homogeneous control of reaction temperature.

Overall, this interplay of parameters outlines continuous flow as a pertinent approach for developing an efficient and productive process of glycidol carbonation.

5.2 THE CATALYTIC COUPLING OF CO_2 AND GLYCIDOL TOWARD GLYCEROL CARBONATE

5.2.1 ABSTRACT

Ambitious environmental objectives have driven research and innovation toward the production of bio-renewable chemicals, such as glycerol carbonate. In particular, the production of glycerol carbonate from the coupling of CO_2 and glycidol has received considerable attention from the Chemistry and Chemical Engineering communities. This route became particularly appealing considering that glycidol is an activated derivative of glycerol, which together with CO_2, is an industrial waste. To keep the chain of value toward high value-added glycerol carbonate as attractive as possible, numerous metal-based and organo-catalysts have been developed. We provide with this review a pragmatic overview of the most promising catalytic protocols toward glycerol carbonate reported over the past 8 years. Special attention is given to inherent mechanistic and structure-(re)activity features as key parameters driving reaction performances. This review also addresses the preparation of a selection of catalysts, as well as the global efficiency and sustainability of the chain of value toward glycerol carbonate. Such a holistic review is intended to feed inspiration for future highly efficient catalytic systems.

5.2.2 INTRODUCTION

The chemical sector is notoriously one of the most energy-, resource- and waste-intensive, industries. These factors have been a particularly significant challenge to the European Union's (EU) Chemical Industry, which despite the reshoring promises of the post-COVID era, continues to struggle to maintain its manufacturing processes. The fast industrial and economic rebounds starting in late 2021 led to an extraordinary demand in energy within a narrow time window. Skyrocketing demand, oil market volatility and progressive depletion, geopolitical instability and climate change extensively stressed the corresponding markets and triggered the current energy crisis.[1] Soaring energy bills are choking the EU Industry, specifically the chemical sector, due to much lower competitiveness on the global market.[2] Reshoring to or developing new chemical production units in the EU also clashes with increasingly restrictive regulatory policies, echoing widespread public awareness of the chemical risks for people and the environment.[3] This global situation also interferes with the EU's ambition to accelerate the green and digital transitions and to strengthen its leadership in replacing fossil-based feedstocks for bio-based renewable alternatives by the end of 2030.[4] A step further was taken to significantly reduce greenhouse gas emissions with the ban of combustion engines by 2035. This has also contributed both to shake up the global energy market and to awaken new needs for sustaining the electrification of the transportation fleet.[5,6]

New chemical production processes must incorporate opportune technologies with lower environmental footprints and high safety.[7] Processes targeting high value-added chemicals at large scales must ideally feed upon bio-renewable sources and/or waste effluents such as CO_2.[8-12] Over a decade of technology and chemical innovation has established robust

foundations upon which new industrial processes can thrive within EU's main environmental ambition, and strategic directions for R&D and production.[13-14]

Among bio-renewable chemicals with a potential significant impact on current industrial processes, glycerol carbonate (**GLC**) is receiving growing attention from the academic and industrial communities. **GLC** has emerged as a versatile chemical with promising applications in major economic sectors including coatings and adhesives. **GLC** also emerges as a promising low volatile organic compound (VOC) solvent that could compete with solvents currently in use (glycols, ketones or esters). Moreover, **GLC** is involved as an intermediate in the production of glycidol (**GD**), which can be then incorporated into polyurethanes through its reactions with amines.[3,4,9,15–19] Lastly, a potentially future growing application stems from the Li-ion battery industry as an electrolyte carrier due to its low flammability and boiling point. Although numerous works report an improved conductivity with **GLC** over current candidates (ethylene and propylene carbonate)[20,21] its hydroxyl group interferes with Li^+ transport. This likely points toward acylated or alkylated derivatives as potential next generation ion carriers. Polymerization of the cyclic carbonate ring with increasing temperature also contributes to the challenges of using **GLC** for Li-ion applications. Some niche markets comprising cosmetics and personal care stand out; yet they represent minor market shares for highly purified **GLC**. Implementation of these applications is, however, hindered due to the high global price of **GLC** ranging between 3000 and 6000 $ per ton (market volume: 10 million $, selling volumes around 10s of tons).[22] The market is not expected to grow in the mid-term, particularly due to the lack of a viable, low-cost production process amenable to commercial scale. The development of a new highly efficient and productive procedure could provide the impulse needed to bring **GLC** to the forefront of the chemical industry.[23]

5.2.3 PRIOR ART AND SCOPE OF THIS REVIEW

Three distinct synthetic approaches are commonly exploited to access **GLC** (Figure 5.2). The direct carbonation involves the reaction between CO or CO_2 with diols (path a). The second strategy relies on the coupling of diols with an activated source of CO_2, such as the transesterification of a carbonating agent such as dimethyl carbonate with glycerol (**GLY**) or the alcoholysis of urea with **GLY** (path b).[24] An alternative pathway exploits **GD**, a highly activated version of **GLY** that is easily carbonated with CO_2 (path c).[25] Path a usually requires expensive, toxic, and increasingly scarce metal catalysts, as well as a large excess of additives under harsh conditions, and is often associated with low yields.[25] Despite its effectiveness, path b suffers from a poor atom economy and a limiting thermodynamic control.[11,12,26–28] Path c feeds upon CO_2 and **GD** in the presence of various catalysts,[29,30] and is usually a highly efficient path to **GLC**. With proper epoxide and/or CO_2 activation, **GLC** can be produced under relatively mild conditions and short reaction times (i.e., compared to path a).[31,32] **GD**'s classification as a toxic chemical is counterbalanced by its potential production from bio-sourced **GLY**, making it an attractive sustainable building block.[4] The synthesis proposed in path c can occur according to two main mechanistic pathways.[29,30] The first one, path c^1, is the most conventional. It relies on the use of catalytic systems, usually combining a halide nucleophile with a Lewis acid center (LA) or a hydrogen bond donor group (HBD). Initial activation of the epoxide via LA or HBD is followed by the

ring opening of the epoxide by the halide nucleophile. In the subsequent step, CO_2 is captured by an intermediate alkoxide species prior to its intramolecular cyclization toward the corresponding cyclic carbonate.[32] The second alternative pathway (path c^2) is often referred to as the proton shuttle mechanism, and consists of the carbonation of the hydroxylated epoxide to yield a hemiester of carbonic acid. Next, the intermediate species undergoes an intramolecular nucleophilic addition to generate the cyclic carbonate.[33] Whereas mechanism c1 can take place with a variety of epoxide substrates, mechanism c^2 relies upon the availability of a β-hydroxyl next to the epoxide, limiting its occurrence to **GD** and other derivatives possessing a β-hydroxyl group.[34]

The attractiveness of the coupling of **GD** with CO_2 strongly depends on the availability of highly performant catalytic systems to provide viable procedures toward industrial production. The design of catalysts endowed with high performance for coupling epoxides and CO_2 still represents one of the most challenging and hottest topics of this past decade.[35] Despite the effectiveness of various homogeneous catalysts, they are usually associated with a very cumbersome downstream separation and purification. In the worst-case scenario, this would preclude their effective recycling and have a deleterious impact on the overall process economics.[35]

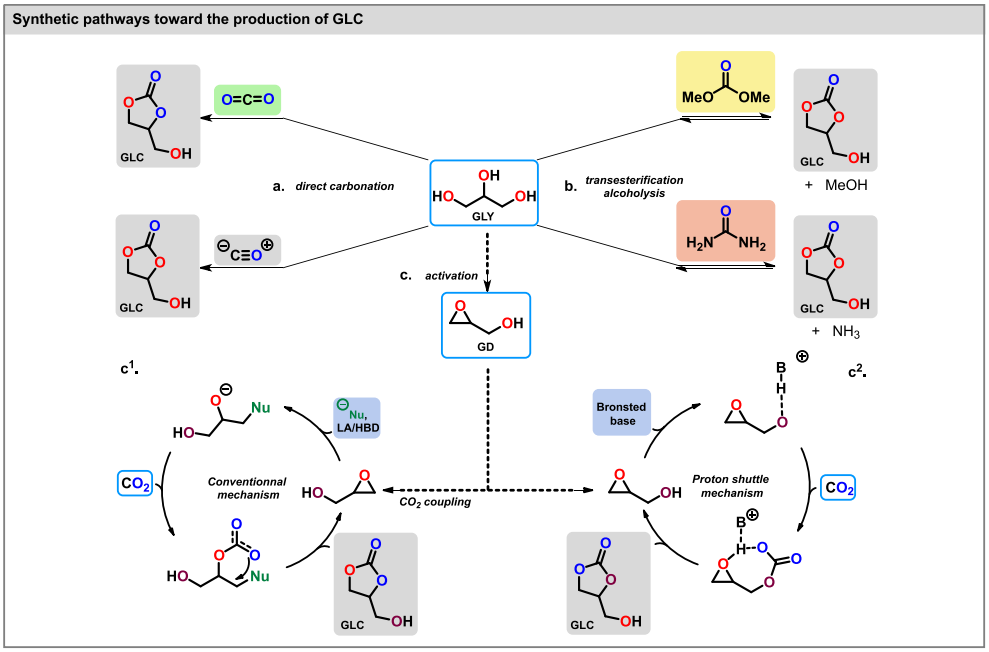

Figure 5.2 Synthetic pathways toward the production of **GLC**. (a) Direct carbonation with CO or CO_2. (b) Transesterification of dimethyl carbonate and alcoholysis of urea with **GLY**. (c) Cycloaddition of CO_2 with **GD** via the conventional (c^1) and the alternative (c^2) proton shuttle mechanisms, respectively.[32,33]

Heterogenization has emerged as a potential compromise for maintaining catalytic activity and easing downstream recycling. Despite the potential for recycling, heterogenized catalysts often suffer from limited mass transfer and lower catalytic performance due to fewer

accessible HBD or/and CO_2 binding sites.[36] These limiting parameters often legitimize the implementation of harsh experimental conditions in order to ensure high product output.[37] Finally, regardless of homogeneous or heterogeneous strategies, most of the time the preparation of the catalysts themselves requires the use of expensive reagents, and time-consuming, complex protocols with significant environmental footprints. Their exploitation at large industrial scale is therefore still very limited.[38] A compromise between performances and ease of preparation should therefore always be aimed at.

Therefore, the development of highly effective yet more sustainable catalysts remains a very timely topic. To ensure convenient recyclability, heterogenized catalysts featuring strongly active nucleophiles, HBD and CO_2 binding/adsorption groups with adequate spatial dispersion within the solid support should be privileged.[37] Furthermore, the porosity of such materials should be engineered to favor mass transfer and therefore accessibility to catalytic sites. Finally, the ideal catalyst should also work under mild experimental conditions, i.e., ideally room temperature and atmospheric pressure,[36] although this requirement is usually associated with extended reaction time.[37,39]

This review aims to provide a pragmatic, detailed, and up-to-date collection of works dealing with the catalytic coupling of CO_2 onto epoxides, with a special emphasis on **GD** and its transformation toward **GLC**. The activities and performances of metal-based catalysts are extensively discussed along with organocatalysts (including ionic liquids), outlining the latest advances in the catalysis of CO_2 fixation. The work of Kleij, who first described the peculiar features of the proton shuttle mechanism, is considered as the starting point of this discussion. As such, only papers produced thereafter are considered in this review. We aim to provide a fine understanding of the most recent catalytic systems to either exploit the proton shuttle mechanism or the conventional pathway. The engineering of catalysts and optimization of procedures have already been extensively covered in the literature.[34,36,40–44] However the mechanistic and structure-reactivity aspects of these catalytic systems are often only superficially discussed. We strongly believe that a thorough mechanistic understanding is a key driver of innovation. Therefore, this work provides in-depth discussions on the specific inherent reaction features, with emphasis on computational support when available and relevant. Moreover, this review also addresses the preparation of these catalytic systems to better evaluate the global efficiency of the processes and their environmental footprint.

To support this sustainability assessment, an Ecoscore scale (Table 5.1) was developed to evaluate all the processes discussed in this work. The scoring system assigns penalties based on various experimental parameters, including the catalyst loading, the use of additives and solvent, reaction temperature, CO_2 pressure, reaction time, and product yield. Each process begins with an Ecoscore of 100, from which penalties are subtracted to determine the final score.

Table 5.1 Guidelines of penalty points and color code for Ecoscores.

C	none	≤ 1 mol%	1 ≤ 5 mol%	> 5 mol%
color code				
penalty	0	1	4	8
solvent	none	low bp (<100°C)	high bp (>100°C)	
color code				
penalty	0	1	4	
T (°C)	25°C	25°C≤ 50°C	50°C≤ 85°C	> 85°C
color code				
penalty	0	1	2	3
P CO_2 (bar)	1 bar	1 ≤ 5 bar	5 ≤ 10 bar	> 10 bar
color code				
penalty	0	1	2	3
t (h)	0 ≤ 4h	4 ≤ 10h	10h ≤ 24h	> 24h
color code				
penalty	0	2	4	8
yield (%)	≥ 90%	90 ≥ 70%	70 ≥ 50%	< 50%
color code				
penalty	(100-yield)/2			

5.2.4 METAL-BASED CATALYSTS

This section does not exhaustively cover the state of the art from primary literature on the metal-catalyzed carbonation of **GD**. Instead, it gives an overview of the most efficient catalytic scaffolds and metal catalysts alongside with their operating conditions. It provides up-to-date and robust foundations for a rational comparison with metal-free, organocatalytic, and ionic liquid-based processes. The section aims to present broadly available, cheap, and harmless metals that nearly fulfill the sustainability requirements of an "ideal catalyst" such as aluminum, iron, zinc, copper, zirconium, and nickel derivatives, as well as some alkaline earth metals. However, other metal catalysts are mentioned to better map of the potential metal centers exploited for the cycloaddition of CO_2.

5.2.4.1 OVERVIEW OF CATALYTICALLY METAL CENTERS

Figure 5.3 provides a snapshot of the literature data illustrating the use of metal catalysts over the past 8 years. Figure 5.3 has been designed to distinguish rare, noxious, and/or expensive metals from more sustainable, abundant alternatives with potent activity in the coupling of epoxides and CO_2. Among transition and post transition metals (Figure 5.3, in blue), examples with Ti-[45,46], Cr-[47,48], Co-[49–51], Ga-[52], Y-[53,54], Ru-[55], Rh-[56], Pd-[57], Cd-[58,59] and In-based[60] catalysts have been documented. Examples of catalysts featuring lanthanides, such as La[61–64], Ce-[65–67], Nd-[54,65], Eu-[68–70], Gd-[64,71], Tb-[72–74], Dy-[64,75], Ho[76], Er[77], Yb[53,54,78] and Lu[79] have also been reported. Apart from Titanium and Chromium, all these metals have a low to medium global availability.[80] In addition, most of the metals and their mining are associated with long-term toxicity and deleterious environmental impact. Good catalytic performance is often outweighed by their low abundance and toxicity, compromising their industrial applications. Therefore, alternative metals featuring high sustainability and low toxicity are privileged. Representative examples include magnesium, calcium, iron, nickel, copper, zinc and aluminum (Figure 5.3, in green).[4] Despite the limited choice of sustainable metal catalysts, numerous reports investigate their reactivity in coupling **GD** with CO_2.

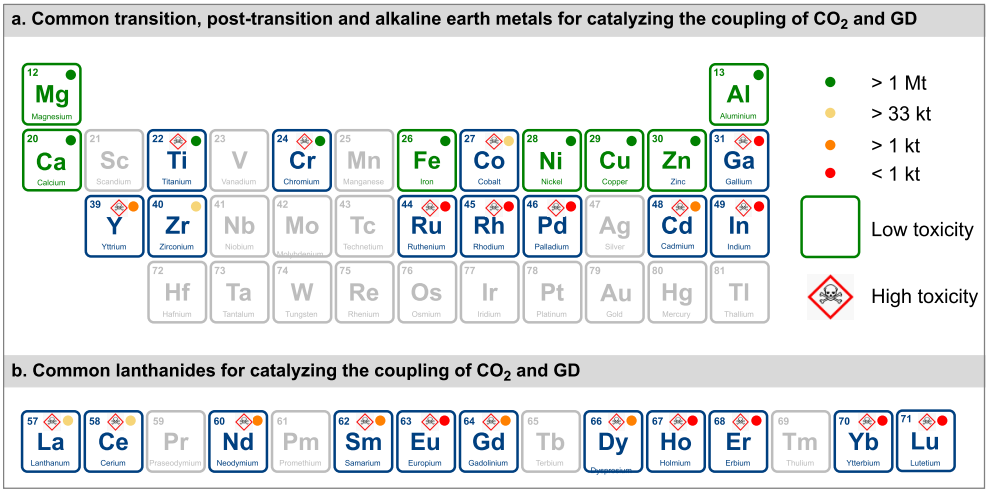

Figure 5.3 Elements with reported activity towards the cycloaddition of CO_2. Elements with low sustainability are highlighted with a blue box, whereas metals featuring high sustainability are in green. High toxicity is indicated by the corresponding symbol when applicable. The worldwide production is indicated with a color dot.[80] (a) Transition, post-transition, alkaline earth metals. (b) Lanthanides.

Aluminum-based catalysts. Lara-Sánchez *et al*. developed a series of stable bifunctional aluminum catalysts supported by NNO-scorpionate ligands (Figure 5.4a). The catalyst incorporated a quaternary amino moiety as counterion to a mechanistically relevant bromide ion. The bromide served as a transient nucleophile during the catalytic cycle converting epoxides to carbonates; however, this ligand was easily degraded due to an intramolecular nucleophilic attack of the bromide on the catalyst, leading to the loss of a benzyl bromide. To address this issue, a new generation of ligands were prepared by changing the alkyl moieties used to build the quaternary amine, from a benzyl to a methyl. Synthesis of the ligand started with deprotonation of bis(pyrazolyl)methane **1** with n-BuLi and addition to 4-(diethylamino)benzophenone (> 90 % yield), followed by alkylation of the amine with iodomethane, affording **2** as a salt in 82% yield. The ligand was reacted with trialkylaluminum to afford catalyst **3**. Bimetallic complexes were also prepared by reacting with 2 equivalents of the alkylaluminium. However, their performance was not better than the mononuclear compounds.[81]

One year later, the same group investigated the influence of the counter-anion on the performances of mono-and bimetallic bifunctional catalysts. Starting from the precursor **4** derived from **1**, the authors prepared a similar ligand by alkylating the amine with methyl methanesulfonate instead of iodomethane. The methanesulfonate salt obtained was then transformed to the chloride, bromide or iodide salts through anion exchange with the appropriate inorganic salts. Further treatment of the resulting salts with 1 equiv. of $AlEt_3$ led to the formation of catalyst **5** (59% yield) (Figure 5.4b).

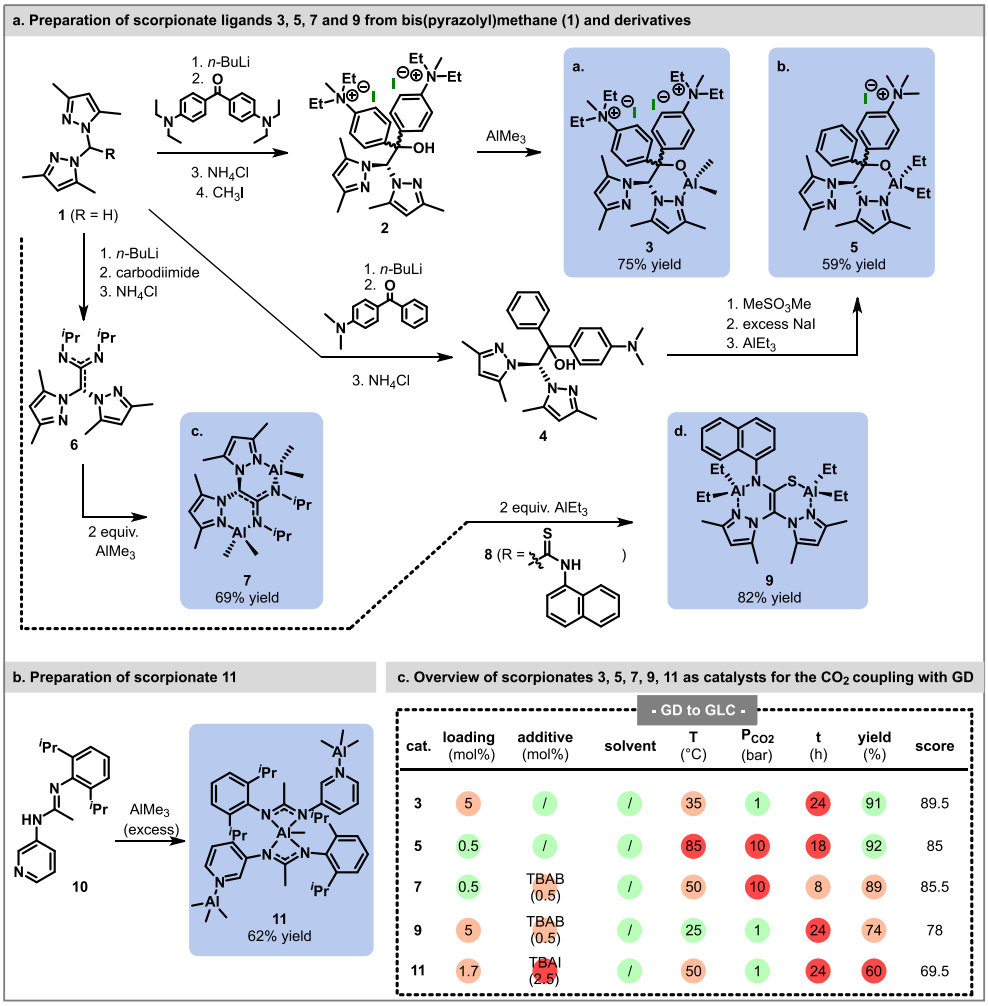

Figure 5.4 (a) Preparation of various scorpionate ligands from bis(pyrazolyl)methane derivatives and the corresponding Al-catalysts **3**, **5**, **7** and **9**.[81–85] (b) Preparation of scorpionate ligand **11**.[86] (c) Comparison of scorpionates Al-complexes **3**, **5**, **7**, **9** and **11** as catalysts for the coupling of CO_2 and **GD** (See Section 6 and Supporting Information for details).

Among the complexes with different halide counterions, the iodide derivative displayed the highest efficiency due to the higher nucleophilicity and leaving group ability of iodide. Furthermore, lower coulombic interactions with the ammonium cation compared to its chloride and bromide analogs contributed to its availability for nucleophilic addition on the epoxide. Additional control experiments emphasized the superior efficiency of monometallic complexes over their bimetallic counterparts.[82]

Another family of Al-based scorpionate compounds was formed from the addition a carbodiimide derivative to bis(pyrazolyl)methane **1**. Figure 5.4c shows the synthesis of ligand **6**, which could be synthesized in 76% yield.[83] Two equivalents of $AlMe_3$ were added to **6** to obtain the dinuclear aluminum complex **7** with an overall yield of 69%. In this case,

tetrabutylammonium bromide (TBAB) was used as a co-catalyst for the production of **GLC** from **GD**, affording the carbonate with an 89% yield.[84] The same authors also developed a series of helical bifunctional heteroscorpionate complexes, such as **9**, which was derived from the reaction between N-naphthyl-2,2-bis(3,5-di-tert-butylpyrazol-1-yl) (**8**) and 2 equivalents of $AlEt_3$ (82% yield). The use of **9** with TBAB as a co-catalyst quantitatively converted **GD** to **GLC** with 94% selectivity (Figure 5.4d).[85]

Another series of scorpionate ligands were developed by Rojas *et al*. They described the synthesis of mono-, bi- and trimetallic alkylaluminium complexes prepared from new amidine ligand precursors. The most efficient of their catalysts began with the preparation of ligand **10** through the addition of N-(2,6-diisopropylphenyl)acetimidoyl chloride to a solution of 2-aminopyridine and Et_3N, affording **10** in 70% yield after column chromatography (Figure 5.4e). Reaction of 2.5 equiv. of $AlMe_3$ to **10** led to the formation of trimetallic complex **11**, containing one pentacoordinate aluminum and two pyridinic nitrogen adducts with the Al Lewis acid center. Complex **11** was isolated in 62% yield. **GLC** could be obtained in 63% yield over 24 h using 1.7 mol% of **11** and 5 mol% of tetrabutylammonium iodide (TBAI) at 50 °C and 1 bar of CO_2.[86]

Focusing on another type of ligand, North and Wu reported the design of a homogeneous bimetallic aluminum(salphen) complex synthesized from commercially available components and using a co-catalyst (TBAB) as an external nucleophile.

The salphen ligand was prepared from the condensation of 1,2,4,5-benzenetetramine with 3,5-di-*tert*-butyl-hydroxybenzaldehyde, which was then treated with 2.2 equiv. of diethylaluminum chloride and filtered to afford complex **12** in 30% cumulated yield (Figure 5.5a). Due to its poor solubility, the use of the catalyst initially resulted in a heterogeneous medium before complete dissolution of the complex. To determine the cooperative or individual behavior of the two metal sites into the catalytic mechanism, two different trials with 0.1 and 0.2 mol% TBAB using a constant amount of **11** were performed.

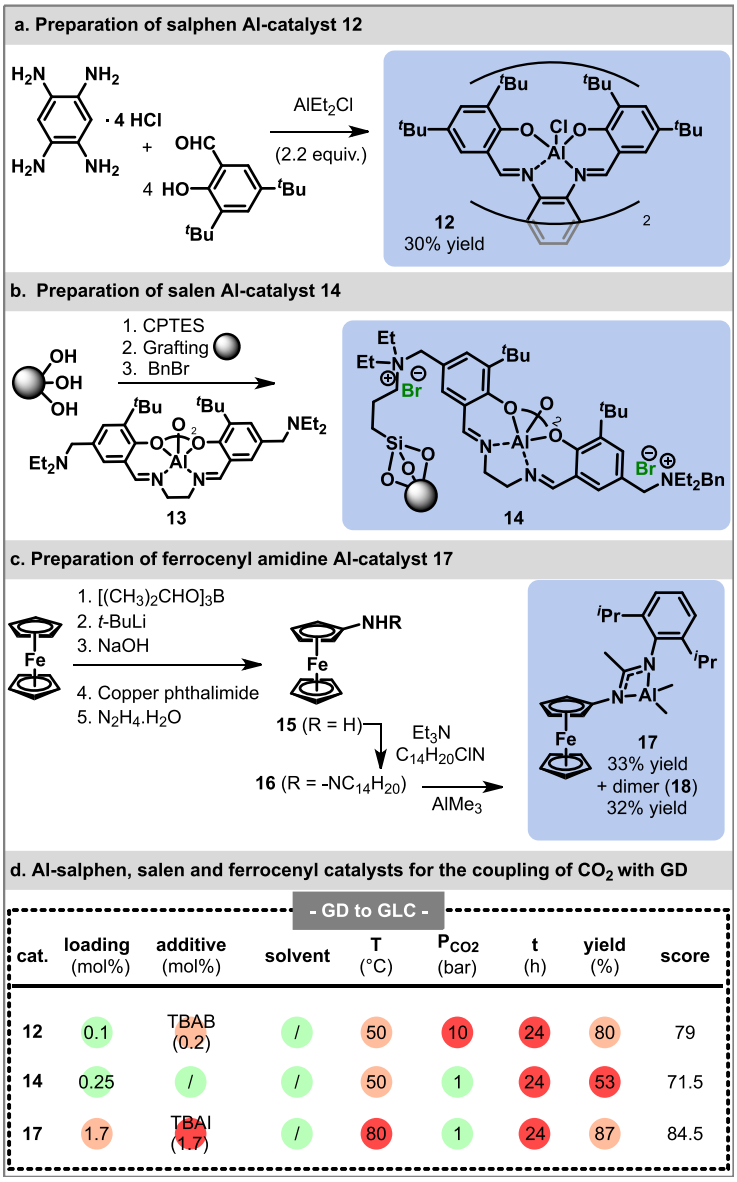

Figure 5.5 (a) Synthesis of a salphen ligand and its corresponding Al-catalyst **12**.[87] (b) Synthesis of a supported salen ligand and its corresponding Al-catalyst **14**.[88] (c) Synthesis of a ferrocenyl amidine ligand and its corresponding Al-catalyst **17**.[89] (d) Comparison of salphen, salen, ferrocenyl amidine ligands and their corresponding Al-complexes **12**, **14**, and **17** as catalysts for the coupling of CO_2 and **GD** (See Section 6 and Supporting Information for details).

The authors rationalized that, in the case of a cooperative behavior, equimolar amounts of TBAB with respect to **12** would be enough to sustain the catalytic activity, as the two Al sites have different roles, catalyzing carbonation of a single **GD** molecule at a time. In the case, however, of separate catalytic activity of both metals, the reaction would benefit from having

a 2:1 molar ratio (TBAB:12), as each Al catalytic site would require one equivalent of TBAB. The results showed only a marginal 9% difference between both modalities (0.2 mol% TBAB/**12**- 94% vs 0.1 mol% TBAB/**12** – 85% conversion), which the authors hypothesized is due to sub-stoichiometric amounts of Br when using 0.1 mol%, caused by exchange with the catalyst's chloride moieties. The authors concluded that both Al centers in the catalyst behave cooperatively, with one Al center activating the epoxide while the neighboring Al traps the CO_2 to promote its insertion in the opened epoxide, leading to terminal cyclization (Figure 5.6). Tributylamine was detected by GC-MS, potentially generated from the retro-Mentschutkin degradation of TBAB. The authors therefore hypothesized that tributylamine could stabilize the CO_2 when bound to Al (**19**).[87]

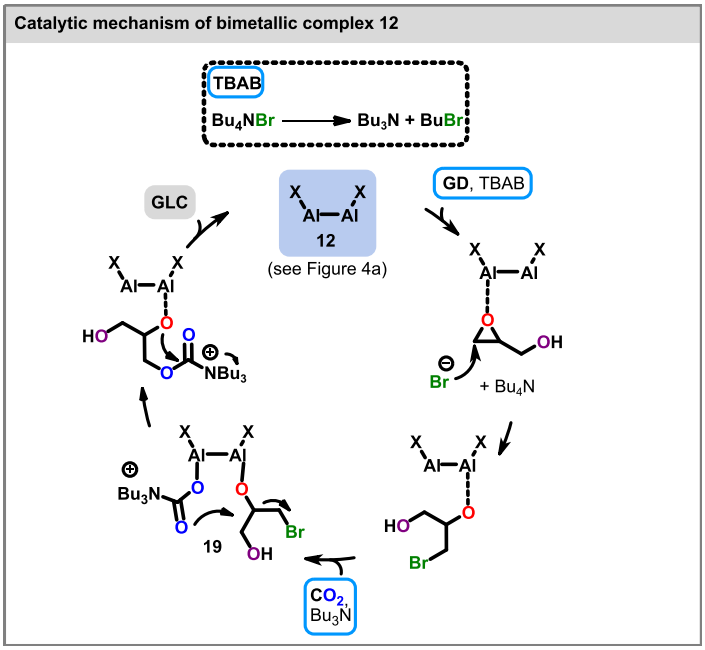

Figure 5.6 Tentative catalytic mechanism of bimetallic complex **12** depicting a dual role for the Al center for substrate activation and binding of CO_2.[87]

Another family of aluminum catalysts was documented by Reiss *et al.*, who prepared heterogeneous bimetallic aluminum(salen) complexes immobilized within mesoporous silica (SAB-15). Specifically, SAB-15 was selected as a support material for its attractive properties including a high surface area and stability, as well as potential tunability of the porosity. A pore-expanded version of SAB-15 was prepared from the dissolution of copolymer P-123 (support template) in aqueous HCl, followed by the addition of trimethylbenzene (micelle expander) and tetraethyl orthosilicate. After 24 h stirring, the mixture was left to stand at ±100 °C for 72 h. A solid was recovered by filtration and calcined at 550 °C for 5 h. Structural characterization of the support material confirmed that the treatment with a micelle expander resulted in an increase in open porosity. The mesoporous silica was functionalized using (3-chloropropyl)triethoxysilane (CPTES) to install reactive 3-chloropropyl moieties on the silica surface, which were then used to anchor

aluminum(salen) complex **13**. Subsequent alkylation of the tertiary amines with benzyl bromide led to the formation of catalyst **14** (Figure 5.5b). The enlarged pores increased mass transfer, facilitating access to the active sites, leading to a **GD** conversion of 53%, compared to 42% for the control catalyst without enlarged pores. Characterization of the catalysts obtained without pore expansion showed that the porosity of the silica was lost after installation of the metal catalyst **13**, reducing the accessibility of the catalytic sites. Recycling of the catalyst was also assessed and showed a progressive loss of performances over 5 runs on *t*-butyl glycidyl ether from approximately 53% to 20% conversion, due to dealkylation of the ammonium group of the catalyst. Catalytic activity could be re-established by treating the catalyst with benzyl bromide to re-alkylate the amine.[88]

A third example based on ferrocene comes from Rojas *et al.*, who prepared a set of alkyl aluminum complexes with non-symmetric ferrocenyl amidine ligands in the presence of TBAI as cocatalyst. The preparation of ligand aminoferrocene **15** consisted of a cumbersome multi-step synthesis starting from a commercially available ferrocene precursor to obtain **15** in a 42% cumulated yield. Further nucleophilic substitution of **15** with an imidoyl chloride derivative gave ligand **16** before its complexation with 0.5 or 1 equiv. $AlMe_3$, producing the tetracoordinate complex **17** (in 33% of cumulated yield) or the pentacoordinate complex **18** (32% yield, Figure 5.5c). Evaluation of their respective performances highlighted **17** as more efficient than **18**. Production of **GLC** using **17** gave 87% yield. The authors explained this difference in due to its higher Lewis acidity and the lower steric hindrance of **17** compared to **18**, which facilitates the interaction between the Al center and the epoxide.[89]

In contrast to the previous works, the next articles illustrate the proton shuttle mechanism involving the β-hydroxyl activation of epoxides and the peculiar behavior displayed by Al complexes. In 2016, Kleij and colleagues reported an unprecedented alternative mechanism toward the activation of CO_2 through a substrate-mediated approach when in the presence of a Lewis Acid catalyst (Figure 5.7a). Using **GD** as a model substrate, they succeeded in predominantly triggering the conventional mechanism when adding an external nucleophile (Figure 5.2c[1]) or the alternative proton shuttle mechanism (Figure 5.2c[2]) depending on the catalytic system.[90] The aluminum catalyst used for this study, **20** (Figure 7a), resulted from the reaction of an aminotriphenolate ligand **19** with an excess of $AlMe_3$.[91] The ligand (**19**) was obtained from a variation of a Mannich reaction involving hexamethylene tetraamine, formaldehyde and a *tert*-butyl phenol derivative. Catalyst **20** gave an excellent yield (93%) of **GLC** after 2 h at 75 °C under 10 bar of CO_2 (Figure 5.7b). Using methyl ethyl ketone (MEK) as a solvent, the combination of the metal catalyst with a halide salt at 25 °C onto substrate **21** led to a distribution of two cyclic carbonates arising from either the epoxide ring opening (**22**) or the activation of the β-OH (**23**) in a **23**/**22** of ratio 22:78 (Figure 5.7c). In contrast, when the reaction was carried out in the absence of the halide co-catalyst, product **22** was selectively formed. The authors argued that its formation proceeded through the formation of carbonic acid hemiester intermediate **24** (Figure 5.7d). The key role played by the free hydroxyl group on **GD** was further confirmed by observing that the reaction on benzyl-protected glycidol gave no conversion.[90]

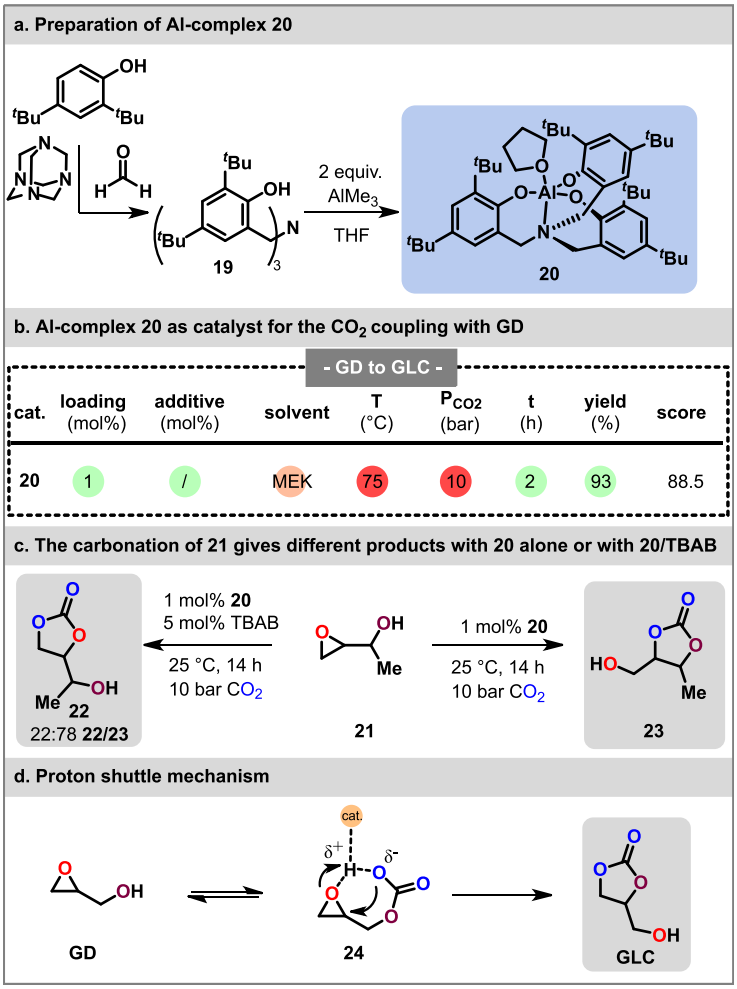

Figure 5.7 (a) Preparation of the Al complex **20** through coordination of an aminotriphenolate ligand with $AlMe_3$. (b) Catalytic performance of Al complex **20** for the coupling of CO_2 et **GD** (See Section 6 and Supporting Information for details). (c) The carbonatation of 1-(oxiran-2-yl)ethanol **21** using solely **20** (1 mol%) gives full conversion to **22**, while in combination with TBAB (5 mol%), a 22:78 **23**/**22** mixture is obtained. (d) Overview of the proton shuttle mechanism involving linear carbonate intermediate **24**.[90]

Two years later, the same group rationalized the proton shuttle mechanism through a multidisciplinary approach.[33] The authors first confirmed that the synthetic path was inherently substrate-dependent when catalyzed by aluminum complex **20**. Accordingly, the carbonation protocol was implemented on deuterated *d*-**GD**, leading exclusively to **25** (Figure 5.8a).

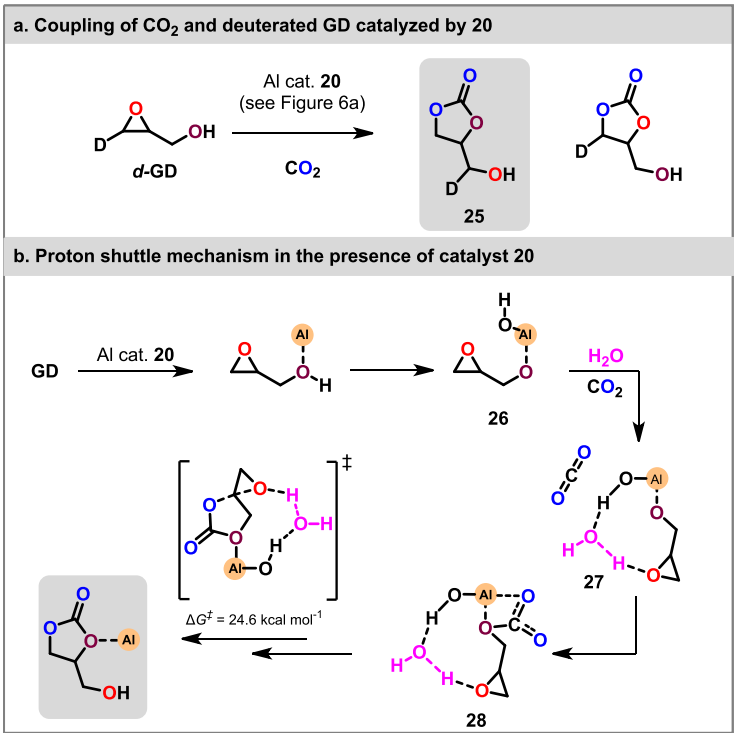

Figure 5.8 (a) Deuterium labeling of **GD** to illustrate the triggering of the proton shuttle mechanism. (b) Detailed mechanism mediated by β-hydroxyl activation of epoxide catalyzed by Al-catalyst **20** and in the presence of H_2O as an additive.[33]

Furthermore, the reaction with (*S*)-**GD** resulted in the formation of (*R*)-**GLC**, suggesting a mechanism similar to SN_2. The kinetics of the reaction featured a first order dependence for the reagents and for the catalyst. A computational study was next undertaken to further strengthen the understanding of the mechanism. The first step involved the coordination of the β hydroxyl group of **GD** with the Al center to form a stable intermediate, followed by its subsequent deprotonation toward an alkoxide species **26**. The second step, i.e., the intramolecular cyclization toward **GLC**, was studied both in the presence and absence of water as an additive. The intramolecular cyclization was identified as the rate-determining step with an overall very high activation barrier ($\Delta G^{\ddagger}$) of 46.2 kcal mol^{-1} (double-hybrid DFT - B2PLYP). The authors, however, found that the addition of water lowered $\Delta G^{\ddagger}$ to 24.6 kcal mol^{-1}. Such acceleration was associated with the favorable formation of a stable anion-CO_2-H_2O complex **27**. The latter complex facilitates the subsequent formation of hemiester intermediate **28** and contributes to a hydrogen-bonding activation of the epoxide. Consequently, the authors concluded that the substrate-activation of CO_2 and subsequent intramolecular cyclization proceed through a concerted mechanism, in contrast with the stepwise process without H_2O (Figure 5.8b). The computational insights were confirmed through additional experiments (50 mol% cat. 20, 50 °C, 10 bar CO_2, 4 h), using anhydrous and normal (wet) conditions, yielding **GLC** in 32% and 62%, respectively. Additional proof

of the mechanism was collected through ATR-IR spectroscopy, providing robust structural evidence on four key intermediates.[33]

Iron-based catalysts. Despite being a less commonly exploited metal, some catalysts with an iron center have also been developed. Kerton *et al.* reported the synthesis of a new set of iron(III) complexes supported by tetradentate amino-bisphenolate ligands. Fe-catalyst **30** was prepared according to a convenient protocol involving a dropwise addition of a methanolic solution of $FeCl_3$ (or $FeBr_3$) to ligand **29** at room temperature (Figure 5.9a).[93] Ligand **29** was prepared using a modified Mannich reaction.[93] Catalyst **30** was obtained after a sequence of evaporation, liquid-liquid extraction and filtration. The structure of the catalyst was studied by X-ray diffraction, revealing a square pyramidal distribution of ligands around the Fe(III) center. TBAB was employed as a co-catalyst to trigger the coupling of propylene oxide (**PO**) with CO_2. The Fe/**PO**/TBAB ratio was optimized, with an optimum at 1:4000:4. Under these conditions, the corresponding propylene carbonate (PC) was obtained in 84%. The authors also studied a small library of catalysts with various ligands. The results emphasized the key role of ortho- and para- electron-withdrawing group (EWG)-substituted phenolate ligands. Stronger EWGs seemed to promote the coordination with the epoxide, hence favoring the reaction. As one of the best catalysts, **30** was then tested on various epoxides. A 78% conversion of **GD** was obtained alongside a turnover number (TON) of 3120 mol_{PC} mol cat^{-1}. Kinetic data was collected through *in situ* IR, confirming a classical mechanism mediated by an external nucleophile. The temperature was identified as a key parameter, with an experimental $\Delta G^{\ddagger}$ of 23.5 kcal mol^{-1}.[94]

Kang *et al.* reported another type of ligands for Fe-based catalysts in the form of bifunctional homoleptic Fe-iminopyridine and heteroleptic Fe-bisiminopyridine complexes bearing both a HBD group and an internal nucleophile. The iminopyridine-derived catalyst was synthesized in a one-pot reaction involving picolinaldehyde, 2-amino-1,3-propanediol and FeI_2 to obtain **31** in 76% yield. The bisiminopyridine (BIP)-derived catalyst **33** required a three-step procedure to synthesize the BIP ligand, before a first addition of iron (II) bromide, followed by the addition of a second ligand (dihydroxybipyridine – dhbpy) to produce **33** in 51% cumulated yield after recrystallization. Using 0.5 or 0.1 mol% of catalysts **31** and **33** (Figure 5.9b), **GLC** was obtained in 72% and 78% yield, respectively, under different experimental conditions. The authors demonstrated that simply adding the components of catalyst **31** (FeI_2, picolinaldehyde, and 2-amino-1,3-propanediol), along with CO_2 and styrene oxide (**SO**) at 80 °C was just as effective in producing styrene carbonate (**SC**) as using the pre-synthesized catalyst **31**. This efficiency, due to the in-situ generation of the catalyst, was not observed in the case of catalyst **33**. The simple mixing of the building blocks for **33** gave a mere 11% yield of SC, compared to 94% yield for the pre-synthesized catalyst (**33**). Computational insights into the mechanism were obtained using DFT, indicating that, after the dissociation of an imino ligand (in catalyst **31**) or of the axial halide anion (in catalyst **33**), the substrate undergoes a dual activation via the Lewis acidic metal and the hydroxyl group (HBD), strongly promoting the ring opening of the epoxide.[95]

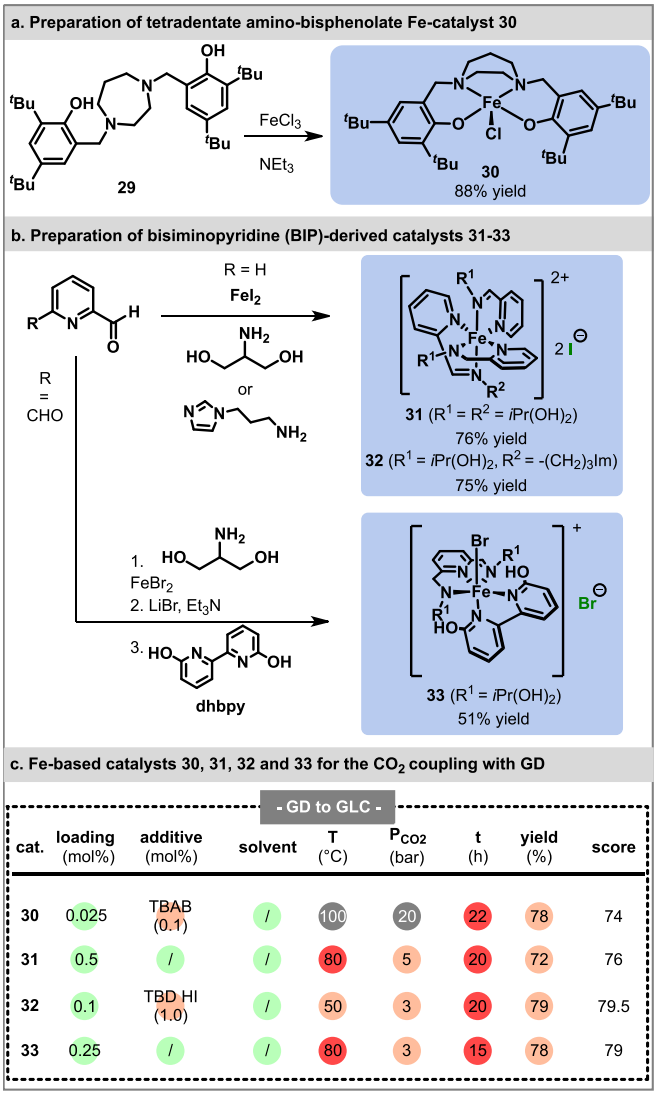

Figure 5.9 (a) Synthesis of tetradentate amino-bisphenolate Fe-catalyst **30**.[94] (b) Synthesis of bisiminopyridine (BIP)-derived Fe catalysts **31**-**33**.[95,96] (c) Comparison of Fe-based catalysts **30**, **31**, **32** and **33** for the coupling of CO_2 and **GD** (See Section 6 and Supporting Information for details).

Two years later, the same authors reported the catalytic properties of other Fe(II) iminopyridine complexes substituted with imidazole groups in the presence of (1,5,7-triazabicyclo[4.4.0]dec-5-ene hydroiodic acid) TBD-HI as co-catalyst. Drawing upon their previous design for **31**, the authors slightly modified the synthetic procedure to add 1-(3-aminopropyl)imidazole to produce the self-assembled catalyst **32** (Figure 5.9b). Interestingly, when performing the reaction using hydroxymethyl substituted derivative **34**, they found that such Fe(II) catalysts led to two distinct products (Figure 5.10a and 5.10b). Synthesis of cyclic carbonates from **34** indicated the concomitant formation of both **35**,

through the conventional mechanism, and **36**, arising from the proton shuttle mechanism in a ratio 1:2 and 67% conversion. The first mechanism involved the assistance of the external nucleophile. Accordingly, the mechanism proceeds through substrate activation mediated by both the metal center and the hydroxyl group of the ligand. Subsequently nucleophilic addition of iodide generates intermediate **37**. Insertion of CO_2 onto to alkoxy intermediate **38** is facilitated through imidazole-CO_2 activation. The final step involves intramolecular cyclization to the desired cyclic carbonate. The second mechanism occurred through substrate activation, involving the β-hydroxyl of **34** and both the metal Lewis acid and TBD co-catalyst.[96]

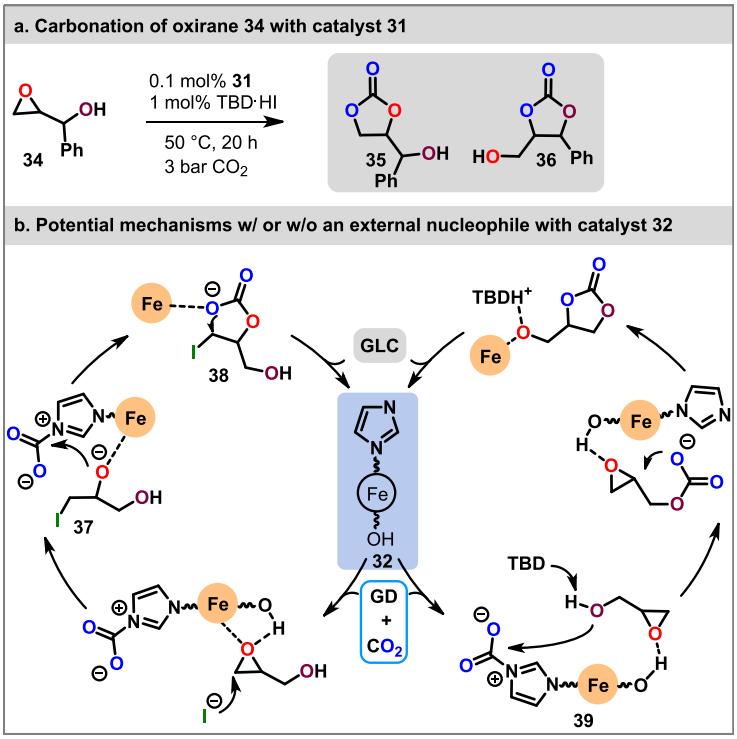

Figure 5.10 (a) Products obtained from the carbonation of oxirane **34** by catalyst **32**. (b) Conventional mechanism in the presence of an external nucleophile (left) and proton shuttle mechanism (right), both catalyzed by **32**.[96]

Islam *et al.* prepared an iron-phosphonate nanoparticle catalyst (HPFP-1(NP)) in combination with a halide salt (TBAB). The protocol of catalyst production simply relied on the mixing of hexamethylenediamine-N,N,N′,N′-tetrakis-(methylphosphonic acid) (HDTMP) with $FeCl_3$ and a subsequent hydrothermal treatment at 150 °C during 24 h to yield the desired compound. The distinctive advantage of this catalytic system was it use under mild experimental conditions to afford SC in high yield (97%). Upon optimization, 88% yield of **GLC** was obtained using 13.5 wt% of catalyst as well as 5 mol% of TBAB and 1 bar CO_2 at 25 °C for 12 h.[97]

Zinc-based catalysts. Islam and colleagues explored the performances of zinc stannate ($ZnSnO_3$) nanocrystals. The catalyst was produced through the mixing of sodium salicylate as a template and diethylamine followed by the addition of metal precursors $ZnCl_2$ and $SnCl_4$ prior to a hydrothermal treatment at 110 °C for 48 h. Analyses of porosity and BET surface emphasized a homogeneous distribution of mesopores, indicating uniform self-assembly of the nanocrystals. Using PEG-600 as a solvent, the reaction catalyzed by $ZnSnO_3$ nanocrystals achieved a high isolated yield of 91% toward **GLC** at 80 °C, over 10 h reaction time (1 bar of CO_2) using 1.2 wt% of the catalyst. Recyclability and recoverability of the catalyst $ZnSnO_3$ were assessed over 5 consecutive runs without significant loss of product yield.[98]

Later, the same group also reported the use of another zinc complex. Polystyrene-supported anthranilic acid was prepared by attaching the acid to a Merrifield resin, which was then complexed with $ZnCl_2$ to prepared catalyst **40** (Figure 5.11a). After reaction optimization, **GLC** was obtained in 89% yield using TBAB as a cocatalyst, at room temperature and 1 bar of CO_2.[99]

Exploiting another category of ligand, He *et al*. described the design and assessment of performances for a Zn salen complex with a multiple HBD scaffold and an internalized halide moiety. This bifunctional component compound was obtained through a two-step synthesis, leading to the formation of the ligand. The first reaction consisted of the condensation of 2,3,4-trihydroxybenzylaldhehyde with N,N'-diethylethylenediamine hydrobromide, followed by the addition of $Zn(OAc)_2 \cdot H_2O$, leading to the formation of complex **41** (Figure 5.11b). Considering the presence of (charged) quaternary amines, (HBD) phenolic groups, and Lewis acidic metal, as well as (nucleophilic) bromide anions within **41**, the authors hypothesized that the mechanism proceeds through simultaneous activation of the epoxide prior to ring opening induced by a bromide anion.[100]

An additional example of a porphyrin-Zn ligand was developed by Dela Cruz and Hung. An N-confused tetraphenylporphyrin (NCTPP) was functionalized with (5-bromopentyl) trimethylammonium bromide and next treated with $ZnCl_2$ to yield 44% of 42 (Figure 5.11c). With a very low loading of **42** (7.5×10^{-5} mol%) and 0.08 mol% TBAB, the authors achieved the preparation of **GLC** in 90% yield. An alternative version of **42** was produced with nickel, yet it displayed a slightly lower catalytic efficiency with 86% yield of cyclic carbonate derived from epichlorohydrin **ECH**.[101]

Lara-Sánchez reported the engineering of mononuclear Zn based complexes with various electronic and steric features. The catalyst was prepared by a three-step protocol starting from precursor **43**, successive transformation into the scorpionate ligand **44**, followed by complexation with $ZnMe_2$ to give **45** in 79% (Figure 5.11d).

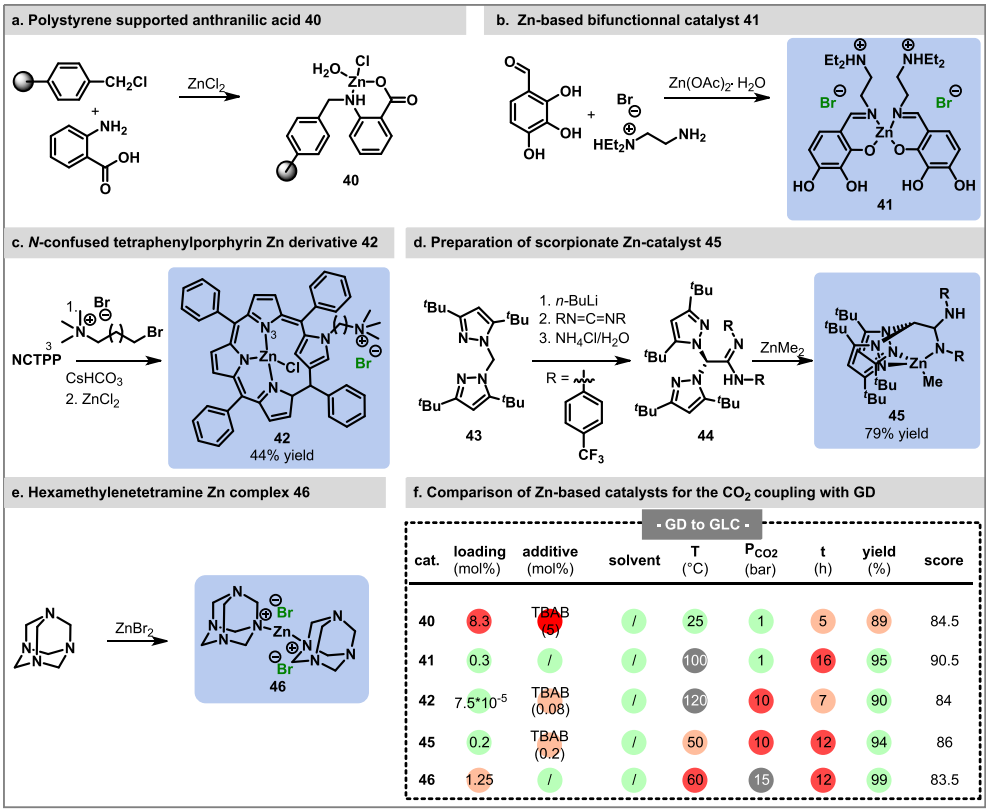

Figure 5.11 (a) Preparation of polystyrene-supported anthranilic acid zinc-based catalyst **40**.[99] (b) Synthesis of Zn-based bifunctional catalyst **41**.[100] (c) Preparation of N-confused tetraphenylporphyrin Zn derivative **42**.[101] (d) Preparation of scorpionate Zn-catalyst **45**.[102] (e) Synthesis of hexamethylenetetramine Zn complex **46**.[103] (f) Comparison of Zn-based catalysts **40**, **41**, **42**, **45** and **46** for the coupling of CO_2 and **GD** (See Section 6 and Supporting Information for details).

Preliminary evaluation of catalyst performance highlighted the beneficial role played by the double functionalization with 4-(trifluoromethyl)aniline moieties, which served as two electron-withdrawing groups (EWG) in **45**, and resulted in an enhanced Lewis acidity of the metal site. However, the synthesis of an analog containing four such EWGs on the same scaffold was shown to be detrimental as the positive effects of EWG were negatively counterbalanced by the increasing steric hindrance, and therefore decreased accessibility of the Zn catalytic center. The catalyst reusability was evaluated by performing multi-feed experiments with substrate removal between runs, which indicated constant performance (80-83% of **PC**) over 6 repetitions. Investigation of reaction kinetics with respect to TBAB and **45** both matched an apparent first-order reaction rate with respect to **SO** consumption.[102]

Yin and colleagues described a cheap and straightforward approach toward the formation of Zn metal complex with hexamethylenetetramine (Hatm) at room temperature for 6 h (Figure 5.11e). In order to unveil the synergetic effects of this bifunctional catalyst **46**, comparative experiments with the components individually considered were performed. The results gave

yields of only 35% and 1% of **PC** for the metal salt $ZnBr_2$ and Hatm, while using a mixture of the ligand and $ZnBr_2$ (i.e., without the pre-formation of complex **46**) achieved a yield of 53%. For these mixtures, the Hatm/$ZnBr_2$ molar ratio of the mixture was also found to influence the outcome, as increasing the relative abundance of the amine from 1 to 2 afforded 79% of **PC**. However, higher catalytic performances were obtained with the synthesized complex **46**, affording **PC** in 99% yield. This observation was explained by the improved coordination between the nitrogen atoms from the ligand and the Lewis acidic metal within the complex. The same procedure was transposed to **GD**, achieving a 99% yield of **GLC**. Interestingly, the additional experiments using **PO** showed that the addition of water up to 12 wt. % as an additive enabled to reduce the reaction time to 8 h, through the enhancement of **46** solubility. However, higher moisture content led to both substrate and product hydrolysis while hampering its recyclability in the medium.[103]

Another straightforward strategy relied on the *in-situ* generation of a catalyst based on a mixture of Zn powder, dimethyl formamide, and benzyl bromide. A typical run reached 99% of **GLC** under 80 °C and atmospheric pressure of CO_2 for 12 h with 5 wt% of catalyst.[104]

Copper-based catalysts. Exploring copper-based catalysts, Rath *et al.* prepared a 2D Cu(II) coordination polymer incorporating high content of nitrogen, aiming to include targeted sites for both CO_2 activation and alkoxide stabilization. Specifically, hexamethylenediamine with CuCN was used as a catalyst. The catalyst was obtained in 50% yield after 6 h at 25 °C. Investigation of compound performances over a broad range of epoxides demonstrated that the catalyst is limited to the conversion of small size substrates, with very poor conversions observed for epoxides such as 1,2-epoxyhexane or 1,2-epoxyoctane. This phenomenon was correlated to the high steric hindrance of substrate preventing their coordination to the metal sites located within the 2D network. Under atmospheric pressure of CO_2 at room temperature, a yield of 96% toward **GLC** was achieved with 1 mol% of catalyst and 1.5 mol% of TBAB over 18 h of reaction.[105]

Four years later, Li *et al.* produced a series of 2D MOF catalysts via a one-pot protocol with concomitant polycoordination and polycondensation using Cu_2O, a nitrogen-rich ligand and trialdehyde linkers. The best 2D MOF catalyst reported had a CO_2 absorption capacity of 16.7 $cm^3\ g^{-1}$, owing to its high copper density. The addition of CO_2 to **ECH** in the presence of 0.2 mol% of the MOF and 15 mol% TBAB was performed with a 94% after 6 h at 55 °C (2 bar of CO_2). Control experiments with only 15 mol% TBAB resulted in a yield of only 64%. On the other hand, the addition of CO_2 to **GD** under similar conditions yielded 63% of **GLC**. The catalyst could be recycled up to 4 times, maintaining an average production of **GLC** around 97%; before a significant decrease of performance (21%) was observed on the fifth cycle.[106]

In the field of three-dimensional networks, Sun *et al.* assembled a heterogeneous protonated copper-phosphonate MOF bearing both Lewis and Bronsted acids. The preparation of the MOF catalyst relied on the hydrothermal treatment (180 °C for 3 days) of a mixture of a tetrahedral cross linker, a nitrogen-containing ancillary ligand and $Cu(OAc)_2$, to achieve 40% yield of the corresponding Cu-derived MOF. In the presence of 0.001 mol% of MOF and 1.5

mol% of TBAB, **GLC** was obtained in 99% yield at 100 °C, after for 3 h under 10 bar of CO_2.[107]

A second example of a catalytic 3D MOF was reported by Wu *et al*., with a Cu-based MOF constructed from the coordination of 5'-5'-(butanede-1,4-diyl)-bis(oxy)-diisophtalic acid ligands (H_4L) with CuI (0.25 equiv.). The 3D catalyst was an assembly of metal cages containing 12 Cu (II) centers each obtained in 52% (starting from H_4L and CuI) after 48 h at 80 °C. A high uptake of CO_2 of 94.4 $cm^3\ g^{-1}$ at 273 K was determined, with a CO_2 adsorption heat (Q_{st}) of 8.36 kcal mol^{-1}. These results were indicative of a high interaction between the catalyst and CO_2. This was later confirmed through a computational study (DFT), which proved that CO_2 adsorption on unsaturated Cu sites was exothermic ($\Delta H°$ = -6.21 kcal mol^{-1}). Electron-rich oxygen atoms of the ligand also participated in the adsorption of CO_2 (ΔH = -2.39 kcal mol^{-1}). Further calculations identified the ring opening of **PO** as rate-determining step with a $\Delta G^{‡}$ = 14.8 kcal mol^{-1}. After optimization of the procedure, **GLC** was formed in 70% yield in the presence of 0.4 mol% of catalyst and 0.5 mol% of TBAB after 12 h at 60 °C (atmospheric pressure of CO_2). The recyclability of the catalyst was tested using **SO** and shown to be recoverable through filtration and used over 10 runs while maintaining a similar performance (88-97% yield).[108]

Cheng *et al.* introduced an alternative catalytic system featuring a heterometallic MOF. It consisted of the coordination between biphenyl-3,3′-disulfonyl-4,4′-dicarboxylic acid dipotassium salt as a ligand source with $Cu(ClO_4)_2{\cdot}6H_2O$ (Figure 5.12.a), yielding 69% of **47** after reaction at 110 °C for 24 h. Analysis of the crystal structure showed that Cu and K centers were specifically linked to both sulfonate and carboxylate groups and that the resulting 3D network had an anionic skeleton. A moderate CO_2 uptake of 49.5 $cm^3\ g^{-1}$ was measured at 273 K. Using 5 mol% TBAB and 5 wt% of MOF **47** (relative to **GD**), **GLC** was obtained in 98% yield (60 °C for 18 h). The recoverability of **47** was evaluated over 5 cycles showing a progressive decrease of performance from 95% to 82% yield of styrene carbonate (**SC**). The authors also provided a tentative mechanism proceeding through the initial activation of CO_2 with sulfonate groups from the ligand, prior to the formation of the carbonate intermediate.[109]

Nickel-based catalysts. Liu and coworkers described the preparation and use of a NiO_3-based MOF, assembled from ligand 5,5,5"-(methylsilanetriyl)triisophthalic acid and $Ni(NO_3)_2{\cdot}6H_2O$ in a mixture of dimethylacetamide and water. This solvothermal reaction proceeded at 150 °C for 72 h to eventually obtain a 40% yield of Ni-based MOF. The corresponding catalyst was then used for the fixation of CO_2 on small terminal epoxides under 10 bar of CO_2 at 100 °C. Complete conversion of **GD** was obtained over 3 h using 1.5 mol% of TBAB combined with 0.025 mol% of the MOF.[110]

Three years later, Bao *et al.* reported the self-assembly of a tetraphosphonic acid ligand derivative with $Ni(NO_3)_2{\cdot}6H_2O$. The reaction (72 h at 150 °C) led to the production of 46% of a Ni-based MOF. Under atmospheric pressure of CO_2 and at room temperature, almost quantitative conversion of **GD** was reached after 48 h (TOF = 41.7 h^{-1}) in the presence of 0.05 and 1.5 mol% of the MOF catalyst and TBAB, respectively. Given the occurrence of both Lewis (P-OH groups) and Bronsted (Ni centers) acids within the catalyst, the authors

suggested that the mechanism likely proceeds through dual activation of the substrate **GD** before the nucleophilic addition of bromide.[111]

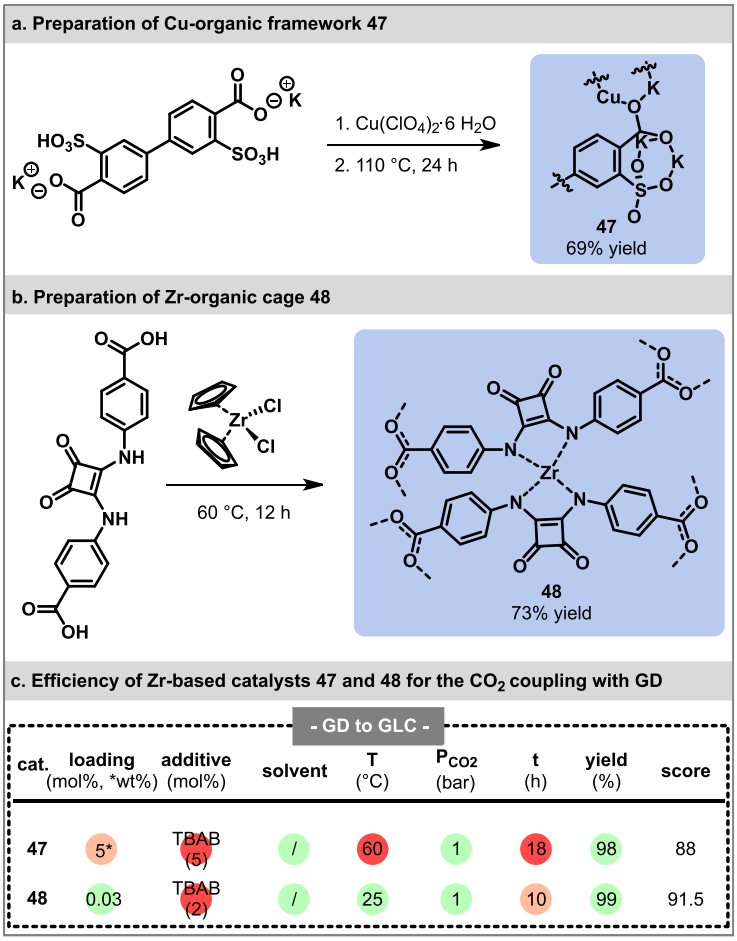

Figure 5.12 (a) Preparation and coordination mode of mono and heterometallic organic framework **47**.[109] (b) Preparation of zirconium metal organic cage **48**.[113] (c) Comparison of the catalytic efficiency of Cu and Zr-based catalysts **47** and **48** for the coupling of CO_2 with **GD** (See Section 6 and Supporting Information for details).

Zirconium-based catalysts. The incorporation of zirconium as an efficient Lewis acid metal was also considered by Islam and coworkers. They developed a mesoporous zirconium oxophosphate catalyst via evaporation-induced self-assembly using Pluronic P-123, zirconium butoxide and orthophosphoric acid as template, metal source and ligand of the catalyst respectively. The BET surface area was determined to be 487 $cm^2\ g^{-1}$ while the total acidity was estimated at 1.05 mmol g^{-1}. A typical run consisted of the conversion of 5 mmol of **GD** with CO_2 (1 bar) at 100 °C for 20 h. In the presence of 10 mol% TBAB and a 6.66 wt% of catalyst, an 80% yield of **GLC** was obtained. The Zr catalyst was recovered by centrifugation and recyclability of the catalyst was studied over 5 successive runs and it maintained similar production of styrene carbonate around 95%[112]

Alternatively, Wang *et al.* reported the preparation of a zirconium metal organic cage (MOC) assembled from Zr_3O clusters with squaramide-based organic linkers (Figure 5.12b). Catalyst **48** was produced in a 73% yield starting from the squaramide linker. Previous use of this type of ligand revealed issues of self-aggregation ascribed to extensive hydrogen bonding interactions within the MOF skeleton. The authors therefore designed MOC compounds constituted of squaramide-bearing capping terminal groups to prevent the infinite extension of the catalytic structure into a 3D network. CO_2 uptake was measured and determined to be 17.6 $cm^3\ g^{-1}$ at 273 K (Q_{st} = 4.30 kcal mol^{-1}), which indicates a fast gas desorption ability. **GD** was fully converted into its corresponding carbonate at room temperature after 10 h of reactions under atmospheric pressure of CO_2 (TON = 3510 $mol_{\mathbf{GD}}\ mol_{cat}^{-1}$). Recyclability and chemical stability were tested over 5 cycles for the reaction with **ECH** without significative change of performance, affording approximatively 97 to 99% of chloropropene carbonate.[113]

Alkaline earth metal-based complexes. This subsection deals with a brief yet representative collection of catalytic systems involving the use of alkaline earth metals (mostly Ca^{2+} and Mg^{2+}) as widely available and low-toxicity materials. Werner and colleagues described a system based on CaI_2 in combination with Et_3N **49** (Figure 5.13). Mechanistic insights were gained via NMR spectroscopy: the authors confirmed the coordination of Et_3N with the Ca^{2+} Lewis acid center through the detection of downfield shifts of methyl and methylene groups of Et_3N. Based on this observation, the authors suggested that the complexation of Ca^{+2} with Et_3N contributes to the suitable tuning of its Lewis acidity to favor the epoxide activation.[114]

Wu *et al.* proposed an analogous catalytic system that exploited methyldiethanolamine as HBD in combination with CaI_2 (**50**, Figure 5.13). Interestingly, the *in-situ* formed complex and its prepared version gave the same efficiency, yielding 99% of **SC**. Implementation of this procedure to **GD** led to **GLC** in 83% yield. A multi-gram preparation of **SC** using 12 g of **SO** was attempted with *in-situ* generated **50** with industrial-grade CO_2 featuring some moisture content. The process resulted in a 96% yield of **SC** after 24 h. The potential role of water as a reaction additive was then investigated through two additional experiments carried out with 10 or 100 mol% of H_2O (*vs* the catalyst). **SO** was converted into **SC** in 96% yield, regardless of the amount of water, therefore ruling out a potential involvement of water. After completion of the reaction, the complex could be precipitated using diethyl ether and recovered through filtration. Constant catalytic performance was observed over 5 consecutive runs.[115]

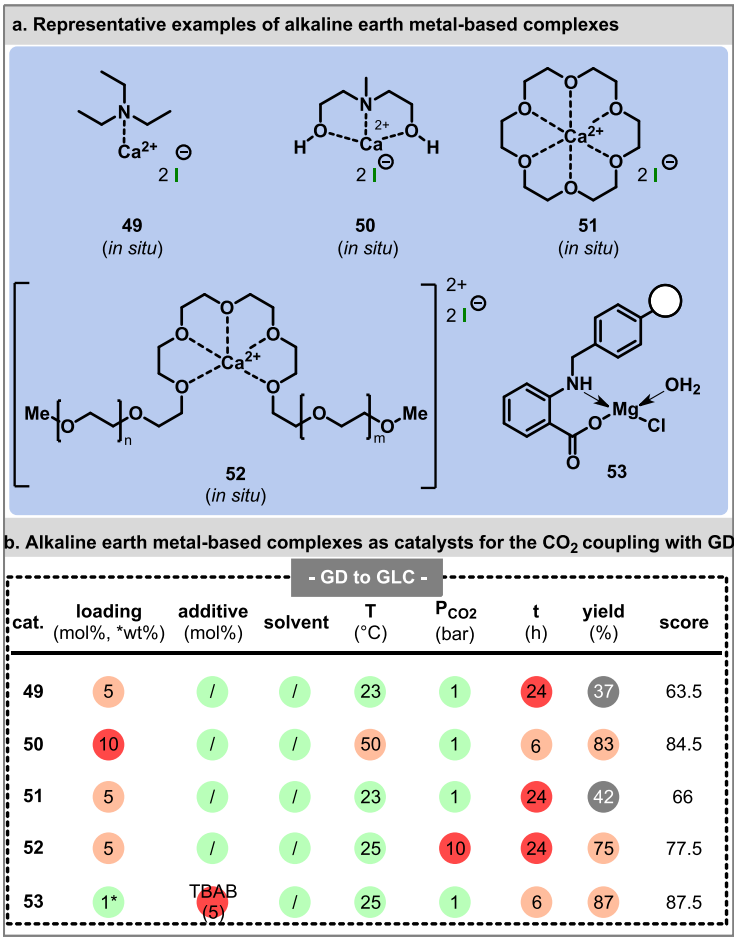

Figure 5.13 (a) Collection of alkaline earth metals used as Lewis acid in combination with various ligands, including Et_3N (**49**),[114] methyldiethanolamine (**50**),[115] Ca^{2+} 18-crown ether complex **51**,[116] dimethyl ether polyether ligands (**52**)[117] and polystyrene-supported magnesium-anthranilic acid complex (**53**).[118] (b) Comparison of alkaline earth metal-based complexes **49**, **50**, **51**, **52** and **53** as catalysts for the coupling of CO_2 with **GD** (See Section 6 and Supporting Information for details).

A third example of *in situ* generated catalyst was reported by Werner and colleagues with the formation of a Ca^{2+}-18-crownether complex (18C6). Various calcium salts including $Ca(OAc)_2$, $Ca(OTf)_2$, $CaCl_2$, $CaBr_2$, CaI_2 were assessed in the presence of 18C6 as a ligand. Salts involving non-nucleophilic anions showed no substrate conversion, as well as in the case of $CaCl_2$, which was likely associated with the poor leaving group ability of the chloride counter-anion. The catalytic system constituted of CaI_2/18C6 (**51**, Figure 5.13) provided good performance, exceeding 60% for the formation of the corresponding cyclic carbonate of *t*-butyl glycidyl ether. By contrast, the use of CaI_2 as the sole catalyst led to a mere 7% of butylene carbonate (**BC**). Based on these results, the authors identified two main roles played by 18C6: (a) the potential enhancement of the catalyst solubility and (b) the improved dissociation and availability of iodide anions. Next, the catalytic process was successfully

applied to various (non)functionalized glycidyl ethers derived from **GD**, with isolated yields >88% after 24 h of reaction. However, the conversion of **GD** only gave 42% of **GLC**, presumably due to the polymerization of the epoxide. The reaction mechanism likely involves oxirane activation, leading to the formation of the nucleophilic alkoxide intermediate stabilized by Ca^{2+} cations.[116]

The same group further investigated the potential of cheap and readily available polyethers as complexing agents and co-catalysts. Screening of a broad variety of linear and branched ligands was performed in the presence of CaI_2. Different structure-reactivity relations for the ligands could be drawn from this extensive screening. Firstly, hydroxyl-terminated polyether groups improved the catalytic performance of CaI_2 more readily than the same material bearing SH-end groups. Butylene oxide (**BO**) was converted to **BC** in 64% with the former *versus* 32% with the latter under the same process conditions. Secondly, comparative trials were conducted using mono- or dimethyl ether ligands (**52**) as well as a ligand substituted with two OH end groups. Results gave **BC** in 90%, 60% and 20%, respectively (Figure 5.13) demonstrating that the absence of the HBD group within the ligand enhanced the reaction performance. The authors ascribed these results to the reduction of iodide ions nucleophilicity caused by the occurrence of H-bonding groups. **GD** was converted to **GLC** in 75% with 5 mol% of the most efficient catalytic system (1:1 ligand/CaI_2 **52**) (Figure 5.13). The activity of the complex was evaluated over 11 successive additions of the fresh substrate. After the seventh run, the catalytic activity started to decrease progressively from 99% to approximately 82% with **BO** as a model substrate.[117]

Keiski et *al*. described the use of magnesium as a Lewis acid center for the activation of epoxides. At 130 °C under 30 bar of CO_2, **GLC** was isolated in 94% yield after 4 h reaction time in the presence of around 8.5 mol% of nanocrystalline LiMgO catalyst.[119]

Another example was provided by Islam *et al.* with a magnesium-anthranilic acid complex supported by polystyrene (**53**). Ligand preparation involved grafting anthranilic acid in DMF on a Merrifield resin over 30 h under reflux, prior to the incorporation of magnesium chloride hydrate in the heterogeneous material for 9 h at 70 °C (Figure 5.13). A typical carbonation of **GD** was performed at room temperature and 1 bar of CO_2, reaching 87% yield of **GLC**.[118]

5.2.5 ORGANOCATALYSTS

5.2.5.1 ORGANOCATALYSTS AS LEGITIMATE ALTERNATIVES TO METAL-BASED CATALYSTS

Despite the recent advances toward efficient metal-based catalysts, many remain cumbersome to prepare. Additionally, their removal from the reaction mixture and potential recycling is often time- and resource-consuming.[120] Organocatalysts stand as promising alternatives as they are usually widely available at moderate costs and often come with lower toxicity and sensitivity to air and moisture.[121,122] Their carbon scaffold also offers countless opportunities for additional functionalization, structural modification, or even immobilization on heterogeneous supports.[123] Despite these appealing assets, the development of organocatalysts remains challenging due to their typically lower reactivity compared to metal catalysts. Current organocatalyzed procedures still require moderate to harsh conditions (> 75 °C, > 10 bar CO_2, > 5 mol% of catalyst) to achieve comparable performances. Consequently, organocatalyzed processes are usually energy-demanding, which can have a negative impact when the greater picture is considered.[122]

This section is divided into subsections dedicated to nitrogen-, phosphorous- and boron-containing organocatalysts. Each subsection aims to present an overview of the broad diversity of catalytic designs as well as the advances made over the past 8 years. Apart from the transpositions of homogeneous to heterogenized versions of some catalysts, their structure-reactivity features are also reported alongside with their peculiar impact into the catalytic mechanism. Indeed, depending on the structural skeleton of the catalytic system, the carbonation reaction can proceed through the activation of either the oxygen from the epoxide or a hydroxyl group at the β position.

5.2.5.2 COMMON ORGANOCATALYSTS

Most recent advances in organophosphorus catalysts for the carbonation of **GD** were reported by Werner *et al*. In 2016, a library of homogeneous catalysts featuring a β-hydroxyphosphonium scaffold was investigated under neat and mild conditions. A library of phosphonium salts was obtained according to a straightforward protocol, *i.e.* a S_N2 reaction of a phosphine nucleophile with a haloalcohol. The authors prepared a variety of structures by altering either the electrophile (carbon chain length and nature of the leaving group) or the phosphine nucleophile. **BO** was used as a model substrate to investigate the performance of tetra-*n*-butylphosphonium scaffolds. As a point of comparison, phosphonium salts not bearing hydroxyl groups were tested and shown to afford only 36%, 25% and 19% yield (at 90 °C, 10 h under 10 bar of CO_2) for the Cl, Br and I salts respectively. Catalysts featuring a β-hydroxyl group as HBD superior performances, while still exhibiting a significant impact of the counter-anion: 57%, 86% and 92% yield were achieved with the chloride, bromide and iodide salts, respectively. Next, the authors investigated variations in the alkyl backbone of the phosphonium salt. Catalysts substituted with hindered alkyl chains led to the highest yields in cyclic carbonates. *n*-Octyl and *n*-cyclohexyl phosphonium **55** and **56** outperformed *n*-butyl derivative **54** (Figure 5.14a). The authors argued that the bulkiness of the alkyl chains contributed to the formation of weaker ion pairs with the halide counter-anion, hence enhancing catalytic efficiency. The process was next transposed to terminal epoxides with

76-98% yield toward the corresponding carbonates. However, when the conditions were applied to the coupling of **GD** with CO_2, **GLC** was obtained in only 56% yield due to polymerization side reactions.

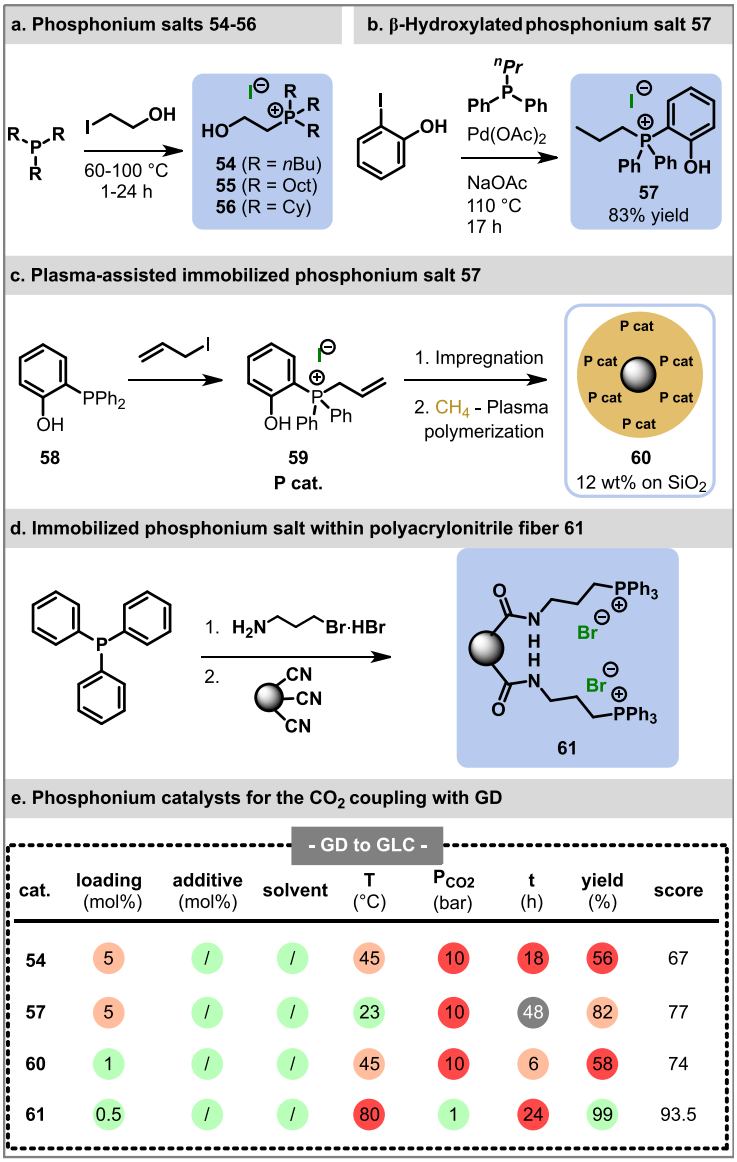

Figure 5.14 (a) Scaffold of most efficient phosphonium salt catalysts **54-56**.[124] (b) Preparation of an alternative version of β-hydroxylated phosphonium catalyst **57**.[125] (c) Preparation of a plasma-assisted immobilized phosphonium salt **60**.[123] (d) Immobilized phosphonium salt within polyacrylonitrile fiber **61**.[126] (e) Comparison of various phosphonium catalysts for the coupling of CO_2 with **GD** (See Section 6 and Supporting Information for details).

The mechanism likely involves a dual activation of the epoxide through both hydrogen bonding via the hydroxyl group on the catalyst side-chain and electrostatic interaction with the phosphonium cation, prior to the nucleophilic addition/ring opening of the less hindered carbon with the external halide (Figure 5.15).[124]

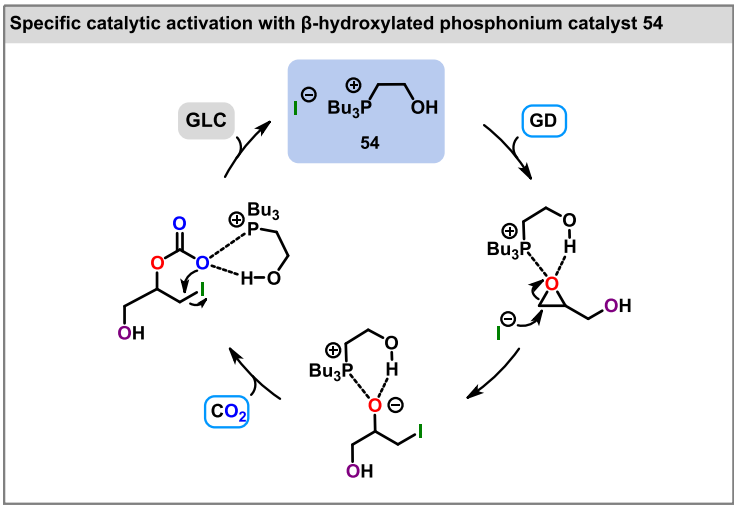

Figure 5.15 Hypothesized mechanism for the coupling of CO_2 with **GD** in the presence of a β-hydroxylated catalyst **54**.[124]

A few years later, the same group reported another generation of hydroxylated phosphonium catalysts. Their catalytic performances were assessed and (2-hydroxyphenyl)-diphenyl(propyl)phosphonium iodide **57** emerged as the most efficient candidate (Figure 5.14b). A kinetic study was carried out to gather insights into the catalytic performance. To this end, catalyst **57** was compared to β-hydroxylated phosphonium iodide **54** as a reference, for the carbonation of **BO**. Despite a promising selectivity toward the desired cyclic carbonate **BC**, the yield obtained with **57** remained low, arguably due to the poor solubility of the phenolic catalyst. The limited solubility translated into an extended induction phase. Consequently, a kinetic experiment was run at 45 °C to speed up the induction phase, with the data indicating a first order reaction. Product inhibition was observed with **54**, hence a Michaelis-Menten model was utilized to account for reversible product inhibition and fit the data. Observed rate constants of 0.0605 h^{-1} and 0.197 h^{-1} were obtained for the aliphatic (**54**) and phenolic (**57**) catalysts, respectively. Moreover, an Arrhenius plot (35 – 65 °C) led to an experimental activation energy (E_a) of 9.3 kcal mol^{-1} for **57**. An additional experiment at 90 °C led to a decreased reaction rate as a consequence of a lower solubility of CO_2 at higher temperatures. When using **GD** as a substrate, the phenolic catalyst (**57**), afforded **GLC** in up to 82% yield. DFT computations further documented the role of the catalyst. The computations confirmed that the activation of the substrate's epoxide proceeds through hydrogen bonding with the phenol. Computed $\Delta G^{\ddagger}$ for the ring opening step emphasized significant differences between the iodide ($\Delta G^{\ddagger} = 17.2$ kcal mol^{-1}) and the bromide ($\Delta G^{\ddagger} =$ 23.2 kcal mol^{-1}) salt versions of **57** ([*n*-PrP(Ph)$_2$PhOH]I and [*n*-PrP(Ph)$_2$PhOH]Br). These

computational results gave support to the experimental superior catalytic performances of the iodide. For the ring closure step, $\Delta G^{\ddagger}$ values of 20.6 and 17.0 kcal mol^{-1} were obtained for the bromide and the iodide anions, respectively. From these results, the authors concluded that the ring opening is the rate-determining step (RDS) for the iodide salt, whereas the ring opening, and closure are kinetically determinant for the bromide catalyst.[125]

The work of D'Elia provides an explanation for the improved yields obtained with phenolic derivative **57** compared to the yield obtained from **54**. The authors studied the pK_a-dependent activity of HBD groups to determine the most efficient range of pk_a to promote the coupling of CO_2 with an epoxide. The optimal region was found between a pK_a of 9 and 11, corresponding to the one exhibited by phenolic moieties. These results provide an explanation for the widespread use of phenolic moieties within organocatalysts for this reaction.[127]

Werner also described the use of plasma techniques for accessing heterogenized organophosphorus catalysts on SiO_2, TiO_2 and FeO. The preparation of the supported catalyst was straightforward, consisting of the impregnation of various inorganic supports with the organocatalyst followed by its immobilization through plasma polymerization. Early design of the catalyst started with the allylation of 2-(diphenylphosphanyl)phenol (**58**) using allyl bromide or iodide to yield the halogenated salt **59** (Figure 5.14c). Next, various inorganic supports were impregnated with the salt and then immobilized within a low-pressure plasma. The catalytic activities for TiO_2, FeO and SiO_2 (**60**) -supported phosphonium salts were assessed with **BO** as a model substrate and gave 93, 72 and 97% yield of **BC**, respectively, after 6 h of reaction. Next, the authors assessed catalyst recyclability. They clearly emphasized the critical role of the plasma treatment to avoid the leaching of the phosphonium salt. Skipping the plasma treatment with only the impregnation of the phosphonium catalyst onto the inorganic support led to a significant drop in catalytic performance (0-31% yield) toward the corresponding cyclic carbonate. Extended plasma treatments from 6.5 to 25 min gave SiO_2 heterogenized catalysts that could be reused for 2 consecutive runs with stable and reproducible outputs (99% yield of **BC**). The TiO_2- and FeO-supported catalysts gave less favorable perspectives for recycling, with a significant drop in catalytic performances (55% and 3%, respectively) for a second run. Longer plasma treatment affected the integrity of the organocatalyst, therefore leading to a loss of catalytic efficiency. The authors demonstrated recyclability of **60** over 5 consecutive runs, however with only 20% yield of **BC** obtained after the fifth run.[123]

Zhang et *al*. reported another example of an immobilized phosphonium salt **61** prepared in 76% yield through the reaction of triphenylphosphine with 3-bromopropylamine, followed by immobilization on polyacrylonitrile fibers (Figure 5.14d). The degree of substitution was estimated at 32% by comparing the weight gain to the initial weight of the support, whereas the degree of functionality was determined at 0.61 $mmol_{Pcat}$ g^{-1}. A typical protocol for CO_2 coupling had a reaction time of 24 h at 80 °C under atmospheric pressure of CO_2 and led to complete conversion of **GD** using 0.5 mol% of catalyst **61**.[126]

Nitrogen-containing organocatalysts. Nitrogen-containing organocatalysts are the most studied organocatalysts for the carbonation of **GD**.

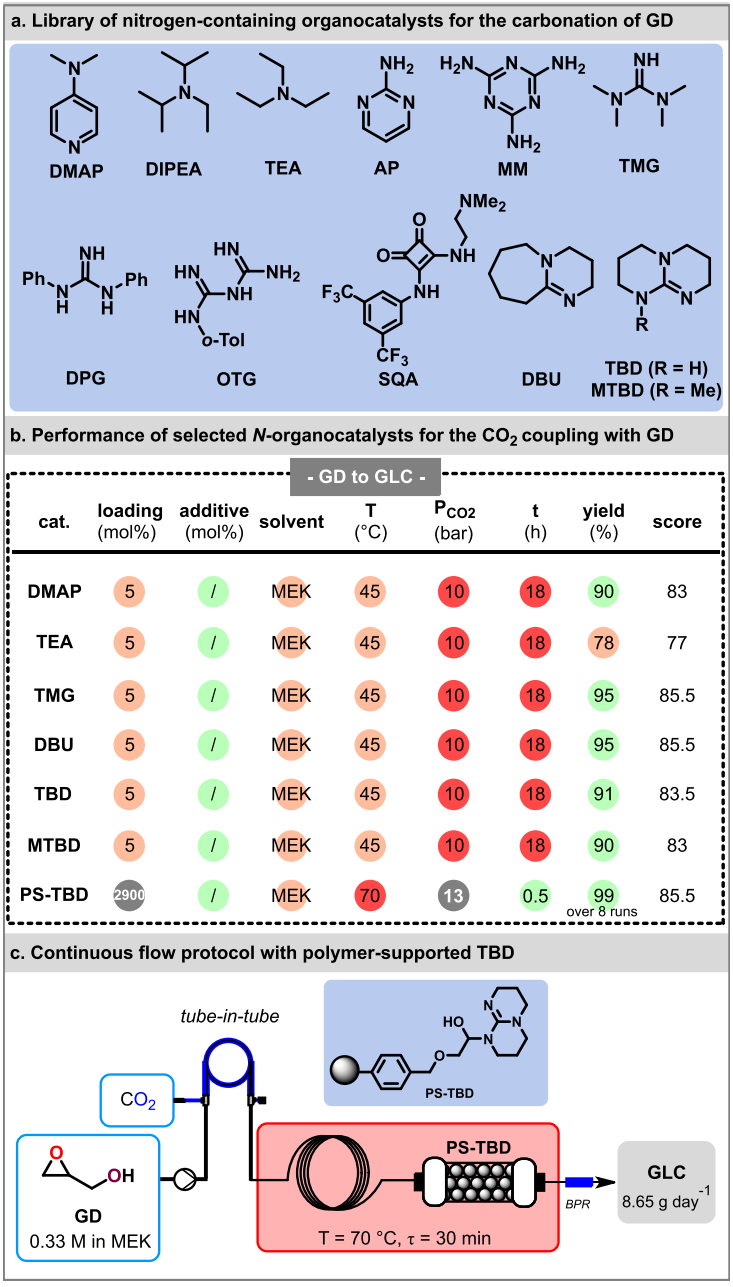

Figure 5.16 (a) Screening of nitrogen-containing organocatalysts for the carbonation of **GD** and resulting yields of **GLC**.[128] (b) Comparison of the catalytic performances of selected N-organocatalysts for the CO_2 coupling with **GD** (See Section 6 and Supporting Information for details). (c) Continuous flow setup featuring a tube-in-tube configuration and a packed-bed column reactor with the heterogenized organocatalyst (PS-TBD).[129]

Kleij and coworkers assessed a series of commercially available nitrogen-containing compounds as homogeneous catalysts for the preparation of **GLC** under mild conditions (Figure 5.16a,b). Among the library of *N*-organocatalysts studied, 1,5,7-triazabicyclo[4.4.0]dec-5-ene (**TBD**), 7-methyl-1,5,7-triazabicyclo[4,40]dec-5-ene (**MTBD**) and 1,8-diazabicyclo(5.4.0)undec-7-ene (**DBU**) provided **GLC** in high yields of 90, 91 and 95%, respectively.[128] Kleij and Pericàs then reported a flow process relying on a packed-bed reactor filled with a heterogenous organocatalyst. The authors heterogenized various nitrogen-containing organocatalysts through covalent grafting on polymer resins. Preliminary screening of various bases and supports pointed towards Merrifield resin beads functionalized with **TBD** (**PS-TBD**) as the most promising heterogeneous catalyst for the preparation of **GLC**. The **PS-TBD** was obtained in 88% yield, used as a packing material in a column and integrated in a microfluidic setup (Figure 5.16c). **GD** and CO_2 were fed in the microfluidic system through a tube-in-tube (Teflon AF-2400) configuration before reacting in the packed column. The conditions led to full conversion toward **GLC** with a productivity calculated at 3.038 mmol h^{-1}. The recycling of the supported catalyst was demonstrated over 8 consecutive runs, though a progressive loss of performance was noticed. The authors argued that mechanical degradations caused by the high operative pressure were responsible for the loss of catalytic efficiency. As a corrective countermeasure, the pressure was decreased to 13.1 bar, resulting in a steady production of **GLC** over 48 h with a daily production of 8.65 g. This work pioneered the preparation of **GLC** under flow conditions with a heterogeneous organocatalyst, although the use of a tube-in-tube setup prevents any further transposition toward larger scales.[129]

Monbaliu et *al.* developed a continuous flow process toward the large-scale production of **GLC** relying on readily available nitrogen-containing bases. An upstream process combining a chlorination-dehydrochlorination sequence on bio-based glycerol was first developed to produce **GD**, further intensifying a previous report from the same team.[130] Concatenation of this sequence provided **GD** in a 75% yield, alongside with 17% of **ECH** as a side product within 110 s of total residence time. The carbonation of **GD** was then investigated under microfluidic conditions, yielding **GLC** in 86% yield with a stochiometric amount of CO_2 and 5 mol% **TBD** as a model catalyst. Next, a selection of homogeneous organic bases was screened, including **TMG**, **DBU**, Barton's base (**BB**), P_1-*t*-Oct and Verkade's base (**VB**). The best results were obtained with **BB**, obtaining 91% with 5 mol%, while a lower catalytic loading of 1 mol% still provided an 82% yield (Figure 5.17a,b). The mechanism appeared to be strongly substrate-dependent as no conversion was observed for **ECH** and *t*-butyl glycidyl ether. DFT calculations were used to rationalize the requirement for both a β-hydroxyl group on the substrate and an organocatalyst with a marked Brønsted basicity. The DFT results uncovered two main consecutive steps: (a) deprotonation of the β-hydroxyl group with the organocatalyst followed by CO_2 capture to yield linear carbonate **62** and (b) a subsequent intramolecular cyclization. While step (a) benefited from a general base catalysis, step (b) was subjected to general acid catalysis. The conjugated acid of the organocatalyst, which is generated during step (a), acts as the active species for step (b), prior to regenerating the free base organocatalyst (Figure 5.17c).

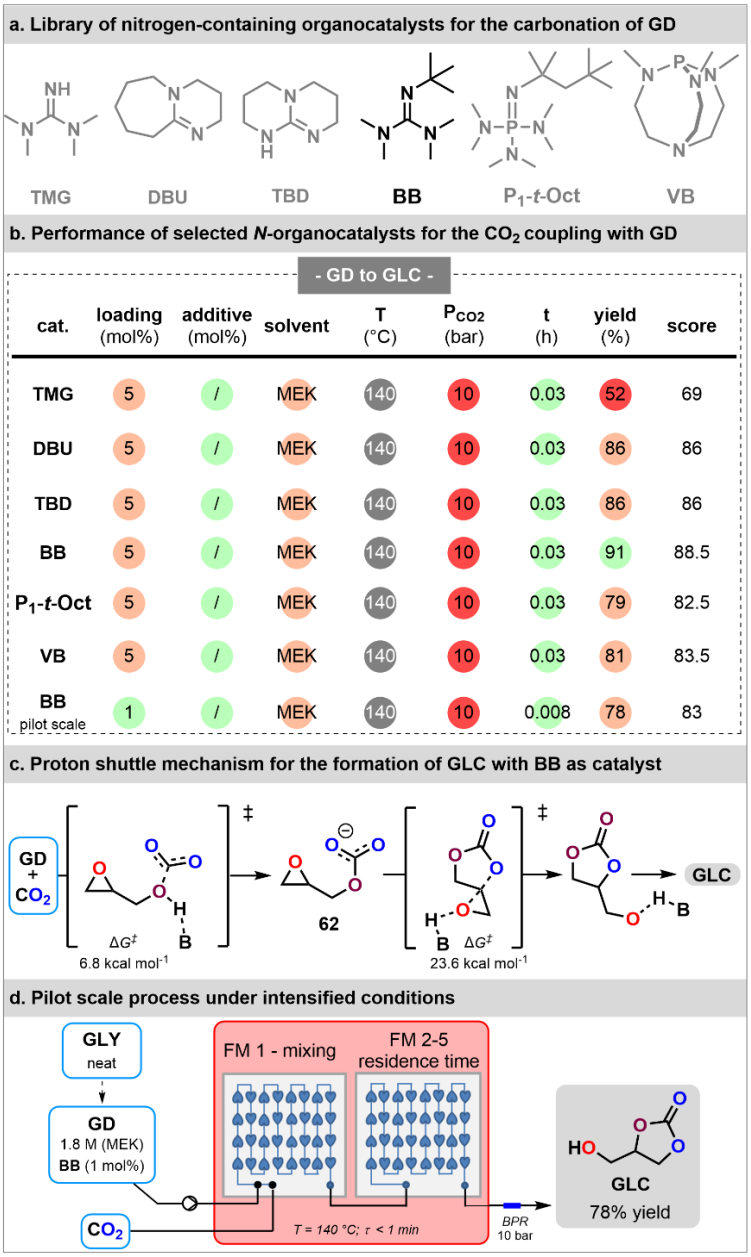

Figure 5.17 (a) Selection of a set of N-containing organic bases. (b) Comparison of the catalytic performances of selected N-organocatalysts for the CO_2 coupling with **GD** under microfluidic conditions and intensified pilot scale mesofluidic conditions (last entry) (See Section 6 and Supporting Information for details). (c) Illustration of the proton shuttle mechanism for the formation of **GLC** (activation barriers were calculated by DFT). (d). Pilot scale process under intensified conditions with a daily productivity of 3.6 kg of **GLC**.[131]

The authors concluded that increasingly stronger bases, despite being more efficient for step (a), result in weaker conjugate acids, thereby diminishing their activity as a Brønsted acid for epoxide activation in step (b). In addition, the overall carbonation process is likely limited by CO_2 solubility in the reaction medium. This justified their selection of MEK as the reaction medium and the utilization of a flow system with enhanced mass transfer. As a final demonstrator of the process robustness, the reaction was implemented under mesofluidic flow conditions with a commercial pilot reactor (Corning® Advanced-Flow Reactor™ G1 with 56 mL of total internal volume). The authors reported a daily productivity of 3.6 kg day^{-1} of **GLC**, with the reaction taking place with a residence time of 28 s (Figure 5.17c.) and an attractive E-factor of 4.7.[131]

Antiñolo *et al.* reported the synthesis of aromatic mono- and bis-guanidines as potential catalysts in combination with external nucleophiles. The preparation of bisguanidines simply relied on the catalytic addition of amines or diamines to carbodiimides (Figure 5.18a). Under optimized conditions, bis-guanidines showed superior catalytic performance over their monoguanidine analogs. The best results were obtained with catalyst **63**, affording **GLC** in 91% yield in 24 h in the presence of 2 mol% of TBAI. The authors argued that a higher content of N-H bonds groups in the bis-guanidines was likely critical to enhance substrate activation through multiple HBD. A supporting NMR study demonstrated that the ring-opening of the substrate is triggered at the most hindered position to yield the iodoalkoxide intermediate.[121]

The same year, Dove *et al.* reported the preparation of alkylated and protonated bicyclic amidines as potential catalysts for the coupling of CO_2 and epoxides. The protocol consisted of the neutralization of DBU with an acid or with an equimolar ammonium halide (catalyst yield between 83% and 97%). The catalysts were tested for the reaction between CO_2 and **SO**, with the best catalytic performance reported using the **DBU·HX** series with X = I (96% conv.) > Br (77% conv.) > Cl (60% conv.). The reaction did not proceed with **DBU** free base. Based on this preliminary set of observations, alkylated DBU derivatives (**RDBU·HX**) were prepared, however they did not reach the same catalytic efficiency as **DBU·HX**. The scope of substrates was then extended to several terminal epoxides including **GD**, which gave **GLC** in 65% yield (Figure 5.18b,c) using **DBU·HI**. Despite its overall effectiveness, the poor solubility of **DBU·HI** in low-polarity substrates drastically limited the scope. The recyclability of **DBU·HI** was, however, validated with 5 consecutive runs. The catalyst recovery step was particularly cumbersome and relied on vacuum distillation of the reaction medium. The mechanism was rationalized through computations (DFT). The 2 different synthetic paths envisioned by the authors are shown in Figure 5.18b, following either a concerted activation of the epoxide and CO_2 fixation (path 1) or a stepwise activation of the substrate prior to the capture of CO_2 (path 2). Computed activation barriers ($\Delta G^{\ddagger}$) were determined to be 20.9 and 30.9 kcal mol^{-1} for paths 1 and 2, respectively, clearly indicating that the mechanism associated with path 1 prevailed. Further computations for the epoxide ring opening (intermediate **64**, path 1) as a function of the nucleophilic counter-anion confirmed the experimental trends with lower activations barriers associated with more nucleophilic anions, with $\Delta G^{\ddagger}$ = 26.8, 26.2 and 20.9 kcal mol^{-1} for X = Cl^-, Br^- and I^-, respectively. The $\Delta G^{\ddagger}$ for the final ring closure toward the cyclic carbonate highlighted the

first step as rate-determining. Increasing leaving group ability of the anion led to decreasing $\Delta G^{\ddagger}$, *i.e.* $\Delta G^{\ddagger}$ = 19.9, 16.7 and 15.6 kcal mol^{-1} for X = Cl, Br and I, respectively.[132]

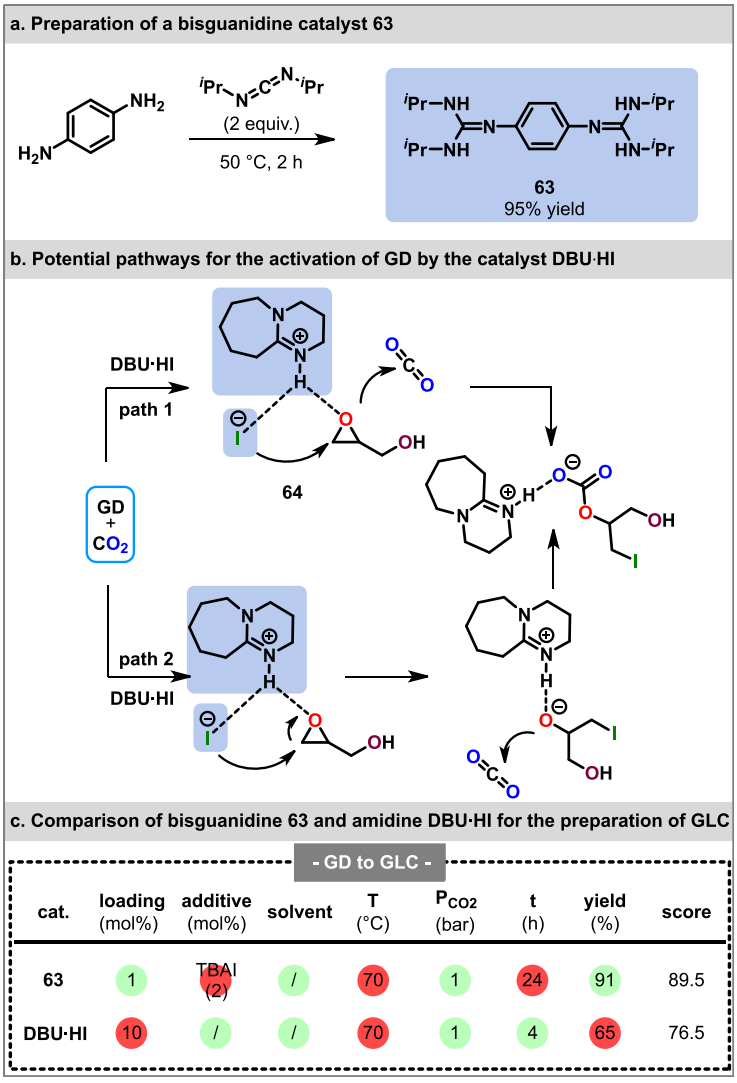

cat.	loading (mol%)	additive (mol%)	solvent	T (°C)	P_{CO2} (bar)	t (h)	yield (%)	score
63	1	TBAI (2)	/	70	1	24	91	89.5
DBU·HI	10	/	/	70	1	4	65	76.5

Figure 5.18 (a) Preparation of a bisguanidine catalyst **63** bearing multiple HBD sites. (b) Potential pathways for the activation of the epoxide by the catalyst DBU·HI and subsequent ring opening of the substrate.[132] (c) Comparison of bisguanidine **63** and DBU·HI as catalysts for the coupling of CO_2 and **GD** (See Section 6 and Supporting Information for details).

Apart from simple amine, amidine and guanidine scaffolds, Kim *et al.* engineered a catalytic system based on computations (DFT) to predict structure (re)activity relationships, eventually leading to novel scorpionate organocatalysts (Figure 5.19a). The design focused on two axes that were identified as critical for the design of an effective catalyst: (a) insertion

of an internal nucleophile on the catalyst backbone and (b) modulation of the proximity between two hydroxyl groups.

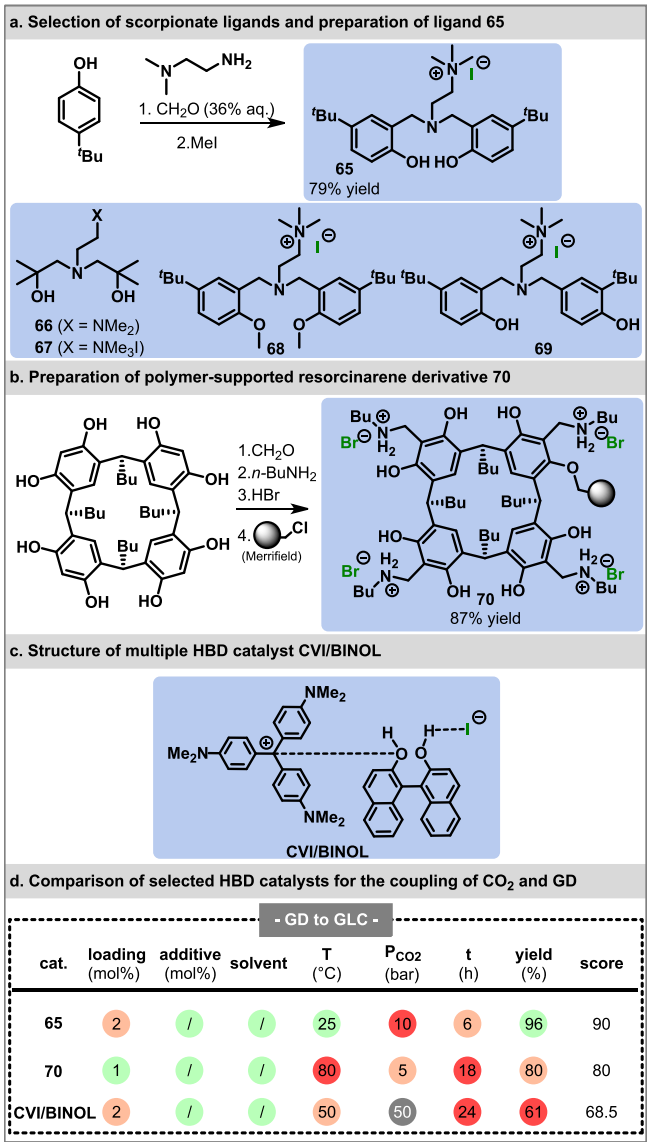

Figure 5.19 Selection of catalytic systems featuring multiple HBD sites. (a) Relevant examples of scorpionate ligands and preparation of ligand **65**.[122] (b) Preparation of polymer-supported resorcinarene derivative **70**.[133] (c) Structure of cationic triarylmethane dye CVI combined to BINOL complexing agent, used as a multiple HBD catalyst.[134] (d) Comparison of scorpionate ligand **65**, polymer-supported resorcinarene derivative **70** and BINOL/CVI as HBD catalysts for the coupling of CO_2 and **GD** (See Section 6 and Supporting Information for details).

The rationale for (a) was to cancel the entropy cost linked to ring opening by an external nucleophile, which could potentially be a significant asset compared to binary systems.

Indeed, the use of catalyst **66** with TBAI as a cocatalyst led to 10% yield of **PC** from **PO**, whereas the use of catalyst **67** under the same conditions afforded **PC** in 29% yield (3-fold increase). To address point (b) of the catalyst design, the initial alkyl fragments in catalyst **67** were replaced with rigid aryl rings to promote the synergistic activation of the substrate with the two hydroxyl groups. The authors tested several aryl moieties and arrived at catalyst **65** as the most efficient catalyst (Figure 5.19a). Conformational analysis indicated that the modification of the alkyl backbone to incorporate aryl groups indeed came with a shortened O-O distance of 2.93 Å (against 6.5 Å for the alkyl groups).[122]

^{1}H-NMR data suggested the occurrence of weak intramolecular hydrogen bonds involving the hydroxyl groups and the ammonium in catalyst **65**. These interactions were highly desirable as they align the hydroxyl functions and create a binding cavity for the coordination of the substrate. These synergistic effects were experimentally confirmed by alkylating a phenolic hydroxyl, which drastically decreased the yield of **PC** from 99% in the presence of **65**, to 11% for **68** (Figure 5.19a). Deeper insights into the catalytic mechanism were then gained from further computational work. Notably, the lowest energy structure of the linear carbonate intermediate clearly showed its double stabilization through the hydroxyl groups (calculated OH-O distance: of 1.73 and 1.92 Å). The elimination of iodide was found to be facilitated by the nitrogen cation with an I-N distance of 4.53 Å. Ring closure toward the cyclic carbonate product was identified as the rate-determining step with $\Delta G^{\ddagger}$ = 24.1 kcal mol^{-1}. The beneficial effect of the two hydroxyl groups in **65** was examined by calculating the transition state for the reaction with one OH group rotated away (conformer **69**), which gave a higher $\Delta G^{\ddagger}$ of 29 kcal mol^{-1}. Finally, analysis of the final cyclization step, consisting in the breaking of hydrogen bond interactions between the linear hemiester and the catalyst, was performed. The analysis supported the installation of electron donating groups (EDG) in the aryl rings to weaken hydrogen bond interactions in the final transition state. For instance, the predicted $\Delta G^{\ddagger}$ for the final cyclization step decreased to 21 kcal mol^{-1} for the catalyst bearing NMe_2 substituents. Experimentally, both *p-tert*-butyl derivative **65** and a *p*-dimethylamino analog performed excellently.[122]

Kleij and coworkers developed amine-functionalized resorcinarene compounds supported by polystyrene as an efficient and cheap catalytic system for the cycloaddition of CO_2 onto epoxides. Bifunctional candidates were produced from the functionalization of resorcin[4]arene precursors with a variety of aliphatic primary amines and subsequent acidification to generate ammonium moieties (Figure 5.19b). The heterogenized version was prepared via etherification with a Merrifield resin (degree of functionalization = 1.09 mmol g^{-1}). Heterogenous catalyst **70** showed comparative epoxide conversions to its homogeneous version. The catalyst could be recycled over 4 cycles while maintaining a similar efficiency. Further reuse of **70** led to a progressive decrease of yield from 96 to 85% at the twelfth reutilization for the carbonation of 1,2-epoxyhexane. This reduction of performance was ascribed to a retro-Menshutkin reaction, resulting in the loss of the nucleophile moieties of the catalyst.[134]

Wu *et al*. developed an innovative design of a bifunctional cross-linked epoxy organocatalyst with a straightforward synthesis. The one-pot preparation involved the polymerization of polyamines with cross-linker epoxides as well as quaternary ammonium salt-derived

epoxides. The morphology of the pre-catalyst was characterized by an irregular surface of agglomerated particles. This feature favored the carbonation of epoxides due to the enhancement of interaction between CO_2 and substrate. A uniform distribution of C, N and Br facilitated both the activation and ring-opening of the substrate due to the physical proximity between catalytic sites. Tests performed using **PO** showed that incorporation of an aromatic structure into the heterogenous skeleton improved the catalytic performance, increasing the yield of **PC** from 33% to 43% (3 h at 100 °C, under 20 bar CO_2 and with 1 mol% of catalyst). The authors argued that such an improvement occurred as a consequence of an increased porosity promoting the interaction of the catalytic sites. Sequential runs were performed to assess the catalyst's recyclability. Comparable yields toward **SC** were obtained after 7 runs on a 100 mmol scale of **SO** over 48 h. Shortening the reaction time to 24 h with **GD** as a substrate led to **GLC** in 74% with a 1 mol% catalytic loading at 100 °C.[135]

Belokon *et al.* reported the use of commercial triarylmethane dyes as stable carbocation catalysts, associated with a halide counter-anion (Figure 5.19c). The authors reasoned that the carbocation species could activate the epoxide through a Lewis acid-base complex. This assumption was confirmed by ^{13}C NMR, which presented a downfield shift for the cationic sp^2 C signal with increasing concentration of the epoxide substrate. The most efficient cation (crystal violet, **CVI**) achieved 32% yield toward **SC** from **SO** as a model substrate. The lower activity of a highly Lewis acidic candidates suggested that low dissociation of the ion pair was reducing the performances of the catalyst. An anion complexing agent was then introduced to enhance ion pair separation. Screening of different complexing agents identified **BINOL** as the best activator. Using 1 mol% of a 1:1 **CVI/BINOL** mixture, **SC** was obtained in 82% yield after 24 h at 50 °C (50 bar of CO_2). Implementation of this procedure to **GD** yielded **GLC** in 61% (see Figure 5.19d for a comparison of selected multiple HBD catalysts).

The generation of a Lewis acid-base complex resulted from the interaction of **CVI** with the phenolic oxygen atoms of **BINOL**, which in turn increased the acidity of the phenol group. The mechanism likely involves the activation of the epoxide through strengthened acidity of **BINOL**. The authors also postulated that the acidity of **BINOL** could favor CO_2 coordination, therefore, facilitating both the carbonation and ring closure. The catalytic system was tested over 4 successive additions of fresh **PO** to assess its recyclability. The results highlighted a progressive decrease of performances, with a reduction from 100% to 74% conversion to **PC**.[133]

Another example of a catalyst incorporating multiple H-bonding donor groups was reported by Quintard et *al*. The catalytic system was composed of 5 mol% of TBAI and a perfluorinated triol, which under optimized conditions, afforded **GLC** in 89% yield after 24 h at 80 °C (under 1 bar of CO_2).[136]

Del Amo *et al.* reported the catalytic performance of a system based on a cholic acid-base bis-primary amine catalyst **71**. The preparation of this steroid was quite time-intensive (7 days), eventually yielding aminated cholic acid-based candidate **71** in 71% (Figure 5.20a). Bisamine **71** alone did not show any conversion of **SO** to **SC**, however the combination with TBAI halide salt led to near reaction completion. A much lower conversion of 47% was

obtained for **SO** with solely TBAI. The authors found that, in the presence of CO_2, the primary amines of **71** reacted to form a bis-carbamic intermediate **72**, which was the catalytically active species. Isolation of bis-carbamic acid **72** allowed to demonstrate it was capable of transferring the CO_2 moieties to **SO**, to form **SC** in 30% yield under a regular air atmosphere (25 mol% of **72**, 1 mol% TBAI). Two potential mechanisms were explored computationally (DFT, B3LYP-6-31+G**) for the reaction between **71** and **PO** as model substrate: (1) the conventional path (path 1) with a classical ring opening mediated by an external nucleophile, and (2) an alternative mechanism (path 2) involving a nucleophilic addition of the carbamic acid moiety leading to the ring opening of the epoxide and formation intermediate **73** (Figure 5.20b). Computations of both paths allowed to identify the CO_2 insertion within the alkoxide intermediate as the rate-determining step. Calculation of their respective $\Delta G^{\ddagger}$ indicated that the conventional mechanism (1) prevails (21.0 kcal mol^{-1}) over the alternative path (2) hypothesis (26.8 kcal mol^{-1}); however, the alternative path could still be relevant under low concentration of CO_2.[137] When the reaction was applied to **GD**, **GLC** was obtained in 70% after 24 h at 80 °C (Figure 5.20c).

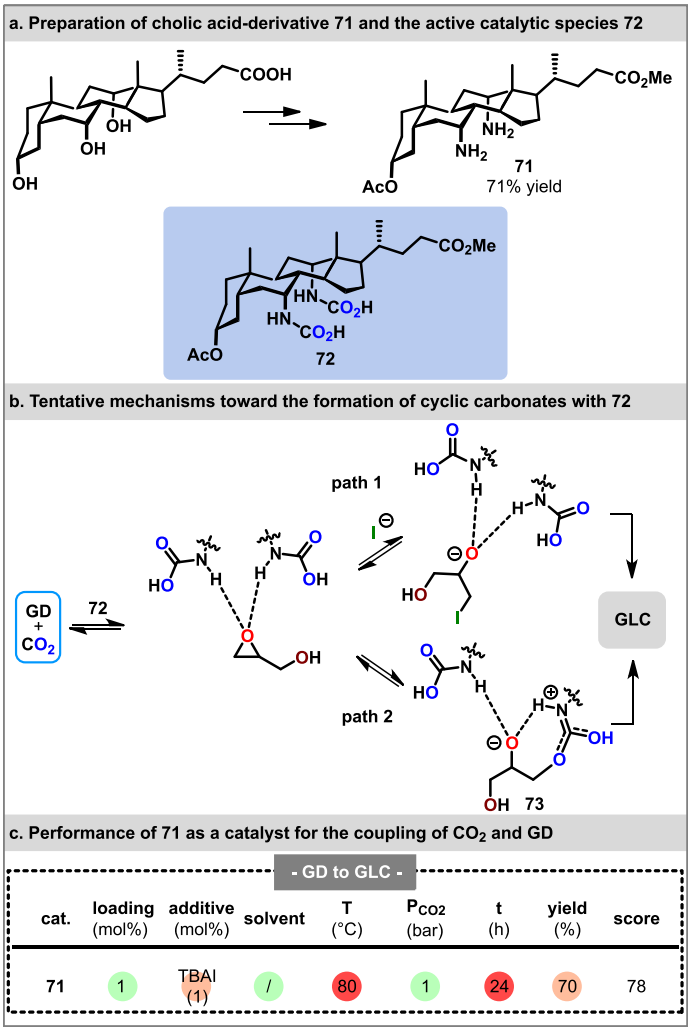

Figure 5.20 (a) Synthesis of cholic acid-base bis-primary amine precursor **71** and its activated form with CO_2, **72**. (b) The two hypothesized mechanisms toward the formation of cyclic carbonates in the presence of active species **72**.[137] (c) Performance of **71**/TBAI for the preparation of **GLC** (See Section 6 and Supporting Information for details).

Organoboron catalysts. Wu *et al.* developed homogeneous bifunctional organoboron catalysts for the coupling of epoxides and CO_2 under neat conditions. The catalysts were prepared according to a high-yielding and scalable (multi-kg) two-step protocol involving an alkylation to form an allylic quaternary ammonium scaffold (with X = Cl, Br or I as counter-anions), followed by a subsequent hydroboration (Figure 5.21a). The catalytic efficiency was first validated on **PO** (0.0005 mol% of the catalyst, 80 °C, 2 h, 20 bar CO_2). With iodide salt **74**, 26% conversion of **PO** (sel. >99%, TOF = 257 h^{-1}) was reported, while the bromide and the chloride salts gave 19% and 14% conversion, respectively. The higher performance of the iodide salt likely relates to an enhanced activation of the epoxide since iodide interacts

poorly with the boron center, while stronger interactions with chloride and bromide ions would compete and decrease the epoxide activation. When the reaction was carried out using catalyst **74** at a higher temperature (120 °C), the conversion of **PO** reached 45% (TOF = 446 h^{-1}). Alternatively, **PC** could be obtained in 32% yield at room temperature and atmospheric pressure within 8 h, with a higher catalyst loading of 1 mol% (TOF = 4 h^{-1}). Catalyst **74** could also be reused for up to 5 consecutive runs without any significant drop in performance. The authors prepared a series of analogs of **74**, including variations to the boron and amine substituents, as well as to the length of the linker between both centers, to study the structure-activity relationship (SAR). Sterically hindered substituents on the boron center such as cyclohexyl groups or low electrophilicity groups (e.g., pinacolborane) were detrimental to the catalytic efficiency. The incorporation of longer linkers that increased the distance between the boron center and the ammonium cation also had a negative impact. In contrast, steric hindrance on the nitrogen center was beneficial as it weakened the ion pair interaction with the halide.

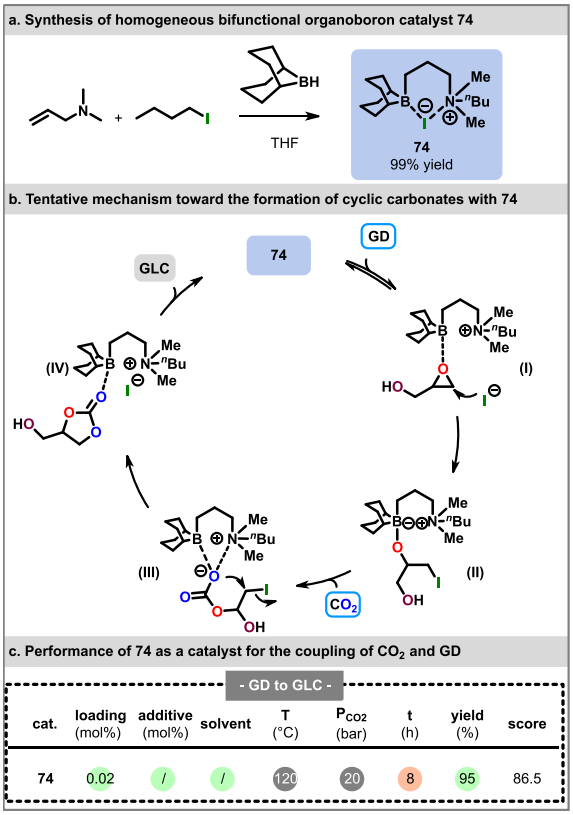

Figure 5.21 (a) Synthesis of homogeneous bifunctional organoboron catalyst **74**. (b) Proposed mechanism for the coupling of CO_2 with **GD** catalyzed by boron derivative **74**.[120] (c) Performance of organoboron catalyst **74** for the preparation of **GLC** (See Section 6 and Supporting Information for details).

The reaction was determined to follow first order kinetics for both **PO** and the catalyst **74** by performing tests under pseudo-first order conditions. On the other hand, the reaction rate was

independent of CO_2 pressure in the range of 3 to 10 bar, pointing to a zero-order dependence. Poor conversion was obtained at 1-3 bar, which was ascribed to the poor diffusion of CO_2 in neat **PO**. Finally, an Arrhenius plot was used to experimentally determine the total activation energy (E_a = 12.1 kcal mol^{-1}). Complementary studies with IR and ^{11}B-NMR reaction monitoring gave further insights. From the spectrometric data, the authors established that the first step consisted of (I) coordination of the Boron center with the epoxide, facilitated by the weak interactions with the iodide counter-anion, and (II) the subsequent ring-opening. Then, (III) CO_2 insertion to form a boron carbonate-species stabilized by the electropositive quaternary ammonium and followed by (IV) the final ring closure to form a five-membered cyclic carbonate (Figure 5.21b).[120] When applied to **GD**, **GLC** was obtained in 95% after 8 h at 120 °C, with only 0.02 mol% of **74** (20 bar of CO_2) (Figure 5.21c).

Quaternary ammonium salt-based catalysts. The three examples included in this section rely on a tetrabutylammonium halide (TBAX) as the main catalyst, in the presence of HBD cofactors. Milione *et al.* investigated **GD**'s dual capacity of being both a substrate and a cocatalyst in the synthesis of **GLC**. Under neat conditions, the authors studied the preparation of **GLC** through the reaction of **GD** with CO_2 (1 h, 80 °C, 10 bar of CO_2) in the presence of 1 mol% of TBAB, providing up to 85% yield of **GLC**. With an extended reaction time of 3 h, full conversion of **GD** was obtained with 5 mol% TBAB at 60 °C (see also Figure 5.22).

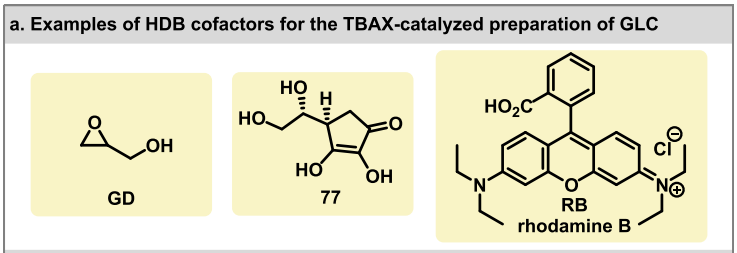

b. Comparison of the performances of TBAX in the presence of HBD cofactors

- GD to GLC -

cat.	loading (mol%)	additive (mol%)	solvent	T (°C)	P_{CO2} (bar)	t (h)	yield (%)	score
TBAB	5	GD	/	60	10	3	99	91.5
TBAI	4	77 (2)	/	25	1	24	85	83.5
TBAB	10	RB (10)	/	100	1	12	64	66

Figure 5.22 (a) Selection of HDB cofactors for the TBAX-catalyzed preparation of **GLC**.[138- 140] (b) Performance of (TBAB and TBAI) in the presence of HBD cofactors for the coupling of CO_2 and **GD** (See Section 6 and Supporting Information for details).

The authors also reported a DFT study of the reaction mechanism considering either **GD, PO**, or methyl glycidyl ether (**MGE**) as model substrates. **PO** and **MGE** were considered in addition to **GD** to assess the impact of the β-hydroxyl group on the reaction mechanism. The reaction path involving **GD** was computed while considering the crucial role of H-binding

networks for all intermediates and transition states. The results emphasized the critical role of the hydroxyl groups based on the lower computed $\Delta G^{\ddagger}$ of **GD**'s ring opening. In all cases, this step appeared as rate-determining with $\Delta G^{\ddagger}$ = 12.4, 16 and 17.6 kcal mol^{-1} for **GD**, **PO** and **MGE**, respectively. Moreover, the values of Gibbs energies computed for the formation of intermediates derived from **PO** and **MGE** were superior compared to those of **GD**. Next, the authors focused on the ability of **GD** to concomitantly form intra- and intermolecular interactions. At high concentrations of **GD**, they found that the substrates formed clusters, later computationally identified as dimeric (10-membered ring **75**) and monomeric species (7-membered ring **76**) as the most stable conformers (Figure 5.23). Computed activation barriers toward **75.A** and **75.B** pointed out that the ring opening step was impacted by these clusters with a lowered $\Delta G^{\ddagger}$ for the 10- and 7-membered rings. $\Delta\Delta G^{\ddagger}$ between the transition state **75.TSA** and the same species in the absence of a cluster gave a value of 2.6 kcal mol^{-1}, whereas the difference with **76.TSA** was about 4.3 kcal mol^{-1}. These decreasing $\Delta G^{\ddagger}$ values are likely caused by the shortening of the distance between the oxy anions and the hydroxyl groups within the cluster. These hydrogen bond interactions are also further involved in the stabilization of intermediates **75.A** and **76.A**.

The following insertion of CO_2 was reported without an enthalpy barrier as solely limited by diffusion. Additionally, no significant decrease of $\Delta G^{\ddagger}$ was observed for intermediates **75.B** and **76.B** when computed in the presence of 7- or 10-membered clusters. Capitalizing on the beneficial effects of cluster formation through HBD, the authors investigated the performances of a binary system composed of **GD**/TBAB. Under these conditions, **PC** was obtained in 84% yield with 5 mol% of a 1:1 **GD**/TBAB mixture. Noteworthy, switching from **GD** to **GLC** as cocatalyst led to similar results, confirming the key role of the β-hydroxyl function as HBD.[138]

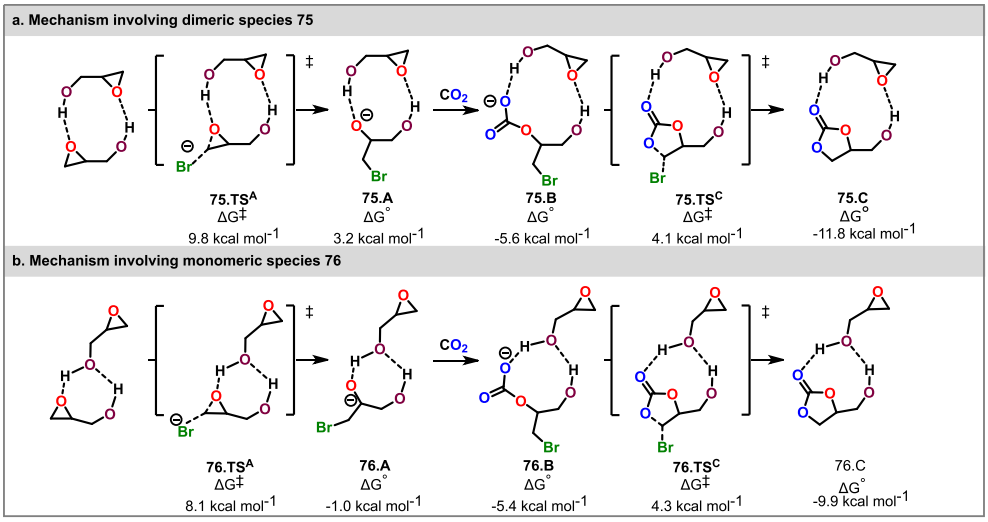

Figure 5.23 Calculated relative free energy for the coupling of **GD** with CO_2 according to two alternative paths, in the presence of bromide as nucleophile (and main active species). The free energies are given in kcal mol^{-1}.[138] (a) Path involving a 10-membered dimer species (**70**). (b) Path involving a 7-membered dimer species (**71**).

Ascorbic acid (**77**) was successfully implemented as a HBD catalyst by Crespy *et al.* in a binary catalytic system with TBAI for the preparation of **GLC** (Figure 5.22a,b). **GD** and CO_2 reacted at room temperature under atmospheric pressure of CO_2, giving **GLC** in 85% yield.[139] Similarly, Cui et Wu studied a binary catalytic system with rhodamine B as HBD (10 mol%) and TBAB (10 mol%) as an external nucleophile. Upon optimization, **GLC** was obtained in 64% yield after 12 h at 100 °C under 1 bar of CO_2 (Figure 5.22a,b).[140]

Bio-based catalyst. D'Elia *et al.* investigated the carbonation of neat **GD** with a broad library of bio-based organic salts under atmospheric pressure of CO_2. After an extensive screening of compounds, including sugars, carboxylic acids, polyols, and ascorbic acid as well as its derivatives, the authors identified sodium citrate **78** as the candidate with the highest potential. Complete conversion and high chemoselectivity were achieved toward **GLC**. The study also emphasized several critical parameters: (a) the key role played by hydrogen bonding moieties for substrate activation, (b) the moderate basicity required to prevent the formation of oligo/polyethers and (c) the nature of the counter-anion to ensure a good solubility of the catalyst. Increasing the temperature and pressure for the reaction did not improve the formation of **GLC**. Additional experiments with **SO** and **ECH** left the substrates unreacted, therefore suggesting the reaction occurred through the proton shuttle mechanism. The authors suggested that the reaction with sodium citrate **78** features a multi-point activation of **GD** prior to the formation of the hemiester intermediate **80** (Figure 5.24a). These valuable insights led the authors to consider analogs of sodium and calcium citrate, such as bio-based ionic alginates. The best results were obtained with calcium alginates, yielding **GLC** in 93%. However, progressive decarboxylation of calcium alginate resulted in a significant decrease of performance, hence hampering its recycling. Contrastingly, Na-alginates (**79**), which came with slightly lower catalytic efficiency, maintained similar performances (89-91% yield of **GLC**) over 3 consecutive runs (Figure 5.24a,b).[141]

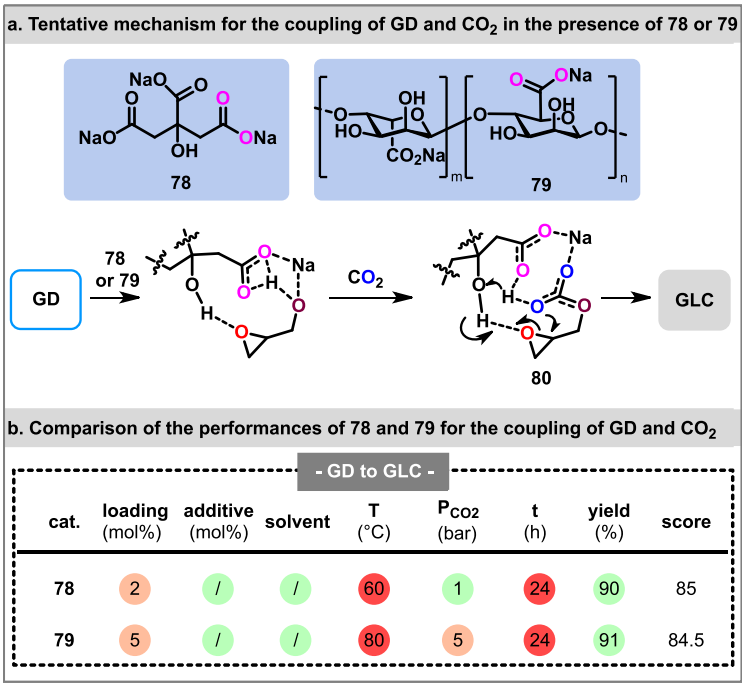

Figure 5.24 (a) Proposed mechanism for the conversion of **GD** into **GLC** in the presence of sodium citrate (**78**) or alginate (**79**).[141] (b) Comparison of the performances of sodium citrate (**78**) or alginate (**79**) for the coupling of CO_2 and **GD** (See Section 6 and Supporting Information for details).

5.2.6 IONIC LIQUIDS A VERSATILE AND HIGHLY MODULAR CATALYSTS

5.2.6.1 PRELUDES ON THE DESIGN OF IL-BASED CATALYSTS

The category of ionic liquids (ILs) gathers a plethora of functional materials featuring a broad diversity of potential scaffolds as well as a high degree of structural modulation, therefore rendering their exploitation very attractive.[35] Simple, homogeneous IL systems provide an anionic nucleophile aiming to promote the ring opening of epoxides as the first step of the conventional path. On the other hand, more elaborated scaffolds, mostly as heterogenized systems, possess HBD groups and/or metallic centers, both of which promote epoxide activation.[36] These solid materials can also display gas adsorption properties. Additional functions, such as carboxylates or thiols can also be introduced within the catalytic system to facilitate the chemisorption of CO_2, rendering it more available in the direct vicinity of catalytic sites.[142]

This section covers the most significant developments in IL catalysis toward **GLC**, from simple ILs used in combination with an external nucleophile toward highly functionalized catalysts bearing HBD and CO_2 adsorption groups. Heterogenized versions of ILs are also discussed with special attention to poorly soluble catalysts,[37,38,143–153] enabling the recycling of the reaction medium.

5.2.6.2 Recent advances on IL-based catalysts

Imidazolium-based catalysts. One of the few examples of homogeneous ionic liquid aiming at the coupling of CO_2 with **GD** was described by Shi *et al*. Synthesis of catalyst **81** consisted of the initial preparation of potassium imidazole salt followed by the addition of 1-ethyl-3-methylimidazolium bromide, yielding 97% of **75** after 24 h at room temperature (Figure 5.25a). Under relatively harsh experimental conditions, the authors obtained **GLC** in 91% (Figure 5.25c).[154]

Among the various reports of imidazolium-based heterogeneous catalysts, Duguet and colleagues developed a commercially available IL catalyst immobilized within thermomorphic polyethylene **82**. Its preparation simply relied on the reaction between 1-methylimidazole and polyethylene iodide at 120 °C for 20 h (Figure 5.25a). This material was particularly appealing thanks to its ease of recovery. Indeed, this material was endowed with a temperature-responsive behavior: its physical state changed from solid to liquid above 100 °C. A library of terminal epoxides was converted to the corresponding cyclic carbonates in satisfying yields ranging between 62 and 92%; however, the carbonation of **GD** gave merely 45% of **GLC** (Figure 5.25c) and predominantly led to polyethers due to polymerization.[155]

Another example of solid catalytic material comes from Zhiani *et al.*, who proposed a *N*-dodecyl imidazolium imidazole IL impregnated onto porous dendritic fibrous nanosilica (DFNS) (Figure 5.25b). The highly branched material enabled high mass transfer and improved access to the IL catalytic sites. Under optimized conditions, neat **GD** reached almost full conversion, offering 94% of **GLC** (Figure 5.25c). The catalytic mechanism is triggered through double hydrogen bond activation between the NH groups in **83** and the epoxide, followed by its ring opening with Cl and CO_2 capture prior to the cyclization step.[156]

Covalently linking *N*-methylimidazole onto Merrifield resin allowed Seo et *al*. to produce a heterogenous catalyst capable of producing **GLC** in 91% yield after 7 h of reaction time at 100 °C and 8 bar of CO_2, with 10 mol% of catalyst.[158] Similarly, Aprile *et al.* described a catalytic system based on Sn-embedded silica nanoparticles functionalized with 1-(2-hydroxypropyl)imidazole moieties (**84**, Figure 25b). In the presence of 1.87 mol% of **84**, conversion of 300 mmol of **GD** reached 27% with a TON of 24 $mols_{GD}$ $mols_{cat}$ (Figure 25c).[157]

Jiang and Ding elaborated a bifunctional Lewis acid-base poly(ionic liquid) catalyst (polyIL@MIL-101) by threading an imidazolium-based ionic liquid through a metal organic framework (MOF - MIL-101). Thermic pretreatment of MIL-101 was performed to expose the Cr(III) Lewis acidic sites of the MOF. The catalyst was then prepared through a one pot *in situ* polymerization of 1-vinyl-3-ethylimidazolium bromide (VEIMBr) in the presence of a cross-linker (*ortho*-divinylbenzene, DVB) and azobisisobutyronitrile (AIBN) within the MOF material.

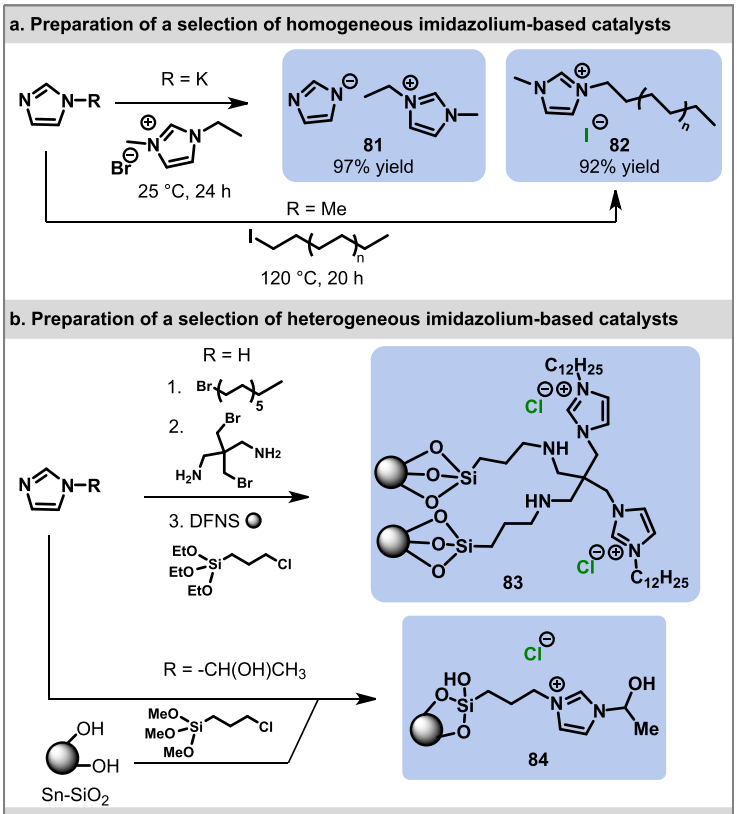

cat.	loading (mol%, *wt%)	additive (mol%)	solvent	T (°C)	P_{CO2} (bar)	t (h)	yield (%)	score
81	3	/	/	120	26	9	91	83.5
82	0.4	/	/	100	5	16	45	61.5
83	6.7*	/	/	70	1	2	94	91
84	1.9*	/	/	50	25	3	27	54.5

Figure 5.25 Elaboration of homogeneous and heterogeneous imidazolium-based catalysts **81-84**.[154-157] (a) Selection of homogeneous imidazolium-based catalysts. (b) Selection of heterogeneous imidazolium-based catalysts. (c) Comparison of homogeneous and heterogeneous imidazolium-based catalysts for the coupling of CO_2 and **GD** (See Section 6 and Supporting Information for details).

Complete characterization of the obtained polyIL@MIL-101 highlighted the good retention of MIL-101 porosity, thus allowing high mass transfer of reagents, as well as efficient adsorption of CO_2 onto the acidic metal centers. Despite having a lower surface area due to its functionalization, polyIL@MIL-101 has a CO_2 uptake of 103 cm^3 g^{-1} at 273 K, which is a superior uptake to the native MIL-101. The authors hypothesized that IL impregnation onto

MIL-101 led to the unexpected additional formation of small pores, hence favoring CO_2 adsorption. Imidazolium VEIMBr and MIL-101 were individually assessed for the carbonation of **ECH** with CO_2 in acetonitrile as a solvent, affording chloropropene carbonate (**CPC**) in 42% and 27% yield, respectively. By contrast, poly@MIL-101 gave 94% yield under the same conditions. These results clearly emphasized the synergy between Lewis basic sites from ILs and Lewis acidity of Cr(III) centers, which contributed to CO_2 enrichment in the direct vicinity of IL sites. An additional trial involving a simple physical mixture of VEIMBr and MIL-101 yielded **CPC** in 90%. However, this unpolymerized mixture made the recovery of the IL catalyst very cumbersome and decreased the overall reaction recyclability. On the other hand, poly@MIL-101 could be successfully recovered by centrifugation, with its performance remaining constant over 10 consecutive runs. The versatility of poly@MIL-101 was next assessed on a small library of epoxides. The coupling reaction with **GD** and CO_2 relied on a large excess of the catalyst of 134 wt% with respect to the substrate, providing **GLC** in 99% yield after 24 h at 70 °C and under 1 bar of CO_2.[159]

Garcia-Verdugo *et al.* developed a flow process toward **GLC** with a 3D-printed reactor grafted with *N*-alkyl imidazole ILs (Figure 5.26). 3D-printing technology was relied upon to address the inherent challenges associated with conventional pack-bed reactors, more specifically the limitations in mass and heat transfer. This was achieved by leveraging the accessibility to a diverse range of complex geometries and raw materials available through 3D printing. Supported catalyst **85** featured a high mechanical resistance and a low swelling, which was desired to prevent a significant change in the volume of the catalytic material within the back-bed column. Its preparation consisted of the polymerization of glycidyl methacrylate monomers in the presence of 1,4-butanediol diacrylate as a cross-linker. In the next step, the polymer was further functionalized with several ILs, including butyl-imidazole chloride. The latter achieved the highest performance with 91% conversion for **SO** conversion after 12 h of reaction time at 100 °C under batch conditions. Then, a proper reactor architecture was designed, incorporating a column composed of a gird with repeated cylindrical patterns.

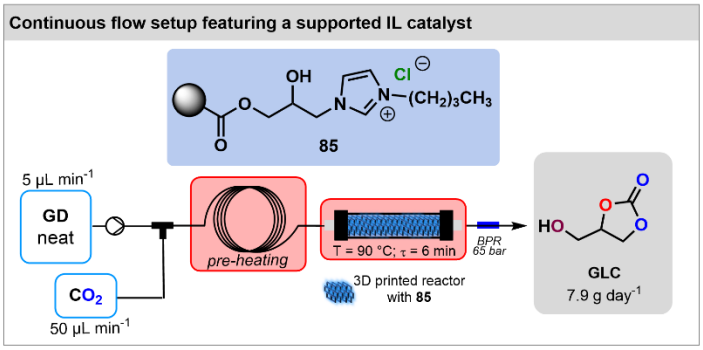

Figure 5.26 Continuous flow set-up equipped with a 3D-printed packed-bed reactor grafted with N-alkyl imidazole ILs **85** as a heterogenized catalyst for the coupling of CO_2 and **GD**.[160]

Superior catalytic performances were demonstrated by comparison with a pack-bed column filled with functionalized commercial spherical polymer beads. As a proof of concept, continuous flow synthesis of over 300 h of run time was shown to sequentially convert a

variety of terminal epoxides including **SO**, **ECH** and **GD**. The results clearly highlighted that the reactor maintained both its mechanical and chemical integrity while offering a daily production of **GLC** around 7.9 g.[160]

Tejeda *et al.* reported the design of a set of homogeneous mono- and dual-component catalytic systems. This class of catalysts featured an imidazole-based scaffold substituted with various alkyl and hydroxyl groups.

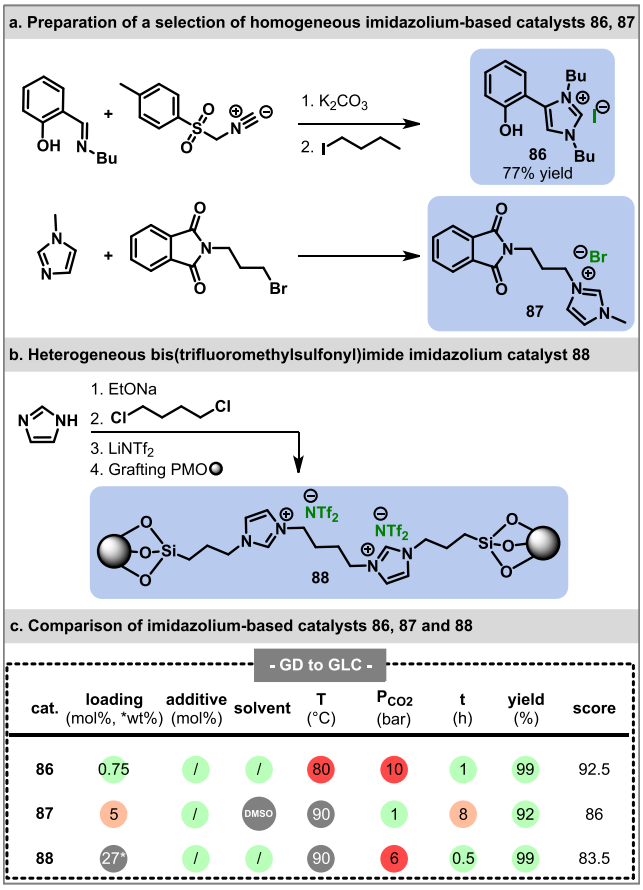

cat.	loading (mol%, *wt%)	additive (mol%)	solvent	T (°C)	P_{CO2} (bar)	t (h)	yield (%)	score
86	0.75	/	/	80	10	1	99	92.5
87	5	/	DMSO	90	1	8	92	86
88	27*	/	/	90	6	0.5	99	83.5

Figure 5.27 (a) Preparation of a selection of homogeneous imidazolium-based catalysts **86**,[161] **87**.[162] (b) Synthesis of heterogeneous bis(trifluoromethylsulfonyl)imide imidazolium catalyst **88**.[35] (c) Comparison of homogeneous and heterogeneous imidazolium-based catalysts **86**, **87** and **88** for the coupling of CO_2 and **GD** (See Section 6 and Supporting Information for details).

Their synthesis started with a base-induced cycloaddition of tosyl methylisocyanide with imines to form phenyl-substituted imidazoles. Once the catalyst was prepared, the authors screened several quaternary ammonium halide salts as nucleophilic cocatalysts. TBAI was identified as the most efficient cocatalyst for the conversion of a large scope of terminal epoxides obtaining yields in the range of 52 to 96%. Further optimization of the catalyst arrived at **86** (Figure 5.27a), which exhibited better solubility and performance than its

predecessors. The use of catalyst **86** boosted the yields up to 82-99% range with low catalytic loading (0.75-1 mol%), for the same substrate scope, without the need for TBAI co-catalysis (Figure 5.27c). The mechanism was investigated with NMR spectroscopy. The authors noticed the broadening of the signal arising from the catalyst phenol group. This observation suggested that the activation of the epoxide proceeds through hydrogen bonding. Moreover, appearance of a CH signal assigned to the opened epoxide highlighted that the ring opening takes part at the most hindered electrophilic center. Catalyst reusability was validated for up to 5 cycles without noticeable loss of performance.[161]

Al-Qaisi et *al*. synthesized homogeneous bifunctional catalysts in the presence of dimethyl sulfoxide as a solvent. The most efficient catalyst was constructed from the S_N2 reaction of *N*-(3-bromopropyl) phthalimide with 1-methylimidazole to recover **87** (Figure 5.27a), achieving an almost quantitative conversion of **GD** (Figure 5.27c).[162]

Hu *et al.* developed a novel heterogeneous dual acid-base bis(trifluoromethylsulfonyl)imide imidazolium catalyst supported by periodic mesoporous organosilica (PMO) (**88**, Figure 5.27b). Using optimized conditions, **GLC** was obtained in 99% yield over 30 min, with a TOF of 1980 h^{-1} (Figure 5.27c). Mechanistic studies showed that silanol groups from PMO enabled both multiple activation of the epoxide and stabilization of alkoxide intermediate **89** (Figure 5.28). The imidazolium amine sites were effective for CO_2 binding and activation.[35]

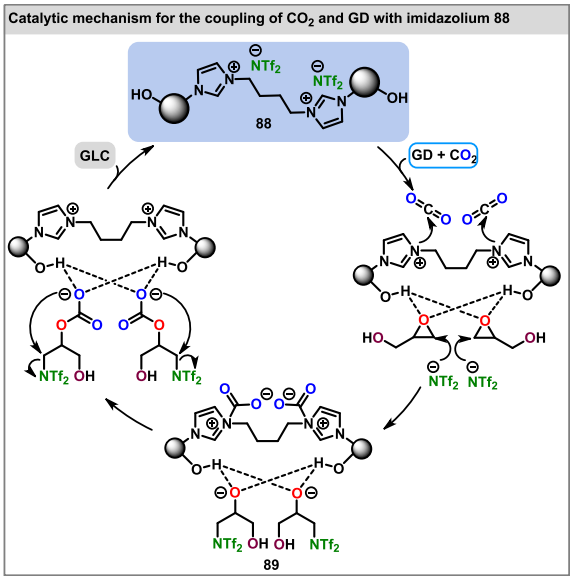

Figure 5.28 Tentative catalytic mechanism for the coupling of CO_2 and **GD** in the presence of dual acid-base bis(trifluoromethylsulfonyl)imide imidazolium **88**.[35]

Another work dealing with a similar catalytic scaffold was described by Chen et *al*. They constructed a series of ionic liquid compounds incorporated in oligomeric octavinylsilsesquioxane. Under optimized conditions, 2 mmol of **GD** was converted to **GLC** over 60 h reaction time, giving 99% of the product at 60 °C under 1 bar of CO_2 in the presence of 33 wt% of catalyst.[163]

A further example of polymer frameworks was reported by Dai and coworkers, who developed a straightforward one-pot strategy for the synthesis of hydroxyl-incorporated bifunctional IL networks (Figure 5.29a). The one-pot synthesis consisted of the nucleophilic substitution of multi-imidazole building blocks (TIPM) with 1,3-dibromo-2-propanol linkers. The resulting functionalized polymer **90** featured a large content of hydroxyl groups, in proximity to bromide anions. The catalysts were insoluble in several polar solvents, including water, alcohols, DMSO, to name a few, therefore ensuring heterogeneous catalysis. FTIR suggested the presence of adsorbed water at the surface of the catalyst. This was later supported by a loss of weight (8%) at 150 °C detected through thermogravimetric analysis (TGA), and further confirmed with X-ray photoelectron spectroscopy (XPS). Additionally, XPS showed that catalysts bearing a hydroxyl group, such as **83**, had lesser electron delocalization of the imidazolium cation compared to the same catalyst lacking hydroxyl groups. As a consequence, the electrostatic interaction between the cation and the bromide anion was weaker for the hydroxylated candidates, resulting in a higher catalytic performance. The comparison between both samples under very mild experimental conditions of 40°C and 78 h confirmed the higher efficiency of hydroxyl-bearing catalyst **90**, yielding carbonated **ECH** in 99%. In contrast, its non-hydroxylated analog afforded around 80% yield. This superior efficiency arguably relates also to its higher content of HBD, arising from the H-bonded molecules of water, the C_2 proton of the imidazolium cation and the hydroxyl groups, hence promoting the CO_2 cycloaddition (Figure 5.29d).[37]

Yang et *al.* developed a set of crosslinked imidazolium-derived polymers, such as **91**, obtained from the reaction of a tetraphenyladamantane derivative with 4,4′-bis(bromomethyl)biphenyl to obtain 97% yield of catalyst **91** (Figure 5.29b). Complete conversion of **GD** was observed using 0.2 mol% of **91** over 8 h at 130 °C (Figure 5.29d).[143]

Implementing a similar approach, Guan *et al.* designed basic porous ionic polymers (PIL) relying on a four-step synthetic route. Firstly, 1-vinylimidazole was alkylated with an amino bromide derivative to obtain an N-alkyl imidazole IL (80 °C, 24 h). Next, this IL underwent a copolymerization with DVB and AIBN, followed by neutralization to give **92**. A further anion-exchange treatment with a solution of NaOH led to the formation of **93**. Finally, bromide anions were exchanged with imidazolide (**94**) or triazolide (**95**) counterions over 72 h (Figure 5.29c). The catalytic activities of these PIL were investigated using **GD** as a model substrate. Higher performances were achieved for imidazolide **94** > triazolide **95** > hydroxide **93** > bromide **92** with yields of 86%, 78%, 77% and 68% (Figure 5.29d), respectively. The results showed that the incorporation of basic anions was beneficial for the catalytic efficiency due to their ability to bind CO_2 compared to bromide **92**. DFT (B3LYP/6-31+G**) was used to compute the binding energies for CO_2 with the various anions assessed in this work. Hydroxyl **93** exhibited a much stronger binding, *i.e.*, formation of stable adducts, with CO_2 at 25.1 kcal mol^{-1} than the two others, which were calculated to be 17.4 kcal mol^{-1} (**94**) and 15.3 kcal mol^{-1} (**95**). The authors explained the higher performance of imidazole **94** by the activation degree of CO_2 (*i.e.*, the COO bond angle of CO_2), which was greater (135.09°) than that of triazole **95** (136.17°).

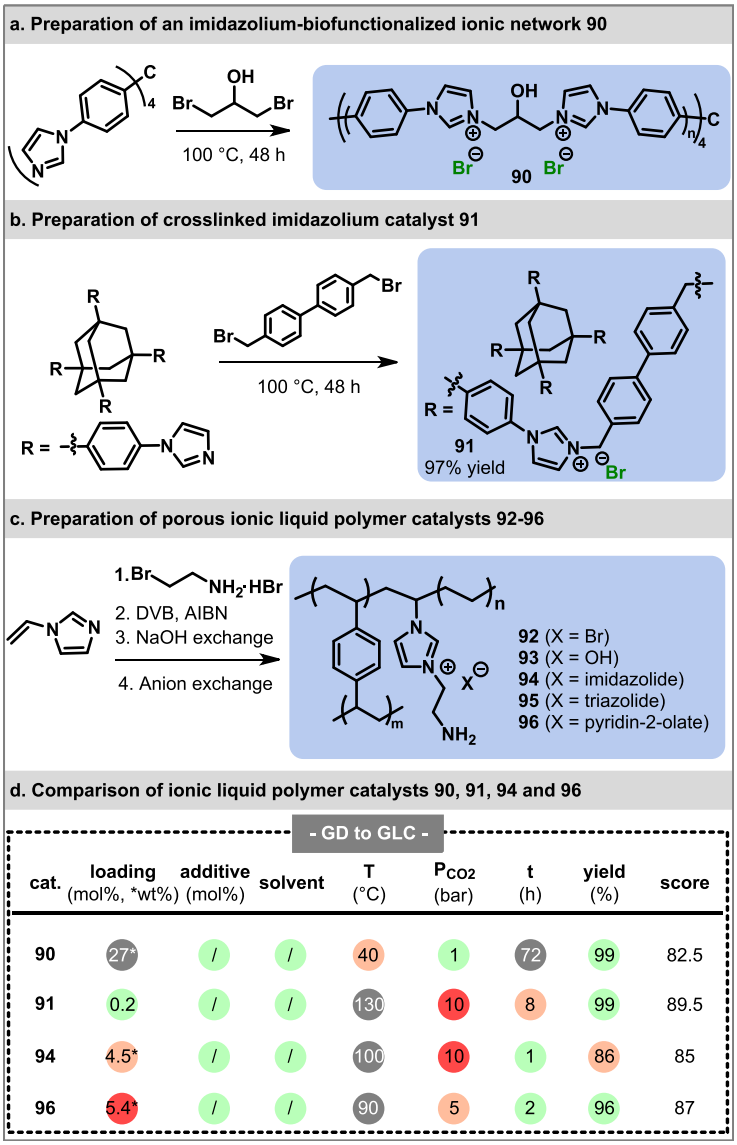

cat.	loading (mol%, *wt%)	additive (mol%)	solvent	T (°C)	P_{CO2} (bar)	t (h)	yield (%)	score
90	27*	/	/	40	1	72	99	82.5
91	0.2	/	/	130	10	8	99	89.5
94	4.5*	/	/	100	10	1	86	85
96	5.4*	/	/	90	5	2	96	87

Figure 5.29 (a) Preparation of an imidazolium-bifunctionalized ionic network **90**.[37] (b) Crosslinked imidazolium catalyst **91**.[143] (c) Porous ionic liquid polymer catalysts with anion counterpart **92-96**.[144,145] (d) Comparison of ionic liquid polymer catalysts **90**, **91**, **94** and **96** for the coupling of CO_2 and **GD** (See Section 6 and Supporting Information for details).

Based on these results, a potential mechanism was proposed (Figure 5.30), with the first step involving the binding of CO_2 by both amino and imidazolium groups. In the next step, the epoxide substrate was activated by the acidic proton from the NH_2-CO_2 adduct, and finally underwent a ring opening via the imidazolium-CO_2 adduct. Once the linear intermediate **97** was formed, its intramolecular cyclization leads to **GLC**.[144]

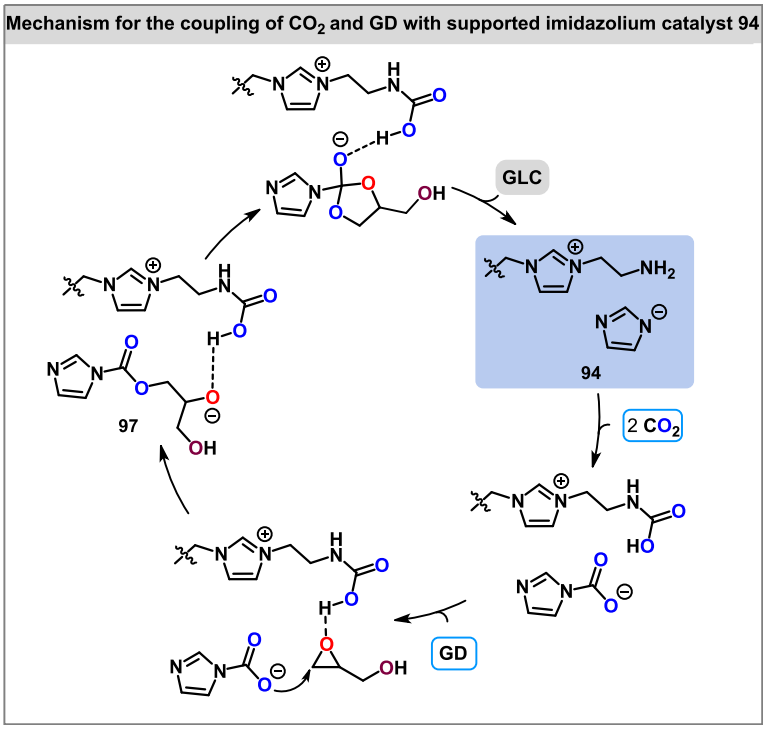

Figure 5.30 Tentative catalytic mechanism for the coupling of CO_2 and **GD** in the presence of catalyst **94** involving the formation of adducts NH_2-CO_2 and Im-CO_2.[144]

One year later, the same group developed a PIL catalyst bearing the pyridin-2-olate anion **96** (Figure 5.29c). DFT (B3LYP/6-31+G**) provided additional support to analyze the nucleophilicity of this anion. It emphasized the oxyanion as more nucleophilic, followed by the tertiary amine site of **96**. Moreover, their corresponding binding energies were very close at 14.5 and 13.6 kcal mol^{-1}, respectively, indicating a fast release of CO_2. Based on these catalytic features, the authors concluded on a similar mechanism than previously reported.[145]

Li *et al.* reported the preparation of novel conjugated acid-base PIL from the copolymerization of 1-(2-carboxylic acid-ethyl)-3-vinylimidazolium-chloride (CEImCl, **98**) and cross-linking agent divinylbenzene (DVB) (Figure 5.31). Typical synthesis of **98** consisted of the nucleophilic substitution of vinyl imidazole with chloroacetic acid at 70 °C for 24 h. Using **GD** as a model substrate, a comparison of performances between **98** and 1-butyl-3-vinylimidazolium chloride showed the beneficial effect of the carboxylic group, with a yield at 79% over 67% for the first. Further introduction of zwitterionic 1-(2-carboxyl-ethyl)-3-vinylimidazolium (CCIm, **99**) to the catalyst formulation provided a higher yield of **GLC** at 87%. The reusability of the catalyst was examined over five runs using the optimized experimental conditions. The different trials gave yields ranging between 92 to 95% of **GLC** (1 h, 90 °C, 10 bar CO_2 and 4.54 wt% of catalyst), demonstrating efficient recovery of catalyst through filtration and its chemical stability. The authors also computationally studied the mechanism of CO_2 chemisorption triggered by **98** and **99** units. The mechanism was initiated

by the carboxylate-induced deprotonation of the proton at the C_2 position of the imidazole ring followed by the covalent bonding of CO_2, trapping the gas in intermediate **99** (Figure 5.31). Although the same processes could be envisioned for **98**, intermediate **99** had a lower energy of adsorption at -17.9 kcal mol^{-1} compared to -13.9 kcal mol^{-1} for **98**. $\Delta G^{\ddagger}$ were computed for solely **98** and in combination with **99**. The concomitant presence of **98** and **99** gave a lower activation barrier of 12.3 kcal mol^{-1}, in contrast to 22.1 kcal mol^{-1} determined for the single use of **98**.[146]

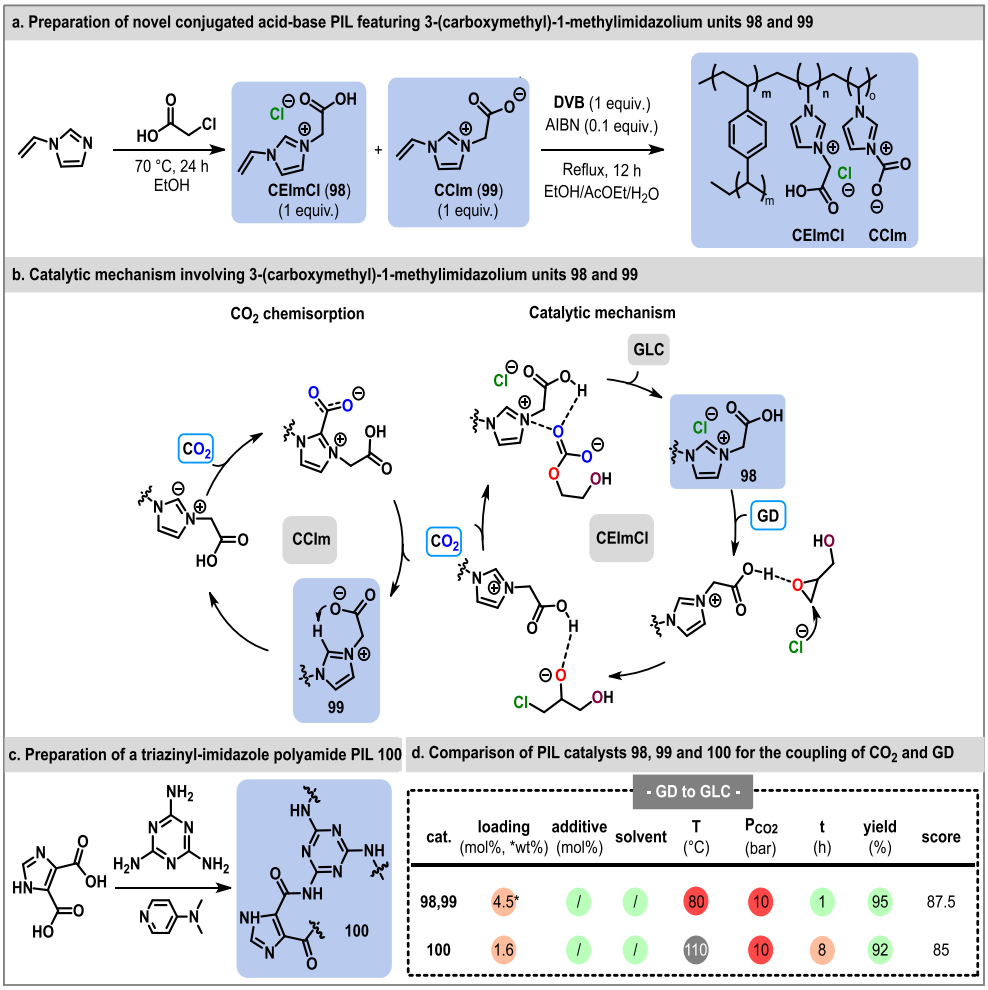

Figure 5.31 (a) Preparation of novel conjugated acid-base PIL featuring 3-(carboxymethyl)-1-methylimidazolium units.[146] (b) Catalytic mechanism involving **98** and **99** units as well as cycle of CO_2 chemisorption proposed for **99**.[146] (c) Preparation of a triazinyl-imidazole polyamide PIL and optimized conditions to produce **GLC**.[147] (d) Comparison of PILs **98**, **99** and **100** for the coupling of CO_2 and **GD** (See Section 6 and Supporting Information for details).

Another example of PIL was developed by Zhi *et al.* with a triazinyl-imidazole polyamide network. This catalyst resulted from the one-pot polycondensation of 4,5-imidazoledicarboxylic acid and melamine, in the presence of 4-dimethylaminopyridine

(DMAP) at 110 °C for 30 h (Figure 5.31c). The mesoporous catalyst **100** gave a 98% yield of **GLC** (Figure 5.31d).[147]

Organic Brønsted bases as catalysts. This subsection gathers a brief collection of catalytic systems containing an organic Bronsted base.

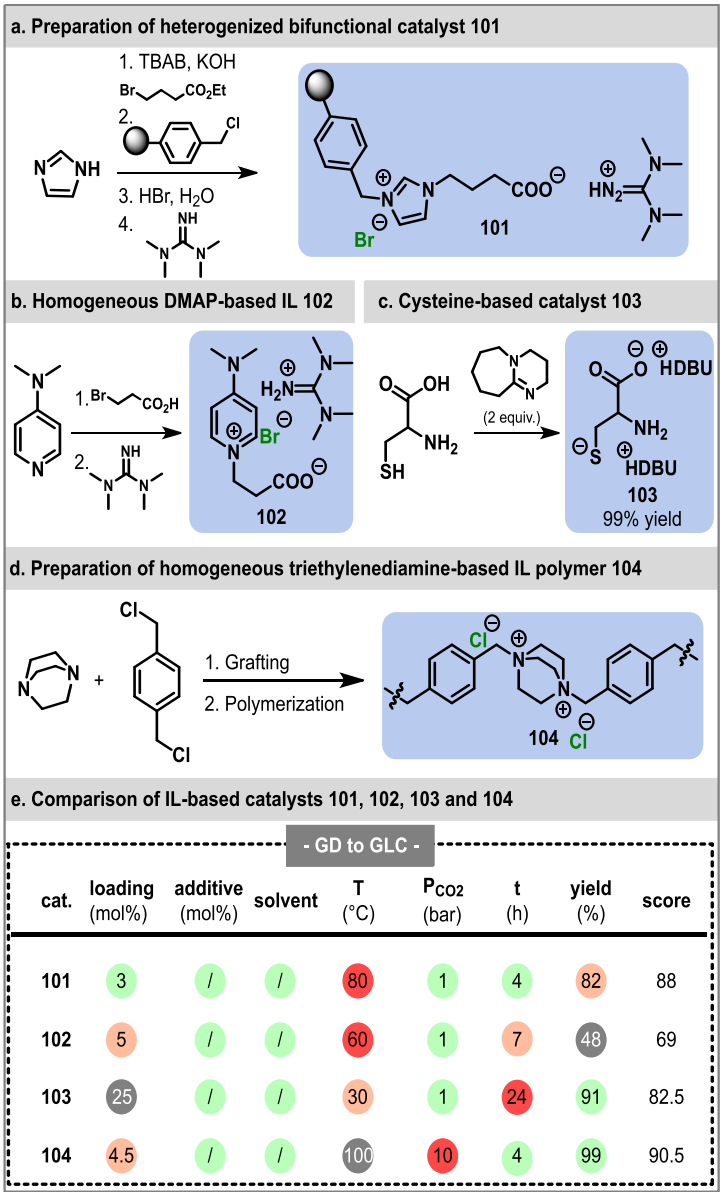

cat.	loading (mol%)	additive (mol%)	solvent	T (°C)	P_{CO2} (bar)	t (h)	yield (%)	score
101	3	/	/	80	1	4	82	88
102	5	/	/	60	1	7	48	69
103	25	/	/	30	1	24	91	82.5
104	4.5	/	/	100	10	4	99	90.5

Figure 5.32 (a) Preparation of heterogenized bifunctional catalyst **101**.[164] (b) Synthesis of homogeneous DMAP-based IL catalyst **102**.[165] (c) Preparation of cysteine-based catalyst **103**.[142] (d) Preparation of homogeneous triethylenediamine-based IL polymer **104**.[148] (e) Comparison of

organic Brønsted base-derivatives **101**-**104** as catalysts for the coupling of CO_2 and **GD** (See Section 6 and Supporting Information for details).

Zhang *et al.* developed a bifunctional catalyst **101** heterogenized on polystyrene and incorporating a trimethylguanidinium cationic counterpart ($TMGH^+$). A multistep approach was required to produce **101**. These steps include the alkylation of the imidazole precursor, grafting on the polystyrene support (Figure 5.32a), hydrolysis and counterion exchange with $TMGH^+$. The loading of the catalyst was determined to be 0.87 mmol g^{-1}. The low uptake of CO_2 was attributed to the inherently non-porous nature of polystyrene. The recyclability of **101** was demonstrated with comparable metrics for up to 7 cycles. Further reuse led to slightly decreased performances from 97 to 91% of chloropropene carbonate, likely caused by IL loss. Mechanistic considerations suggested that CO_2 capture proceeds through the carboxylate groups of **101**.[164]

Similarly, Zhang *et al.* elaborated a homogeneous DMAP-based ionic liquid bearing $TMGH^+$ counterpart. Preparation of catalyst **102** simply involved the alkylation of DMAP with bromopropionic acid for 12 h at 80 °C before reaction with TMG (Figure 5.32b). 48% yield of **GLC** was obtained after optimization of experimental conditions.[165]

Ahlquist *et al.* followed a similar approach relying on the neutralization of 1-carboxylpropyl imidazolium bromide with tetramethylguanidine. 10 mol% of corresponding binary catalyst yielded **GLC** in 80% after 5 h at 50 °C atmospheric pressure of CO_2.[166]

Deng and coworkers designed cysteine-based catalyst **103** prepared from the neutralization of both the thiol and carboxylic groups of cysteine with two equivalents of DBU (Figure 5.32c).A similar protocol was expanded to other amino acids lacking a thiol, and the corresponding catalysts were significantly less performant. This result emphasized the critical role of the SH group. An alternative candidate derived from cysteine and trimethylguanidine was also assessed, displaying a lower catalytic efficiency with a 57% yield for chloropropene carbonate. The authors argued that the lower pK_{aH} of trimethylguanidine accounted for the lower catalytic performance. Further increase of catalytic loading led to a highly viscous reaction medium, which limited the overall mass transfer.

Based on these experimental observations, the authors hypothesized that the mechanism depends on the presence of two nucleophilic groups as well as the protonated base (Figure 5.33). Both COO^- and S^- groups were assumed to be involved in the activation of two molecules of CO_2. Meanwhile, protonated DBU interacted with the substrate via hydrogen bonding **103**. In the next stage, the activated CO_2 would react with the most electrophilic carbon of the epoxide to form a linear carbonated species **105** before the intramolecular cyclization toward **GLC**.[142]

Ma et *al*. described the elaboration of a triethylenediamine-based IL polymer **104** (Figure 5.32d) endowed with a high degree of functionalization (4.10 mmol g^{-1}). The high density of active sites was obtained due to the preliminary nucleophilic addition of the monomer precursor 1,4-bis(chloromethyl)benzene with the diamine before the polymerization step. A

typical run with **GD** as substrate led to complete conversion to **GLC** after 4 h at 100 °C under 10 bar of CO_2 with 4.54 wt% of **104**.[148]

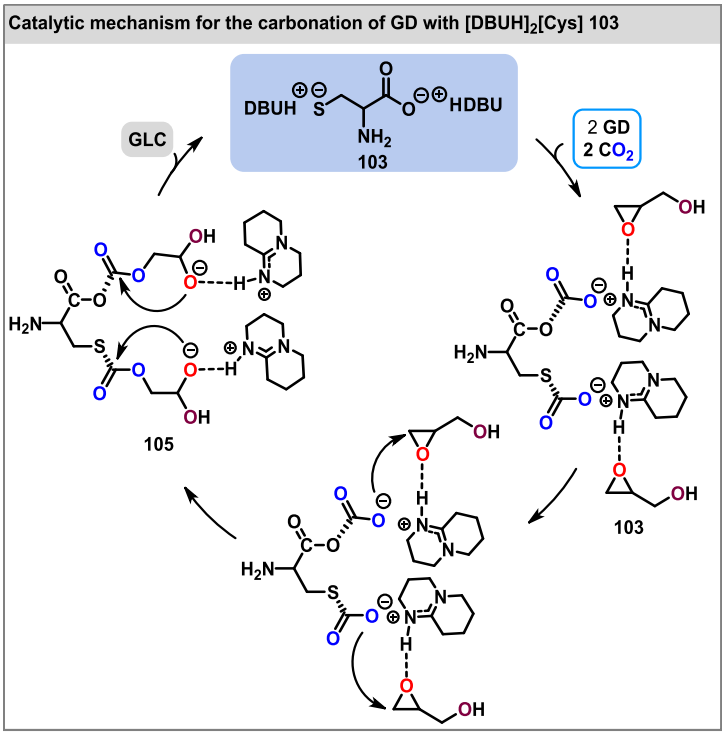

Figure 5.33 Tentative mechanism for the carbonation of **GD** catalyzed by $[DBUH]_2[Cys]$ **103**.[142]

Pyridinium-based catalysts. Duan and Wang synthesized a heterogeneous pyridinium derived ionic polymer (PIP) catalyst incorporating either a urea or thiourea moiety as dual HBD. The Sonogashira coupling of bispyridinium derivative **106** with 2,4,6-triethynylaniline yielded 98% of PIP **107**. This species **107** was then reacted with 3,5-bis(trifluoromethyl)phenyl isocyanate over 5 days at room temperature, resulting in the formation of PIP-urea **108** (Figure 5.34a). A series of experiments evaluating the catalytic performances of PIP, PIP-urea and its analog PIP-thiourea on the carbonation of **ECH** gave the corresponding carbonate in 58, 97 and 86% yield, respectively. The higher efficiency of PIP-urea was attributed to the enhanced activation of the oxirane, stemming from its higher acidity compared to PIP-thiourea. Additionally, its greater porosity and higher specific surface area improved substrate mass transfers along with CO_2 adsorption.[149]

Guan et *al.* designed a set of mesoporous pyridine-functionalized binuclear poly(ionic-liquid)s generated from the radical polymerization of IL imidazole derivative **109**, 4-vinylpyridine (**VP**) and **DVB** at 100 °C for 24 h to yield 80% of **110** (Figure 5.34b).

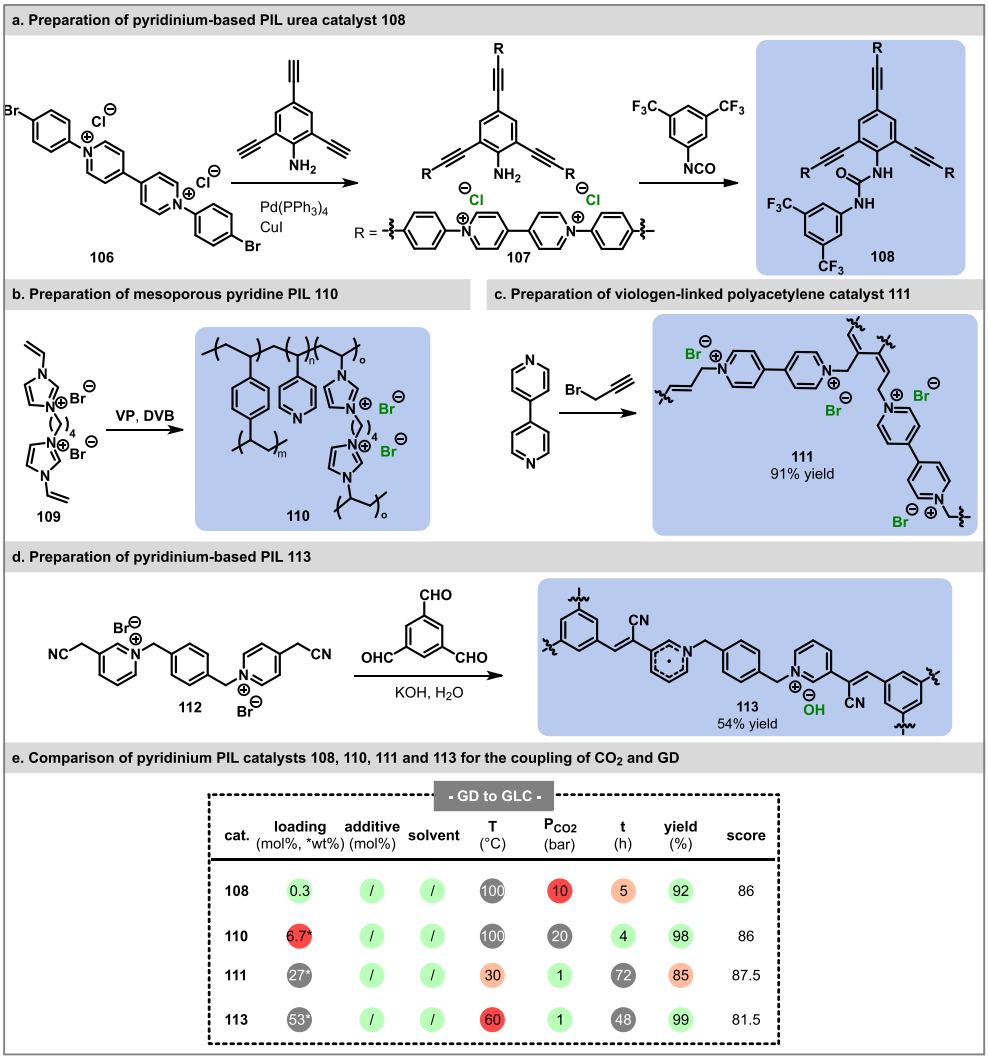

Figure 5.34 (a) Preparation of pyridinium-based PIL urea catalyst **108**.[149] (b) Preparation of mesoporous pyridine PIL **110**.[150] (c) Preparation of viologen-linked polyacetylene catalyst **111**.[151] (d) Preparation of pyridinium-based PIL **113**.[152] (e) Comparison of pyridinium-based PIL catalysts **108**, **110**, **111** and **113** for the coupling of CO_2 and **GD** (See Section 6 and Supporting Information for details).

The role of **VP** in the uptake of CO_2 was thoroughly studied. The results emphasized the critical role of pyridinium groups in facilitating CO_2 capture, yielding 11.75 mL g^{-1} for **110**. A similar structure lacking **VP** exhibited a reduced CO_2 capture of 9.69 mL g^{-1}. The activation degree of the imidazolium and pyridinium moieties to CO_2 was computed by DFT. Calculations were based on the postulate that CO_2 activation occurs through the induction of a geometrically curved state. CO_2 bond angles were determined to be 175.57° and 176.35° in the presence of **VP** and **VIM,** whereas their corresponding binding energies were 24.2 kcal mol^{-1} and 22.7 kcal mol^{-1}, respectively. DFT calculations thus pointed out **VP** as the most

efficient activator of CO_2. Reducing the density of catalytic sites from **110** was detrimental, leading to a decreased performance from 95 to 72% yield of chloropropene carbonate.[150]

Chen *et al.* documented a single-step approach that merged the alkylation of commercially available 4,4'-bipyridine with propargyl bromide and simultaneous polymerization towards the production of heterogeneous viologen-linked polyacetylene catalyst **111**. A 91% yield of **111** was obtained after 24 h at 100 °C (Figure 5.34c). Under very mild conditions, these highly crosslinked polymers showed high efficiency for small epoxide substrates such as **GD**, with a **GLC** yield of 85 % after 72 h of reaction at 30 °C. Epoxides with higher steric congestion required harsher conditions. Typically 72 h of reaction at 80 °C had to be implemented to achieve similar metrics. The authors ascribed this phenomenon to the lack of porosity within **111**, preventing an efficient mass transfer between the substrate and the catalytic centers. Catalyst **111** was reused up to 5 times through centrifugation, maintaining a similar production of chloropropene carbonate.[151]

The same group published another straightforward strategy for the synthesis of a pyridinium-based PIL, which involved the simultaneous presence of hydroxide anions and pyridinyl radicals. Catalyst **113** was prepared through a basic Knoevenagel condensation of acetonitrile functionalized pyridinium IL **112** and benzene-1,3,5-tricarbaldehyde (Figure 5.34d). The desired catalyst **113** was recovered in 54% after 72 h at 120 °C by simple filtration. Regarding the structural features of **113**, Fourier transform infrared detected the presence of adsorbed water, while pyridinyl radicals ($Py^{\cdot}$-N) were detected via electron paramagnetic resonance. X-ray photoelectron spectroscopy determined the molar ratio of Py-N^+ to $Py^{\cdot}$-N radicals to be around 1:1.53 Py-N^+/$Py^{\cdot}$-N based on their atomic concentrations.

Catalyst **113** (4 mol%) gave full conversion of **GD** within 48 h of reaction under atmospheric pressure of CO_2. Next, a tentative mechanism relying on the formation of HCO_3^- species was proposed. Two different modes of CO_2 activations were examined, proceeding through either (a) the basic hydroxide anions or (b) $Py^{\cdot}$-N radical groups. Regarding mode (a), OH^- species could directly react with CO_2 to yield a bicarbonate (HCO_3^-, see **114**, Figure 5.35). In the case of mode (b), $Py^{\cdot}$-N moieties form carbamate adducts with CO_2, and further react with H_2O to also generate bicarbonate anions (**115**). The epoxide substrate undergoes a dual H-bonding activation through H_2O and the polarized α-proton of the pyridinium groups. This is followed by the rate-determining ring opening by bicarbonate, the final intramolecular cyclization leads to the desired cyclic carbonate (Figure 5.35).[152]

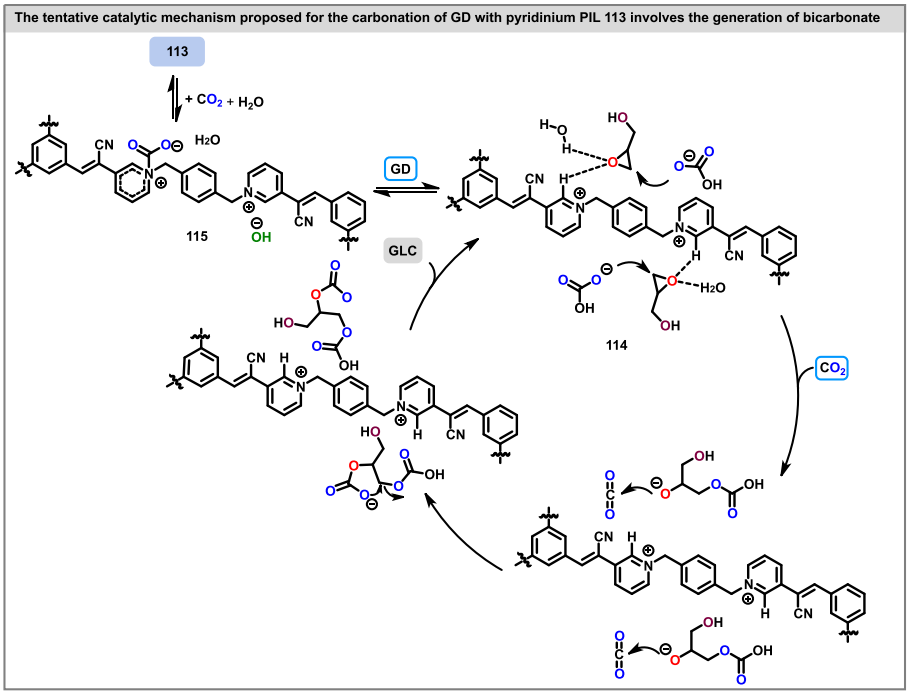

Figure 5.35 Tentative catalytic mechanism proposed for **113**, involving the generation of a bicarbonate (HCO_3^-) according to two different modes of CO_2 activation.[152]

Pyrazolium-based catalyst. In addition to imidazolium and pyridinium-based catalysts, researchers have recently explored other categories of ionic liquids. For instance, Wang *et al.* described a three-component pyrazolium-based IL (Figure 5.36a) on mesoporous organosilica embedded onto cobalt nanoparticles (Co-PMO-IL) **118**.[167] The simple acid-base reaction of benzyltrimethylammonium hydroxide with carboxylethyl imidazolium derivative **116** led to catalytic complex **117**. Extensive screening of a collection of common pyrazolium species outlined the importance of the introduction of a CO_2-trapping group along with a strong nucleophile to achieve high catalytic performance. Using 15 mol% of the most efficient catalyst **117** resulted in the modest formation of **GLC** (58%), more likely caused by the limited solubility of **117**. Evaluation of **117** recyclability proved to be inconclusive with decreasing performance from 88 to 80% yield of **CPC** after the third run. NMR analysis of the reused catalyst showed the degradation of **117**, through the loss of the pyrazolium moiety to eventually generate benzyltrimethylammonium bromide.

DFT computations indicated that the binding of CO_2 with the carboxylate group of the pyrazolium moiety slightly facilitated the epoxide ring opening. A small decrease of the activation barrier from 24.1 to 23.0 kcal mol^{-1} was observed in the presence of CO_2 within the complex (Figure 5.36a). The efficiency of the catalyst was also correlated to the multiple activation of the epoxide via HBD (Figure 5.36a), as well as the subsequent stabilization of the various intermediates.[39]

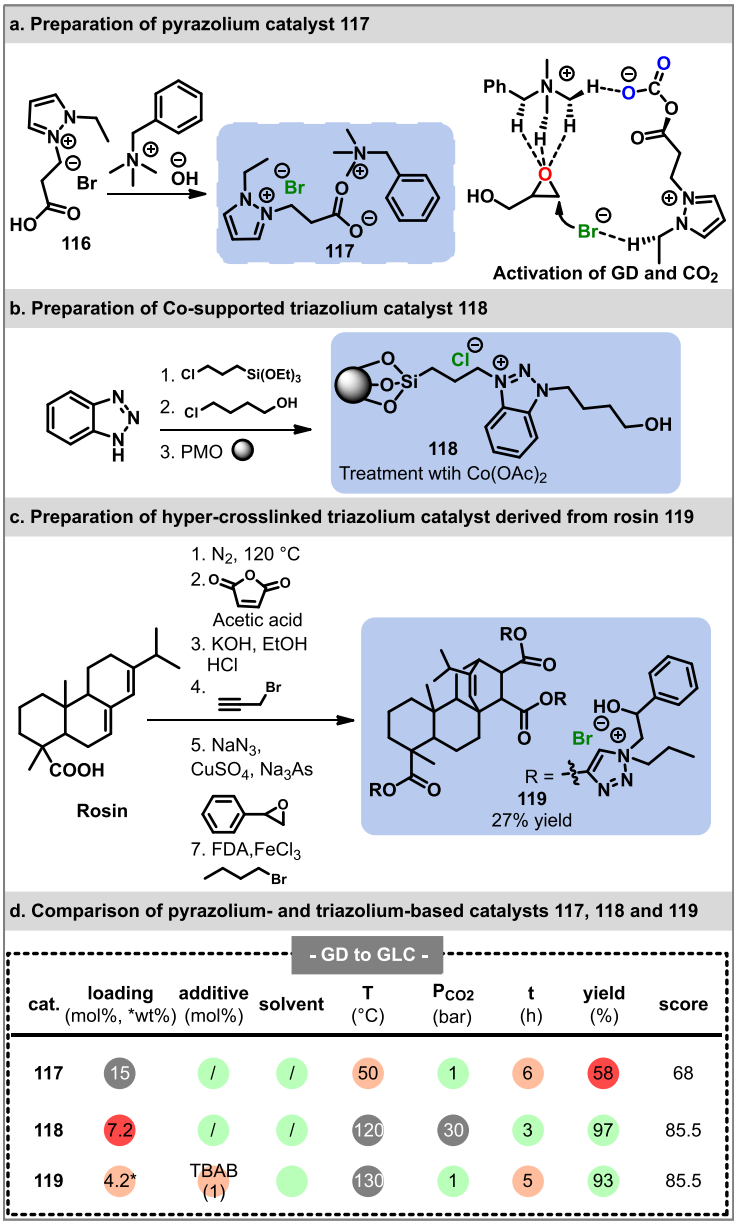

cat.	loading (mol%, *wt%)	additive (mol%)	solvent	T (°C)	P_{CO2} (bar)	t (h)	yield (%)	score
117	15	/	/	50	1	6	58	68
118	7.2	/	/	120	30	3	97	85.5
119	4.2*	TBAB (1)		130	1	5	93	85.5

Figure 5.36 (a) Preparation of pyrazolium catalyst **117** and illustration of the activation of **GD** via multiple hydrogen bonding interactions with **117**.[39] (b) Elaboration of a grafted benzotriazolium IL on mesoporous organosilica embedded onto cobalt nanoparticles (Co-PMO-IL) **118**.[167] (c) Synthesis of a hyper-crosslinked polymer derived from bio-based rosin and functionalized with triazole moieties **119**.[153] (d) Comparison of pyrazolium- and triazolium-based catalysts **117**, **118** and **119** for the coupling of CO_2 and **GD** (See Section 6 and Supporting Information for details).

Triazolium-based catalyst. Hu *et al.* reported a multifunctional catalytic system consisting of grafted benzotriazolium IL on mesoporous organosilica embedded with cobalt nanoparticles (**118**, Figure 5.36b). Complete characterization revealed an expected reduction of the surface area, pore volume and size due to the functionalization with the ILs. However, these structural changes still allowed sufficient diffusion of the substrate toward the catalytic active sites. Various ratios of ILs/PMO were examined to determine the optimal composition, with a molar ratio of 1.0 producing the most efficient candidate. The reaction catalyzed by **118** yielded **GLC** in 97% after 3 h at 120 °C (Figure 5.36d). Performances of bulk IL and PMO alone gave yields around 54% and 30% of **PC** respectively, highlighting the synergistic effect of cobalt sites and ILs on the catalytic efficiency. Both moieties contributed to the enhancement of epoxide activation and alkoxide stabilization. The catalyst's recyclability and recoverability were tested over 5 cycles through filtration providing similar results over the consecutive runs.[167]

Xiong et *al*. documented the design of a hyper cross-linked porous polymer derived from bio-based rosin and functionalized with triazole moieties (**119**). The synthesis of **119** was cumbersome, requiring a multi-step protocol with the isolation of several intermediates (Figure 5.36c). Catalyst recyclability was possible over 10 successive cycles without any loss of performance.[153]

As an additional example, Gao *et al.* described a catalytic species from a lignin-modified deep eutectic solvent in combination with TBAB. Under 10 bar of CO_2 at 110 °C, **GLC** was obtained in 95% yield with 10 mol% of additive and 13.5 wt% of catalyst.[38]

5.2.7 GLOBAL ASSESSMENT OF PROCESS EFFICIENCY AND E-FACTOR

In this section, we present a global process evaluation for selected examples of metal, organic, and IL-based catalytic systems for the coupling of **GD** with CO_2 (Table 5.1). These examples were selected for their sustainability regarding the nature of the catalyst, their attractive yield towards the preparation of **GLC** from **GD** and CO_2, as well as the use of mild or moderate experimental conditions. This analysis encompasses two main indicators (See Supporting Information for details): (a) an evaluation of the burden associated with the preparation of the catalytic systems and (b) an efficiency assessment of the catalyzed coupling of **GD** and CO_2. For the evaluation of the preparation of the catalysts, it includes the cost/time efficiency and intrinsic waste generation linked to their synthesis. The efficiency of the overall process toward the production of **GLC**, including the synthesis of the catalyst, will then be inspected to calculate a fair and representative E-factor alongside with a discussion feeding upon both aspects.[168] Considering **GLC** as a fine chemical, benchmark values of E-Factors for its synthetic procedure should range between 1 to 50.[169,170] For the efficiency assessment of the catalyzed coupling of GD and CO_2, we are introducing a scoring system inspired by the EcoScale,[171] where penalty points are deducted based on categories of impactful factors (yield, catalytic loading, use of additive, use of solvents, pressure of CO_2, technical specificities of the setup, process temperature, reaction time; see Supporting Information for details on the categories of penalties and color codes, which are used through this manuscript in the table sections giving scores and in Table 5.1). These scores are indicative only, and do not take the scale (or potential for scalability into account).

The first consideration is the number of steps required for the preparation of the catalyst and the cumulated reaction time. Most catalysts were synthesized in a 2- to 4-step strategy (6 to 67 h reaction time). Every intermediate had to be purified prior to its further conversion, therefore resulting in a significant additional cost that could not be accurately estimated for the analysis. Two exceptions are entries 3 and 12 (Table 5.2), where straightforward approaches were implemented with only one final purification toward the catalyst. However, the efficiency of one stage protocols was found to always be negatively impacted by extended reaction time at 48 and 24 h (Table 5.2, entries 3 and 12). Alternatively, a one pot carbonation of **GD** could be accomplished with an *in-situ* generation of a homogeneous CaI_2/PEG complex (entry 5). However, the catalyst could not be recovered. Focusing on heterogeneous catalysts (entries 4 and 11), their preparation was based on the preparation of the active moiety prior to its incorporation into the material. In both cases, this latter stage was highly energy consuming with extended reactions time (32-36 h) at high temperatures (110-153 °C). On the other hand, all homogeneous metal candidates were associated with low cumulated yields from 38 to 53% (entries 1-3), in contrast, the synthesis of organo- and IL- based catalysts was more waste efficient, exhibiting cumulated yields between 80 to 99% (entries 6-12). Average prices of homogeneous catalysts were estimated to be approximately 16.98, 2.95 and 2.36 € g^{-1} for metals, organocatalysts and ILs (including PILs), respectively. Ideally, catalyst preparation should rely on a straightforward or *in-situ* approach, with high yield, facile purification, and under mild conditions, while catalyzing the desired reaction with high efficiency. Furthermore, commercially available chemicals should always be privileged. While some of the examples discussed above, especially CaI_2/ligand complex, Barton base, Boron-based catalyst and pyridinium-based PIL (entries 5, 7, 9, 12), meet several of these criteria, the engineering of a protocol to fulfill all these criteria at once remains highly challenging.

Most of the reported catalysts afford **GLC** under mild experimental conditions. The authors usually played on the loading of catalysts, the use of potential cocatalysts as external nucleophiles, as well as extended reaction times to ensure a high yield of **GLC** (75-99%, entries 1, 3-6, 8, 11-12). When transposition of these procedures to multi-gram scale is attempted, similar performances can only be maintained with a drastic increase of reaction time up to several days.[135,151,152,157] Despite the efficiency of these processes, they suffer from very low overall productivity when it comes to largescale production of **GLC**. A potential solution to increase productivity could lie in flow technology. Indeed, transposition of the formation of **GLC** from **GD** and CO_2 from microfluidic to pilot scale was successfully demonstrated with a daily productivity reaching 3.6 kg in a Corning® Advanced-Flow Reactor™ G1 (Table 5.2, entry 7).

The E-factor is a simple, handy, and relevant green metric to compare waste generation.[168] Determination of the E-factor for the same selection of examples was therefore performed. Apart from the Aluminum scorpionate complex (entry 1), all the processes assessed exhibited a favorable E-factor between 0.5 and 15, suggesting their suitability for the preparation of **GLC**. Five out of the remaining eleven catalysts contained a heterogeneous support (entries 4 and 6) or a poorly soluble scaffold (entries 10-12), which enables their recycling over multiple runs through an additional purification step. Although not usually considered in the calculation of E-factor, their exploitation over successive reaction cycles often leads to

decreasing performances due to degradation, leaching, or clogging of their intrinsic porosity.[36]

The scoring system developed in this work offers a practical and convenient tool for comparing the experimental conditions of the various examples in Table 5.2. Scoring values range from 79.5 to 93.5 which indicate good to excellent process efficiency of the synthetic procedures.[171] The use of high loading of catalyst along prolonged reaction times are identified as the most detrimental parameters for the design of efficient processes of **GD** carbonation. Only two reactions require the use of halide salts (entries 3 and 4), highlighting the overall scientist willingness to switch toward bifunctional candidates with internalized nucleophiles. Moreover, most entries implemented the combination of a low temperature and catalytic loading, therefore always requiring a long reaction time above 20 h to exceed 75% yield of **GLC** output (entries 1-3, 5,6,12). In contrast, lower reaction time could be achieved while increasing the reaction time as observed with entries 2,7 and 10, but negatively impacting the overall process efficiency.

This summary of examples illustrates some of the main considerations to design and engineer cost/efficient processes toward **GLC**. The choice of a sustainable catalyst is of paramount importance, as well as the price of the procedure for the preparation of the catalyst and the cost of reagents. Moreover, the productivity of **GLC** directly depends on its performance. Therefore, the balance between catalyst design and its resulting performance must be carefully weighed to provide the best financial and environmental compromise between catalyst preparation and its intrinsic efficiency. Figure 5.37 summarizes the key features gathered in this work concerning the research and development of efficient and cost effective **GLC** production at an industrial scale, as well as a global assessment of the potential industrialization prospect of **GLC** as widely applicable value-added molecule.

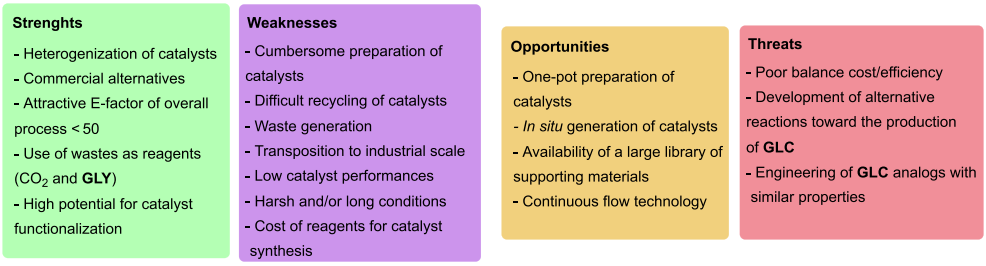

Figure 5.37 Presentation of current strengths, weaknesses, opportunities, and threats linked to the preparation of catalysts as well as following carbonation of **GD** with CO_2.

5.2.8 PERSPECTIVES TOWARD THE PRODUCTION OF BIO-BASED GLC AT THE INDUSTRIAL SCALE

Regarding the industrialization potential to produce **GLC**, two continuous flow pilot-scale processes implementing either the fixation of CO_2 onto **GD** or the transesterification of **GLY** with dimethyl carbonate (**DMC**) are discussed (Figure 5.38).

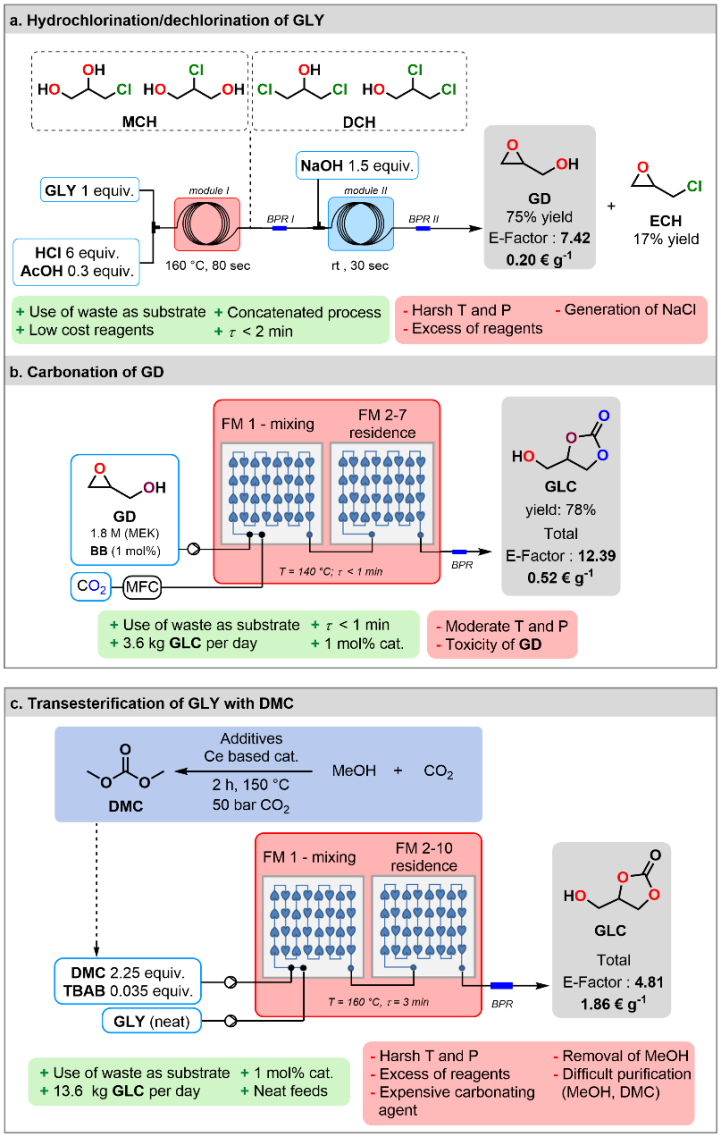

Figure 5.38 Preparation of **GLC** starting from **GLY**, including the calculation of total cost and E-factor. (a) Chlorination-dehydrochlorination of **GLY** to **GD** under intensified continuous flow conditions at pilot scale. (b) Intensified continuous flow (pilot scale) coupling of **GD** with CO_2 in

the presence of BB as organocatalyst.[131] (c) The synthesis of the carbonation agent DMC, followed by is transesterification with **GLY**.[28,174-175]

We have previously shown that the preparation of bio-based **GD** can be achieved according to an intensified concatenated process.[131] It involves the upgrading of **GLY**, a widely available chemical that can be sourced from waste, through (di)chlorination and subsequent dehydrochlorination to yield the corresponding epoxides (**GD** and **ECH**). Despite being associated with a less favorable E-factor of 7.42, the conversion of **GLY** towards **GD** only relies on widely available and cheap reagents (~0.2 € g^{-1} for bio-based **GD**). More importantly, the overall productivity of the chlorination-dehydrochlorination sequence yields **GD** in 75% from bio-based **GLY** (Figure 5.38) in only 110 s. The application of this procedure in pilot scale was already successfully demonstrated by Monbaliu and coworkers with a productivity of 0.717 kg per day for **GD**.[130] These performances can be strengthened when combined with the downstream module of carbonation (Figure 5.38), achieving a cumulated E-factor of 12.39 with a total price estimated at 0.52 € g^{-1}. Relying on a similar flow strategy and 3.5 mol% of TBAB, the transesterification of **DMC** with neat **GLY** is also very appealing, offering a daily productivity of 13.6 kg of **GLC**.[28] The absence of solvent led to a low E-factor of 4.81, whereas the end-to-end cost, including the preparation of **DMC** starting from MeOH, was estimated to be 1.86 € g^{-1}. This latter example features a lower waste generation and allows the preparation of **GLC** from **GLY** in one step by using an activated carbonate (**DMC**). However, the preparation of **DMC** is much more time-consuming than the activation of **GLY** to form **GD**, which in turn allows the use of CO_2 as a carbonation agent. Considering the same daily production of **GLC**, the efficiency/cost balance of both processes was determined. The transesterification of **DMC** with **GLY** has a slightly more attractive price of 1860€ t^{-1}, compared to 1924 € t^{-1} for the carbonation of **GD**. However, the use of an excess of **DMC** combined with the release of MeOH makes the purification step cumbersome and expensive. To conclude, these examples illustrate the complex duality of process productivity versus cost efficiency. Furthermore, these projections are only based on the price of the reagents and do not include key parameters such as the purification, the energy consumption, as well as the working force, to name of few.

5.2.9 CONCLUSION

Stimulated by the EU's impulse to meet ambitious environmental objectives by 2030, new strategies toward the manufacturing of high value-added bio-based molecules are thriving. Both the chemical and chemical engineering communities have been very responsive and creative, triggering a global effort to design innovative processes to access marketable bio-based products. Among them, **GLC** is currently under the spotlight, with promising applications and favorable perspectives toward industrial production. Over the past two decades, numerous works have been published on the coupling of **GD** with CO_2 toward **GLC**. The first effort is dedicated to the development of highly performant catalytic systems. Soon enough, the literature was flooded with a wide range of metal, organic, and ionic liquid-based catalysts. The fruitfulness of these 20 last years led to the need of understanding the nature of the interactions between the catalyst and the substrates, and the structural features that drive the formation of **GLC**. This understanding is a critical step toward the rational design of better catalysts. Two main distinct mechanisms for the coupling of **GD** with CO_2 have

been elucidated using multidisciplinary approaches, often with the support of computational chemistry. The most conventional path requires assistance by a nucleophile, while a second path involves a proton shuttle mechanism, mediated by substrate activation of CO_2. Numerous catalytic cores have been explored for both metal- and organo- catalysts. Multiple designs for these catalysts have been investigated, focusing on activation of the epoxide, chemisorption of CO_2, activation of CO_2, as well as catalysts showing synergetic behaviors.

After elucidating the inherent mechanistic features and undergoing several rounds of catalyst optimization, significant progress has been made in achieving high yields of **GLC**. Among the challenges that persist, we highlight the separation and recyclability of catalysts, which continue to undermine the overall efficiency of the process, even for heterogeneous catalysts. Significant drops in performance are frequently reported after only a few cycles. Some seemingly overengineered catalytic systems are time- and resource-intensive to access. In other cases, unsuccessful downstream recovery of the product closes the door to potential industrial developments. The investigation of the global efficiency of some representative examples highlighted the necessity to develop performant, sustainable, and cost-efficient syntheses of catalysts. Indeed, downstream repercussions on the total price of the carbonation process are a critical parameter to bear in mind. Apart from very few processes under continuous conditions, the overall productivity of many of these processes does not seem to favor transposition to commercial scales.

To sum up, despite significant advances converging toward more efficient production routes for **GLC**, the development of economically viable and sustainable large-scale processes for the coupling of **GD** and CO_2 remains a significant challenge for the Chemistry and Chemical Engineering communities. Several years ago, the industrial forecast for **GLC** was very optimistic; however, its anticipated market growth has not been realized. It is evident that further reductions in overall production costs are vital. Future research efforts should now focus on (a) developing of the production of **GD** from waste **GLY**, (b) developing low-cost, sustainable, and recyclable catalysts, ideally compatible with low-purity **GD** and CO_2 from waste gaseous effluents, and (c) capitalizing on scalable process technologies from the early stages of development.

Table 5.2 Global assessment including the steps for catalyst preparation and for carbonation of GD, for selected examples discussed in this work.

Catalyst preparation				Carbonation of GD with CO_2						
Category	Catalytic site assessment[79 a]	Number of steps; Total reaction time; E-factor [b]	Global price; [c] Cumulated yield	Catalyst loading (mol%/wt %)	Additive loading (mol%) and solvent	Temperature (° C)	CO_2 Pressure (bar)	Reaction time (h)	GLC yield (%) E-factor [d] Score	Ref.
Entry				1						
Homogeneous metal	A1 $3.98*10^4$ Mt $year^{-1}$ 2k € t^{-1}	4, 28 h, 241.08	47% yield 17.18 € g^{-1}	5	/	35	1	24	91 94.71 89.5	[81]

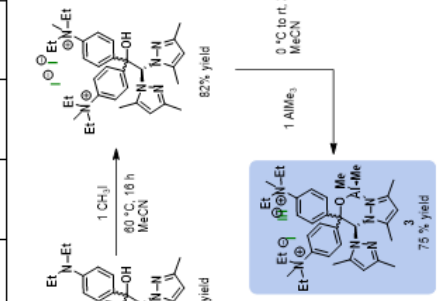

Catalyst preparation				Carbonation of GD with CO_2						
Category	Catalytic site assessment[79] [a]	Number of steps; Total reaction time; E-factor [b]	Global price; [c] Cumulated yield	Catalyst loading (mol%/wt %)	Additive loading (mol%) and solvent	Temperature (° C)	CO_2 Pressure (bar)	Reaction time (h)	GLC yield (%) E-factor [d] Score	Ref.
Entry										2
Homogeneous metal	Al $3.98*10^4$ Mt $year^{-1}$ 2k € t^{-1}	2, 6 h, 75.11	- 16.29 € g^{-1}	1	/ MEK	75	10	2	93 14.44 88.5	90,92, 172

Catalyst preparation				Carbonation of GD with CO_2							
Entry				3							
Category	Catalytic site assessment[79 a]	Number of steps; Total reaction time; E-factor [b]	Global price; [c] Cumulated yield	Catalyst loading (mol%/wt %)	Additive loading (mol%) and solvent	Temperature (° C)	CO_2 Pressure (bar)	Reaction time (h)	GLC yield (%) E-factor [d] Score	Ref.	
Homogeneous metal	Fe $12*10^6$ Mt year^{-1} 1.7k € t^{-1}	1, 48 h, 16.38	75% yield 17.57 € g^{-1}	0.1	TBD-HI 1.0	50	3	20	79 0.39 79.5	96	

Catalyst preparation				Carbonation of GD with CO_2						
Entry				4						
Category	Catalytic site assessment[79 a]	Number of steps; Total reaction time; E-factor [b]	Global price; [c] Cumulated yield	Catalyst loading (mol%/wt %)	Additive loading (mol%) and solvent	Temperature (° C)	CO_2 Pressure (bar)	Reaction time (h)	GLC yield (%) E-factor [d] Score	Ref.
Heterogeneous metal	Zn $1.25*10^4$ Mt $year^{-1}$ 1.82k € t^{-1}	2, 42 h, 11.07	- 4.18€ g^{-1}	8.3	TBAB 5.0	25	1	6	89 1.15 84.5	[99]

Catalyst preparation				Carbonation of GD with CO_2						
Entry				5						
Category	Catalytic site assessment[79 a]	Number of steps; Total reaction time; E-factor [b]	Global price; [c] Cumulated yield	Catalyst loading (mol%/wt %)	Additive loading (mol%) and solvent	Temperature (° C)	CO_2 Pressure (bar)	Reaction time (h)	GLC yield (%) E-factor [d] Score	Ref.
Homogeneous earth metal	Ca $3.16*10^4$ Mt $year^{-1}$ -	*In-situ*, 24 h, 1	*In-situ* 1.88 € g^{-1}	5	/	25	1	24	75 0.51 77.5	11 7

Catalyst preparation				Carbonation of GD with CO_2						
Entry										6
Category	Catalytic site assessment[79 a]	Number of steps; Total reaction time; E-factor [b]	Global price; [c] Cumulated yield	Catalyst loading (mol%/wt %)	Additive loading (mol%) and solvent	Temperature (° C)	CO_2 Pressure (bar)	Reaction time (h)	GLC yield (%) E-factor [d] Score	Ref.
Homogeneous organophosphorus	-	2; 26 h; 31.41	- 1.8 € g^{-1}	0.5	/	80	1	24	99 0.32 93.5	[12] [6]

Catalyst preparation				Carbonation of GD with CO_2						
Category	Catalytic site assessment[79 a]	Number of steps; Total reaction time; E-factor [b]	Global price; [c] Cumulated yield	Catalyst loading (mol%/wt %)	Additive loading (mol%) and solvent	Temperature (° C)	CO_2 Pressure (bar)	Reaction time (h)	GLC yield (%) E-factor [d] Score	Ref.
Homogeneous organocatalyst	-	2, 8 h, 9.42	82% yield 5.40 € g^{-1}	1	/	140	10	0.008	78 4.56 83	[13] 1,173

Catalyst preparation				Carbonation of GD with CO_2						
Entry				8						
Category	Catalytic site assessment[79 a]	Number of steps; Total reaction time; E-factor [b]	Global price; [c] Cumulated yield	Catalyst loading (mol%/wt %)	Additive loading (mol%) and solvent	Temperature (° C)	CO_2 Pressure (bar)	Reaction time (h)	GLC yield (%) E-factor [d] Score	Ref.
Homogeneous organocatalyst	-	2, 36 h, 37.44	80% yield 1.69 € g^{-1}	2	/	25	10	6	99 2.52 90	[12] [2]

Catalyst preparation				Carbonation of GD with CO_2						
Category	Catalytic site assessment[79 a]	Number of steps; Total reaction time; E-factor [b]	Global price; [c] Cumulated yield	Catalyst loading (mol%/wt %)	Additive loading (mol%) and solvent	Temperature (° C)	CO_2 Pressure (bar)	Reaction time (h)	GLC yield (%) E-factor [d] Score	Ref.
Homogeneous organocatalyst	-	2, 36 h, 13.17	99% yield 2.94 € g^{-1}	0.02	/	120	20	8	95 1.11 79.5	[120]
									Entry	9

Catalyst preparation				Carbonation of GD with CO_2							
Category	Catalytic site assessment[79 a]	Number of steps; Total reaction time; E-factor [b]	Global price; [c] Cumulated yield	Catalyst loading (mol%/wt %)	Additive loading (mol%) and solvent	Temperature (° C)	CO_2 Pressure (bar)	Reaction time (h)	GLC yield (%) E-factor [d] Score	Ref.	Entry
Porous ionic liquid	-	3 48 h, 8.50	- 1.78 € g^{-1}	4.5	/	80	10	1	87 0.50 89.5	[146]	10

Catalyst preparation				Carbonation of GD with CO_2						
Entry				11						
Category	Catalytic site assessment[79 a]	Number of steps; Total reaction time; E-factor [b]	Global price; [c] Cumulated yield	Catalyst loading (mol%/wt %)	Additive loading (mol%) and solvent	Temperature (° C)	CO_2 Pressure (bar)	Reaction time (h)	GLC yield (%) E-factor [d] Score	Ref.
Heterogeneous ionic liquid	-	4 67 h, 14.96	- 8.97€ g^{-1}	3	/	80	1	4	82 9.78 88	[134]

Catalyst preparation				Carbonation of GD with CO_2							
Category	Catalytic site assessment[79] [a]	Number of steps; Total reaction time; E-factor [b]	Global price; [c] Cumulated yield	Catalyst loading (mol%/wt %)	Additive loading (mol%) and solvent	Temperature (° C)	CO_2 Pressure (bar)	Reaction time (h)	GLC yield (%) E-factor [d] Score	Ref.	Entry
Porous ionic liquid	-	1 24 h, 10.44	91% yield 2.94€ g^{-1}	27*	/	30	1	72	85 2.04 82.5	15 1	12
c. 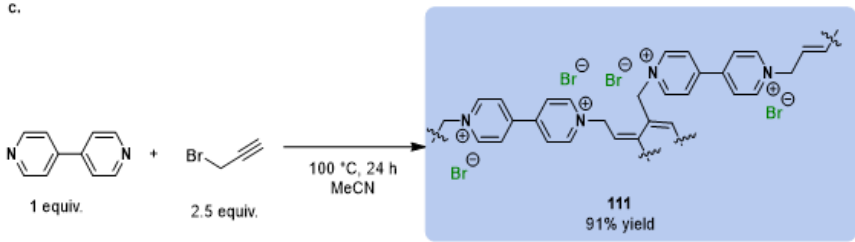											

[a] Prices and global production of catalytic metals are reported. [b] All the reagents and solvents involved in the calculation of the E-factor are considered as not recyclable. [c] All the costs of reagent and solvent used to calculate the total price of catalyst preparation were found on Sigma-Aldrich and VWR websites.[80] [d] Calculated with the formula *E-factor = (mass of total inputs) – (mass of valuable products)/mass of valuable products*. E-factor calculation includes CO_2 (gas volume fixed to reactor volume) and solvent. The catalyst is not usually considered in the calculation of the E factor. However, numerous papers indicate that the performances of their catalysts decrease over the time. Therefore, the mass of catalyst that is lost for every run is considered. See supporting information for details on calculations

5.2.10 REFERENCES

[1] *https://www.iea.org/topics/global-energy-crisis*, accessed 2022-12-22.

[2] *https://cefic.org/media-corner/newsroom/energy-crisis-the-eu-chemical-industry-is-reaching-breaking-point/*, accessed 2022-12-22.

[3] Sonnati, M. O.; Amigoni, S.; Taffin De Givenchy, E. P.; Darmanin, T.; Choulet, O.; Guittard, F. Glycerol Carbonate as a Versatile Building Block for Tomorrow: Synthesis, Reactivity, Properties and Applications. *Green Chem.* **2013**, *15*, 283–306.

[4] Muzyka, C.; Monbaliu, J.-C. M. Perspectives for the Upgrading of Bio-Based Vicinal Diols within the Developing European Bioeconomy. *ChemSusChem* **2022**, *15* (5), e202102391.

[5] *https://energy.ec.europa.eu/topics/renewable-energy/renewable-energy-directive-targets-and-rules/renewable-energy-directive_en*, accessed 2022-12-22.

[6] *https://www.europarl.europa.eu/committees/fr/renewable-energy-directive-red-ii-/product-details/20220214CDT09123*, accessed 2022-12-22.

[7] Chen, Y.; Cattoen, M.; Monbaliu, J.-C. M. 8 Mitigation of Chemical Hazards under Continuous Flow Conditions. Darvas, F.; Dormàn, G.G; Hessel, V.; Ley, S. V.; Eds.; *In Flow Chemistry -Fundamentals*, Vol. 1; De Gruyter: Berlin, **2021**, 269–312.

[8] Dabral, S.; Schaub, T. The Use of Carbon Dioxide (CO_2) as a Building Block in Organic Synthesis from an Industrial Perspective. *Adv. Synth. Catal.* **2018**, *361*, 223–246.

[9] Grignard, B.; Gennen, S.; Jérôme, C.; Kleij, A. W.; Detrembleur, C. Advances in the Use of CO_2 as a Renewable Feedstock for the Synthesis of Polymers. *Chem. Soc. Rev.* **2019**, *48*, 4466–4514.

[10] Seo, H.; Nguyen, L. v.; Jamison, T. F. Using Carbon Dioxide as a Building Block in Continuous Flow Synthesis. *Adv. Synth. Catal.* **2019**, *361* (2), 247–264.

[11] Limburg, B.; Cristòfol, À.; della Monica, F.; Kleij, A. W. Unlocking the Potential of Substrate-Directed CO_2 Activation and Conversion: Pushing the Boundaries of Catalytic Cyclic Carbonate and Carbamate Formation. *ChemSusChem* **2020**, *13* (23), 6056–6065.

[12] Hasan, M. M. F.; Rossi, L. M.; Debecker, D. P.; Leonard, K. C.; Li, Z.; Makhubela, B. C. E.; Zhao, C.; Kleij, A. Can CO_2 and Renewable Carbon Be Primary Resources for Sustainable Fuels and Chemicals? *ACS Sustainable Chem. Eng.* **2021**, *9* (37), 12427–12430.

[13] Kaisin, G.; Bovy, L.; Joyard, Y.; Maindron, N.; Tadino, V.; Monbaliu, J.-C. M. A Perspective on Automated Advanced Continuous Flow Manufacturing Units for the Upgrading of Biobased Chemicals toward Pharmaceuticals. *J. Flow Chem.* **2022**, *13*, 77–90.

[14] Monbaliu, J.-C. M.; Legros, J. Will the next Generation of Chemical Plants Be in Miniaturized Flow Reactors? *Lab Chip* **2023**, *23*, 1349–1357.

[15] Monie, F.; Grignard, B.; Thomassin, J.-M.; Mereau, R.; Tassaing, T.; Jerome, C.; Detrembleur, C. Chemo-and Regioselective Additions of Nucleophiles to Cyclic Carbonates for the Preparation of Self-Blowing Non-Isocyanate Polyurethane Foams. *Angew. Chem. Int. Ed.* **2020**, *59*, 17033–17041.

[16] Carré, C.; Ecochard, Y.; Caillol, S.; Avérous, L. From the Synthesis of Biobased Cyclic Carbonate to Polyhydroxyurethanes: A Promising Route towards Renewable Non-Isocyanate Polyurethanes. *ChemSusChem* **2019**, *12* (15), 3410–3430.

[17] Maisonneuve, L.; Lamarzelle, O.; Rix, E.; Grau, E.; Cramail, H. Isocyanate-Free Routes to Polyurethanes and Poly(Hydroxy Urethane)s. *Chem. Rev.* **2015**, *115*, 12407–12439.

[18] Gomez-Lopez, A.; Elizalde, F.; Igo Calvo, I.; Sardon, H. Trends in Non-Isocyanate Polyurethane (NIPU) Development. *Chem. Commun.* **2021**, *57*, 12254–12265.

[19] Li, R.; Bobbink, F. D.; Van Muyden, A. P.; Dyson, P. J. En Route to CO_2-Containing Renewable Materials: Catalytic Synthesis of Polycarbonates and Non-Isocyanate Polyhydroxyurethanes Derived from Cyclic Carbonates. *Chem. Commun.* **2019**, *55*, 1360–1373.

[20] Evarts, E. C. Lithium Batteries: To the Limits of Lithium. *Nature* **2015**, *526*, S93–S95.

[21] Pescarmona, P. P. Cyclic Carbonates Synthesised from CO_2: Applications, Challenges and Recent Research Trends. *Curr. Opin. Green Sustain. Chem.* **2021**, *29*, 100457.

[22] Gesval. Market Analysis on Glycerol Carbonate. **2023**.

[23] Newry. Glycerol Carbonate Market Assessment. **2023**.

[24] Gérardy, R. G.; Debecker, D. P.; Estager, J.; Luis, P.; Monbaliu, J.-C. M. Continuous Flow Upgrading of Selected C2 −C6 Platform Chemicals Derived from Biomass. *Chem. Rev.* **2020**, *120*, 7219–7347.

[25] Aomchad, V.; Cristòfol, À.; Monica, F. della; Limburg, B.; D'elia, V.; Kleij, A. W. Recent Progress in the Catalytic Transformation of Carbon Dioxide into Biosourced Organic Carbonates. *Green Chem.* **2021**, *23*, 1077–1113.

[26] Zanda, N.; Sobolewska, A.; Alza, E.; Kleij, A. W.; Pericàs, M. A. Organocatalytic and Halide-Free Synthesis of Glycerol Carbonate under Continuous Flow. *ACS Sustainable Chem. Eng.* **2021**, *9*,4391–4397.

[27] Wang, Z.; Gérardy, R.; Gauron, G.; Damblon, C.; Monbaliu, J.-C. M. Solvent-Free Organocatalytic Preparation of Cyclic Organic Carbonates under Scalable Continuous Flow Conditions. *React. Chem. Eng.* **2018**, *4* (1), 17–26.

[28] Gérardy, R.; Estager, J.; Luis, P.; Debecker, D. P.; Monbaliu, J.-C. M. Versatile and Scalable Synthesis of Cyclic Organic Carbonates under Organocatalytic Continuous Flow Conditions. *Catal. Sci. Technol.* **2019**, *9* (24), 6841–6851.

[29] Zanda, N.; Zhou, L.; Alza, E.; Kleij, A. W.; Pericàs, M. Continuous Organocatalytic Flow Synthesis of 2-Substituted Oxazolidinones Using Carbon Dioxide. *Green Chem.* **2022**, *24* (11), 4628–4633.

[30] Poolwong, J.; Aomchad, V.; del Gobbo, S.; Kleij, A. W.; D'Elia, V. Simple Halogen-Free, Biobased Organic Salts Convert Glycidol to Glycerol Carbonate under Atmospheric CO_2 Pressure. *ChemSusChem* **2022**, *15* (17), e202200765.

[31] Rintjema, J.; Kleij, A. W. Substrate-Assisted Carbon Dioxide Activation as a Versatile Approach for Heterocyclic Synthesis. *Synthesis* **2016**, *48* (22), 3863–3878.

[32] Kleij, A. W. Advancing Halide-Free Catalytic Synthesis of CO_2-Based Heterocycles. *Curr. Opin. Green Sustain. Chem.* **2020**, *24*, 72–81.

[33] Huang, R.; Rintjema, J.; González-Fabra, J.; Martín, E.; Escudero-Adán, E. C.; Bo, C.; Urakawa, A.; Kleij, A. W. Deciphering Key Intermediates in the Transformation of Carbon Dioxide into Heterocyclic Products. *Nat. Catal.* **2019**, *2* (1), 62–70.

[34] Guo, L.; Lamb, K. J.; North, M. Recent Developments in Organocatalysed of Epoxides and Carbon into Cyclic Carbonates. *Green Chem.* **2021**, *23*, 77–118.

[35] Jin, T.; Dong, F.; Liu, Y.; Hu, Y. L. Novel and Effective Strategy of Dual Bis(Trifluoromethylsulfonyl)Imide Imidazolium Ionic Liquid Immobilized on Periodic Mesoporous Organosilica for Greener Cycloaddition of Carbon Dioxide to Epoxides. *New J. Chem.* **2019**, *43*, 2583–2590.

[36] Li, G.; Dong, S.; Fu, P.; Yue, Q.; Zhou, Y.; Wang, J. Synthesis of Porous Poly(Ionic Liquid)s for Chemical CO_2 Fixation with Epoxides. *Green Chem* **2022**, *24*, 3433–3460.

[37] Zhang, Y.; Chen, G.; Wu, L.; Liu, K.; Zhong, H.; Long, Z.; Tong, M.; Yang, Z.; Dai, S.; Li, R. Two-in-One: Construction of Hydroxyl and Imidazolium-Bifunctionalized Ionic Networks in One-Pot toward Synergistic Catalytic CO_2 Fixation. *Chem. Commun.* **2020**, *56*, 3309–3312.

[38] Xiong, X.; Zhang, H.; Lin Lai, S.; Gao, J.; Gao, L. Lignin Modified by Deep Eutectic Solvents as Green, Reusable, and Bio-Based Catalysts for Efficient Chemical Fixation of CO_2. *React. Funct. Polym.* **2020**, *149*, 104502.

[39] Liu, F.; Hu, Y.; Zhou, J.; Zhang, Z.; Zhu, Z.; Zhang, J.; Wang, L. "Responsive" Ionic Liquids to Catalyze the Transformation of Carbon Dioxide under Atmospheric Pressure. *Appl. Catal. A Gen.* **2021**, *623*, 118241.

[40] Alves, M.; Grignard, B.; Mereau, R.; Jerome, C.; Tassaing, T.; Detrembleur, C. Organocatalyzed Coupling of Carbon Dioxide with Epoxides for the Synthesis of Cyclic Carbonates: Catalyst Design and Mechanistic Studies. *Catal. Sci. Technol.* **2017**, *7*, 2651–2684.

[41] Luo, H.; Ren, J.; Sun, Y.; Liu, Y.; Zhou, F.; Shi, G.; Zhou, J. Recent Advances in Chemical Fixation of CO_2 Based on Flow Chemistry. *Chin. Chem. Lett.* **2023**, *34* (5), 107782.

[42] D'Elia, V.; Kleij, A. W. Surface Science Approach to the Heterogeneous Cycloaddition of CO_2 to Epoxides Catalyzed by Site-Isolated Metal Complexes and Single Atoms: A Review. *Green Chem. Eng.* **2022**, *3*, 210–227.

[43] Usman, M.; Rehman, A.; Saleem, F.; Abbas, A.; Eze, V. C.; Harvey, A. Synthesis of Cyclic Carbonates from CO_2 Cycloaddition to Bio-Based Epoxides and Glycerol: An Overview of Recent Development. *RSC Adv.* **2023**, *13*, 22717–22743.

[44] Aomchad, V.; Cristòfol, À.; Monica, F. Della; Limburg, B.; D'Elia, V.; Kleij, A. W. Recent Progress in the Catalytic Transformation of carbon Dioxide into Biosourced Organic. *Green Chem.* **2021**, *23*, 1077–1113.

[45] Chowdhury, A. H.; Chowdhury, I. H.; Islam, S. M. Titanium Phosphate with Flower-like Morphology as an Effective Reusable Catalyst for Chemical Fixation of CO_2 at Mild Reaction Conditions. *Ind. Eng. Chem. Res.* **2019**, *58* (27), 11779–11786.

[46] Lin Hu, Y.; Bo Wang, H.; Wei Chen, Z.; Guang Li, X.; Hu, Y. L.; Wang, H. B.; Chen, Z. W.; Li, X. G. Titanium Incorporated Mesoporous Silica Immobilized Functional Ionic Liquid as an Efficient Reusable Catalyst for Cycloaddition of Carbon Dioxide to Epoxides. *ChemistrySelect* **2018**, *3*, 5087–5091.

[47] Park, J.; Cho, K.; Ko, Y.-J.; Hyun Kim, M.; Song, T.; Ryung Seo, U.; Eun Park, J.; Moon Lee, S.; Jin Kim, H.; Keun Chung, Y.; Son, S. Hollow and Microporous Catalysts Bearing Cr(III)-F Porphyrins for Room Temperature CO_2 Fixation to Cyclic Carbonates. *J. Mater. Chem. A* **2017**, *5*, 23612-23619.

[48] Liu, Y.; Li, S.; Yu, X.; Chen, Y.; Tang, X.; Hu, T.; Shi, L.; Pudukudy, M.; Shan, S.; Zhi, Y. Cellulose Nanofibers (CNF) Supported (Salen)Cr(III) Composite as an Efficient Heterogeneous Catalyst for CO 2 Cycloaddition. *Mol. Catal.* **2023**, *547*, 113344.

[49] Tong, Y.; Cheng, R.; Dong, H.; Liu, B. Efficient Cycloaddition of CO_2 and Epoxides to Cyclic Carbonates Using Salen-Based Covalent Organic Framework as a Heterogeneous Catalyst. *J. Porous Mater.* **2022**, *29*, 1253–1263.

[50] Yao, N.; Chen, C.; Li, D. J.; Lin Hu, Y. Cobalt Nanoparticles Embedded over Periodic Mesoporous Organosilica Functionalized with Benzotriazolium Ionic Liquid for Efficient and Heterogeneous Catalytic Transformation of Carbon Dioxide to Cyclic Carbonates. *J. Environ. Chem. Eng.* **2020**, *8*, 103953.

[51] Li, Y.; Weng, S.; Wang, S.; Zhang, G.; Liu, F.; Liu, M. Engineering the Activity and Stability of ZIF-8(Zn/Co)@g-C_3N_4 Nanocomposites and Their Synergistic Action in Converting Atmospheric CO_2 into Cyclic Carbonates. *J. Colloid. Interface Sci.* **2023**, *656*, 24–34.

[52] Álvarez-Miguel, L.; Burgoa, J. D.; Mosquera, M. E. G.; Hamilton, A.; Whiteoak, C. J. Catalytic Formation of Cyclic Carbonates Using Gallium Aminotrisphenolate Compounds and Comparison to Their Aluminium Congeners: A Combined Experimental and Computational Study. *ChemCatChem* **2021**, *13*, 4099–4110.

[53] Cheng, J.; Lu, C.; Zhao, B. Cycloaddition of Carbon Dioxide and Epoxides Catalyzed by Rare Earth Metal Complexes Bearing a Trost Ligand. *New J. Chem.* **2021**, *45*, 13096–13103.

[54] Hua, L.; Li, B.; Han, C.; Gao, P.; Wang, Y.; Yuan, D.; Yao, Y. Synthesis of Homo- And Heteronuclear Rare-Earth Metal Complexes Stabilized by Ethanolamine-Bridged Bis(Phenolato) Ligands and Their Application in Catalyzing Reactions of CO_2 and Epoxides. *Inorg. Chem.* **2019**, *58*, 8775–8786.

[55] Ho J.; Nord T. M.; Stafford P. J.; Stylianou C. K. Ruthenium-Based Metal–Organic Framework Catalyst for CO_2 Fixation onto Epoxides. *Catal. Sci. Technol.* **2022**, *12*, 6998–7002.

[56] Liu J.; Fan, Y.-Z.; Li X.; Xu Y-W; Zhang L.; Su, C.-Y. Catalytic Space Engineering of Porphyrin Metal-Organic Frameworks for Combined CO_2 Capture and Conversion at a Low Concentration. *ChemSusChem* **2018**, *11*, 2340–2347.

[57] Khatun, R.; Bhanja, P.; Mondal, P.; Bhaumik, A.; Das, D.; Islam, S. M. Palladium Nanoparticles Embedded over Mesoporous TiO_2 for Chemical Fixation of CO_2 under Atmospheric Pressure and Solvent-Free Conditions. *New J. Chem.* **2017**, *41*, 12937–12946.

[58] Rani, P.; Husain, A.; Bhasin, K. K.; Kumar, G. Metal−Organic Framework-Based Selective Molecular Recognition of Organic Amines and Fixation of CO_2 into Cyclic Carbonates. *Inorg. Chem.* **2022**, *2022*, 6977–6994.

[59] Liu, S.; Hu, T.; Yang, K.; Zhang, X. Robust $\{Cd_4\}$-Organic Framework for Efficiently Catalyzing CO_2 Cycloaddition and Knoevenagel Condensation. *Cryst. Growth Des.* **2023**, *23*, 3320–3329.

[60] Liu, S.; Chen, H.; Fan, L.; Zhang, X. Highly Robust $\{In_2\}$-Organic Framework for Efficiently Catalyzing CO_2 Cycloaddition and Knoevenagel Condensation. *Inorg. Chem.* **2023**, *62*, 3562–3572.

[61] Sinchow, M.; Semakul, N.; Konno, T.; Rujiwatra, A. Lanthanide Coordination Polymers through Design for Exceptional Catalytic Performances in CO_2 Cycloaddition Reactions. *ACS Sustainable Chem. Eng.* **2021**, *9*, 8581–8591.

[62] Hoseini, K. S.; Razaghi, M.; Nouri, T.; Khorasani, M. Direct Coupling of CO_2 with Epoxides Catalyzed by Lanthanum(III) Supported on Magnetic Mesoporous Organosilica Nanoparticles. *Sci. Rep.* **2023**, *13*, 5521.

[63] Martínez, J.; Fernández-Baeza, J.; Sánchez-Barba, L. F.; Castro-Osma, J. A.; Lara-Sánchez, A.; Otero, A. An Efficient and Versatile Lanthanum Heteroscorpionate Catalyst for Carbon Dioxide Fixation into Cyclic Carbonates. *ChemSusChem* **2017**, *10*, 2886–2890.

[64] Wang, W. M.; Cheng, R. R.; Wu, Z. L.; Cui, J. Z. Bifunctional Lanthanide-Based Coordination Polymers: Conversion of CO_2 and Highly Selective Luminescence Sensing for Acetylacetone. *Inorg. Chem.* **2023**, *62*, 14902–14911.

[65] Gao, J.; Yue, C.; Wang, H.; Li, J.; Yao, H.; Wang, M. Y.; Ma, X. CeO_2-ZrO_2 Solid Solution Catalyzed and Moderate Acidic–Basic Sites Dominated Cycloaddition of CO_2 with Epoxides: Halogen-Free Synthesis of Cyclic Carbonates. *Catalysts* **2022**, *12* (6), 632.

[66] Yang, Q.; Wang, Y.; Tang, X.; Zhang, Q.; Dai, S.; Peng, H.; Lin, Y.; Tian, Z.; Lu, Z.; Chen, L. Ligand Defect Density Regulation in Metal-Organic Frameworks by Functional Group Engineering on Linkers. *Nano. Lett.* **2022**, *22* (2), 838–845.

[67] Das, S. K.; Chatterjee, S.; Bhunia, S.; Mondal, A.; Mitra, P.; Kumari, V.; Pradhan, A.; Bhaumik, A. A New Strongly Paramagnetic Cerium-Containing Microporous MOF for CO_2 Fixation under Ambient Conditions. *Dalton Trans* **2017**, *46*, 13783–13792.

[68] Lv, H.; Chen, H.; Fan, L.; Zhang, X. Heterometallic {ZnEu}-Metal–Organic framework for Efficient Chemical Fixation of CO_2. *Dalton Trans* **2020**, *49*, 14656–14664.

[69] Li, L.; Zou, J. Y.; You, S. Y.; Zhang, L. Ratiometric Fluorescence Thermometry, Quantitative Gossypol Detection, and CO_2 Chemical Fixation by a Multipurpose Europium (III) Metal-Organic Framework. *Inorg. Chem.* **2023**, *62*, 14168–14179.

[70] Qiao, N.; Xin, X.-Y.; Wang, W.-M.; Wu, Z.-L.; Cui, J.-Z. Two Novel Ln8 Clusters Bridged by CO3 Convert CO_2 into Oxazolidinones and cyclic Carbonates. *Dalton Trans* **2023**, *52*, 10725–10736.

[71] Chen, H.; Fan, L.; Lv, H.; Zhang, X. Robust Anionic LnIII-Organic Frameworks: Chemical Fixation of CO_2, Tunable Light Emission, and Fluorescence Recognition of Fe_3+. *Inorg. Chem.* **2020**, *59*, 13407–13415.

[72] Miao, C.-Q.; Yan, J.-C.; Yang, C.; Wang, J.-L.; Ding, J.-L.; Chen, S.-R.; Ge, J.-X.; Wang, N.; Hou, Y.-L. Two Tetranuclear Tb(III)-Based Clusters: Crystal Structures and Effectively Catalyze the Cycloaddition of CO_2 with Epoxides. *Polyhedron* **2023**, *243*, 116509.

[73] Lv, H.; Chen, H.; Fan, L.; Zhang, X. Nanocage-Based Tb3+-Organic Framework for Efficiently Catalyzing the Cycloaddition Reaction of CO_2 with Epoxides and Knoevenagel Condensation. *Inorg. Chem.* **2022**, *61*, 15558–15568.

[74] Chen, H.; Fan, L.; Zhang, X.; Ma, L. Nanocage-Based InIII$\{TbIII\}_2$-Organic Framework Featuring Lotus-Shaped Channels for Highly Efficient CO_2 Fixation and I_2 Capture. *ACS Appl. Mater. Interfaces* **2020**, *12*, 27803–27811.

[75] Li, R.; Dalton, Wang, G.; Xu, C.; Wang, L.; Liu, W. Highly Efficient 3d/4d–4f Coordination Polymer Catalysts for Carbon Dioxide Fixation into Cyclic Carbonates. *Dalton Trans* **2018**, *47*, 12711–12717.

[76] Wang, W. M.; Qiao, N.; Xin, X. Y.; Wu, Z. L.; Cui, J. Z. Octanuclear Ln(III)-Based Clusters Assembled by a Polydentate Schiff Base Ligand and a β-Diketone Co-Ligand: Efficient Conversion of CO_2 to Cyclic Carbonates and Large Magnetocaloric Effect. *Cryst. Growth Des.* **2023**, *23*, 87–95.

[77] Zhao, J.-Y.; Yang, C.; Bian, X.-Y.; Qiu, J.; Ren, S.-Y.; Fang, M. A Tetranuclear Er(III)-Based Cluster with Bifunctional Properties: Efficient Conversion of CO_2 and Slow Magnetic Relaxation Behavior. *Inorg. Chim. Acta* **2023**, *556*, 121560.

[78] Zhang, R.; Wang, L.; Xu, C.; Yang, H.; Chen, W.; Gao, G.; Liu, W. Anion-Induced 3d–4f Luminescent Coordination Clusters: Structural Characteristics and Chemical Fixation of CO_2 under Mild Conditions. *Dalton Trans* **2018**, *47*, 7159–7165.

[79] Gao, Y.; Guo, L.; Zhang, X. A Highly Robust Lutecium(III)-Organic Framework for the High Catalytic Performance on the Chemical Fixation CO_2. *J. Mol. Struct.* **2023**, *1272*, 134192.

[80] Vesborg, P. C. K.; Jaramillo, T. F. Addressing the Terawatt Challenge: Scalability in the Supply of Chemical Elements for Renewable Energy. *RSC Adv.* **2012**, *2*, 7933–7947.

[81] De La Cruz-Martínez, F.; Martínez, J.; Gaona, M. A.; Fernández-Baeza, J.; Sánchez-Barba, L. F.; Rodríguez, A. M.; Castro-Osma, J. A.; Otero, A.; Lara-Sánchez, A. Bifunctional Aluminum Catalysts for the Chemical Fixation of Carbon Dioxide into Cyclic Carbonates. *ACS Sustainable Chem. Eng.* **2018**, *6*, 5322–5332.

[82] Martínez, J.; De La Cruz-Martínez, F.; Gaona, M. A.; Pinilla-Pealver, E.; Fernández-Baeza, J.; Rodríguez, A. M.; Castro-Osma, J. A.; Otero, A.; Lara-Sánchez, A. Influence of the Counterion on the Synthesis of Cyclic Carbonates Catalyzed by Bifunctional Aluminum Complexes. *Inorg. Chem.* **2019**, *58*, 3396–3408.

[83] Alonso-Moreno, C.; Garcés, A.; Sánchez-Barba, L. F.; Fajardo, M.; Fernández-Baeza, J.; Otero, A.; Lara-Sánchez, A.; Antiñolo, A.; Broomfield, L.; López-Solera, M. I.; Rodríguez, A. M. Discrete Heteroscorpionate Lithium and Zinc Alkyl Complexes. Synthesis, Structural Studies, and ROP of Cyclic Esters. *Organometallics* **2008**, *27*, 1310–1321.

[84] Navarro, M.; Sánchez-Barba, L. F.; Garcés, A.; Fernández-Baeza, J.; Fernández, I.; Lara-Sánchez, A.; Rodríguez, A. M. Bimetallic Scorpionate-Based Helical Organoaluminums for the Efficient Carbon Dioxide Fixation into a Variety of Cyclic Carbonates. *Catal. Sci. Technol.* **2020**, *10*, 3265–3278.

[85] Gaona, M. A.; De La Cruz-Martínez, F.; Fernández-Baeza, J.; Sánchez-Barba, L. F.; Alonso-Moreno, C.; Rodríguez, A. M.; Rodríguez-Diéguez, A.; Castro-Osma, J. A.; Otero, A.; Lara-Sánchez, A. Synthesis of Helical Aluminium Catalysts for Cyclic Carbonate Formation. *Dalton Trans* **2019**, *48*, 4218-4227.

[86] Rios Yepes, Y.; Quintero, C.; Osorio Meléndez, D.; Daniliuc, C. G.; Martínez, J.; Rojas, R. S. Cyclic Carbonates from CO_2 and Epoxides Catalyzed by Tetra- and Pentacoordinate Amidinate Aluminum Complexes. *Organometallics* **2019**, *38*, 469–478.

[87] Wu, X.; North, M. A Bimetallic Aluminium(Salphen) Complex for the Synthesis of Cyclic Carbonates from Epoxides and Carbon Dioxide. *ChemSusChem* **2017**, *10*, 74–78.

[88] Carvalho, P. A.; Comerford, J. W.; Lamb, K. J.; North, M.; Reiss, P. S. Influence of Mesoporous Silica Properties on Cyclic Carbonate Synthesis Catalysed by Supported Aluminium(Salen) Complexes. *Adv. Synth. Catal.* **2019**, *361*, 345–354.

[89] Rios Yepes, Y.; Martínez, J.; Rangel Sánchez, H.; Quintero, C.; Carmen Ortega-Alfaro, M.; López-Cortés, J. G.; Daniliuc, C. G.; Antiñolo, A.; Ramos, A.; Rojas, R. S. Aluminum Complexes with New Non-Symmetric Amidine Ligands and Their Application in CO_2 Transformation into Cyclic Carbonates. *Dalton Trans.* **2020**, *49*, 1124–1134.

[90] Rintjema, J.; Epping, R.; Iulia Fiorani, G.; Martín, E.; Escudero-Adµn, E. C.; Kleij, A. W. Substrate-Controlled Product Divergence: Conversion of CO_2 into Heterocyclic Products. *Angew. Chem. Int. Ed.* **2016**, *55*, 3972–3976.

[91] Whiteoak, C. J.; Kielland, N.; Laserna, V.; Castro-Gõmez, F.; Martin, E.; Escudero-Adán, E. C.; Bo, C.; Kleij, A. W. Highly Active Aluminium Catalysts for the Formation of Organic Carbonates from CO_2 and Oxiranes. *Chem. Eur. J.* **2014**, *20*, 2264–2275.

[92] Kol, M.; Shamis, M.; Goldberg, I.; Goldschmidt, Z.; Al, S.; Hayut-Salant, E. Titanium(IV) Complexes of Trianionic Amine Triphenolate Ligands. *Inorg. Chem. Commun.* **2001**, *4*, 177–179.

[93] Alhashmialameer, D.; Ikpo, N.; Collins, J.; Dawe, L. N.; Hattenhauer, K.; Kerton, F. M. Ring-Opening Polymerization of Rac-Lactide Mediated by Tetrametallic Lithium and Sodium Diamino-Bis(Phenolate) Complexes. *Dalton Trans.* **2015**, *44*, 20216–20231.

[94] Alhashmialameer, D.; Collins, J.; Hattenhauer, K.; Kerton, F. M. Iron Amino-Bisphenolate Complexes for the formation of Organic Carbonates from CO_2 And Oxiranes. *Catal. Sci. Technol.* **2016**, *6*, 5364–5373.

[95] Seong, E. Y.; Kim, J. H.; Kim, N. H.; Ahn, K. H.; Kang, E. J. Multifunctional and Sustainable Fe-Iminopyridine Complexes for the Synthesis of Cyclic Carbonates. *ChemSusChem* **2019**, *12*, 409–415.

[96] Kim, J. H.; Lee, H.; Kim, N. H.; Kang, E. J. Sustainable Synthesis of Five-Membered Heterocycles Using Carbon Dioxide and Fe-Iminopyridine Catalysts. *J. CO_2 Util.* **2021**, *50*, 101595.

[97] Ghosh, S.; Bhanja, P.; Salam, N.; Khatun, R.; Bhaumik, A.; Islam, S. M. Porous Iron-Phosphonate Nanomaterial as an Efficient Catalyst for the CO_2 Fixation at Atmospheric Pressure and Esterification of Biomass-Derived Levulinic Acid. *Catal. Today* **2018**, *309*, 253–262.

[98] Roy, S.; Banerjee, B.; Bhaumik, A.; Islam, S. M. CO_2 Fixation at Atmospheric Pressure: Porous ZnSnO3 Nanocrystals as a Highly Efficient Catalyst for the Synthesis of Cyclic Carbonates. *RSC Adv.* **2016**, *6*, 31153–31160.

[99] Ghosh, S.; Mondal, P.; Das, D.; Tuhina, K.; Islam, S. M. Use of PS-Zn-Anthra Complex as an Efficient Heterogeneous Recyclable Catalyst for Carbon Dioxide Fixation Reaction at Atmospheric Pressure and Synthesis of Dicoumarols under Greener Pathway. *J Organomet. Chem.* **2018**, *866*, 1–12.

[100] Lang, X.-D.; Yu, Y.-C.; He, L.-N. Zn-Salen Complexes with Multiple Hydrogen Bonding Donor and Protic Ammonium Bromide: Bifunctional Catalysts for CO_2 Fixation with Epoxides at Atmospheric Pressure. *J. Mol. Catal. A Chem.* **2016**, *420*, 208–215.

[101] Dela Cruz, J. A. B.; Hung, C. H. Ni and Zn N-Confused Porphyrin Complexes as Recyclable Catalysts for High Efficiency Solvent-Free CO_2 fixation into Cyclic Carbonates. *Catal. Sci. Technol.* **2021**, *11*, 2144–2154.

[102] Navarro, M.; Garcés, A.; Sánchez-Barba, L. F.; González-Lizana, D.; Lara-Sánchez, A. Very Efficient Organo-Zinc Scorpionates for CO_2 into a Variety of Cyclic Carbonates: Synthesis, Coordination Ability and Catalytic Studies. *Dalton Trans.* **2023**, *52*, 6105–6116.

[103] Lan, D.-H.; Chen, K.; Zhu, H.-J.; Shen, J.; Wu, S.-S.; Au, C.-T.; Yi, B.; Yin, S. Hexamethylenetetramine Complexes as Easy-to-Handle and Efficient Lewis Acid−Base Heterogeneous Catalysts for Coupling of CO_2 under Mild Conditions. *Ind. Eng. Chem. Res.* **2022**, *61*, 11390–11396.

[104] Zhang, S.; Han, F.; Yan, S.; He, M.; Miao, C.; He, L. N. Efficient Catalysts In Situ Generated from Zinc, Amide and Benzyl Bromide for Epoxide/CO_2 Coupling Reaction at Atmospheric Pressure. Chem. *Eur. J.* **2019**, *2019*, 1311–1316.

[105] Trivedi, M.; Yadav, A. K.; Singh, G.; Kumar, A.; Kumar, G.; Husain, A.; Rath, N. P. Synthetic, Spectral, Structural and Catalytic Activity of Infinite 3-D and 2-D Copper(II) Coordination Polymers for Substrate Size-Dependent Catalysis for CO_2 Conversion. *Dalton Trans.* **2019**, *48*, 10078–10088.

[106] Song, J. Y.; Chen, X.; Wang, Y. M.; Luo, X.; Zhang, T. E.; Ning, G. H.; Li, D. Tuning the Catalytic Activity of Covalent Metal-Organic Frameworks for CO_2 Cycloaddition Reactions. *Asian J. Chem.* **2023**, *18*, e202300857.

[107] Ai, J.; Min, X.; Gao, C.-Y.; Tian, H.-R.; Dang, S.; Sun, Z.-M. A Copper-Phosphonate Network as a High-Performance Heterogeneous Catalyst for the CO_2 Cycloaddition Reactions and Alcoholysis of Epoxides. *Dalton Trans.* **2017**, *46*, 6756–6761.

[108] Wang, W. M.; Wang, W. T.; Wang, M. Y.; Gu, A. L.; Hu, T. D.; Zhang, Y. X.; Wu, Z. L. A Porous Copper-Organic Framework Assembled by [Cu12] Nanocages: Highly Efficient CO_2 Capture and Chemical Fixation and Theoretical DFT Calculations. *Inorg. Chem.* **2021**, *60*, 9122–9131.

[109] Yang, Y.; Tu, C.; Shi, J.; Yang, X.; Liu, J. J.; Cheng, F. New Stable Cu-K Metal-Organic Framework Constructed by a Bifunctional Ligand: Structure, Application in Dye Adsorption, and Catalytic CO_2 Cycloaddition Reaction. *Cryst. Growth Des.* **2022**, *22*, 4813–4820.

[110] Yang, Y.; Guo, Z.; Chen, X.-H.; Liu, J. A Ni3O-Cluster Based Porous MOF for Catalytic Conversion of CO_2 to Cyclic Carbonates A Novel Ni3O-Based MOF, *J. Solid State Chem.* **2019**, *276*, 190–193.

[111] Gao, C. Y.; Yang, Y.; Xu, N.; Liu, J.; Duan, L.; Chen, X.; Bao, M. A NiII Phosphonate as an Efficient Catalyst for the Synthesis of Cyclic Carbonate under Ambient Conditions. *Cryst. Growth Des.* **2021**, *21*, 1413–1417.

[112] Islam, S. S.; Bhanja, P.; Ghosh, K.; Molla, R. A.; Yasmin, N.; Das, D.; Islam, S. M. Mesoporous Zirconium Oxophosphate: An Efficient Catalyst for the Synthesis of Cyclic Acetals and Cyclic Carbonates under Solvent-Free Conditions. *ChemistrySelect* **2017**, *2*, 10595–10602.

[113] Zhao, X.; Tang, Y.; Wang, Y.; Rong, X.; Wu, P.; Li, Z.; Cai, N.; Deng, X.; Wang, J.; Li, R. C. Zirconium Metal-Organic Cage Decorated with Squaramides Imparts Dual Activation for Chemical Fixation of CO 2 under Mild Conditions. *Chem. Commun.* **2023**, *59*, 10944–10947.

[114] Terazzi, C.; Laatz, K.; Von Langermann, J.; Werner, T. Synthesis of Cyclic Carbonates Catalyzed by CaI2-Et3N and Studies on Their Biocatalytic Kinetic Resolution. *ACS Sustainable Chem. Eng.* **2022**, *10*, 13335–13342.

[115] Zhao, T.; Zhang, Y.; Liang, J.; Li, P.; Hu, X.; Wu Y. Multisite activation of epoxides by recyclable CaI_2/N-methyldiethanolamine catalyst for CO_2 fixation: A facile access to cyclic carbonates under mild conditions. *Mol. Catal.* **2018**, *450*, 87–94.

[116] Steinbauer, J.; Spannenberg, A.; Werner, T. An in Situ Formed Ca2+–Crown Ether Complex and Its Use in CO_2-Fixation Reactions with Terminal and Internal Epoxides. *Green Chem.* **2017**, *19*, 3769–3779.

[117] Hu, Y.; Steinbauer, J.; Stefanow, V.; Spannenberg, A.; Werner, T. Polyethers as Complexing Agents in Calcium-Catalyzed Cyclic Carbonate Synthesis. *ACS Sustainable Chem. Eng.* **2019**, *7*, 13257–13269.

[118] Kumar Mondal, R.; Riyajuddin, S.; Ghosh, A.; Ghosh, S.; Ghosh, K.; Islam, S. M. Polymer Immobilized [Mg@PS-Anthra] Complex: An Efficient Recyclable Heterogeneous Catalyst for the Incorporation of Carbon Dioxide into Oxiranes at Atmospheric Pressure and Knoevenagel Condensation Reaction under Solvent Free Condition. *J. Organomet. Chem.* **2019**, *880*, 322–332.

[119] Rasal, K. B.; Yadav, G. D.; Koskinen, R.; Keiski, R. Solventless Synthesis of Cyclic Carbonates by Direct Utilization of CO_2 Using Nanocrystalline Lithium Promoted Magnesia. *Mol. Catal.* **2018**, *451*, 200–208.

[120] Zhang, Y.; Yang, G.; Xie, R.; Yang, L.; Li, B.; Wu, G. Scalable, Durable, and Recyclable Metal-Free Catalysts for Highly Efficient Conversion of CO 2 to Cyclic Carbonates. *Angew. Chem. Int.* **2020**, *132*, 23491–23498.

[121] Mesías-Salazar, Á.; Martínez, J.; Rojas, R. S.; Carrillo-Hermosilla, F.; Ramos, A.; Fernández-Galán, R.; Antiñolo, A. Aromatic Guanidines as Highly Active Binary Catalytic Systems for the Fixation of CO_2 into Cyclic Carbonates under Mild Conditions. *Catal. Sci. Technol.* **2019**, *9*, 3879–3886.

[122] Hong, M.; Kim, Y.; Kim, H.; Cho, H. J.; Baik, M. H.; Kim, Y. Scorpionate Catalysts for Coupling CO_2 and Epoxides to Cyclic Carbonates: A Rational Design Approach for Organocatalysts. *J. Org. Chem.* **2018**, *83*, 9370–9380.

[123] Hu, Y.; Peglow, S.; Longwitz, L.; Frank, M.; Epping, J. D.; Brüser, V.; Werner, T. Plasma-Assisted Immobilization of a Phosphonium Salt and Its Use as a Catalyst in the Valorization of CO_2. *ChemSusChem* **2020**, *13*, 1825–1833.

[124] Büttner, H.; Steinbauer, J.; Werner, T. Synthesis of Cyclic Carbonates from Epoxides and Carbon Dioxide by Using Bifunctional One-Component Phosphorus-Based Organocatalysts. *ChemSusChem* **2016**, *8*, 2655–2669.

[125] Hu, Y.; Wei, Z.; Frey, A.; Kubis, C.; Ren, C. Y.; Spannenberg, A.; Jiao, H.; Werner, T. Catalytic, Kinetic, and Mechanistic Insights into the Fixation of CO_2 with Epoxides Catalyzed by Phenol-Functionalized Phosphonium Salts. *ChemSusChem* **2021**, *14*, 363–372.

[126] Li, X.; Feng, J.; Cao, J.; Ma, N.; Tao, M.; Zhang, W. Multi-Dimensional Application of Quaternary Phosphonium Salt Functionalized Fiber with High Polarization Performance: Efficient Adsorption of SDBS and Green Conversion of CO_2. *Polymer* **2023**, *280*, 126044.

[127] Yingcharoen, P.; Kongtes, C.; Arayachukiat, S.; Suvarnapunya, K.; Vummaleti, S. V. C.; Wannakao, S.; Cavallo, L.; Poater, A.; D' Elia, V. Assessing the PKa-Dependent Activity of Hydroxyl Hydrogen Bond Donors in the Organocatalyzed Cycloaddition of Carbon Dioxide to Epoxides: Experimental and Theoretical Study. *Adv. Synth. Catal.* **2019**, *361*, 366–373.

[128] Sopeña, S.; Cozzolino, M.; Maquilón, C.; Escudero-Adán, E. C.; Martínez Belmonte, M.; Kleij, A. W. Organocatalyzed Domino [3+2] Cycloaddition/Payne-Type Rearrangement Using Carbon Dioxide and Epoxy Alcohols. *Angew. Chem. Int. Ed.* **2018**, *57*, 11203–11207.

[129] Zanda, N.; Sobolewska, A.; Alza, E.; Kleij, A. W.; Pericàs, M. A. Organocatalytic and Halide-Free Synthesis of Glycerol Carbonate under Continuous Flow. *ACS Sustainable Chem. Eng.* **2021**, *9*, 4391–4397.

[130] Morodo, R.; Gérardy, R.; Petit, G.; Monbaliu, J.-C. M. Continuous Flow Upgrading of Glycerol toward Oxiranes and Active Pharmaceutical Ingredients Thereof. *Green Chem.* **2019**, *21*, 4422–4433.

[131] Muzyka, C.; Renson, S.; Grignard, B.; Detrembleur, C.; Monbaliu, J.-C. M. Intensified Continuous Flow Process for the Scalable Production of Bio-Based Glycerol Carbonate. *Angew. Chem. Int. Ed.* **2024**, *63*, e202319060.

[132] Fanjul-Mosteirín, N.; Jehanno, C.; Ruipérez, F.; Sardon, H.; Dove, A. P. Rational Study of DBU Salts for the CO_2 Insertion into Epoxides for the Synthesis of Cyclic Carbonates. *ACS Sustainable Chem. Eng.* **2019**, *7*, 10633–10640.

[133] Rulev, Y. A.; Gugkaeva, Z. T.; Lokutova, A. V.; Maleev, V. I.; Peregudov, A. S.; Wu, X.; North, M.; Belokon, Y. N. Carbocation/Polyol Systems as Efficient Organic Catalysts for the Preparation of Cyclic Carbonates. *ChemSusChem* **2017**, *10*, 1152–1159.

[134] Jose, T.; Cañellas, S.; Pericàs, M. A.; Kleij, A. W. Polystyrene-Supported Bifunctional Resorcinarenes as Cheap, Metal-Free and Recyclable Catalysts for Epoxide/CO_2 Coupling Reactions. *Green Chem.* **2017**, *19*, 5488-5493.

[135] Lu, C.; Zhang, Y. Y.; Zhu, X. F.; Yang, G. W.; Wu, G. P. Simultaneous Activation of Carbon Dioxide and Epoxides to Produce Cyclic Carbonates by Cross-Linked Epoxy Resin Organocatalysts. *ChemCatChem* **2023**, *15*, e2023003.

[136] Sperandio, C.; Rodriguez, J.; Quintard, A. Organic & Biomolecular Chemistry Organocatalytic Carbon Dioxide Fixation to Epoxides by Perfluorinated 1,3,5-Triols Catalysts. *Org. Biomol. Chem.* **2020**, *18*, 2637–2640.

[137] Fanjul-Mosteirín, N.; Martín, J.; Valdés, C.; Concellón, C.; Del Amo, V. Broadening the Scope of Steroidal Scaffolds: The Umpolung of a Bis-Primary Amine Precatalyst for the Insertion of CO_2 into Epoxides. *Org. Lett.* **2020**, *22*, 6988–6992.

[138] Della Monica, F.; Buonerba, A.; Grassi, A.; Capacchione, C.; Milione, S. Glycidol: An Hydroxyl-Containing Epoxide Playing the Double Role of Substrate and Catalyst for CO_2 Cycloaddition Reactions. *ChemSusChem* **2016**, *9*, 3457–3464.

[139] Yadav, N.; Seidi, F.; Gobbo, S. Del; D'Elia, V.; Crespy, D. Polymer Chemistry Versatile Functionalization of Polymer Nanoparticles with Carbonate Groups via Hydroxyurethane Linkages. *Polym. Chem.* **2019**, *10*, 3571–3584.

[140] Wu, F.-T.; Wu, L.; Cui, C.-N. The Catalytic System "Rhodamine B/Additive" for the Chemical Fixation of CO_2. *Tetrahedron* **2021**, *83*, 131965.

[141] Poolwong, J.; Aomchad, V.; Del Gobbo, S.; Kleij, A. W.; D'Elia, V. Simple Halogen-Free, Biobased Organic Salts Convert Glycidol to Glycerol Carbonate under Atmospheric CO_2 Pressure. *ChemSusChem* **2022**, *15*, e202200765.

[142] Gong, Y.; Li, Y.; Hu, J.; Wang, Z.; Deng, T. Sulfur-Containing Amino Acid-Derived Ionic liquid as a Halogen-Free Catalyst for CO_2 Mild into Cyclic Carbonates. *New J. Chem.* **2021**, *45*, 19215–19218.

[143] Wang, Y.; Nie, J.; Lu, C.; Wang, F.; Ma, C.; Chen, Z.; Yang, G. Imidazolium-Based Polymeric Ionic Liquids for Heterogeneous Catalytic Conversion of CO_2 into Cyclic Carbonates. *Microporous Mesoporous Mat.* **2020**, *292*, 109751.

[144] He, Y.; Li, X.; Cai, W.; Lu, H.; Ding, J.; Li, H.; Wan, H.; Guan, G. One-Pot Multiple-Step Integration Strategy for Efficient Fixation of CO_2 into Chain Carbonates by Azolide Anions Poly(Ionic Liquid)s. *ACS Sustainable Chem. Eng.* **2021**, *9*, 7074–7085.

[145] He, Y.; Li, X.; Li, H.; Ding, J.; Wan, H.; Guan, G. Understanding the Ingenious Dual Role-Playing of CO_2 in One-Pot Pressure-Swing Synthesis of Linear Carbonate. *ACS Sustainable Chem. Eng.* **2022**, *10*, 2556–2568.

[146] Jiang, D.; He, Y.; Zhang, J.; Yin, J.; Ding, J.; Wang, S.; Li, H. Conjugate Acid-Base Bi-Functional Polymeric Ionic Liquids (CAB-PILs) as Efficient Catalysts for CO_2 Capture and Subsequent Glycidol Cycloaddition Reaction. *J. Mol. Liq.* **2023**, *375*, 121284.

[147] Yue, Z.; Hu, T.; Zhao, W.; Su, H.; Li, W.; Chen, Z.; Chen, Y.; Li, S.; Wang, L.; Liu, Y.; Zhang, H.; Shan, S.; Zhi, Y. Triazinyl-Imidazole Polyamide Network as an Efficient Multi-Hydrogen Bond Donor Catalyst for Additive-Free CO_2 Cycloaddition. *Appl. Catal. A: Gen.* **2022**, *643*, 118748.

[148] Chen, C.; Sun, T.; Chen, Y.; Zhang, Y.; Feng, N.; Wan, H.; Guan, G.; Ma, J. Anchoring High-Density Cooperative Catalytic Sites within Triethylenediamine-Based Ionic-Liquid Polymers via Microenvironment Modulation for Efficient CO_2 Fixation. *Sep. Purif. Technol.* **2024**, *330*, 125348.

[149] Wang, Y.; Duan, J. Urea and Thiourea-Functionalized, Pyridinium-Based Ionic Polymers Convert CO_2 to Cyclic Carbonate under Mild Conditions. *ACS Appl. Polym. Mater.* **2022**, *4*, 5851–5860.

[150] Wang, P.; Lv, Q.; Tao, Y.; Cheng, L.; Li, R.; Jiao, Y.; Fang, C.; Li, H.; Geng, C.; Sun, C.; Ding, J.; Wan, H.; Guan, G. One-Pot Efficient Fixation of Low-Concentration CO 2 into Cyclic Carbonate by Mesoporous Pyridine-Functionalized Binuclear Poly(Ionic Liquid)s. *Mol. Catal.* **2023**, *544*, 113157.

[151] Xu, Z.; Liu, K.; Huang, H.; Zhang, Y.; Long, Z.; Tong, M.; Chen, G. Quaternization-Induced Catalyst-Free Synthesis of Viologen-Linked Ionic Polyacetylenes towards Heterogeneous Catalytic CO_2 Fixation. *J. Mater. Chem. A* **2022**, *10*, 5540–5549.

[152] Liu, K.; Xu, Z.; Huang, H.; Zhang, Y.; Liu, Y.; Qiu, Z.; Tong, M.; Long, Z.; Chen, G. In Situ Synthesis of Pyridinium-Based Ionic Porous Organic Polymers with Hydroxide Anions and Pyridinyl Radicals for Halogen-Free Catalytic Fixation of Atmospheric CO_2. *Green Chem.* **2022**, *24*, 136–141.

[153] Lai, S.; Gao, J.; Xiong, X. Rosin-Based Porous Heterogeneous Catalyst Functionalized with Hydroxyl Groups and Triazole Groups for CO_2 Chemical Conversion under Atmospheric Pressure Condition. *React. Funct. Polym.* **2021**, *165*, 104976.

[154] Chen, F.; Wei, W.; Gao, Y.; Wang, Y.; Yan, Z.; Zhang, Z.; Yu, H.; Xu, G.; Shi, L. Synthesis of Highly Effective [Emim]IM Applied in One-Step CO_2 Conversion to Dimethyl Carbonate. *J. CO_2 Util.* **2022**, *65*, 102178.

[155] Grollier, K.; Vu, N. D.; Onida, K.; Akhdar, A.; Norsic, S.; D'Agosto, F.; Boisson, C.; Duguet, N. A Thermomorphic Polyethylene-Supported Imidazolium Salt for the Fixation of CO_2 into Cyclic Carbonates. *Adv. Synth. Catal.* **2020**, *362*, 1696–1705.

[156] Zhang, P.; Zhiani, R. Synthesis of Ionic Liquids as Novel Nanocatalysts for Fixation of Carbon Dioxide with Epoxides by Using a Carbon Dioxide Balloon. *Catal. Letters* **2020**, *150*, 2254–2266.

[157] Jadhav, A. H.; Thorat, G. M.; Lee, K.; Lim, A. C.; Kang, H.; Gil Seo, J. Effect of Anion Type of Imidazolium Based Polymer Supported Ionic Liquids on the Solvent Free Synthesis of Cycloaddition of CO_2 into Epoxide. *Catal. Today* **2016**, *265*, 56–67.

[158] Comès, A.; Fiorilli, S.; Aprile, C. Multifunctional Heterogeneous Catalysts Highly Performing in the Conversion of Carbon Dioxide: Mechanistic Insights. *J. CO_2 Util.* **2020**, *37*, 213–221.(159)Ding, M.; Jiang, H. L. Incorporation of Imidazolium-Based Poly(Ionic Liquid]s into a Metal-Organic Framework for CO_2 Capture and Conversion. *ACS Catal.* **2018**, *8*, 3194–3201.

[160] Valverde, D.; Porcar, R.; Zanatta, M.; Alcalde, S.; Altava, B.; Sans, V.; García-Verdugo, E. Towards Highly Efficient Continuous-Flow Catalytic Carbon Dioxide Cycloadditions with Additively Manufactured Reactors. *Green Chem.* **2022**, *24*, 3300–3308.

[161] Castro-Osma, J. A.; Martínez, J.; De La Cruz-Martínez, F.; Caballero, M. P.; Fernández-Baeza, J.; Rodríguez-López, J.; Otero, A.; Lara-Sánchez, A.; Tejeda, J. Development of Hydroxy-Containing Imidazole Organocatalysts for CO_2 Fixation into Cyclic Carbonates. *Catal. Sci. Technol.* **2018**, *8*, 1981–1987.

[162] Eftaiha, A. F.; Qaroush, A. K.; Hasan, A. K.; Helal, W.; Al-Qaisi, F. M. CO_2 Fixation into Cyclic Carbonates Catalyzed by Single-Site Aprotic Organocatalysts. *React. Chem. Eng.* **2022**, *7*, 1807–1817.

[163] Li, R.; Dalton, L.; Zhang, Y.; Liu, K.; Wu, L.; Huang, H.; Xu, Z.; Long, Z.; Tong, M.; Gu, Y.; Qin, Z.; Chen, G. POSS and Imidazolium-Constructed Ionic Porous Polymers with Multiple Active for Synergistic Catalytic CO_2 Transformation. *Dalton Trans.* **2021**, *50*, 11878–16916.

[164] Liu, Y.; Hu, Y.; Zhou, J.; Zhu, Z.; Zhang, Z.; Li, Y.; Wang, L.; Zhang, J. Polystyrene-Supported Novel Imidazolium Ionic Liquids: Highly Efficient Catalyst for the Fixation of Carbon Dioxide under Atmospheric Pressure. *Fuel* **2021**, *305*, 121495.

[165] Zhang, Z.; Li, J.; Yu, G.; Zeng, C.; Wang, M.; Huang, S.; Wang, L.; Zhang, J. Efficient Synthesis of Cyclic Carbonates under Atmospheric CO_2 by DMAP-Based Ionic Liquids: The Difference of Inert Hydrogen Atom and Active Hydrogen Atom in Cation. *Green Chem. Eng.* **2023**, *4*, 285–293.

[166] Wang, T.; Zheng, D.; An, B.; Liu, Y.; Ren, T.; Ågren, H.; Wang, L.; Zhang, J.; Ahlquist, M. S. G. Dual-Ionic Imidazolium Salts to Promote Synthesis of Cyclic Carbonates at Atmospheric Pressure. *Green Energy and Environ.* **2022**, *7*, 1327–1339.

[167] Yao, N.; Chen, C.; Li, D. J.; Lin Hu, Y. Cobalt Nanoparticles Embedded over Periodic Mesoporous Organosilica Functionalized with Benzotriazolium Ionic Liquid for Efficient and Heterogeneous Catalytic Transformation of Carbon Dioxide to Cyclic Carbonates. *J Environ. Chem. Eng.* **2020**, *8*, 103953.

[168] Sheldon, R. A. The E Factor 25 Years on: The Rise of Green Chemistry and Sustainability. *Green Chem.* **2017**, *19*, 18–43.

[169] Kassin, V.-E. H.; Morodo, R.; Toupy, T.; Jacquemin, I.; Van Hecke, K.; Robiette, R.; Monbaliu, J.-C. M. A Modular, Low Footprint and Scalable Flow Platform for the Expedient α-Aminohydroxylation of Enolizable Ketones. *Green Chem.* **2021**, *23*, 2336–2351.

[170] Sheldon, R. A. Green Solvents for Sustainable Organic Synthesis: State of the Art. *Green Chem.* **2005**, *7*, 267–278.

[171] Van Aken, K.; Strekowski, L.; Patiny, L. Ecoscale, a Semi-Quantitative Tool to Select an Organic Preparation Based on Economical and Ecological Parameters. *Beilstein J. Org.* Chem. **2006**, *2* (3), 1–7.

[172] Dargaville, T. R.; De Bruyn, P. J.; Lim, A. S. C.; Looney, M. G.; Potter, A. C.; Solomon, D. H.; Zhang, X. Chemistry of Novolac Resins. II. Reaction of Model Phenols with Hexamethylenetetramine. *J. Polym. Sci. A: Polym. Chem.* **1997**, *35* (8), 1389–1398.

[173] Mihara, M.; Moroga, K.; Iwasawa, T.; Nakai, T.; Ito, T.; Ohno, T.; Mizuno, T. Selective Synthesis of Carbonates from Glycerol, CO_2, and Alkyl Halides Using Tert-Butyltetramethylguanidine. *Synlett* **2018**, *29* (13), 1759–1764.

[174] Zhang, Y.; Khalid, S.M.; Meng, W.; Gao L. New Strategies on Green Synthesis of Dimethyl Carbonate from Carbon Dioxide and Methanol over Oxide Composites. *Molecules* **2022**, *27*, 5417–23498.

[175] Unnikrishnan P., Srinivas, D. Direct synthesis of dimethyl carbonate from CO_2 and methanol over CeO_2 catalysts of different morphologies. *J. Chem. Sci.* **2016**, *128*, 957–965.

Author Contributions

Claire Muzyka: Conceptualization, Writing - Original Draft

Diana V. Silva-Brenes: Writing – review & editing
Bruno Grignard: Writing - review & editing

Christophe Detrembleur: Funding acquisition, Writing - review & editing.

Jean-Christophe M. Monbaliu: Conceptualization, Project Administration, Supervision, Funding acquisition, Writing – review & editing.

5.3 INTENSIFIED CONTINUOUS FLOW PROCESS FOR THE SCALABLE PRODUCTION OF BIO-BASED GLYCEROL CARBONATE

5.3.1 ABSTRACT

A subtle combination of fundamental and applied organic chemistry toward process intensification is demonstrated for the large-scale production of bio-based glycerol carbonate under flow conditions. The direct carbonation of bio-based glycidol with CO_2 is successfully carried out under intensified flow conditions, with Barton's base as a potent homogeneous organocatalyst. Process metrics for the CO_2 coupling step (for the upstream production, output: 3.6 kg day^{-1}, Space Time Yield (STY): 2.7 kg h^{-1} L^{-1}, Environmental factor (E-factor): 4.7) outclass previous reports. High conversion and selectivity are achieved in less than 30 s of residence time at pilot scale with a stoichiometric amount of CO_2. Supporting DFT computations reveal the unique features of the mechanism in presence of Brønsted bases.

5.3.2 INTRODUCTION

Ambitious R&D and production directives in Europe now favor the integration of disruptive technologies for reducing the environmental impact, for enhancing safety measures and for lifting the extensive reliance on petro-based chains of value.[1–5] In this context, significant efforts have been dedicated to the upgrading of glycerol (**1**) into industrially relevant bio-based platform compounds, such as glycidol (**2**) and glycerol carbonate (**3**).[5,6] In this context, **3** has rapidly accessed the status of rising star. It has several advantages over other petro-based carbonates such as ethylene and propylene carbonates, which are key electrolyte carriers in lithium batteries.[7] The flammability of **3** is much lower in comparison to ethylene/propylene carbonates, thus significantly reducing the inherent fire hazards associated with Li-based batteries.[8] By condensation with dicarboxylic acids or diacyl chlorides,[8] **3** has also served as a building block for the construction of bicyclic carbonates suitable for non-isocyanate polyurethanes (**NIPU**) by polyaddition with polyamines. However, the use of **3** in **NIPU** chemistry remains marginal.[5,8–15] Carbonate **3** can also be used as a bio-lubricant, formulating agent or alternative green solvent.[5]

The global production of **3** is still limited, estimated to *ca.* 3 Mt y^{-1} in 2020,[16] which most likely relates to the overall inefficiency of current industrial processes.[5] There are currently three main synthetic routes to access **3** (A-C, Figure 5.39a). [6,17–21] The most economically viable processes feed on activated glycerol derivatives such as **2** and CO_2.

However, the alleged inert nature of CO_2 leads to extended reaction times, hampering the global process efficiency.[26–29] Various carbonation protocols using CO_2 on oxiranes with homogeneous and heterogeneous catalysts have been reported under flow conditions,[30–33] among which only two reports specifically disclosed the carbonation of **2** (Figure 5.39b,c)[22,25] with low overall productivities.

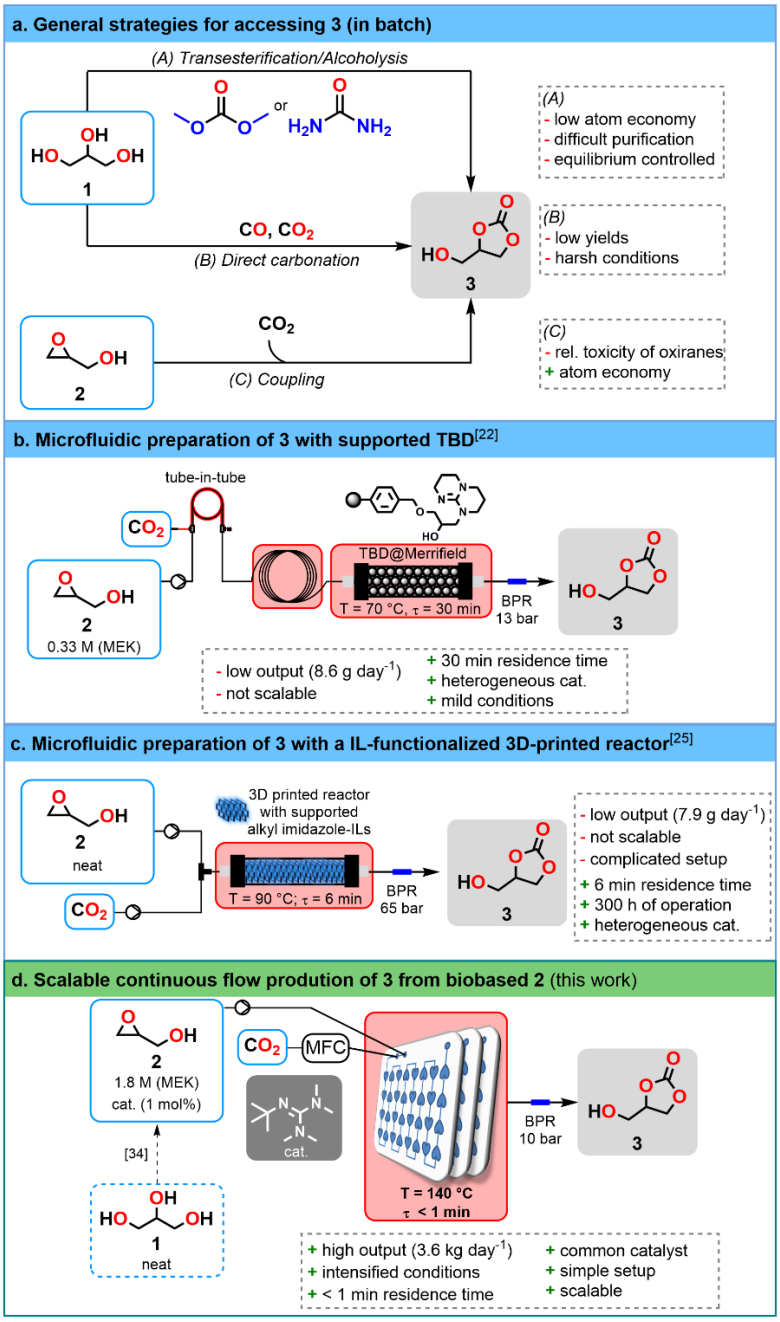

Figure 5.39 (a) Typical preparations of **3** (A: transesterification/alcoholysis of **1**; B: direct carbonation of **1** with CO or CO_2; C: coupling of **2** with CO_2); (b) Microfluidic preparation of **3** from **2** and CO_2 with a heterogenized catalyst and featuring a tube-in-tube configuration;[22–24] (c) Microfluidic preparation of **3** from **2** and CO_2 with a 3D-printed reactor;[25] with covalent ionic liquid functionalization; (d). This work: scalable and intensified flow preparation of **3** from biobased **2** with a homogeneous catalyst.

5.3.3 RESULTS AND DISCUSSION

Our previous studies established an intensified and scalable flow process to convert bio-based **1** into the corresponding oxiranes, including **2** with high selectivity (Section S5, Supporting Information).[34] With the invaluable opportunities in terms of scalability, safety and intensification brought by flow process technology,[18,34–39] we sought for further downstream valorization of **2** and for a concrete solution to access **3** at large scale (Figure 5.39d). We hereby present a DFT-guided homogeneous catalytic process to access carbonate **3**.[35,40] Structure reactivity relationships were established among a library of nitrogen-containing homogeneous organocatalysts displaying a range of pK_{aH} to maximize the reaction selectivity, conversion and output. A DFT study further rationalized the mechanism. The process conditions relied on a stoichiometric amount of CO_2, a low catalyst loading and a short residence time with very high conversion and selectivity. The scalability and intensification of the process were validated with favorable metrics (3.6 kg day^{-1}).

To ensure seamless scalability, specific technical and chemical options were selected: CO_2 was fed into the reactor setup with a mass flow controller and homogenous catalysis in 2-butanone (methyl ethyl ketone, MEK) was privileged.[41] 1,5,7-Triazabicyclo[4.4.0]dec-5-ene (**TBD**) was selected as a model catalyst for the direct coupling of gaseous CO_2 with **2**.[22] The influence of temperature, counter-pressure and CO_2 flow rate on the reaction outcome were assessed with 5 mol% of **TBD** in a microfluidic reactor (Figure 5.40, Section S6.1, Supporting information). The preliminary scouting of reaction conditions led to conditions striking a balance between yield and selectivity under intensified conditions. These conditions involved processing **2** at 140 °C (10 bar) with 2 min of residence time and 10 mL_N/min of gaseous CO_2.

Next, a library of potential nitrogen-containing homogeneous organocatalysts was investigated. The series of homogeneous organocatalysts (Figure 5.40b) featured 1,1,3,3-tetramethylguanidine (**TMG**),1,8-diazabicyclo[5.4.0]undec-7-ene (**DBU**), 2-*tert*-butyl-1,1,3,3-tetra- methylguanidine (Barton's base, **BB**), *tert*-octylimino-tris(dimethylamino)phosphorane (**P$_1$-*t*-Oct**), as well as 2,8,9-trimethyl-2,5,8,9-tetraza-1-phosphabicyclo-[3.3.3]undecane (Verkade's base, **VB**). All selected bases were evaluated under standardized process conditions (Section S6, Supporting Information). Starting with the lowest pK_{aH} (e.g., **TMG**, **DBU** and **TBD**), **3** was obtained in up to 86% yield, with the formation of increasing amounts of **1** (up to 14%). **BB** afforded the best compromise with a high yield (91% in **3**) with only a minor amount of **1**. Stronger bases than **BB** (**P$_1$-*t*-Oct** and **VB**) significantly increased the formation of **1**. With **BB** as the most promising catalyst, further optimization eventually led to **3** in 82% with only 1 mol% of catalyst (Section 6.2, Supporting Information) and a stoichiometric amount of CO_2. Lowering the catalytic loading to 0.5 and 0.1 mol% drastically decreased the conversion to 53 and 12%, respectively.

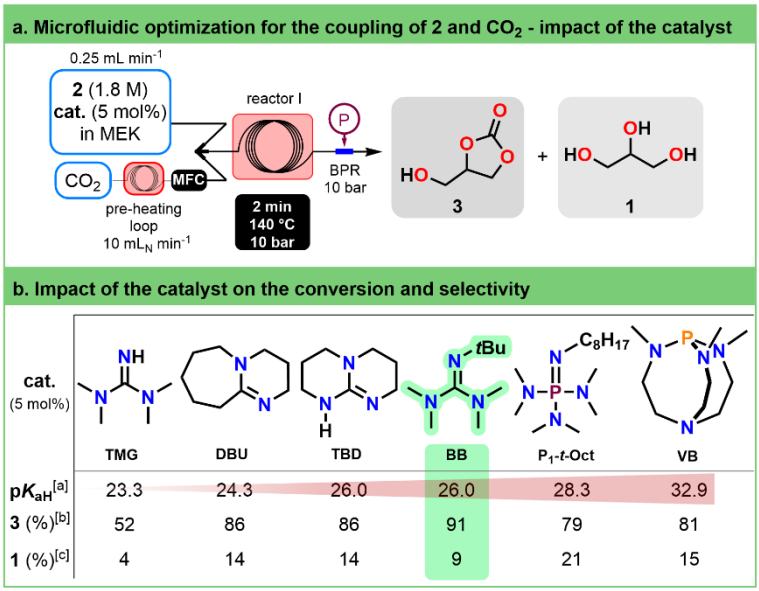

Figure 5.40 (a) Microfluidic prototype for the screening of catalyst. Conditions: 2 (1.8 M in MEK with 5 mol% cat.) at 0.25 mL min^{-1}; CO_2 (gas, 1 equiv.) at 10 mL_N min^{-1}, 140 °C, 10 bar, 2 min estimated residence time. MFC = Mass Flow Controller; (b) Screening of various homogeneous nitrogen-containing organic bases for the coupling of bio-based **2** with CO_2 (see a.). [a] Indicative values for experimental pK_{aH} in MeCN reported in the literature[42,43]. [b] Yield of **3** determined by ^1H NMR. [c] Yield of **1** determined by ^1H NMR.

The scalability of the process was next evaluated in commercial mesofluidic glass reactors (Corning® Advanced-Flow™ Reactors (AFR), Section S6.5, Supporting Information). Temperatures from 120 to 150 °C (10 bar) were assessed first in a lab scale mesofluidic system with a feed solution of **2** (1.8 M in MEK) and 1 equiv. of CO_2 in the presence of 1 mol% of **BB** (Table 5.3). Comparable trends to the microfluidic experiments were collected: increasing the temperature had a positive impact on the reaction outcome. At 140 °C and 70 s of residence time, **3** was obtained in 88% yield (1 mol% **BB**). A further increase of both the temperature and residence time did not improve the selectivity. At the highest flow rate, implementing 150 °C led to the clogging of the reactor, most likely due to ring opening polymerization of **2**.[44,45] The influence of the residence time independently of the mixing was also studied (Table 5.3, entries 8-12). A decrease of the residence time had a moderate impact from 70 to 41 s with a loss of 10% yield for **3**, whereas further shortening to 27 s and 13.5 s lowered the yields (63 and 31%, respectively).

Additional data points were considered with **DBU** and **TBD** (1 mol%) under similar conditions. In both cases, clogging of the first fluidic module was observed. **DBU** is known to easily form an adduct with CO_2,[46] which is poorly soluble in most organic solvents. **TBD** was unsuccessful as well, since it triggered the polymerization of **2**,[47] starting at 120 °C. This clogging issue was also observed for the experiment with 1 mol% of **BB** at 150 °C, therefore also underlining the thermal limitation of the reaction with **BB**.

Table 5.3 Scalability trials for the carbonation of **2** in a mesofluidic lab scale glass reactor (total internal volume = 13.5 mL) for various temperature and residence times using 1 mol% of Barton's base (**BB**).

Entry	T (°C)	Residence time (s)	**2** conv. (%)	**3** yield (%)	**1** yield (%)
1	120	50	55	52	3
2	120	70	66	62	4
3	120	140	76	66	10
4	130	50	71	66	6
5	130	70	86	80	6
6	130	140	82	76	6
7	140	50	84	77	6
8[a]	140	70	95	88	7
9[a]	140	54	91	82	8
10[a]	140	41	87	78	9
11[a]	140	27	69	63	6
12[a]	140	13.5	34	31	3
13	140	140	93	85	8
14	150	50	92	85	7
15	150	70	97	88	9
16	150	140	95	88	7

[a] Experiments performed with a liquid flow rate of 1.82 mL min^{-1} and with a gaseous flow rate of 72.9 mL_N min^{-1}.

The carbonation process was then carried out in a pilot mesofluidic reactor with **BB** (1 mol%). A representative flow chart is depicted in Figure 5.41. Further intensification led to conversions of up to 85% within remarkably short residence times (43 s: 80%, 28 s: 78%, 21 s: 67%) at 140 °C. These results simply outperform all conditions reported in the primary literature so far. The attractiveness of this process is emphasized by its high throughput and

low footprint, which translates to a Space Time Yield (STY) of 2.7 kg h^{-1} L^{-1} and an E-factor of 4.7 for the upstream carbonation process (Section S6.5.6, Supporting Information).[48] Crude carbonate **3** was purified with a simple liquid-liquid extraction with water (1% NaCl) and methyl isobutyl ketone (MIBK), affording **3** in 71% isolated yield (> 95% purity) (Section S7, Supporting Information). The end-to-end process comes with an E-factor of 1.99,

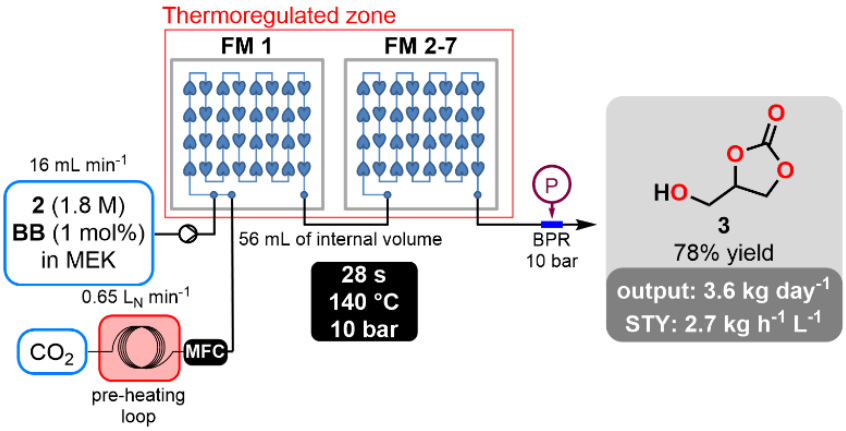

Figure 5.41 Intensified mesofluidic pilot-scale process (Corning® AFR™ G1, 7 glass fluidic modules in series) for the coupling of **2** and CO_2. Conditions: **2** (1.8 M in MEK with 1 mol% **BB**) at 16.18 mL min^{-1} CO_2 (gas, 1 equiv.) at 648 mL_N min^{-1}, 140 °C, 10 bar, 28 s estimated residence time. FM = Fluidic Module, MFC = Mass Flow Controller. Up to 4% glycerol (**1**) was detected in the crude reactor effluent

provided that MIBK and MEK are recovered through vacuum distillation (Section S6.5.6, Supporting Information).

Experimental observations highlighted that the β-OH group on **2** plays a critical role, thus suggesting a direct substrate activation with **BB** (Section S9.1, Supporting Information). Indeed, the carbonation of oxiranes lacking a β-OH group, such as epichlorohydrin and *t*-butyl glycidyl ether, gave no conversion. When a 2.25:1 mixture of **2** and epichlorohydrin was subjected to the same conditions, selective coupling occurred with **2**, leaving epichlorohydrin unreacted (Section S6.4.2, Supporting Information). However, by contrast to Kleij's work,[49] the addition of water did not improve CO_2 capture: control experiments under strictly anhydrous conditions gave marginal differences (2-4%) for the conversion to **3**. The potential involvement of a CO_2-adduct with nitrogen-containing organocatalysts was also ruled out.[50,51]

The mechanism was studied computationally with the Gaussian 16 software package[52] (Section S9, Supporting Information) for a selection of organocatalysts (**TMG**, **DBU**, **TBD**, **BB** and **P1-*t*-Oct**). The mechanism (Figure 5.42a) features two steps: (a) an intermolecular CO_2 capture (step 1) and (b) an intramolecular cyclization toward **3** (step 2).

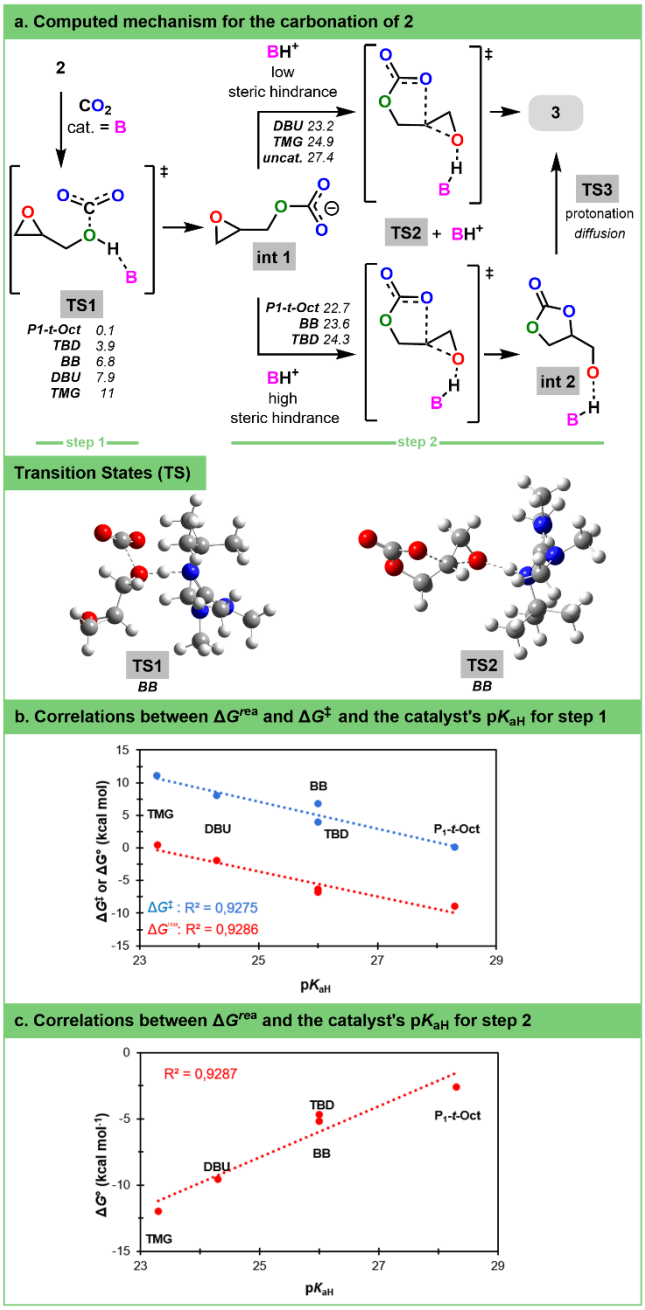

Figure 5.42 (a) Mechanism for the organocatalyzed coupling of CO_2 and **2** toward **3**, computed at the B3LYP-GD3BJ/6-31+G*//M08HX/6-311++G** level of theory (SMD = MEK, 413 K). Activation barriers ($\Delta G^{\ddagger}$) are given in kcal mol^{-1} and mentioned near the acronyms of the various bases. (b). Free Gibbs energy of reaction (ΔG^{rea}), in red) and activation barriers ($\Delta G^{\ddagger}$, in blue) as a function of pK_{aH} of the catalysts for step 1. (c) Calculated Free Gibbs energy of reaction (ΔG^{rea}) for step 2. Experimental pK_{aH} were collected from the literature and measured in MeCN. (Section S9, Supporting Information).

Step 1, which involves the catalyst, the hydroxyl group of **2** and CO_2, leads to **int 1**. It proceeds through low activation barriers ($\Delta G^{\ddagger}$) ranging from 0.1 (**P$_1$-*t*-Oct**) to 11 kcal mol^{-1} (**TMG**) depending on the catalyst, thus indicating a fast CO_2 capture. $\Delta G^{\ddagger}$ can be linearly correlated with the pK_{aH} of the catalyst (Figure 5.42b, blue): decreasing $\Delta G^{\ddagger}$ are associated with an increasing Brønsted basicity. Regarding the thermodynamics (ΔG^{rea}) of the process, the high stability of CO_2 is overcome with the favorable acid-base reaction at the hydroxyl group of **2**. This assumption is supported by a negative value of ΔG^{rea} for **DBU**, **TBD**, **BB** and **P$_1$-*t*-Oct**, thus ensuring a favorable CO_2 capture, which also correlates with the pK_{aH} of the catalyst (Figure 5.42b, red).

Step 2 is promoted through the activation of **int 1** by the conjugated acid of the catalyst (produced in step 1) through another proton shuffle. There are, however, two distinct mechanisms depending on the steric hinderance of the catalyst. Catalysts with a lower steric congestion (e.g., **TMG** and **DBU**) directly lead to the final products (**3** and the regenerated active catalytic species). It involves an asynchronous concerted TS, where both the intramolecular cyclization and the proton transfer to the alkoxide occur. Values of $\Delta G^{\ddagger}$ range from 23.2 (**DBU**) to 24.9 kcal mol^{-1} (**TMG**), depending on the catalyst. A change of the mechanism from concerted to stepwise is noticed with highly hindered bases (e.g., **BB** and **P$_1$-*t*-Oct**). The intramolecular cyclization occurs first, where the oxirane ring is activated through H-bonding with the conjugated acid of the catalyst, yielding **int 2**. The latter is then protonated (**TS3**, diffusion-limited) to give **3** with the concomitant recovery of the catalyst. For **TBD**, the stepwise pathway seems to be favored due to the symmetry of its protonated form. The uncatalyzed intramolecular cyclization appeared uncompetitive with a much higher $\Delta G^{\ddagger}$ (27.4 kcal mol^{-1}). Moreover, the presence of the catalyst shifts the equilibrium toward the formation of the products by drastically lowering ΔG^{rea}. The thermodynamics of the second step are again dictated by the acid-base equilibrium (Figure 5.42c).

5.3.4 CONCLUSION

In summary, a range of nitrogen-containing organocatalysts were assessed experimentally and computationally. Computations emphasized the unique features of a double H-shuffle mechanism for the coupling of CO_2 and glycidol according to a 2-step mechanism. The catalyst's basicity is of paramount importance for step 1. Indeed, a high pK_{aH} ensures a fast and favorable CO_2 fixation with the formation of a highly stable conjugated acid along with a linear carbonate intermediate. Step 2 is drastically accelerated in the presence of the conjugated acid of the catalyst, which acts as a general Brønsted acid catalyst for the activation of the epoxide, though it remains overall rate-determining. Contrasting trends are observed in the activation energies of the two steps of carbonation. This observation provides insight into why Barton's Base emerged with the most favorable results for the entire transformation process. When a stronger base is employed, it leads to a weaker conjugate acid, which in turn acts as a less effective Brønsted acid for the activation of the epoxide. Given the fast kinetics of both steps, the carbonation is likely limited by the solubility of CO_2 in the reaction medium, therefore justifying both the selection of MEK as reaction medium and flow technology for high mass transfer. The process was validated at the pilot scale in a commercial mesofluidic reactor, affording high yields and selectivity within 28 s with an unprecedented productivity at low catalyst loading (1 mol%). This constitutes a significant improvement of existing conditions toward the intensified and scalable preparation of glycerol carbonate.

5.3.5 REFERENCES

[1] "Chemicals strategy," can be found under https://single-market-economy.ec.europa.eu/sectors/chemicals/chemicals-strategy_en, accessed on January 1, 2024.

[2] "Transition pathway," can be found under https://single-market-economy.ec.europa.eu/sectors/chemicals/transition-pathway_en, accessed on January 1, 2024.

[3] "A more robust bioeconomy could help the EU accelerate its progress towards a circular and low-carbon economy," can be found under https://rea.ec.europa.eu/news/more-robust-bioeconomy-could-help-eu-accelerate-its-progress-towards-circular-and-low-carbon-economy-2023-11-27_en, accessed on January 1, 2024.

[4] "Bio-based products," can be found under https://single-market-economy.ec.europa.eu/sectors/biotechnology/bio-based-products_en, accessed on January 1, 2024.

[5] C. Muzyka, J.-C. M. Monbaliu, *ChemSusChem* **2022**, *15*, e202102391.

[6] R. Gérardy, D. P. Debecker, J. Estager, P. Luis, J.-C. M. Monbaliu, *Chem. Rev.* **2020**, *120*, 7219–7347.

[7] E. C. Evarts, *Nature* **2015**, *526*, S93–S95.

[8] M. O. Sonnati, S. Amigoni, E. P. T. De Givenchy, T. Darmanin, O. Choulet, F. Guittard, *Green Chem.* **2013**, *15*, 283–306.

[9] C. Carré, Y. Ecochard, S. Caillol, L. Avérous, *ChemSusChem* **2019**, *12*, 3410–3430.

[10] S. Dabral, T. Schaub, *Adv. Synth. Catal.* **2018**, *361*, 223–246.

[11] S. Gennen, B. Grignard, T. Tassaing, H. Jérôme, C. Detrembleur, *Angew. Chem. Int. Ed.* **2017**, *56*, 10530–10534.

[12] L. Maisonneuve, O. Lamarzelle, E. Rix, E. Grau, H. Cramail, *Chem. Rev.* **2015**, *115*, 12407–12439.

[13] M. Bourguignon, B. Grignard, C. Detrembleur, *Angew. Chem. Int. Ed.* **2022**, *61*, e202213422.

[14] B. Quienne, N. Kasmi, R. Dieden, S. Caillol, Y. Habibi, *Biomacromolecules* **2020**, *21*, 1943–1951.

[15] D. S. Wunschik, K. N. Ingenbosch, M. Zähres, J. Horst, C. Mayer, M. Jäger, V. Strehmel, M. Dornbusch, K. Hoffmann-Jacobsen, *Green Chem.* **2018**, *20*, 4738–4745

[16] G. M. Lari, G. Pastore, M. Haus, Y. Ding, S. Papadokonstantakis, C. Mondelli, J. Pérez-Ramírez, *Energy Environ. Sci.* **2018**, *11*, 1012–1029.

[17] B. Limburg, À. Cristòfol, F. della Monica, A. W. Kleij, *ChemSusChem* **2020**, *13*, 6056–6065.

[18] Z. Wang, R. Gérardy, G. Gauron, C. Damblon, J.-C. M. Monbaliu, *React Chem Eng* **2018**, *4*, 17–26.

[19] R. Gérardy, J. Estager, P. Luis, D. P. Debecker, J.-C. M. Monbaliu, *Catal. Sci. Technol.* **2019**, *9*, 6841–6851.

[20] V. Aomchad, À. Cristòfol, F. della Monica, B. Limburg, V. D'Elia, A. W. Kleij, *Green Chem.* **2021**, *23*, 1077–1113.

[21] J. Poolwong, V. Aomchad, S. del Gobbo, A. W. Kleij, V. D'Elia, *ChemSusChem* **2022**, *15*, e202200765.

[22] N. Zanda, A. Sobolewska, E. Alza, A. W. Kleij, M. A. Pericàs, *ACS Sustain Chem. Eng.* **2021**, *9*, 4391–4397.

[23] C. J. Mallia, I. R. Baxendale, *Org. Process Res. Dev.* **2016**, *20*, 327–360.

[24] L. Yang, K. F. Jensen, *Org. Process Res. Dev.* **2013**, *17*, 927–933.

[25] D. Valverde, R. Porcar, M. Zanatta, S. Alcalde, B. Altava, V. Sans, E. García-Verdugo, *Green Chem.* **2022**, *24*, 3300–3308.

[26] J. A. Castro-Osma, J. Martínez, F. de La Cruz-Martínez, M. P. Caballero, J. Fernández-Baeza, J. Rodríguez-López, A. Otero, A. Lara-Sánchez, J. Tejeda, *Catal. Sci. Technol.* **2018**, *8*, 1981–1987.

[27] J. Rintjema, R. Epping, G. Fiorani, E. Martín, E. C. Escudero-Adán, A. W. Kleij, *Angew. Chem. Int. Ed.* **2016**, *55*, 3972–3976.

[28] Y. Zhang, G. Yang, R. Xie, L. Yang, B. Li, G. Wu, *Angew. Chem. Int. Ed.* **2020**, *132*, 23491–23498.

[29] J. Steinbauer, A. Spannenberg, T. Werner, *Green Chem.* **2017**, *19*, 3769–3779.

[30] D. Rigo, R. Calmanti, A. Perosa, M. Selva, G. Fiorani, *ChemCatChem* **2021**, *13*, 2005–2016.

[31] Y. Wu, Y. Ding, J. Xu, Y. Wang, K. Mumford, G. W. Stevens, W. Fei, *Green Energy Environ.* **2021**, *6*, 291–297.

[32] A. Rehman, A. M. López Fernández, M. F. M. G. Resul, A. Harvey, *J. CO2 Util.* **2018**, *24*, 341–349.

[33] M. R. Li, M. C. Zhang, T. J. Yue, X. B. Lu, W. M. Ren, *RSC Adv.* **2018**, *8*, 39182–39186.

[34] R. Morodo, R. Gérardy, G. Petit, J.-C. M. Monbaliu, *Green Chem.* **2019**, *21*, 4422–4433.

[35] P Bianchi, J.-C. M. Monbaliu, *Angew. Chem. Int. Ed.* **2023**, e202311526

[36] N. N. Tshibalonza, J.-C. M. Monbaliu, *Green Chem.* **2017**, *19*, 3006–3013.

[37] N. N. Tshibalonza, R. Gérardy, Z. Alsafra, G. Eppe, J.-C. M. Monbaliu, *Green Chem.* **2018**, *20*, 5147–5157.

[38] L. Capaldo, Z. Wen, T. Noël, *Chem. Sci.* **2023**, 14, 4230–4247.

[39] N. Kockmann, P. Thenée, C. Fleischer-Trebes, G. Laudadio, T. Noël, *React. Chem. Eng.* **2017**, *2*, 258-280.

[40] Y. Chen, S. Renson, J.-C. M. Monbaliu, *Angew. Chem. Int. Ed.* **2022**, *61*, e202210146.

[41] X. Gui, Z. Tang, W. Fei, *J. Chem. Eng. Data* **2011**, *56*, 2420–2429.

[42] R. Schwesinger, J. Willaredt, H. Schlemper, M. Keller, D. Schmitt, H. Fritz, *Chem. Ber.* **1994**, *127*, 2435–2454.

[43] Ishikawwa T., *Superbases for Organic Synthesis: Guanidines, Amidines and Phosphazenes and Related Organocatalysts*, John Wiley & Sons, Ltd, Chichester, UK, **2009**.

[44] A. Thomas, S. Mü, H. Frey, *Biomacromolecules* **2014**, *15***,** 1935–1954.

[45] S. Liu, L. Liu, Y. Zhou, Y. Chen, J. Zhao, *Polym. Chem.* **2022**, *13*, 3650.

[46] M. Lv, P. Wang, Y. Yao, *ChemCatChem* **2016**, *9*, 4451–4455.

[47] L. Simón, J. M. Goodman, *J. Org. Chem.* **2007**, *72*, 9656–9662.

[48] D. J. C. Constable, A. D. Curzons, V. L. Cunningham, *Green Chem.* **2002**, *4*, 521–527.

[49] R. Huang, J. Rintjema, J. González-Fabra, E. Martín, E. C. Escudero-Adán, C. Bo, A. Urakawa, A. W. Kleij, *Nat Catal* **2019**, *2*, 62–70.

[50] C. Maquilón, B. Limburg, V. Laserna, D. Garay-Ruiz, J. González-Fabra, C. Bo, M. Martínez Belmonte, E. C. Escudero-Adán, A. W. Kleij, *Organometallics* **2020**, *39*, 1642–1651.

[51] V. Laserna, E. Martin, E. C. Escudero-Adán, A. W. Kleij, *ACS Catal.* **2017**, *7*, 5478–5482.

[52] Gaussian 16, Revision C.01, M. J. Frisch, G. W. Trucks, H. B. Schlegel, G. E. Scuseria, M. A. Robb, J. R. Cheeseman, G. Scalmani, V. Barone, G. A. Petersson, H. Nakatsuji, X. Li, M. Caricato, A. V. Marenich, J. Bloino, B. G. Janesko, R. Gomperts, B. Mennucci, H. P. Hratchian, J. V. Ortiz, A. F. Izmaylov, J. L. Sonnenberg, D. Williams-Young, F. Ding, F. Lipparini, F. Egidi, J. Goings, B. Peng, A. Petrone, T. Henderson, D. Ranasinghe, V. G. Zakrzewski, J. Gao, N. Rega, G. Zheng, W. Liang, M. Hada, M. Ehara, K. Toyota, R. Fukuda, J. Hasegawa, M. Ishida, T. Nakajima, Y. Honda, O. Kitao, H. Nakai, T. Vreven, K. Throssell, J. A. Montgomery, Jr., J. E. Peralta, F. Ogliaro, M. J. Bearpark, J. J. Heyd, E. N. Brothers, K. N. Kudin,V. N. Staroverov, T. A. Keith, R. Kobayashi, J. Normand, K. Raghavachari, A. P. Rendell, J. C. Burant, S. S. Iyengar, J. Tomasi, M. Cossi, J. M. Millam, M. Klene, C. Adamo, R. Cammi, J. W. Ochterski, R. L. Martin, K. Morokuma, O. Farkas, J. B. Foresman, and D. J. Fox, Gaussian, Inc., Wallingford CT, **2019**.

Author Contributions

Claire Muzyka: Conceptualization, Experimental work, Writing - Original Draft

Sebastien Renson: Experimental work, Computations, Review & Editing

Bruno Grignard: Writing - review & editing

Christophe Detrembleur: Funding acquisition, Writing - review & editing.

Jean-Christophe M. Monbaliu: Conceptualization, Project Administration, Supervision, Funding acquisition, Writing – review & editing.

6 CONCLUSION AND PERSPECTIVES

6.1 CONCLUSION

This thesis explores new perspectives toward the valorization of bio-based polyols through two complementary, yet distinct strategies: one grounded in computational science and the other in reactor technologies. Both approaches aim to tackle key challenges, including selectivity control and the low efficiency of current synthetic processes involving bio-based polyols. By proposing innovative solutions to these limitations, this work contributes to the broader effort to integrate bio-based polyols in industrial applications by offering innovative solutions to their inherent limitations. A consistent methodology is applied to both strategies, beginning with a comprehensive literature review to precisely define the research problem prior to addressing its resolution.

In lieu of a conclusion, we present below the main take-home messages arising from the research findings discussed in Chapters 2 to 5:

- **Identification of reactions bearing a huge potential in polyol valorization (Chapter 2)**: The research began with a detailed overview of synthetic methodologies flagged as industrially relevant (olefins, epoxides, chlorinated species, carbonates and ketals), and an assessment of their sustainability and overall efficiency. While small polyols such ethylene glycol or glycerol are widely used, more complex substrates such as *meso*-erythritol, xylitol or sorbitol are barely investigated. This strongly highlights the need to develop tools enabling to map complex reactions with multiple reactive sites to facilitate polyol exploitation.
- **Development of a methodology to tackle complex reaction systems relying on computational science (Chapter 3)**: This strategy was implemented as a workflow of two user-friendly Python scripts, using a dynamic covalent exchange toward orthoesters as the model subject system. The first script performed tensorial decomposition of raw NMR data obtained from a kinetic study, providing an estimation of the number of species involved. Building on these findings and careful characterization of the reaction medium, the second script enables the numerical resolution of kinetic systems. Model elaboration is assisted by statistical tools that assess both the model accuracy and the trade-off between complexity and accuracy. Once a validated and robust model was developed, it was used to quantitatively evaluate the effect of various experimental parameters on the reaction network. In parallel, a comprehensive DFT study was conducted to elucidate the underlying mechanisms, emphasizing the crucial role of inter- and intramolecular hydrogen bonds in governing the reaction dynamics.
- **Elucidation of the acid-catalyzed deoxydehydration mechanism of bio-based orthoesters (Chapter 4)**: This work performed DFT calculations to elucidate the mechanisms leading to the formation of key intermediates next undergoing deoxydehydration. Dioxocarbene species were found to be generated via an asynchronous pathway, involving initial protonation and elimination of the orthoester ethoxy group, and followed by deprotonation of the acidic proton to yield the dioxocarbene. Conversely, intramolecular stabilization of the ethoxy group by a free alcohol or carboxylic acid group (unrestrained by ring geometry)

led to a stepwise mechanism involving carbocation intermediates. A combination of intra- and intermolecular stabilization was shown to further lower the activation barrier of carbocation formation, from 15.6 to 12.6 kcal mol^{-1}. The final deoxydehydration of dioxocarbenes exhibited reduced activation barriers for the intermediates substituted with electron withdrawing groups, decreasing from 12-13 kcal mol^{-1} for polyol- derived carbenes to less than 6 kcal mol^{-1} for diols substituted with ester or carboxylic acid groups. Overall, this work gave an overview of potentially reachable olefins from renewable feedstocks.

- **Design of a high throughput and efficient process toward added value glycerol carbonate** (**Chapter 5**): This chapter is divided in two subsections. Subsection 1 presents an in-depth review of the literature on epoxide and β-hydroxylated epoxides carbonatation with gaseous CO_2 (epoxides accessible from bio-sourced polyols). The focus is placed on structure activity relationships within catalytic systems, addressing both mechanistic insights and reaction performance. The review also includes a combined analysis of sustainability and productivity, with a thorough examination of experimental conditions, carbonate yields, and E-factors. Despite the extensive development and screening of catalysts, reactors technologies have received little attention. Therefore, subsection 2 aims to bridge this gap, exploring the use of continuous flow technologies for the carbonation of glycidol using nitrogen based organocatalyst. A straightforward process was engineered and successfully scaled up from microfluidic conditions to mesofluidic reactors, achieving a daily productivity of 3.6 kg of glycerol carbonate with a very attractive E-factor at 4.7 (140 °C, 28 s of residence time, 10 bar and 1 mol% of catalyst). A supporting DFT study was also conducted to rationalize the mechanism, validating the choice of Barton's base as catalyst.

Despite the successful development of these two strategies, a critical assessment is necessary to both enhance current performances and explore new avenues of research capitalizing on the **chapter 3** (Figure 6.1), **chapter 4** and **chapter 5** (Figure 6.2).

6.2 PERSPECTIVES OF CHAPTER 3

- **Strengths**: The development of the workflow set a new benchmark in computational chemistry, offering user-friendly and open access Python scripts. Designed to minimize manual input, the workflow guides users through intuitive dialog boxes to ensure smooth execution of both codes. Script 1 effectively processes and decomposes complex raw NMR data with high accuracy, while script 2 led to the development of kinetic models that strike an optimal balance. Moreover, the second script demonstrates versatility through its successful application to various reaction systems. Extensive computations analyses supported and validated kinetic modeling, enforcing the reliability and robustness of the developed strategy. Overall, this strategy revisits the empirical classical studies of mechanism elucidation, leveraging computational science to explore new reaction systems and offer rapid and in-depth analyses. Considering dynamic covalent chemistry, elucidation of the mechanisms brings novel insights to control the tailored tuning of such systems to reach specific 3D architectures.

- **Opportunities:** The implementation of this strategy on a set of kinetic studies, investigating experimental conditions (e.g. temperature, solvents, catalysts, reagents, to name a few), allows for the rapid mapping of complex reaction networks. Based on the screening, predictive models can be developed, eventually leading to precise control of selectivity through the fine tailoring of reaction parameters. Such models could also provide kinetic and thermodynamic information by applying Eyring equation, predict reaction time, and identify the most suitable reactor technology (relying on Levenspiel diagram) for the synthesis of the target system.
- **Weaknesses:** (a) Kinetic monitoring of complex reaction usually requires powerful analytical techniques able to resolve nearly identical species. In our study, we use 700 MHz NMR for monitoring, which, while effective, remains costly and limits the broader applicability of this strategy.
  (b) For script 1, the non-negative Tucker decomposition (NNT) algorithm was used to analyze spectral data. However, this algorithm lacks a penalization term to control model sparsity. In kinetic studies involving several intermediates and products, integrating sparsity would help by shrinking the contribution of the intermediates to zero once they are fully consumed. Currently, this is not the case, which hampered the accuracy of concentration profile predictions and the reconstruction of pure NMR spectra for each species.
  (c) Regarding script 2, initialization of the rate constants is arbitrary, which slow down calculations and negatively impact the quality of the adjusted model.
  (d) Furthermore, script 2 does not provide an automated workflow to compare multiple models, hindering the systematic application of this approach.
  (e) Finally, although computations gave valuable insights into kinetics and thermodynamics of the reaction, this approach lacks a comprehensive screening of functionals and bases, preventing an accurate reflection of reality.
- **Threats:** The implementation of this workflow is resource-intensive. Script 2 demonstrated limited effectiveness in adjusting for compounds present in trace amounts. Additionally, elucidation of reaction mechanisms can be very laborious and time-consuming, which may hinder the theoretical validation of the kinetic model.

Based on this critical assessment, we propose solutions to address the identified weaknesses of the strategy and present perspectives of improvements of the overall strategy.

- **Experimental set-up and analytics**: While a detailed characterization of the medium was initially required to begin kinetic monitoring, preliminary tests using a benchtop NMR 43 MHz demonstrated sufficient resolution to track main intermediates and products. Quantification was possible through integration of signal from unreacted reagent, though incorporating an internal standard would enhance reliability. However, this method required supplementary deconvolution script to ensure accurate quantification. Implementing in-line analytic methods significantly streamline kinetic monitoring and allow for simultaneous data treatment.

If in-line monitoring proves inadequate due to resolution or sensitivity limitations, alternative approaches like in-line liquid or gas chromatography could be considered. These would involve periodic sampling via injection loops with predefined volumes for analysis. However, such set-up configuration presents greater technical complexity compared to standard in-line analytical systems. Finally, complete automation of this set-up would significantly increase the reliability and efficiency of the kinetic study, and prevent any potential human errors.

- **Tensorial decomposition algorithm**: Sparse non-negative Tucker decomposition (SN-Tucker) provides a framework for introducing sparsity constraints in the core tensor. However, balancing sparsity and reconstruction accuracy requires specific tuning of the regularization parameter λ. While Bayesian optimization offers automated alternative to the manual screening for identifying the optimal value of the parameter, this approach is data-specific, meaning that re-optimization of regularization parameters is mandatory for every new dataset.
  Tensors often possess modes (= time, chemical shifts and intensities) with intrinsic dimensional mismatch. Forcing the same rank across all modes usually results in overfitting. Therefore, the use of adaptative rank strategies such as Bayesian rank constraints or adaptive tensor networks could upgrade traditional grid optimization. Such algorithms would enable automated data-driven optimization of the rank search, finding the best trade-off between complexity and accuracy while reducing the computational resource requirement.
- **Kinetic modeling**: Although this script delivers accurate statistical evaluation for individual model, it lacks a systematic framework for comparative analysis across multiple models' workflow. Incorporating such functionality would significantly enhance model development efficiency by enabling rapid identification of the optimal kinetic model.
- **Computations**: Accurate kinetic constants could be efficiently predicted via preliminary computational screening of functionals and basis sets. This approach streamlines parameter initialization of script 2, reducing its convergence time while mitigating local minima traps. Molecular dynamics simulations offer a powerful approach to investigate hydrogen bond dynamics in orthoester covalent systems. By monitoring the formation of alcohol by-product over time, these simulations would allow for visualization of the evolving solvation cages. They would also enable observation of the motion of reactive species over the course of the reaction, providing deeper understanding of species reactivity. This approach could also deepen our understanding of water behavior in such systems, particularly in the context of hydrophilic and hydrophobic catalyst use.

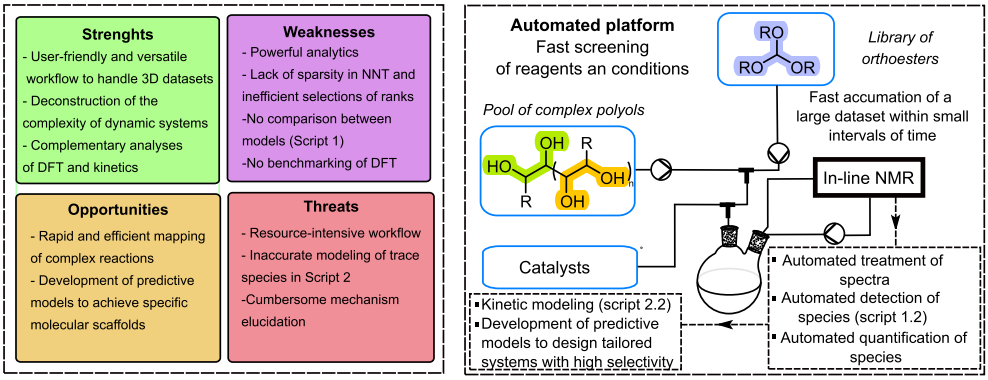

Figure 6.1 (a) SWOT analysis of the computer-aided kinetic network modeling of complex orthoester-polyol dynamic covalent exchanges and (b) perspectives toward a unify and automated platform for kinetic elucidation.

Compared to existing literature, the thesis introduces a novel strategy toward the kinetic modeling of complex dynamic systems. Specifical emphasis was placed on developing workflows specifically tailored for the organic chemistry community, addressing a gap that has received limited attention to date. This chapter directly complements the pioneering contributions of Von Delius, whose research focus on the engineering of self-assembling orthoester scaffolds with encapsulation capabilities. The combination of meticulous kinetic modeling and quantum chemical calculations presented in Chapter 3 offer new parameters and mechanistic insights that can be harnessed to design dynamic systems with tailored properties.

6.3 PERSPECTIVES OF CHAPTER 4

In contrast to Chapter 3, which developed a strategy to address polyol complexity in DCE, this chapter proposes mechanistic hypotheses based on a DFT study. The aim is to provide new insights on dioxocarbene formation and further deoxydehydration reaction, thereby opening new avenues of research. The following paragraph discusses the broader perspectives and implications of this work.

- **Computations:** Molecular dynamics simulations could provide valuable insights into dioxocarbene formation mechanisms by tracking the evolution of both intra- and intermolecular hydrogen bond networks surrounding reactive species. This approach might reveal previously overlooked competitive reaction pathways. To fully characterize the system, quantum calculations should be performed to establish the singlet-triplet state energetics of the generated dioxocarbenes, as spin multiplicity significantly influences carbene reactivity. Additionally, hydrogen bond networks could modulate spin-state transitions in the system. Comprehensive benchmarking of DFT methodologies against experimental data remains crucial to ensure reliable comparison between theoretical predictions and observed reaction outcomes.
- **Experimental work:** The hypotheses proposed in Chapter 4 require experimental validation, starting with the observation and isolation of carbocation and carbene intermediates. A comprehensive kinetic study is also essential to support the

computational findings along to explore both elucidated and potentially overlooked reaction pathways. This study should span a range of temperatures to accurately assess how reaction selectivity and outcomes vary as a function of temperature. Based on the insights gained in Chapter 4, substrate selection could be strategically adapted. For instance, the formation of dioxocarbenes could be attempted using cyclic substrates such as orthoesters derived from quinic acid, which are expected to proceed via an asynchronous mechanism. In contrast, simpler substrates derived from glycerol could be more suitable for kinetic experiments as it features a stepwise pathway.

6.4 PERSPECTIVES OF CHAPTER 5

- **Strengths**: In contrary to previously reported methods of glycidol carbonation, our strategy employed the use of an equimolar ratio of CO_2 (in respect to GD) and utilized a simple organocatalyst. The straightforward and simple experimental setup we developed greatly facilitated the transposition from microfluidic to mesofluidic conditions. This scaling-up, featuring an improved mass transfer inherent to the reactor scale, resulted in an efficient intensification of the reaction, decreasing the residence time below 30 seconds. Specifically, we achieved a unprecedent productivity of 3.6 kg day^{-1} of glycerol carbonate, while minimizing the overall generation of waste translated by the low E-factor at 4.7.
- **Opportunities**: This process can, in theory, be fully engineered using bio-based feedstocks and industrial waste streams. Glycidol can be synthetized from glycerol, a widely recognized by-product from biofuel manufacturing, while industrial effluents highly concentrated in CO_2 could serve as a primary carbon source. As such, this synthetic path holds strong potential for advancing sustainability by reducing reliance on fossil-derived inputs. By leveraging a dual feedstocks strategy, it also offers a way to overcome costs barriers associated with glycerol carbonate production. Moreover, combining a low-cost procedure to the scalability advantages of continuous flow technologies would make this process highly appealing for industrials. This strategy could give a second breath to research and development efforts, aiming to unlock novel applications from glycerol carbonate.
- **Weaknesses**: (a) Main concerns are in regard to the toxic nature of glycidol, which are red-flagged by the REACH policy, though partially mitigated using flow technologies.
  (b) Sustainability and cost efficiency of the strategy are hampered by the use of homogeneous base, which is not recyclable.
  (c) Similarly, the use of solvent, although primordial for the solubilization of CO_2, requires thermic energy to be recycled.
  (d) Fluid dynamics were not quantitively defined and monitored over the course of the reaction. We only assumed that the use of mesofluidic reactors would enhance mixing efficiency, thereby closing the door to optimizing the flow regime. Therefore, a critical gap remains: no robust framework exists to systematically correlate flow regime (laminar vs. turbulent) with experimental conditions such as flow rates, reactor geometry and operating conditions.

- **Threats**: Alternative carbonation pathways demonstrating higher overall performances than CO_2 cycloaddition could shift research focus away from CO_2 use. Moreover, analogs with comparable physico-chemical properties may lead to competition with glycerol carbonate in similar application areas.

Similarly to **chapter 3** and **4**, new perspectives and potential solutions to mitigate weaknesses of our strategy are now discussed.

- **Safety considerations**: mitigation of glycidol-related hazard could be achieved by integrating the flow synthesis of the epoxide with its subsequent conversion with CO_2. While the telescoped conversion of bio-sourced glycerol to glycidol in flow has already been reported, it involves the use of aqueous hydrochloric acid (HCl). This results in a high excess of water relative to the epoxide, leading to both low epoxide concentration and significant hydrolysis of glycerol carbonate back to glycerol. It is anticipated that this issue will be addressed by the use of gaseous HCl as chlorinating agent, thereby minimizing water content and unlocking the overall potential of the end-to-end synthesis of glycerol carbonate. Such route is currently investigated by another PhD student.
- **Catalyst loss**: The heterogenization of Barton's base could be envisioned to prevent its loss. Chemically inert solid materials such as polystyrene present a promising option. Additionally, Lewis acidic supports like mesoporous silica or zeolithes offer attractive alternatives, as they could theoretically activate the epoxide, further stabilize the reaction intermediate (e.g hemiester of carbonic acid) and facilitate intramolecular cyclization of the proton shuttle mechanism; identified as the rate determining step in **chapter 5**.
- **Productivity of glycerol carbonate**: A concentration of 1.8 M glycidol was used as the reaction medium. Further improvement in reaction performance could be achieved by increasing this concentration and considering a solventless synthesis of the carbonate.
- **Fluid dynamics**: Gas-liquid reactions are commonly limited by mass transfer at the gas-liquid interface. Continuous flow systems offer higher mixing efficiency due to rapid molecular diffusion within narrow channels and the potential for turbulence regime under specific conditions. In our case, the reaction starts with two low-viscosity reagents, glycidol (4 mPa s^{-1}) and methyl ethyl ketone (0.4 mPa s^{-1}), and produces highly viscous glycerol carbonate (44 mPa s^{-1}). This represents a 10-fold increase of the viscosity over the course of the reaction, which significantly hinders performance by reducing mass transfer efficiency. We believe that the future lies in the development of integrated tools that combine fluid dynamics modelling under micro- and mesofluidic conditions with predictions of gas solubility (via's Henry law and Laplace pressure) and kinetic modelling. Such tools hold great promise in delivering optimized experimental conditions tailored to maximize mass transfer and productivity of a library of epoxides. It could also assist in designing experimental setups by identifying areas with poor mixing efficiency (Figure 6.2b). Overall, improving the efficiency of reaction mixing could allow for lower temperature, pressure, and catalyst loading, thereby reducing the process footprint.

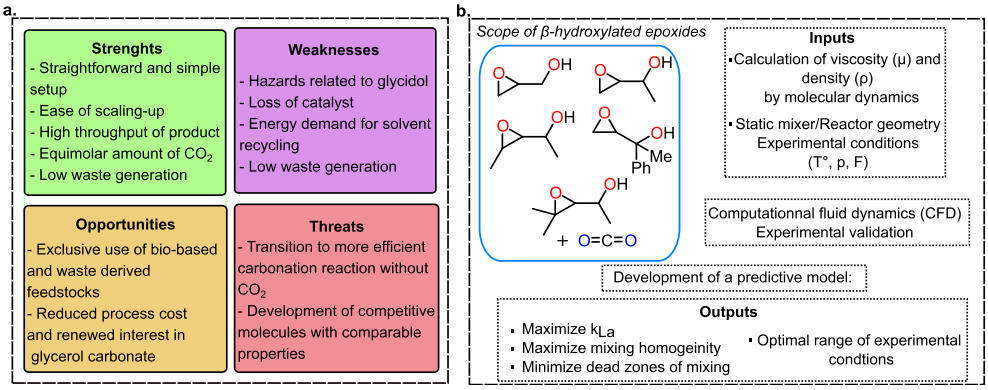

Figure 6.2 (a) SWOT analysis of the catalytic coupling of glycidol with CO_2 and (b) perspectives toward the development of predictive model to optimize mass transfer efficiency in gas liquid reactions.

This chapter introduces a straightforward and effective strategy to address the thermodynamic stability of CO_2 through appropriate activation of both the substrate and carbon dioxide. To date, only two examples of glycidol carbonation in flow have been reported (e.g. Kleij and Garcia-Verdugo), both demonstrating very low productivity, limited to gram-scale yields, and highlighted the inability to scale up their experimental set-up. Conversely, our work offers a new perspective on CO_2 utilization and establishes a solid foundation for developing carbonation reactions applicable to a broad library of β-hydroxylated-epoxides, including di- or tri-substituted carbonates, which are particularly known for their challenging reactivity.

This research aimed to advance the valorization of bio-based polyols by addressing key limitations through innovative strategies in vicinal diol chemistry. By developing alternative pathways and processes that rival petrochemistry in term of efficiency and atom economy, we position biomass-derived polyols as competitive and sustainable feedstocks for industrial application. The structural complexity of polyols is overwhelming, yet, offering unique opportunities for novel valorization strategies, enabling to reach scaffolds with peculiar functionalities and significant untapped potential. To overcome challenges posed by this complexity, multidisciplinary approaches that integrate green chemistry principles with scalable technologies are essential. This PhD work contributes to global efforts to align economic viability with the development of a circular and climate-neutral chemical industry.